Towards Sustainable Machining of Difficult-to-Cut Materials using Nano-Cutting Fluids

by

Hussien Hegab

A Thesis Submitted in Partial Fulfillment of the Requirements for the Degree of Doctor of Philosophy

In

The Faculty of Engineering and Applied Science

Department of Automotive, Mechanical and Manufacturing Engineering

University of Ontario Institute of Technology

May, 2018

Copyright © by Hussien Hegab, 2018

Abstract

Providing environmentally friendly conditions and optimizing energy consumption are two essential requirements in order to achieve sustainable machining processes. One of the major sustainable machining concerns is the implementation of cutting fluids due to its significant impact on the machining quality characteristics. In addition, several economic, environmental, and health problems take place due to the inappropriate application of cutting fluids, therefore, previous research has introduced advanced cutting fluids technologies in order to optimize the cutting fluids usage during machining. However, there are still issues related to machining difficult-to-cut materials that have not been addressed and need to be improved. These materials have superior characteristics such as high strength to weight ratio, corrosion resistance, temperature resistance, and chemical stability, allowing them to be materials of choice in the aerospace, automotive, oil and gas, and bio-medical industries. Despite their desired characteristics, the wide spread applications of these materials has been compromised by several difficulties that arise during machining.

Flood cooling is a typical cooling strategy used in industry to dissipate the high heat generated during machining difficult-to-cut materials; however, the use of flood coolant has raised environmental and health concerns which call for different alternatives. Minimum Quantity Lubricant (MQL) has been successfully utilized as an acceptable coolant strategy; however, its potential to dissipate heat is much lower than the one achieved by flood coolant. One of the best techniques to enhance MQL heat capacity is the application of nano-cutting fluids as they offer significant enhancement in the tribological and heat transfer characteristics.

The main objective of the proposed research is to fully investigate and understand the influence and role of dispersed multi-walled carbon nano-tubes (MWCNTs) into vegetable oil by implementing the minimum quantity lubrication (MQL) technique during turning Ti-6Al-4V titanium alloy and Inconel 718. The Investigations include study of the energy consumption, tool wear behavior, chip morphology, and surface quality when using nano-cutting fluids based MQL. The study revealed that nano-fluid based MQL improves the tool performance and proves clear advantage over the traditional/classical MQL.

In order to provide a solid physical understanding of the studied cutting processes using MQL-nano-fluids, the tribological aspects of the process and heat transfer mechanisms have been analyzed and investigated. The study presented a comparative performance analysis between MWCNTs and aluminum oxide (Al_2O_3) nano-cutting fluids. Additionally, an integrated finite element (FE) model has been developed in order to simulate the thermal and frictional effects of the MQL-nano-fluid to study various unique cutting aspects such as generated cutting temperature and residual stresses.

Furthermore, a general and detailed assessment model is developed and used to assess the sustainability of machining processes. Energy consumption, machining costs, waste management, environmental impact, and personal health and safety have been used to express the overall sustainability assessment index. It should be stated that the model predictions agree with the experimental findings. As such, the developed model offers a valuable tool to optimize the sustainability aspects of machining process.

Acknowledgements

I would like to express my special thanks and gratitude to my supervisor, Professor H A. Kishawy, for his great support and encouragement to conduct this research. Professor Kishawy's extensive knowledge and significant experience has not only helped me throughout my research, but has also allowed me to overcome any obstacles throughout this process. My family has been my source of love, guidance, and inspiration throughout this journey. They were always there whenever I needed support. I would also like to expresses my sincere appreciation to the members of the supervisory committee for their helpful comments and discussions. Finally, I would like to thank my colleagues at the Machining Research Laboratory (MRL) for their continuous support and motivation.

Dedication

To my beloved parents; Mrs. Bothina Abdelhamid & Mr. Abdelaziz Hegab

Table of Contents

Nomenclature

A	The initial yield strength (MPa) of the material at room temperature
A_s	The protective film surface area
A_{CS}	The interference cross-sectional area of nano-additive
A_N	Nominal area
ANOVA	Analysis of Variance
$AWSI_{jn}$	The average weighted sustainable index for each machining characteristic (j)
$AWSI_{kn}$	The average weighted sustainable index for each sustainable metric (k)
B	The hardening modulus
B’	The dimensionless velocity gradient
Bi	Biot number
BUE	Built up edge
C	The resultant nano-fluid specific heat
c	The coefficient dependent on the strain rate
C_{bf}	The base fluid specific heat
C_c	The cost of tool changing
C_{ctd}	The cost of cutting tool disposal (unit cost/Kg)
C_{ctr}	The recycling cost of cutting tool (unit cost/Kg)
C_e	The cost of a cutting edge
C_l	The cutting fluid preparation costs
C_m	The machining cost
C_{mist}	The nano-fluid mist specific heat
C_n	The cost associated with non-machining time
C_p	The nano-additive specific heat
C_p	The protective film specific heat
C_t	The tool cost per piece
C_{co}	The production cost of cutting oil (unit cost/liter)
C_{ad}	The cost of additives (unit cost/liter)
C_{di}	The required cost to disperse the additives into the main cutting oil
C_{setup}	The required cost for lubrication/cooling system setup
C_{dis}	The cost of cutting fluid disposal (unit cost/liter)
C_{lr}	The recycling cost of cutting fluid (unit cost/liter)
d	The separation distance between the workpiece and cutting tool surfaces
D	Damage (fracture) of an element
$D_{1\text{-}5}$	Johnson–Cook progressive damage model parameters
D_{AVG}	Nano-additive average size
$\dot{E}_{in}$	Input thermal energy rate
$\dot{E}_{out}$	Output thermal energy rate
$E_{\text{ cutting edge}}$	The energy per cutting edge
E_{cfd}	The required energy to dispose of the used cutting fluid
E_{cfp}	The required energy for production of the used cutting fluid
E_{cfr}	The required energy to recycle/recover the used cutting fluid

E_{ctd}	The required energy to dispose of scrap parts (cutting tool)
E_{ctp}	The required energy for production the used cutting tool
E_{ctr}	The required energy to recycle/recover scrap parts (cutting tool)
E_{tool}	The energy footprint of the cutting tool
E_{wd}	The required energy to dispose of the scrap parts (workpiece)
E_{wp}	The required energy for production of the used workpiece
E_{wr}	The required energy to recycle/recover scrap parts (workpiece)
f_c	The cutting force
G(Pr)	Prandtl number function
h	The nano-fluid mixture convection coefficient
HPC	High-Pressure Coolant
I	The design parameter levels counter
I^{kp}	Value for each sustainable indicator (p)
IW_{kp}	The weighting importance factor for each sustainable indicator (p)
J	The machining responses counter
k	The specific cutting energy (J/mm^3)
K	The sustainable metrics counter
K_e	The resultant nano-fluid thermal conductivity
K_m	The base fluid thermal conductivity
K_{mist}	The nano-fluid mist thermal conductivity
K_p	The nano-additive thermal conductivity
L	The nano-additives sliding distance
Lc	The characteristic length
l_g	The labor rate for a tool room operator
l_m	The labor cost of a production operator per unit time
m	The thermal softening coefficient
M	Number of selected machining quality characteristics (responses)
m_{film}	The protective film mass
MQL	Minimum Quantity Lubrication
MQW_j	Weighting importance factor for each machining response (j)
Mr_j	Value for each machining response (j)
MWCNTs	Multi-Walled Carbon Nano-Tubes
m_{sr}	The total mass of remanufactured scrap parts
m_s	The total mass of scrap parts
m_{dc}	The total mass of disposed of chips
m_{src}	The total mass of recycled scrap parts
m_{sd}	The total mass of disposed of scrap parts
m_{rc}	The total mass of recycled chips
m_c	The total mass of chips
$\overline{Nu_{L_c}}$	The average nano-fluid mist Nusselt number
n	The work-hardening exponent
N	Number of experimental cutting tests
N	The cutting tests counter
NCFL	Nano-Cutting Fluid Lubrication
NDM	Near-dry machining
N_{dp}	Number of selected design parameters

N_k	Number of selected indicators for each sustainable metric (k)
N_{li}	Number of levels per each design parameter (i)
NM	Number of studied sustainable metrics
N_{NA}	Number of nano-additives
NP	Nano-particles
NT	Nano-tubes
NT	Nodal temperature
OA	Orthogonal array
$OAWS_{In}$	The overall average weighted sustainable index for each cutting test (n)
o_g	The overhead rate for the tool room operation
o_m	The overhead charge for the machine
OS_{hss}	An operational safety index used to express the high-speed surface exposure
OS_{hts}	An operational safety index used to express the temperature surface exposure
OS_{tc}	An operational safety index used to express the toxic chemicals exposure
p	The normal pressure at the contact point where chip shear stress determined
P	The sustainable indicators counter
P_{ac}	A personal health index used to express the working environment conditions
P_i	A personal health index used to express the working illumination level
P_n	A personal health index used to express the working environment noise level
Pr	Prandtl number
$\dot{P}$	The applied pressure of the used cutting fluid
q'''	Amount of heat generation
R	The nano-additive radius
Ra	The average surface roughness
$Re_{mist,Lc}$	The nano-fluid mist Reynolds number
R_m	Measure response value
R_P	Predicted response value
RSM	Response Surface Methodology
s	The protective film thickness
SF_{kpjn}	The sustainable factor for each cutting test (n)
SI_{kpjn}	The sustainable index for each cutting test (n)
SMW_k	The weighting importance factor for each sustainable metric (k)
SWCNTs	Single-Walled Carbon Nano-Tubes
T	The cutting tool life
T_∞	The ambient temperature
t_{ac}	The actual cutting time per piece
t_{cus}	The cutting usage time
$t_{cutting}$	The required cutting time
T_{film}	The protective film temperature
t_g	The time required to grind and change a cutting edge
$T_{interface}$	The cutting interface temperature
t_m	The machining time per piece
T_{metl}	Melting temperature
t_o	The undeformed chip thickness
T_{S1}	The workpiece surface temperature
t_{setup}	The cutting process required setup time

$t_{toolchange}$	The required time to change the cutting tool
$TWSI_n$	The total weighted sustainable index for each cutting test (n)
τ	The chip shear stress
τ_c	The critical friction stress
τ_{th}	The threshold value related to material failure
T	The cutting tool life
v	The cutting velocity
V_{film}	The protective film volume
VB	Flank tool wear
V_{mist}	The average mist velocity
V_{NA}	The wear volume induced by nano-additive
v_s	Nano-additive sedimentation velocity
$\dot{V}$	Material removal rate (mm^3/min)
$\dot{W}_o$	The machine's power consumption with the spindle turned off
W_{rc}	The ratio of recycled chips
W_{sd}	The ratio of disposed of scrap parts
W_{src}	The ratio of recycled scrap parts
W_{sr}	The ratio of remanufactured scrap parts
W_{dc}	The ratio of disposed of chips

Greek Symbols

ρ_m	The base fluid density
ρ_p	The nano-additive density
ρ_e	The resultant nano-fluid density
μ_e	The resultant nano-fluid viscosity
μ_m	The base fluid viscosity
υ_p	The nano-additive volume fraction
η	The nano-additive viscosity
Δ	The average percentage of deviation
ε	The normally distributed error
$n_p(y)$	The number of nano-additives per nominal area of contact
ø	The size distribution of nano-additive
ω	The nano-additive indentation
σ_{avg}	Standard deviation of nano-additive size
ν_2	The workpiece Poisson ratio
ΔE_{stored}	The change of thermal energy content
ρ_{film}	The protective film density
α	The protective film thermal diffusivity
ρ_{mist}	The nano-fluid mist density
μ_{mist}	The nano-fluid mist viscosity

$\bar{\sigma}$	The equivalent stress
$\bar{\varepsilon}$	The equivalent plastic strain
$\dot{\bar{\varepsilon}}$	The normalized strain rate
$\dot{\bar{\varepsilon}}_o$	The reference strain rate
$\Delta\bar{\varepsilon}$	The increment of equivalent plastic strain
$\bar{\varepsilon}^f$	The equivalent strain to fracture

List of Figures

List of Tables

Chapter 1 Introduction

1.1. Preamble

It is a well-acknowledged fact that the major environmental concerns have arisen because of the pollution and consumption of natural resources. Thus, the implementation of sustainable systems is an essential requirement in modern manufacturing to address these concerns and present effective solutions. There is no universal definition for the term sustainability; however, the most acceptable illustration of this term was proposed by Norway's previous Prime Minister and Director-General of the World Health Organization (WHO), Gro Harlem Bruntland, who expressed as *"meeting the needs of the present without compromising the ability of future generations to meet their own needs"* [1]. Jawahir and Wanigarathne showed that the main aspects of sustainability are focused on the environmental, economic, and social directions in order to achieve better requirements through effective utilizing of the available resources [1, 2].

Each sustainable aspect has specific objectives that should be achieved in order to create and implement the efficient term of sustainability. The main objectives of the social sustainability are focused on the health improvement, safety, quality of life enhancement, and ethics. When looking at the environmental sustainability, cleaner air, water, soil, regulations implementation, and eco-balance efficiency support this goal. With respect to the economic sustainability, the main pillars are product and process development, new employment, and large-scale new business opportunities [1].

The concept of sustainable manufacturing can be identified and analyzed through three main levels which are product, process, and system levels. The interaction among the three levels provide the required sustainable target. In regards to the product level, the perspective of sustainable manufacturing focuses on the new 6R approach (i.e. reduce, reuse, recover, redesign, remanufacture, recycle) instead of the 3R approach (i.e. reduce, reuse, recycle) of green manufacturing, as it theoretically achieves a closed loop and multiple life-cycle paradigms [3-5]. At the process level, reducing energy consumption, hazards, and toxic wastes can be accomplished through using an optimized technological process associated with an effective process planning methodology, while using an efficient supply chain system considering all life-cycle stages (i.e. pre-manufacturing, manufacturing, use and post-use) can provide a promising sustainable system level [3, 6, 7]. The expectations of a sustainable manufacturing process can be concluded as following [1, 2, 4]:

- Energy consumption reduction.
- Waste elimination/reduction.
- Product durability improvement.
- Health hazards and toxic dispersion elimination (health conditions improvements).
- Higher quality of manufacturing.
- Recycling, reuse, and remanufacturing enhancement.
- Development of renewable energy sustainable resources.

Five major elements are implemented for the assessment of sustainable machining process (ProcSI) as following [8]:

- **Energy consumption:** as a result of the global impact of energy production and consumption, this element is considered as an effective part of any manufacturing process assessment. Energy consumption includes manufacturing operation/process, coolant pumps consumption, production supporting facilities, in-plant transportation, etc.

- **Machining costs:** during the manufacturing process, this element focuses on direct and indirect costs for capital, environment, and society related factors. It has a high potential effect to ensure the economic soundness and technological validity.

- **Waste management:** achieving zero waste and no emissions is the main target of this element which is extremely difficult to achieve. The effort related to this element is focused on the generation and post-treatment of all waste produced during and after production activities, and achieving a closed-loop material flow with minimal waste and emissions.

- **Personal health and operational safety:** it covers the direct working environment which affects the individual's shop floor and supervisory personnel' health with the immediate and long-term impacts of the manufacturing processes. It involves standard industrial and governmental regulations (e.g., EPA, OSHA and NIOSH), established personnel's health records, and historic data.

- **Environmental impact:** its main concerns focus on resource consumption, emissions, and waste disposal. There is no universal benchmarking method established for measuring this element. Thus, analysis and comparison would be feasible only among similar processes.

Various studies have been performed to investigate, develop, model and optimize efficient energy systems in order to minimize the energy consumption during machining processes. One of the major sustainable machining concerns is using of cutting fluid as it has a significant impact on the machining quality characteristics, and it is one of the cost contributors. Furthermore, the cutting fluid usage has a social and environmental impact (e.g. shop floor personnel's health effects) [8]. Major advances in the lubrication and cooling techniques have been presented throughout the literature such as near dry machining (NDM), minimum quantity lubrication (MQL), cryogenic cooling, high-pressure coolant (HPC), compressed air cooling, and nano-cutting fluid lubrication (NCFL) [9-11].

Several studies focused on machining difficult-to-cut materials as they are associated with low productivity and high machining cost due to the excessive heat generation, difficulties in chip formation, and heat dissipation at the cutting zone in the presence of high material hardness and strength. The main problems associated with machining difficult-to-cut materials are short tool life and poor surface integrity. However, despite the above-mentioned issues, these materials have superior characteristics such as high strength to weight ratio, corrosion resistance, temperature resistance, chemical stability that make them a material of choice in aerospace, automotive, oil and gas, and biomedical industries. Examples of difficult-to-cut materials include titanium alloys, nickel-based alloys, structural ceramics, composites, polymers and magnesium alloys [12-15]. As a result, machining difficult-to-cut materials should be thoroughly studied from a sustainability point of view to achieve the most feasible cutting strategy.

1.2. Research Scope and Objectives

The current work focuses on the improvement of quality characteristics (e.g., tool wear, surface quality) when machining titanium and nickel-based alloys.

Several properties make titanium and its alloy the primary candidate to attain weight and functional advantages because of its promising properties (e.g., high strength to weight ratio, high corrosion resistivity, high yield stress, high wear resistance, and high toughness) [16]. A comparative study among Ti-6Al-4V, high-strength steel (34CrMo4), high-strength aluminum alloy (AlZnMg-Al7075), and high strength magnesium alloy (AZ80) has been presented in terms of their properties and applications. Ti-6Al-4V showed a significant advantage when structural components are designed for higher strength or fatigue strength [17]. Although titanium alloys have superior properties, some inherent characteristics such as high chemical reactivity and low thermal conductivity lead to poor machinability and result in premature tool failure and shortened tool life. Furthermore, other major issues associated with machining of titanium alloys include generation of high mechanical pressure, high dynamic loads, high cutting temperature, and tendency to adhesion and forming built up edge [12, 18]. In view of their potential market, lots of large companies (e.g., Rolls Royce) present different studies to develop appropriate techniques for machining titanium alloys in order to minimize machining cost, achieve excellent surface quality, and achieve reasonable production rates by considering the unique characteristics of titanium alloys and developing new sustainable energy systems [12, 19].

Nickel based alloys have also superior mechanical, thermal, and chemical properties (e.g., hot strength and hot hardness, high creep resistance, and chemical stability at elevated temperatures). Furthermore, nickel alloys have unique properties such as high erosion resistivity, high thermal fatigue resistivity, high melting temperature, and resistance to thermal shock. During machining of nickel-based alloys, the heat generated can't be dispersed through the workpiece and chips because of its very low heat conductivity and high generated temperature, creating undesirable forces during the cutting process. It has been shown that the increase in the cutting temperature over 650°C leads to low surface quality, excessive tool wear, altering the microstructure, micro cracks and micro-hardness variations, high hardness and non-sufficient machinability in general [20, 21]. Another mechanical property in some nickel-based alloys (e.g. Inconel 718, Hastelloy, Nimonic) is the strain hardening due to the presence of molybdenum and niobium in the material.

Generally, it has been shown that nickel based alloys machining is associated with poor surface and subsurface quality, short tool life, low cutting speeds and high machining costs. Nickel-based alloys can be categorized as hard-to-cut materials due to the following reasons [22-24]:

- High strain hardening, hot strength, hardness, shear strength, and cutting forces.
- Low thermal conductivity.
- Formation of built-up edge.
- Hard carbide particles presence in the microstructure which leads to abrasive wear.
- Small tool–chip contact area which leads to high mechanical and thermal properties.
- High chemical reactivity with cutting tool materials.

In terms of the cutting fluid usage, the main functions are cooling at high cutting speeds and lubricating at low speeds. Flood cooling is a typical cooling strategy used in industry to reduce the high temperature generated during machining nickel and titanium alloys. However, the use of flood coolant has raised environmental and health concerns which call for different alternatives. Thus, proposing new environmental cooling and lubricant systems is highly required specially to improve the cutting quality characteristics and achieve a sustainable machining system. It was investigated that minimum quantity lubrication (MQL) provides an economically applied amount to the cutting zones. Most studies consider MQL as an effective method rather than the conventional flood cooling. MQL has been successfully introduced as an acceptable coolant strategy; however, its potential to dissipate heat is much lower than the one achieved using flood coolant. In this study, the important key to improve the cooling and lubrication performance of MQL system is using special cutting fluids such as nano-cutting fluids which could improve the wettability characteristics of the base fluid [25, 26].

MQL-nano-cutting fluid is one of the suggested techniques to further improve the performance of MQL particularly when machining difficult-to-cut materials. Nano-cutting fluids have shown promising effects on the cutting performance characteristics through different cutting operations such as turning, milling and grinding as has been presented in some previous studies [27-32]. One of the nano-additives which have superior properties is carbon nano-tubes (CNTs). CNTs have diameters ranging from a few nanometers to hundreds of nanometers and their lengths vary from tens of nanometers to several centimeters. They have superior mechanical properties; Young's modulus is over 1 TPa and tensile strength is estimated to be 10 – 60 GPa, which makes them ideal for applications like reinforced composites and Nano Electro Mechanical Systems (NEMS).

Furthermore, the carbon nano-tubes show superior thermal properties such as thermal conductivity over 2000 W/m K for single-walled carbon nanotubes (SWCNTs) and about 3000 W/m K for multi-walled carbon nanotubes (MWCNTs) [33-35]. In addition, CNT's surface area to volume ratio is much larger in million times than micro-particles. This property enhanced flow, heat transfer and other characteristics; for example, the heat convection is predicted to be as high as 6,000 (W/m K) at room temperature.

The application of titanium and nickel-based alloys can be further spread through providing new techniques to decrease the problems associated with its machining process. The focus of this work is mainly to understand and investigate the effects of dispersed multi-wall carbon nanotubes (MWCNTs) into the conventional fluid (vegetable oil) under minimum quantity lubrication (MQL) technique during turning of Ti-6Al-4V titanium alloy and Inconel 718. Cutting tests are carried out to study the generated power consumption, tool wear behavior, chip morphology, and surface quality. The following specific objectives will be discussed in this work:

- Performing bar turning experiments for both Ti-6Al-4V titanium alloy and Inconel 718 using dispersed multi-wall carbon nanotubes (MWCNT) in the base oil (nano-cutting fluid) under (MQL) technique. The input process parameters are cutting speed, feed rate, and percentage of added MWCNT (%wt.). Standard Taguchi orthogonal array (L9OA) is applied to study the entire design parameters space through performing the experimental trials.

- Employing analysis of variance (ANOVA) in order to analyze the influence of the design parameters on the measured machining quality characteristics which are the average surface roughness, energy consumption, and flank tool wear. This objective includes determining the significant design parameters for each measured response, selecting an optimal level for each significant parameter, and verifying the improvement of quality characteristics using the optimal level of design parameters.

- Building mathematical models for the measured average surface roughness, energy consumption, and flank tool wear (VB) as a function of the significant process parameters using Response Surface Methodology (RSM). Validation of mathematical models will be provided through this step by comparing the measured and predicted values of previously measured machining quality characteristics.

- Analyzing the cutting tool wear modes and their associated wear mechanisms. The role of dispersed MWCNTs into the base oil can be clearly investigated throughout this objective and can also be correlated with other characteristics such as the generated cutting forces;

- Examining the chip morphology in terms of chip thickness, shape, and color in order to provide details about the effects of the proposed nano-fluid with MQL on the chip-tool interface temperature;

- Comparing the machining quality characteristics results when using MWCNTs nano-fluid with another nano-cutting fluid (i.e., aluminum oxide nano-particles; Al_2O_3);

- Studying and analyzing the nano-cutting fluid tribological and heat transfer mechanisms through conducting a comparative performance analysis between MWCNTs and Al_2O_3 nano-cutting fluids (i.e., nano-tubes vs. nano-particles);

- Developing an integrated finite element model to analyze various unique aspects of the studied cutting processes, including the resultant nano-cutting fluid heat transfer characteristics, the interactions between the cutting tool and workpiece, the generated cutting temperature at cutting zones, and the resulting residual stresses;

- Developing a general assessment model for machining processes using five major sustainable indicators (i.e., energy consumption, machining costs, waste management, personal health and operational safety, environmental impact) in order to express the overall sustainability assessment index;

- Implementing the proposed assessment model into the studied cases (i.e., turning Ti-6Al-4V and Inconel 718 alloys using MWCNT and Al_2O_3 nano-cutting fluids under using MQL).

1.3. Thesis Outline

This thesis consists of ten chapters. The first chapter presents an introduction which provides the study motivation, scope, and objectives. Chapter 2 contains a literature survey of publications which are related to sustainable manufacturing/machining concepts and problems related to the machining of difficult-to-cut materials. A literature review of the research progress in nano-cutting fluids technology is discussed in chapter 3.

Chapter 4 presents the experimental setup. This includes the selection of the measured cutting responses and their measured techniques, the independent process parameters and their levels, the properties for the used alloys (e.g. mechanical and thermal properties, and chemical compositions), CNC machine setup, MQL setup, preparation and characterization of the nano-cutting fluids, and the plan of cutting experimentation.

Modeling and optimization of the cutting processes characteristics (i.e., flank wear, surface roughness, energy consumption, cutting tool wear modes/mechanisms and chip morphology examination) when using MQL-nano-fluids for cutting Ti-6Al-4V and Inconel 718 are presented and discussed in Chapters 5 and 6, respectively. Moreover, the nano-cutting fluid tribological and heat transfer mechanisms for both MWCNTs and Al_2O_3 nano-cutting fluids are presented and discussed throughout Chapter 7.

Chapter 8 presents the developed integrated finite element model of the studied cutting processes when using MQL-nano-fluids. The proposed assessment algorithm of sustainable machining processes is developed, discussed, and verified in Chapter 9. The implementation of the proposed assessment model into the studied cutting processes is also provided and discussed in Chapter 9. Finally, the conclusions of the thesis findings and the roadmap for future investigations are provided in Chapter 10.

Chapter 2 Difficult-to-Cut Materials and Machining Sustainability

2.1. Preamble

This chapter presents a literature survey of reported machining studies of difficult-to-cut materials. It showed the problems associated with machining difficult-to-cut materials (e.g., Ti-6Al-4V, and Inconel 718). It also provides an overview about the sustainability of machining processes. There is a significant technological advancement in order to achieve better machining performance and sustainable machining systems; however, major problems associated with machining of difficult-to-cut materials still exist. Thus, several studies are focused on the cutting processes development through achieving energy consumption reduction with health condition improvements. In this chapter, the most significant publications in the field of lubrication and cooling techniques from the sustainability perspective are presented. Also, the achievements of researchers in the relevant topics are reviewed.

2.2. Machining of Difficult-to-Cut Materials

In this section, a review to illustrate the characteristics of difficult-to-cut materials is provided and analyzed, especially for titanium and nickel-based alloys. The Difficult-to-cut materials can be categorized into three types; non-homogeneous materials, hard materials, and ductile materials as shown in Figure 2-1. Difficult-to-cut materials have been widely employed in many engineering applications, including automotive and aeronautical designs because of their effective properties including high strength-to-weight ratio and better capability to resist the induced corrosion [1]. However, other characteristics; for example, high hardness and low thermal conductivity has negatively affected the induced surface quality and tool life, and consequently the overall machinability of such materials. An understanding of the influence of different machining design variables (e.g. cutting velocity, tool geometry, coolant strategy, feed rate, depth of cut), has a significant role in improving machinability, productivity, and reducing the total machining cost. Several studies have been conducted with an aim to specify the optimal machining variables and select the better coolant strategy as machining of hard-to-cut materials is still facing different problems particularly, ceramics, titanium alloys, polymers, nickel-based alloys, composite based materials, and hardened steels [12-15].

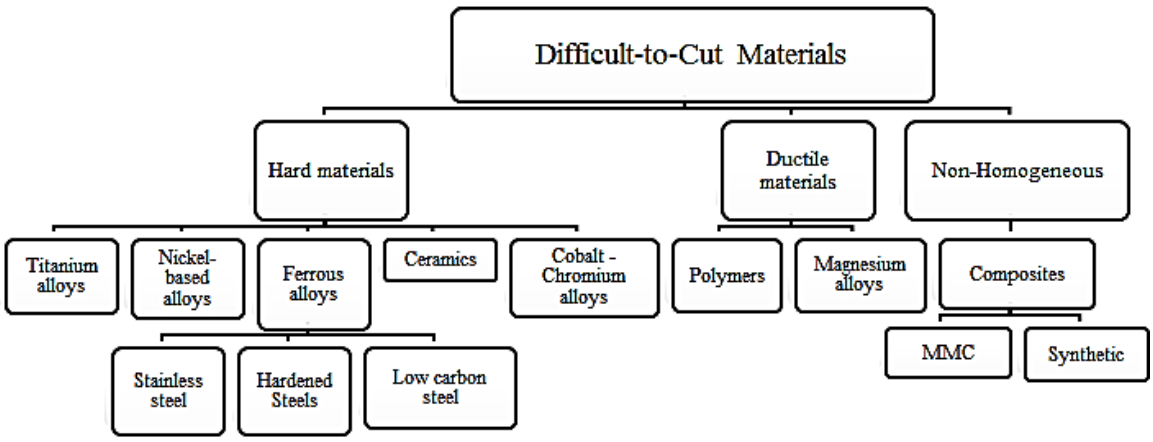

Figure 2-1 Difficult to machine materials classification [1]

In spite of improving the service life of the components using advances in the metallurgy of engineering alloys, a lot of difficulties are still facing the components developments throughout their machinability behavior [12]. High hardness, low thermal conductivity, and high strength are considered as the main properties of hard-to-machine materials. Different associated problems can be taken place due to these properties. For example, short tool life, poor surface quality, and low productivity are among noted problems.

Also, polymers and low carbon steels are among the difficult-to-cut materials as they exhibit high elongation percentage and ductility. Their problems are mainly related to the geometrical accuracy, surface quality, and chip formation.

Composites materials are positioned in a different category as they are made of a combination of a different material with different properties which result in achieving non-chemically combined and non-homogenous materials. Thus, dealing with the resultant material characteristics is a difficult aspect in terms of the cutting parameters requirements [12, 36, 37].

2.2.1. Titanium Alloys Machinability

Titanium alloys have potential industrial applications (e.g., automotive, aerospace) due to their superior mechanical, physical, and chemical properties such as high yield strength, high strength to weight ratio, high toughness, very high creep and corrosion resistivity, and high wear resistance [16]. Furthermore, titanium and its alloys have other potential properties such as maintaining their hardness and strength at very high temperatures [38]. Despite all these favorable characteristics, titanium is categorized as a difficult-to-cut material due to the high stresses and high cutting temperature generated during the cutting process. During machining titanium alloys, the generated heat is dissipated through the cutting tool and cooling media because of low thermal conductivity of the workpiece.

Conventional cooling methods except flood coolant (i.e. non-sustainable approach) are not effective when machining titanium and its alloys as the coolant cannot penetrate into the cutting zone and tool-chip interface. As a result, most of the cutting tool materials suffer from the thermal softening because titanium alloys maintain their strength even at high cutting temperatures. This reflects on several cutting difficulties associated to titanium alloys. Moreover, the resultant chip shape when machining titanium is serrated or saw-tooth which is formed due to the localized adiabatic shear that exists in the primary shear zone because of the high chip–tool interface temperature and dynamic shear strength of titanium alloys.

The titanium alloys have been classified as difficult-to-cut materials because of the following [12]:

- Low thermal conductivity and elastic modulus
- High thermal capacity, strain hardening, and chemical reactivity with cutting tool materials
- Tendency to adhesion to the cutting tool and form built-up edge
- High dynamic shear strength

2.2.2. Nickel-based Alloys Machinability

Nickel –based alloys have superior mechanical, thermal, and chemical properties such as hot strength and hardness, high-temperature resistance, high creep resistance, and maintaining chemical and mechanical properties at elevated temperatures. In spite of these properties, the machining of nickel-based alloys has a lot of difficulties because of its very low heat conductivity, high generated temperature, and forces which are produced during the cutting process. Furthermore, the poor quality of the machined surface and cutting tool life are the most important considerations during machining nickel-based alloys in order to govern its machinability. The chip–tool welding, work-hardened layer, and attrition wear are the main causes of generating notching at the depth of cut region.

Another important consideration which affects the tool wear rate during machining nickel-based alloys is the presence of different atmospheres. It can be shown that presence of oxygen can provide a reduction in the generated notching while severe effects can be noticed in presence of argon of nitrogen [39, 40].

In terms of wear behavior and tool life, mechanical and thermal fatigue, abrasion wear and diffusion usually take place when machining nickel-based alloys, and that could cause sever flank wear and chipping. Regarding the cooling techniques during machining nickel based alloys, the high-pressure coolant plays an important role in decreasing the cutting area overall temperature, improving the chip segmentation, and reducing the induced fatigue generated from the cutting tool and hot chip contact. In spite of the previous advantages, the high-pressure coolant increases the cutting edge stresses because of its significant reduction in the chip–tool contact length/area.

In addition, the major sufficient cutting tools for machining nickel based alloys are CBN tools, modern ceramic cutting tools (e.g. sialon, SiC whisker-reinforced alumina ceramics), and multi-layer coated carbide tools; however, CBN tools are commanly used in comparison with other mentioned cutting tools. Furthermore, a lot of studies have been focused on using coated cemented carbide cutting tool materials which are considered as a suitable recommendation for cutting nickel-based alloys [39].

2.2.3. Machining Considerations of Titanium and Nickel-based Alloys

In order to accomplish economical machining of titanium and nickel-based alloys, some practical considerations and guidelines have been suggested. Regarding material hardness, it is recommended that the machining process take places under solution treated condition (i.e., the softest state possible) until it is near to be dimensionally finished. After that, age hardening process is required before final finishing passes in order to eliminate the heat treatment distortion and achieve the desired surface roughness. In terms of cutting tool geometry, positive rake geometry has been recommended in order to minimize the work hardening of the induced surface because of shearing the chip away from the workpiece. Additionally, improving the surface finish and preventing the material build-up can be achieved by employing light hones or even sharp insert edges.

Furthermore, reinforcing the cutting edge, preventing localized damage, and decreasing the force at any one point have been obtained during using a large nose radius. Also, the modern CNC programming has the capability to achieve a continuous shifting of the tool–workpiece contact length/area (ramping), and therefore, the tool wear distribution over large cutting edge region can be noticed, and it could result in reducing the cutting tool notching. Some of the practical guidelines for machining titanium and nickel-based alloys are provided as shown in Table 2-1. Other recommendations to improve the machinability of titanium and nickel alloys have been given and discussed through the literature such as using high coolant supply, use of self-propelled rotary tooling (SPRT) technique, cryogenic machining, and employing nano-additives to improve the wet-ability characteristics of the base cutting oil [20, 41, 42].

Table 2-1 Practical guides and considerations for machining titanium and nickel-based alloys [20]

Machining titanium and nickel-based alloys
1. Machine alloys in the softest state possible
2. Use a positive rake insert
3. Use relatively sharp edges
4. Use a rigid set-up
5. Avoid part deflection
6. Use a high lead angle
7. Vary the depth of cut through applying different number of passes

2.3. Sustainable Machining Processes

The evolution of sustainable manufacturing is provided in Figure 2-2. It can be seen that sustainable manufacturing evolves through several generations, namely; traditional manufacturing, lean manufacturing, green manufacturing and in its most developed phase sustainable manufacturing [11].

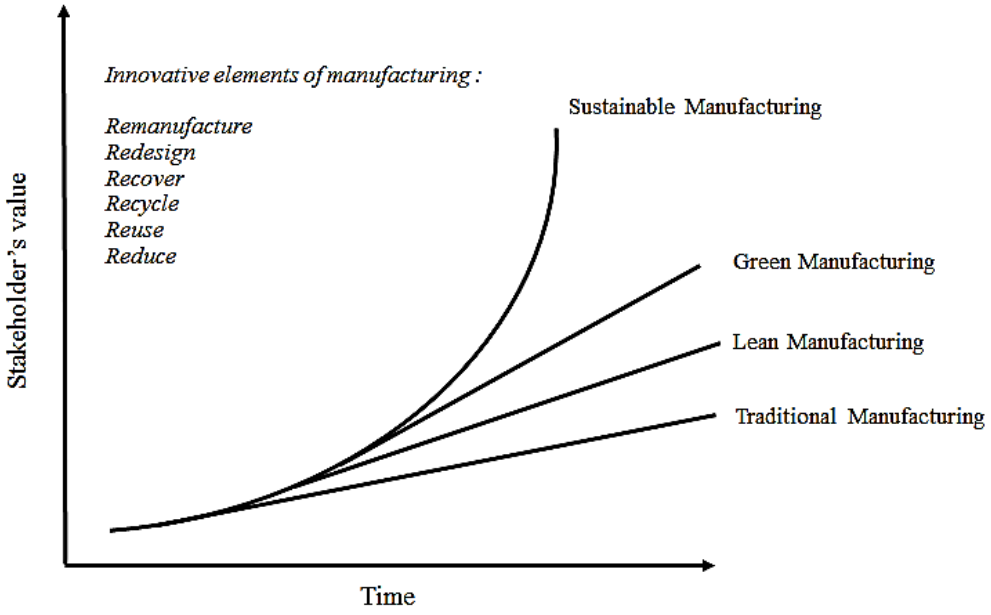

Figure 2-2 Sustainable manufacturing evolutions [11]

The 6R approach adds 3 new elements to modify the classic approach (3R); these elements are recover, redesign and remanufacture. The recover stage deals with collecting end-of-life products through post-use activities. On the other hand, the redesign element provides a sufficient environmental consideration by simplifying the future post-use processes, while the product performance can be improved through the remanufacture element since it works on saving natural resources, energy, and cost and reducing the generated wastes [1, 2].

One of the most important aspects of building and enhancing the sustainable manufacturing system is obtaining some basic keys for implementation. Through different studies [4, 43, 44], it is investigated that implementation of the sustainable model is addressed by three major phases as following:

- **Research:** in order to develop, evaluate and examine the specific sustainability requirements such as energy and resource use, pollution and climate change impacts. This phase of the model has a high potential as it helps to ensure the sustainability at the pre-competitive level and focuses on the manufacturing environmental issues.

- **Development:** using appropriate methods and tools to improve the environmental performance such as environmental footprint assessment, life cycle analysis, and design for environment.

- **Commercialization:** in order to refine the previous phases and co-operate with suppliers, vendors, and customers.

2.3.1. Environmental and Health Considerations of Machining Processes

Six major elements are usually used in order to obtain the main blocks of a machining system. These blocks are given as follows [45]:

- Material production

- Tool preparation

- Machine tool construction

- Material removal

- Cutting fluid preparation

- Cleaning

Identification of the major elements of a machining system is essential to address and provide a detailed assessment of energy investigation and materials flows. Several research works have studied the environmental impacts of the machining process. These studies presented several analytical models in order to utilize the application of cutting fluids by studying the chip formation effects, tool life behavior, and generated wastes [46]. A more quantitative analysis model for investigation the environmental impacts has been presented to obtain the effects of the amount of cutting fluids, the number of cutting tools, and the amount of chip produced on the electricity consumption of the machine tool [47]. Different studies have focused on providing an assessment of metalworking fluids utilization. It has been noticed that the direct contact between the metalworking fluids with chip and cutting tool makes it more prone to be contaminated, so filtration, disposal, or replacing are the main available solutions. Furthermore, the cost of disposal of cutting fluids is very expensive due to the environmental regulations, so more common techniques have been developed to recycle the used cutting fluids [45].

It has been approximated that 16% of the total manufacturing costs are associated with cutting fluids, while about 20% to 30% can be consumed in machining difficult-to-cut materials, while 2% to 4% of the total manufacturing costs are consumed in the tooling setup costs [48-50]. The previous results indicate that more attention must be paid in order to develop and optimize the cutting fluid systems. It can be concluded from several environmental and health concerns associated with production that the main source of environmental issues of machining processes is related to the application of cutting fluids. Also, it has been reported in the open literature that increasing the risk of various types of cancer such as prostate and colon can be observed, especially for those whom are exposed to cutting fluids in the automotive sector. The main reasons behind these risks are airborne particles of cutting fluid and the cutting fluid aerosols effects. Thus, more studies have focused on eliminating the cutting fluids usage (e.g. dry machining), and others are focused on optimizing the use of cutting fluids to achieve environmentally-friendly cutting fluids (e.g. minimum quantity lubrication) [48-51]. In the next section, modern environmentally conscious machining technologies are presented and discussed. In addition, several studies which employed these environmentally conscious technologies during cutting titanium alloys are obtained and discussed.

2.3.2. Modern Environmentally Conscious Machining Technologies

As previously mentioned, different economic, environmental, and health problems may occur due to the improper use of cutting fluids during cutting operations. Eliminating cutting fluids have already been considered in dry cutting techniques; however, the dry cutting technique has shown problems associated with excessive tool wear and poor surface quality [49]. Furthermore, cryogenic coolant is considered as another alternative for enhancing the machinability and dissipating the generated heat from the cutting zone as it affects the properties of the cutting tool and workpiece using a super cold medium with liquefied gasses with a temperature lower than $120^{o}K$ (e.g. Liquid nitrogen:LN_2) [12]. Different achievements and issues related to the environmentally conscious machining technologies performance are summarized in Table 2-2. Flood cooling is a typical cooling strategy used in industry to reduce the high temperature generated during machining nickel and titanium alloys. The use of flood coolant has raised environmental and health concerns which call for different alternatives. Thus, proposing new environmental cooling and lubricant systems is highly required specially to improve the cutting quality characteristics and achieve a sustainable machining system. Several environmentally conscious cooling and lubrication technologies during machining processes have been presented such as; dry cutting, minimum quantity lubrication (MQL), and cryogenic technology. Eliminating the cutting fluids usage can be performed using dry cutting techniques; however, dry cutting techniques are associated with some machining difficulties such as excessive tool wear and poor surface quality [49]. Another conscious technology has been investigated in order to improve the machinability known as MQL and the resulting mist is sprayed directly into the working zone using an optimal amount of cutting fluid with compressed air [52, 53] ;however, the excessive heat generation problem hasn't been completely solved. Also, several techniques have been discussed through the open literature to improve the machinability of difficult-to-cut materials [54]. For example, a previous work [55] used a typical rotary tool in tube-end machining to reduce the induced tool wear as only a short segment of cutting edge is engaged with the workpiece. Consequently, the proposed technique could significantly enhance the frictional behavior.

Proposing new nano-cutting fluids can contribute in facing the heat dissipation challenge during cutting processes as it offers a higher observed thermal conductivity value in comparison with the base lubricants. Additionally, it is shown that nano-cutting fluids have superior cooling properties due to their good heat extraction capabilities [56, 57]. A nano-fluid can be defined as a new fluid that results from the dispersion of metallic/nonmetallic nanoparticles or nanofibers with a certain size less than 100 nm into the base cutting fluid [58]. The nano-cutting fluids have shown promising results in improving the base cutting fluid properties; however, these improvements can't be clearly observed without applying an adequate dispersion technique. These improvements are mainly on the thermal, tribological, and rheological properties. Several studies [27, 59, 60] have focused on using nano-cutting fluids and their effects on the cutting performance characteristics, and promising results have been revealed particularly in reducing the tool wear and cutting forces. MWCNTs and Al_2O_3 nano-additives are among the nano-additives that have superior thermal, mechanical and tribological properties [61]; however, only a few studies have investigated their effects on different machining operations.

2.4. Summary

Providing environmentally friendly conditions and optimizing the energy consumption are two essential requirements in order to achieve sustainable machining processes. One of the major sustainable machining concerns is the implementation of cutting fluids due to its significant impact on the machining quality characteristics. In addition, several economic, environmental, and health problems are taken place due to the inappropriate application of cutting fluids; therefore, several studies have already been published in the open literature to introduce advanced cutting fluids techniques in order to optimize the cutting fluids performance during machining.

However, there is still a lot of rooms for improvement, especially in machining difficult-to-cut materials that have not been yet addressed and need to be improved. These materials have superior characteristics such as high strength to weight ratio, corrosion resistance, temperature resistance and chemical stability that make them a material of choice in aerospace, automotive, oil and gas, and biomedical industries.

Despite their desired features, the wide spread applications of these materials has been compromised by several difficulties that arise during their machining. One of the techniques to protect the cutting tool during machining difficult-to-cut materials is the application of nano-cutting fluids technology. The characterization of nano-fluid technology will be discussed in Chapter 3.

Table 2-2 Achievements and problems associated with MQL, cryogenic cutting, and dry cutting

MQL		Cryogenic cutting		Dry cutting	
Achievements	Problems	Achievements	Problems	Achievements	Problems
Providing low volume and low-pressure lubrication through a system consists of air compressor, gas based coolant lubricants (CLs) container, tunings, flow control system and spray nozzles [12, 52]. Using of cutting fluid (10–100 ml/h) mixed with compressed air results in lower friction coefficient with (CLs) evaporation. It can be obtained that no needs for disposal of the cutting fluid, maintenance, and any required cost [9, 62]. Ability to increase the tool life up to 8 times in drilling aluminum alloys [49]. 40% tool wear reduction in comparison with other traditional techniques through milling of A380 wrought aluminum has been observed [(0.06 ml/h) of biodegradable oil+ compressed air] [63]. Cutting forces reduction has been investigated during machining AISI 1045 in comparison with the dry cutting [12] MQL advantages have been presented such as; reduction of cutting fluids use, improve the tool life and performance of the process [51, 64]	There are not significant effects on the cutting zone temperature during machining AISI 1045 steel because of the coolant penetration position [12] MQL has limitations in machining of difficult-to-machine materials such as titanium and nickel-based alloys where excessive heat generation exists. The reason behind that the poor cooling capability of MQL system because it is considered as a lubricating method rather than cooling [65] General MQL disadvantages have been presented such as; usage of toxic cutting fluids, and new equipment installation [51]	Reduction of cutting zone temperature using a super cold medium with liquefied gasses (lower than 120^{o}K) through directed into the cutting zone [12] Usage of non-hazardous gasses (e.g., nitrogen, helium) provides an environmentally sustainable system [51, 66] As a result of lowering the temperature, an increase of strength and hardness for workpiece or tool has been investigated [12] Reductions of chip–tool interface temperature, chemical reactivity, and diffusion wear have been noticed through spraying cryogenic coolant at the cutting zone [67-69] 77% and 66% reduction in crater and flank wear have been observed through applyingLN_2 as a coolant in turning Ti–6Al–4Valloy [70] Cryogenic machining has presented some advantages such as; better surface quality and tool life [51]	Usage of liquid carbon dioxide could reduce the workplace safety as it could cause oxygen deficiency problems because of CO_2 accumulation [51, 66] Heavy investment and installation of new equipment are still required [51]	Eliminating cutting fluids usage completely has been presented under using dry cutting techniques, and it results in reduction of the machining costs and ecological hazards [49, 71] Lower thermal shock and tool life improvement can be accomplished through dry machining [12] Decreasing of coolants cost, leakage flow and achieving environmental sustainable systems can be observed through using dry cutting techniques [72]	Dry cutting has some problems which associated with excessive tool wear and poor surface quality [12]. During end milling of Titanium alloy, with uncoated carbide tools, brittle fracture of the cutting edge and localized flank wear have been observed in term of tool failure modes [22] During end milling of Inconel 718, high local temperature at the cutting zone has been observed and it results in formation of BUE on the flank face [73]. Also, more expenses are required for introducing better tool materials, coatings or tool geometries to compensate the effects of the cutting fluids elimination [12]. An Indirect cooling system of the cutting tool/ W.P using heat pipes may be required to enhance the heat conduction [74]

Chapter 3 Nano-Cutting Fluids Technology

3.1. Preamble

Increasing the heat dissipation area is an essential requirement during the cutting processes as it offers effective results in terms of tool life, energy consumption, and production rates. The conventional technique for increasing the heat dissipation for several industrial applications has focused on increasing the heat exchanging area; however, it associates with a problem of the thermal management system size [58]. Thus, proposing new environmental cooling and lubrication systems is highly required specially to improve the cutting quality characteristics. Several environmentally conscious cooling/lubrication technologies during machining processes have been presented in the open literature (e.g. dry cutting, minimum quantity lubrication (MQL), and cryogenic technology). Eliminating the cutting fluids usage can be performed using dry cutting techniques; however, dry cutting techniques are associated with some machining difficulties (i.e., the excessive tool wear and poor surface quality) [49]. Previous studies investigated another conscious technology in order to improve the machinability of difficult-to-cut materials, known as minimum quantity lubricant (MQL), and it could be penetrated into the cutting zone using an optimal amount of cutting fluid with compressed air [52].

Furthermore, the cryogenic technique is considered as another effective alternative for enhancing the machinability and dissipating the generated heat at the cutting zone as it affects the properties of the cutting tool as well as the workpiece using a super cold medium of liquefied gasses at a temperature lower than $120^{o}K$ (e.g. Liquid nitrogen, LN_2) [12].

Proposing new nano-cutting fluids to face the heat dissipation challenge during the cutting processes is encouraged since it offers a highly-observed thermal conductivity value in comparison with the base lubricants. Additionally, it has been proven that nano-cutting fluids are characterized with superior cooling properties due to its good heat extraction capabilities [56]. Nano-fluid can be defined as a new fluid result from the dispersion of metallic/nonmetallic nano-particles or nano-fibers with a certain size less than 100 nm into the base cutting fluid [58]. Nano-additives can be categorized into several types which are non-metallic, mixing metallic, carbon, and ceramic nano-particles [75]. Various advantages of using nano-fluids in different applications have been presented as following [76]:

- The heat transfer surface between particles and fluids is high due to the nano-fluids' high specific surface area;

- The dispersion stability is high;

- The power consumption in intensification of pure liquid can be reduced since it can offer the desired heat transfer properties;

- The surface wettability and heat transfer properties can be controlled by changing the nano-additives concentrations.

Examples of several applications that implemented nano-fluid technology in order to improve the applications' thermal, rheological, and stability properties are reported in various studies such as cooling of electronics, engine cooling, solar water heating, cooling of welding, engine transmission oil, nuclear systems cooling, and nano-fluids in different cutting operations [77-79].

This chapter is mainly focused on presenting a comprehensive literature survey of publications which are related to techniques of nano-cutting fluids preparation, characterization of nano-cutting fluids stability, nano-cutting fluids thermal and rheological properties, machining quality characteristics improvements due to employing of nano-cutting fluids, and current challenges associated with the nano-fluids implementation.

3.2. Techniques of Nano-Cutting Fluids Preparation

In order to achieve optimum thermal properties during the preparation of nano-cutting fluids, two main factors need to be considered, namely durability and stability. Achieving a lower sedimentation velocity of nano-additives is an essential requirement to ensure the nano-fluid's stability. The sedimentation velocity varies proportionally to the square of nano-additive radius according to the Stokes' law reported in equation (3.1), where v_s is the sedimentation velocity, R is the nano-additive radius, μ_m is the base fluid viscosity, ρ_p is the nano-additive density, and ρ_m is the base fluid density. However, using a lower particle radius leads to decreasing the sedimentation velocity, the surface energy of the nano-additives is increased, and that can result in an aggregation of nano-additives. Thus, selecting an optimal value of the nano-additive size and performing a homogeneous dispersion are highly required in order to avoid both higher sedimentation velocities and aggregation [58, 80, 81].

$$V = \frac{2R^2}{9\mu_m}(\rho_p - \rho_m)\, g \tag{3.1}$$

There are two main techniques for nano-fluids preparation, namely; single step and two-step techniques. While the two-step technique refers to manufacturing of nano-additives using physical vapor deposition with two separate steps, the single step technique depends on simultaneously making both of them.

In regards to the two-step technique, it is more suitable during dispersion of oxide particles and carbon nano-tubes and its results showed a great potential for metal-nano-particles. However, regardless that this technique requires two steps to disperse the nano-additives into the base fluid, it is more simple than the other technique, which it is associated with several problems, such as nano-additives agglomeration. Thus, some methods are used to overcome the aforementioned problem using ultrasound and/or high shear approaches. Also, it has been observed that the two-step technique can fit more volume concentration values higher than 20% [82, 83]. In terms of the single step technique, drying, storage, and transportation of the nano-additives are included, hence, a stable and durable Nano-fluid can be achieved as both the nano-additives agglomeration and sedimentation are avoided. However, the high observed efficiency of the single step technique, in terms of Nano-fluids' stability and durability, they can't fit the applications with high volume concentration values [84, 85].

Nano-additives dispersion into the base fluid is an important consideration that affects the thermal conductivity as well as the viscosity of the resultant nano-cutting fluid. Dispersion of nano-additives into the base cutting fluid can be performed using an ultrasonic machine followed by a stirring stage using a magnetic stirrer to ensure the full desperation of nano-additives. Furthermore, the processing time of each step depends on the weight fraction (wt. %) of the nano-additives [86, 87]. The Nano-additive weight concentration into the base cutting fluid can be determined using equation (3.2). Another two alternatives to the dispersion of Nano-additives powder into the base fluid have been obtained, namely; chemical precipitation or organic reduction [88].

$$\%\ \text{of weight cocentration} = \frac{\text{nanoadditive weight}}{\text{nanoadditive weight} + \text{the base fluid weight}} \tag{3.2}$$

3.3. Characterization of Nano-Cutting Fluids Stability

Nano-cutting fluids, resulted from the suspension of nano-additives into the base cutting fluid, can be expressed using four design parameters as following [11]:

- **Nano-additives:** metallic particles, non-metallic particles, and carbon tubes/graphene

- **Base fluid:** water-based oil, organic liquids, vegetable oil, and polymeric solutions

- **Other additives:** surfactants, anti-wear/corrosion additives, and fungicides

- **Scale:** percentage of weight/volume concentration

During the nano-fluid manufacturing process, these design parameters are selected based on the required thermal, tribo-chemical, physical, and rheological properties, which need to be met in the resultant nano-fluid since the functional requirements for each nano-fluid type are different. Dispersion of nano-additives into the base fluid is considered a difficult challenge due to the strong van der Waals interactions, which result in nano-additives agglomeration, clogging, and sedimentation. Consequently, using physical or chemical treatments, such as surfactants, is recommend in order to achieve powerful forces on the clustered nano-additives that ensure a sufficient dispersion and obtain some enhancements in thermal conductivity and viscosity [89-91]. Two principles have been studied in order to establish a high suspension quality for nano-additives into the base oil, namely; diffusion and zeta potential. The former ensures the Nano-additives are well scattered and dispersed into the liquid medium. The latter is mainly focused on achieving a higher zeta potential value, which produces a repulsive force among the Nano-additives [92]. Depending on previous studies [93-99] three main methods have been implemented to control and offer a high suspension/stability performance in order to avoid the nano-additives agglomeration, clogging, and sedimentation, namely:

- **Surfactant:** the purpose of using surfactant is modifying the nano-additives to be more hydrophilic, and increasing the nano-additives surface charges, hence the repulsive forces between the nano-additives are increased [100, 101]. Consequently, improving the suspension of Nano-additives into the base fluid. On the other hand, selecting the optimal amount of surfactant is an important factor that affects the resultant electrostatic repulsion. Another limitation is the difficulty in dealing with applications associated with temperature values above 60^{o} Celsius as the repulsive forces can be damaged [97]. Various examples of surfactant have been used, e.g. Sodium dodecyl Sulfate, dodecyl trimethylammonium bromide, and polyvinylpyrrolidone [58];

- **pH control:** the nano-fluid pH can control the stability and also improve the thermal conductivity as it is related to its electro-kinetic properties. Using simple chemical treatment techniques cause a conversion for the nano-additives shape, which results in higher surface discharge density, electric repulsion force, and zeta potential value. Thus, agglomeration, clogging, and sedimentation effects can be decreased and high suspension quality of the resultant nano-fluid can be accomplished [101-103]. It has been investigated during the dispersion of Al_2O_3 nano-particles into water as a base fluid that the agglomeration size has been decreased at a pH level of 1.7. However, an increase of the agglomeration size has been noticed at a pH level of 7.66 [104]. Furthermore, another study provided the effects of pH on the electrostatic repulsion and van der Waals attraction energies (total energy) at different inter-particle distances using metal oxide nano-particles. Subsequently, it can be observed that the total energy is inversely proportional to pH values at lower levels of inter-particle distances; however, no significant effects of pH were observed at higher levels of inter-particle distance, as shown in Figure 3-1 [103];

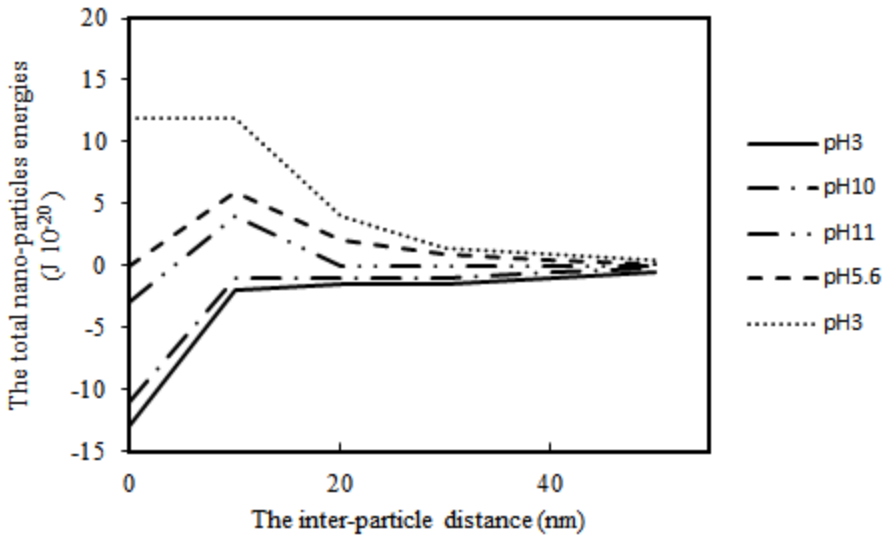

Figure 3-1 The inter-particle distance versus the total nano-particles energies [90]

- **Ultrasonic vibrations:** a technique that aims to break down the agglomerations among nano-additives and it revealed promising results in term of the process stability. Nevertheless, optimizing the processing time is required as it can lead to fast clogging and sedimentation of nano-additives [105]. The ultrasonic disruptor is the most popular apparatus used method to disperse the nano-additives into the base fluid. The applied mechanisms includes three stages, namely; strong and irregular shock on the system wall, micro-bubbles formation, and high flow shear rate, that guarantee process stability and decreasing the clogging and agglomeration size [106].

Many researchers presented several employed instrumentation techniques in order to assess the nano-fluid suspension performance such as sediment photograph capturing [107], UV–Vis spectrophotometer [104], transmission electron microscopy, scanning electron microscopy, and light scattering [108]; however, the zeta potential analysis and analyzing the gathered data are the popular techniques used to check the process stability. Table 3-1 shows the suspension stability at different zeta potential levels [109].

Table 3-1 The suspension stability at different zeta potential levels

Z potential absolute value	Stability Status
0	Little or no stability
15	Some stability but settling lightly
30	Moderate stability
45	Good stability, possible settling
60	Very good stability, little settling likely

3.4. The Thermal and Rheological Nano-Cutting Fluid Properties

The Nano-cutting fluids have shown promising results in improving the base cutting fluid properties that cannot be clearly observed without applying an adequate dispersion technique as previously mentioned. Such improvements are mainly focused on the thermal, tribological, and rheological properties. The thermal conductivity is one of the most important indications to express the system heat transfer. Regarding the improvements of the thermal properties, a previous review study [88] has focused on the thermal conductivity enhancements for different nano-particles types, sizes, and volume fraction percentages using water as base fluid, whose summary is provided in Table 3-2. The summary shows various analytical models to express the nano-fluid thermal conductivity.

The Maxwell equation [110] shown in equation (3.3) can be used to predict the resultant thermal conductivity is (K_e) as a function of the base fluid's thermal conductivity (K_m), the nano-additive thermal conductivity (K_p), and the nano-additive volume fraction (U_p).

$$K_e = K_m + 3\,U_p \frac{K_p - K_m}{2\,K_m + K_p - U_p(K_p - K_m)} K_m \tag{3.3}$$

Another modified model, equation (3.4) [111] has been obtained to calculate the nano-fluid thermal conductivity, where ρ_p, C_p, T, η, and R stand for the nano-additive density, specific heat, temperature, viscosity, and radius, respectively.

$$\frac{K_e}{K_m} = \frac{K_p+2K_m-2U_p\,(K_m-K_p)}{K_p+2K_m+2U_p\,(K_m-K_p)} + \frac{\rho_p U_p Cp}{2\,K_m}\sqrt{\frac{K_p\,T}{3\pi R\eta}} \tag{3.4}$$

On the other hand, the transient hot-wire method, called transient line heat source method [112, 113], has been alternatively used in various studies to predict the thermal conductivity. In addition, through investigating the effective heat transfer ratio (nano-fluid heat transfer coefficient/base fluid heat transfer coefficient) for different nano-additives types, sizes, and volume fractions [114], the nano-fluids have shown highly favorable results to enhance the heat transfer coefficient. Furthermore, two analytical models have been developed to predict another heat indicator, known as the specific heat. The first model [115], equation (3.5), is based on the nano-additive volume fraction while the other model [116] depends on the heat capacity concept. Where C_{bf} is the base fluid's specific heat and C is the nano-fluid specific heat

$$C = C_{bf}(1 - U_p) + U_p C_p \tag{3.5}$$

Another effective property, in terms of nano-fluids dynamics, is the viscosity as it is an important consideration for the heat transfer applications. Furthermore, the nano-fluids rheological behavior can be obtained through investigating its effects [58]. Several analytical models have been implemented to calculate the effective nano-fluid viscosity ratio (i.e., nano-fluid viscosity/base fluid viscosity) as shown in Table 3-3.

These models vary depending on the nano-additive volume fraction and the dynamics of their interactions [96, 117]. The nano-fluid rheological behavior has been classified into four main sections [118]:

- Nano-fluids of volume fraction values less than 0.1%, and its viscosity associated with the Einstein model (without shear thinning);

- Nano-fluids of volume fraction values between 0.1 and 5% (no obvious shear thinning);

- Nano-fluids of volume fraction values between 5 and 10 % (observed shear thinning);

- Nano-fluids of volume fraction values greater than 10 % (Nano-additives interpenetration);

Table 3-2 The nano-fluid viscosity analytical models

Model	The effective nano-fluid viscosity ratio	Application
Einstein	$1+ \eta \, \upsilon p$	At no nano-additives interactions & υ_p is less than 1%
Batchelor	$1+ \eta \, \upsilon_p+(\eta \, \upsilon_p)^2$	Brownian motion & interactions of nano-additives
Ward	$1+ \eta \, \upsilon_p+(\eta \, \upsilon_p)^2+(\eta \, \upsilon_p)^3$	υ_p is greater than 35%

Table 3-3 Literature summary of the thermal conductivity enhancements for various nano-fluids (water-based)

Reference	Nano-additive type	Nano-additives Diameter (nm)	Volume fraction %	The percentage of thermal conductivity improvement %
[119]	Cu	100	7.5	78
[120]	CuO	36	5	60
[121]	MWCNT	100	0.6	38
[103]	CuO	23	9.7	34
[119]	TiO_2	10	5	33
[122]	Al_2O_3	13	4.3	30
[122]	Al_2O_3	13	4.3	30
[119]	TiO_2	15	5	30
[121]	MWCNT	130	0.6	28
[123]	Cu	100	0.1	24
[124]	Cu	100	2.5	22
[125]	Al_2O_3	36	10	22
[126]	Au	10	0.026	21
[127]	Al_2O_3	68	5	21
[127]	Al_2O_3	60.4	5	20
[103]	CuO	23	4.5	17
[126]	Ag	60	0.001	17
[127]	Sic	26	4.2	16
[103]	Al_2O_3	33	4.3	15
[125]	Al_2O_3	36	2	15
[128]	CuO	28.6	4	14
[103]	CuO	36	3.4	12
[103]	CuO	23.6	3.5	12
[89, 100]	Al_2O_3	28	3	12
[129]	Ag	15	0.39	11
[122]	TiO_2	27	4.3	10.8
[103]	Al_2O_3	38.4	4	10
[130, 131]	Al_2O_3	42	1.59	10
[128]	Al_2O_3	38.4	4	9
[132]	Al_2O_3	11	1	9
[122]	TiO_2	27	3.25	8.4
[132]	Al_2O_3	47	4	8
[119]	TiO_2	10	0.5	8
[127]	Al_2O_3	60.4	1.8	7
[127]	MWCNT	15	1	7

3.5. Improvements of Machining Quality Characteristics

Several research works have focused on using various nano-cutting fluids and their effects on the cutting performance characteristics within different cutting operations (e.g., turning, milling and grinding). A recent literature review study has presented a summary of the findings obtaining for different nano-additive types and its size, base oil, and cutting operation, as reported in Table 3-4. Another summary for the used lubrication/cooling system, workpiece materials, and selected machining parameters for the same studies provided in the previous table has been presented in Table 3-5 [27]. Recently, other researchers have focused on adding multi-walled Carbon Nano-tubes (MWCNTs) into the base fluid, where high improvements up to 150% and 200% in the thermal conductivity have been reported in comparison with based fluid thermal conductivity [133]. In terms of the friction between the cutting tool and workpiece, it has been reported that the addition of graphite nano-particles into the conventional lubricant helps in reducing the induced friction coefficient. Thus, better workpiece dimensional accuracy, good surface quality, and reduction of cutting forces could be achieved [134].

Additional study has confirmed that increasing the nano-particle concentration and decreasing the nano-particles size into the base cutting fluid have critical roles in improving the thermal conduction during the cutting processes [135]. Some studies have presented promising results in terms of improving the machining quality characteristics when using carbon nano-tubes as nano-additives into the conventional cutting fluids. MQL system with nano-cutting fluid based on MWCNTs has been applied when turning high Carbon-high Chromium AISI D2 using tungsten carbide insert (CNMG 120408). Taguchi method has been implemented to study the effects of cutting parameters on the surface finish and cutting zone temperature. In comparison with the MQL technique based on conventional cutting fluid, promising results have been observed by the proposed technique (MQL-Nano-fluid) [86].

Table 3-4 Literature summary for investigation of nano-cutting fluid effects on different machining operations (part I)

Reference	Nano-additive type	Size (nm)	Conventional fluid	Machining operation	Findings
[136]	xGnP	10	Vegetable oil	Milling	The lowest friction coefficient is obtained at 0.1 wt. % xGnP (1mm dia. and 10 nm thickness)
[137]	SiO_2	5-15	ECOCUT SSN 322 mineral oil	Milling	The proposed technique can reduce the cutting power, and forces
[138]	Carbon onions	5-20	Aluminum oil	Milling	Highest carbon onion concentration (1.5 wt. %) have provided minimum cutting force and surface roughness
[139]	MoS_2	20-60	ECOCUT HSG 905S oil	Milling	0.5 wt. % MoS_2 has shown best surface and surface quality deteriorated because MoS_2 concentration increased to 1 wt. %
[140]	SiO_2	5-15	ECOCUT SSN 322 oil	Milling	0.2% SiO_2 produced thin protective film and increase of SiO_2conc. has provided a reduction in surface roughness
[141]	SiO_2	5-15	ECOCUT SSN 322 oil	Milling	0.2 wt. % SiO_2, high air pressure, and 60° nozzle angle showed minimum cutting force. 1 wt. % SiO_2, 2 bar air pressure, and 30° nozzle angle have given best surface quality
[142]	MoS_2	20-60	ECOCUT HSG 905S oil	Milling	1 wt. % MoS_2, 4 bar air pressure and 30° nozzle angle showed minimum cutting force. 0.5 wt. % MoS_2, 4 bar air pressure, and 60° nozzle angle showed the best surface quality
[143]	MoS_2	<100	Paraffin oil, CANMIST oil and Soybean oil	Grinding	High MoS_2 concentration showed high G-ratio with MQL and low G-ratio with flood lubrication
[144]	Al_2O_3	40,100,200	Deionized water	Grinding	4 wt. % Al_2O_3 showed best G-ratio while best surface quality was given under flood cooling
[145]	XGnP™	5-10	IPA, TRIM SC200	Grinding	Large size platelets were obtained to be more effective than small ones. 1 wt. % graphite platelets generated best surface finish quality

[146]	ND	30,150	Paraffin oil	Grinding	30 nm size showed smoother surface than 150 nm particles. Size did not affect grinding force while nano-particle conc. did not have an effect on surface quality, 4% ND with 30 nm generated the best surface quality
[147]	MWCNT	10-20	SAE-20W40 oil	Grinding	Improvement in surface roughness from micro-level to nano-level is obtained.
[148]	Al_2O_3	30,150	Paraffin oil	Grinding	Al_2O_3 are more promising than diamond nanoparticles due to their lower hardness. 2% Al_2O_3 (30 nm) showed lowest surface roughness quality
[149]	Al_2O_3	40	Water	Grinding	4 vol. % Al_2O_3 have obtained minimum generated grinding forces
[150]	MoS_2	<100	Paraffin oil & Soybean oil	Grinding	MoS_2 has shown better for steel with soybean oil. Regarding cast iron, it showed better results with paraffin oil. Lower energy consumption, friction coefficient, and increasing the G-ratio are obtained
[151]	MoS_2	40-70	Paraffin oil	Grinding	8% nano MoS_2 showed lower peak temperature. It has observed that lowest has been showed with flood cooling. MoS_2 gives lower force-ratio, wheel wear, and specific energy
[152]	CNT	10-20	SAE-20W40 oil	Grinding	Increasing in both of the flash and fire points of the fluid. Higher surface quality has been observed
[153]	Al_2O_3	40	Deionized water	Grinding	Reduction in grinding temperature, and forces and higher surface quality
[154]	Al_2O_3	60	Deionized water	Grinding	Surface roughness, grinding forces, and temperature were reduced using angularly spraying of nano-fluid toward grinding wheel
[155]	ND	30	Paraffin oil and vegetable oil	Drilling	Paraffin with 1% ND and vegetable oil (2% ND) showed the lower torque and thrust force. Nano-fluid improved the tool life
[156]	Nano-boric acid	50	SAE-40 oil and coconut oil	Turning	0.5% nano-boric acid in coconut oil performed better in terms of cutting temperature, tool wear, and surface roughness.
[157]	CNT	-	-	Turning	Nodal temp was decreased using Up to 2% CNT inclusion, but higher than 2%, the change was minimal. High CNT % gives lower flank wear

Table 3-5 Literature summary for investigation of nano-cutting fluid effects on different machining operations (part II)

Reference	Cutting speed/wheel speed (grinding)	Feed rate/ workpiece speed	Depth of cut (mm)	Workpiece materials	Lubrication/cooling system
[136]	3500, 4500 rpm	2500	1	AISI 1045 Steel	MQL
[137]	5000 mm/min	100	5	Aluminum AA6061-T6	MQL
[138]	75.408 m/min	100	1	Duralumin AL-2017-T4	-
[139]	5000 mm/min	100	5	Aluminum AL6061-T6	MQL
[140]	5000 mm/min	100	5	Aluminum AL6061-T6	MQL
[141]	5000 mm/min	100	5	Aluminum AL6061-T6	MQL
[142]	8000 mm/min	2100	5	Aluminum AL6061-T6	MQL
[143]	30 m/s	2400	10	Dura-Bar 100-70-02	MQL
[144]	30 m/s	2400	10	Dura-Bar 100-70-02	MQL
[145]	25 m/s	750	50	D-2 tool steel (62 HRC)	MQL

[146]	80000 rpm	120	5	SK-41C tool steel	MQL
[147]	80000 rpm	120	5	AISI D2 Tool steel	MQL
[148]	80000 rpm	120	5	SK-41C tool steel	MQL
[149]	10.89 m/s 16.34 m/s 21.79 m/s	3000 9000 1500	10 20 30	Ti-6AL-4 V	MQL
[150]	30 m/s	0.06 m/s	10,20	Cast Iron 100-70-03 durabar EN24 alloy steel	MQL
[151]	30 m/s	0.06 m/s	10,20	Cast Iron 100-70-03 durabar EN24 alloy steel	MQL
[152]	2000 rpm	1.9 mm/rev	0.2	AISI D3 tool steel (256 VHC)	-
[153]	31.4 m/s	0.05 m/s	10	AISI 52100 Steel	MQL
[154]	31.4 m/s	0.05 m/s	10	AISI 52100 Steel	MQL
[155]	60000 rpm	50	0.4	Aluminum 6061	MQL
[156]	100 m/min 80 m/min 60 m/min	0.2 mm/rev 0.16 mm/rev 0.14 mm/rev	1	AISI 1040 Steel	Supply under atmospheric pressure and flow rate of 10 mL/min
[157]	102 m/min	0.44 mm/rev	0.5	-	MQL

Another study has investigated the effects of MWCNT/MQL system during the high-speed milling of AISI 1050 and AISI P21. The results have been compared to dry and wet cutting. It has been observed that the MWCNTs/nano-fluid has a significant role in reducing the tool wear as well as improving the surface finish because of the excellent heat conductivity of MWCNTs nano-fluids [158]. In addition, the high-speed turning of AISI 4140 steel with a TiN-top coated multilayered carbide insert has been conducted using small quantity lubrication (SQL) technology. The use of 3vol. % alumina and 1vo. l% MWCNT nano-fluid instead of soluble oil has shown a substantial reduction of the cutting forces and tensile residual stresses. Furthermore, enhancement of surface quality has been observed due to the improvement in retention of cutting tool edges sharpness [159].

Another work has concerned with controlling the friction behavior in the grinding processes as the contact between the abrasive grains and workpiece is highly affecting the machining quality characteristics such as; the wheel wear and grinding forces. Different volume concentrations of Al_2O_3 and CuO nano-particles have been added to water as a base fluid. The grinding process has been performed on Ti-6Al-4V using MQL system. The wheel morphology, surface integrity of ground surface, grinding forces, friction coefficient, and chip formation have been investigated. The nano-cutting fluid and MQL have noticeably reduced the coefficient of friction and tangential forces. Moreover, the short C-type chip formation has been observed, hence it could imply a cooling effect of the proposed lubrication system [160].

Another work studied the effects of the dispersed MoS_2 nano-particles into vegetable oil (i.e. soybean oil) on several machining quality characteristics during grinding of 45 steel. Various lubrication strategies have been employed (i.e., flood, MQL, and dry cutting). It has been observed that the lubrication property can be improved due to the high nano-cutting fluid viscosity, and the heat transfer performance can be consequently enhanced. On the other hand, the optimal mass concentration for MoS_2 nano-particles into the base cutting fluid was 6 wt.% since it is an important factor to be selected in order to avoid the agglomeration of nano-particles [161].

Achieving a sustainable machining process is an essential requirement as it offers various environmental, societal, and economical advantages, however enhancing the machining processes performance is still required besides building a sustainable environment. A previous study obtained that using nano-additives with vegetable oil as a base cutting fluid with MQL could fulfill the two desired objectives; enhancing the machining quality characteristics since the nano-additives improve the friction and thermal behavior, and accomplishing a sustainable process as using vegetable oils provides effective environmental benefits [162]. Also, a previous study investigated different wear mechanisms during end-milling of Aluminum alloy AA6061 under using MQL system and water-based TiO_2 nano-cutting fluid. The findings have been compared with other lubrication techniques (i.e., MQL with conventional cutting fluid, and flood cooling technique). The nano-cutting fluid-based method has presented promising results in terms of reducing the edge chipping and fracture due to its cooling effects, which lead to decrease the cutting zone temperature [163].

Another work applied Taguchi methodology, neural networks, and fuzzy logic techniques to analyze the effects of using CNT-nano-fluids to enhance the induced surface roughness during turning AISI D3 Tool steel. The ANOVA results have revealed that the most significant parameters are the cutting speed and mass concentration. Also, the artificial neural network and fuzzy logic techniques have presented two models to investigate the relationship between the machining parameters and the measured surface roughness, where 10.31% and 9.23% model accuracies have been achieved, respectively [164]. Also, it has been found from the literature that there is a research gap in investigating the nano-fluids effects when machining nickel-based alloys. A summary of these studies and their findings are provided in Table 3-6. In addition, reviewing the open literature has shown that there is no–previous attempt in using MQL-MWCNTs-nano-fluid in enhancing the machinability of Inconel 718.

Table 3-6 Summary for investigation of nano-fluids effects on machining nickel-based alloys

Reference	Nano-additives type	Machining operation	Nickel alloy type	Findings
[165]	Al_2O_3 under using MQL	Turning	Inconel 600	The measured cutting force, and temperature have been reduced using 6 vol. % Al_2O_3
[166]	Zinc oxide (ZnO) under using MQL	Grinding	Inconel 718	Low cutting forces, friction coefficient, and surface roughness have been observed
[167]	Hybrid nano-fluid (MoS_2-CNTs)	Grinding	GH4169	8% MoS_2-CNTs improved the surface quality, and the frictional behavior.
[168]	graphene nano-platelets under using MQL	Grinding	Inconel 718	The results show that graphene nano-platelets lower the grinding force, temperature, and surface roughness

3.6. Nano-Fluids Challenges

In spite of all previous superior properties of nano-fluids, there are still several challenges, which face the development and implementation of nano-fluid technologies. The main challenges facing such growing technology are [78];

- There is no a sufficient agreement between the results obtained in various studies
- Poor suspension / stability characterization
- More understanding needs to be investigated in terms of properties changes mechanisms

On the other hand, the challenges that face the growth of Nano-cutting fluids applications are summarizes as follows:

- **Long-term stability for nano-fluid dispersion:** it is one of the most important requirements needed as the nano-particles are easily aggregated due to the very strong van der Waals interactions. A lot of proposed solutions have been applied and presented (e.g. using surfactant); however, the time period after preparing the nano-fluid is a critical factor as the nano-particles agglomeration can occur [120];

- **The nano-fluids/Nano-additives production** (e.g. sedimentation, clustering, agglomeration): an effective recommendation to tackle such a challenge is to establish a multi-disciplinary approach that can link the thermal, mechanical, chemical, and materials science aspects [169];

- **The high cost of nano-fluids** [170];

- **The nano-fluids thermal behavior for turbulent flow cases:** more researches are required to investigate the convective heat transfer and thermal conductivity in cases of turbulent flows. However, few studies have obtained good results by using Nano-fluids in turbulent flow cases [171, 172]. Also, producing analytical models to express the flow mechanisms effects are highly required.

3.7. Summary

In this chapter, a comprehensive literature survey of publications related to the nano-cutting fluid technology has been presented and discussed. It has been reported that the two commonly used techniques in nano-fluids preparation are the two-step and single step techniques. The former is more suitable during dispersion of oxide particles and carbon nano-tubes and it does not show potential results for metal-nano-particles; however, higher efficiency in term of nano-fluid stability can be noticed during using the single step technique. In spite of the advantage of using the single step, it can’t fit the applications with high volume concentration values. Besides, three main methods, using a surfactant, pH control, or ultrasonic vibrations, have been used to control and offer a high

suspension/stability performance in order to avoid the nano-additives agglomeration, clogging, and sedimentation. The nano-cutting fluids have shown promising results in improving the base cutting fluid properties; however, these improvements can't be clearly observed without applying an adequate dispersion technique. Such improvements are mainly focused on the thermal, tribological, and rheological properties where several studies have established different empirical and analytical models to express the relationship between the process parameters and the improved properties.

In addition, the nano-cutting fluids have revealed promising results in terms of machining quality characteristics improvements such as reducing the generated cutting forces, improving the friction behavior and tool wear, and decreasing the induced cutting temperature. Despite the previous improvements, a number of challenges still face its implementation; for example, the long-term stability for nano-fluid dispersion, difficulties associated with the turbulent flow cases, the high cost of nano-fluids, and challenges associated with the nano-fluids/nano-additives production process.

Finally, some significant points have been concluded after reviewing the achievements of researchers in the relevant topics through chapters 2 and 3 as following:

- More investigations are still required in order to improve the machinability of titanium and nickel alloys;
- Research, development, and commercialization are the basic keys to implementing a sustainable machining process;
- Dry cutting, MQL, and cryogenic machining are considered as environmentally conscious machining technologies; however, more developments are still required to overcome their associated problems;
- Flood cooling is a typical cooling strategy used in industry to dissipate the high temperature generated during machining Inconel 718. The use of flood coolant has raised environmental and health concerns which call for different alternatives. Minimum Quaintly Lubricant (MQL) has been successfully introduced as an acceptable coolant strategy; however, its potential to dissipate heat is much lower than the one achieved using flood coolant;

- MQL-nano-cutting fluid is one of the suggested techniques to further improve the performance of MQL particularly when machining difficult-to-cut materials. MQL-nano-fluid technique offers two main advantages; (a) enhancing the machining process performance as the employed nano-additives improve the thermal and friction behavior, and (b) accomplishing a sustainable process as using vegetable oils based on MQL provide effective environmental benefits;
- Multi-walled carbon nanotubes (MWCNTs) have obtained promising results as nano-additive into the conventional cutting fluid; however, only a few studies studied its effects on different machining operations especially in cutting Ti-6Al-4V and Inconel 718;
- It is obtained from the literature review that there is a research gap in investigation the nano-fluids technology effects when machining titanium and nickel-based alloys;
- Developing a general assessment methodology in order to express and evaluate the sustainable machining metrics and machining quality characteristics is an essential requirement;

Chapter 4 Experimental Setup and Design

4.1. Experimentation

It is an important requirement to develop and investigate new proposed techniques to face the machinability problems (e.g., short tool life and poor surface integrity) associated with cutting titanium and nickel-based alloys as these alloys have promising applications in aerospace, automotive, oil and gas, and biomedical industries. The nano-cutting fluids have shown promising results in terms of machining quality characteristics improvements (e.g., cutting forces, friction behavior, tool wear, and cutting zone temperature) through different previous studies; however, it is investigated that there is a research gap in the investigation of the nano-fluids technology effects when machining titanium and nickel-based alloys. In order to investigate the influence of dispersed MWCNTs and Al_2O_3 nanoparticles into the conventional cutting fluid on the cutting quality performance, different cutting experiments are carried out by bar turning of two round bars of Ti-6Al-4V and Inconel 718. In this chapter, the experimental setup and design's frame during machining Inconel 718 and Ti-6Al-4V using MQL-nano-cutting fluids have been presented in detail.

Inconel 718 (ASTM SB 637) and Ti-6Al-4V (UNS R56400) are utilized as the experiments workpieces. Chemical composition and some other properties for both Inconel 718 (ASTM SB 637) and of Ti-6Al-4V (UNS R56400) are provided in Tables 4-1 and 4-2, respectively. The tests were performed on a CNC lathe machine (Hass ST-10 CNC) using standard carbide turning inserts and tool holders as shown in Table 4-3. Cutting tests are performed under using MQL strategy, at different levels of cutting speed, feed rate, and weight percentages of added nano- additives (i.e., MWCNTs or Al_2O_3 nanoparticles). The depth of cut for each cutting pass is 0.2 mm. The sensitivity analysis of cutting performance results are employed to select the cutting conditions values for cutting speed and feed rate levels.

Table 4-1 Inconel 718 (ASTM SB 637) properties

Inconel 718 (ASTM SB 637)
Chemical composition-wt.%:Ni:50-55%, Fe: Bal, Cr:17-21%, Mo:2.8-3.3%, Ti:0.65-1.15%, Al:0.2-0.8%, Co:0.17-1%, Si:0.12-0.35%, Mn:0.07-0.35%, Cu:0.07-0.3%, C:0.03-0.08%, P:0.01-0.15%,Nb:4.75-5.5%,S:0.015%]
Density: 8193.25 Kg/m^3
Young's modulus(at 23^{o}C): 198.57 GPa
Poisson's ratio (at 23^o C): 0.3
Tensile strength: 930 MPa
Yield strength @ 0.2% offset: 482 MPa
Elongation: 45% Hardness: 43 Rc
Specific Heat (at 23°C): 435 J/kg °C
Thermal Conductivity (at 23^{o}C): 11.2 W/m °C
Melting Point: 1350 °C

Table 4-2 Ti-6Al-4V (UNS R56400) properties

Ti-6Al-4V (UNS R56400)
Chemical composition-wt.%: Ti: 90%, Al:5.5-6.75%, V:3.5-4.5%, C:0.1%, Fe:0.3%, O:0.2%, N:0.05%, H:0.0125%
Density: 4470 Kg/m^3
Young's modulus(at 23°C): 114 GPa
Poisson's ratio (at 23°C): 0.3
Tensile strength: 895 MPa
Yield strength @ 0.2% offset: 828 MPa
Elongation: 10%
Hardness:30-34 (Rc)
Specific Heat (at 23°C): 560 J/kg °C
Thermal Conductivity (at 23°C): 7.2 W/m °C
Melting Point: 1649 °C

Table 4-3 The used cutting inserts and tool holders

	Ti-6Al-4V cutting processes	Inconel 718 cutting processes
Cutting insert	Coated carbide insert (CNMG 120416MR (ISO))	CNMG 432MMH13A (ANSI) – from Sandvic-Inc.
Tool holder	SANDVICK SCLCR-2525M12 with clearance angle 5° and rake angle 0°, nose radius of 1.588 mm (Honed edge)	KENNAMETAL MCLNL-164DNC5 with clearance angle 0° and rake angle -5°, nose radius of 0.793 mm (Honed edge)

Regarding the MQL system, the air-oil mixture was supplied by stand-alone booster system (Eco-Lubric) which was installed on the machine tool with a nominal oil flow rate of 40 ml/hr and air pressure of 0.5 MPa, similarly as used in a previous research work [173]. In addition, ECOLUBRIC E200 was employed as a vegetable oil used for experimentation which is a cold-pressed rapeseed oil type without additives. This base cutting fluid, ECOLUBRIC E200, is comprised of vegetable oil devoid of additives, allowing this cold-pressed rapeseed oil to not only assist in carrying out favorable outcomes when used in these specific tests, but also provides less abrasive effects on the environment. The position and the angle of the MQL nozzle were adjusted by experimental observation to avoid being blocked by chips. The air-oil mixture ratio is 1.25:1.

The cutting performance is studied in terms of average surface roughness (Ra), flank tool wear (VB), energy consumption, chip morphology examination and wear mechanisms investigations. Through the use of a toolmaker's microscope, flank wear was measured subsequent to each cutting pass. This type of wear takes place due to the friction between the flank tool and the machined surface. The width of generated wear land in the flank tool is used to measure its value. Also, it should be stated that the increase in the flank wear leads to a significant increase in the cutting forces. During the experimentation phase, A maximum flank wear of 0.4 mm [174] is used as the tool life criteria otherwise, in case of not reaching the end of tool life criteria, the cutting stopped after nine cutting passes.

The average surface roughness parameter is used to evaluate the machined surface quality using a surface roughness tester (Mitutoyo SJ.201). Ra is the arithmetic average height of surface component (profile) irregularities from the mean line within the measuring length used to describe the vertical dimension of roughness [175]. Ra is commonly recognized, and the most used parameter to evaluate the machined surface roughness. The used cut-off length is 0.8 mm. After each cutting test, the surface roughness tester is used in five random regions along the machined surface, and the average value is considered. The cutting tests are replicated three times and average response value is calculated. In addition, a Power Sight Manager was employed throughout the machining process in effort to assist with logging power consumption for each machining run.

The collected chips were analyzed and the chip thickness and shape, were recorded after each test. Thus, the effects of dispersed MWCNTs/ Al_2O_3 nano-additives on the chip-tool interface temperature can be investigated. The deformed chip thickness has been measured by analysis of micrographs captured using a digital optical microscope (KEYENCE VHX-1000) and ImageJ software under different feed rate levels. Also, the change in modes of tool was also recorded. Therefore, the nano-additives effects on the tool wear behavior can be easily obtained and the associated wear mechanisms can be demonstrated. A digital optical microscope (KEYENCE VHX-1000) has been used to investigate the wear modes occurred at different cutting conditions. Schematic diagram of the experimental setup is provided as shown in Figure 4-1. Also, the experimental setup view when machining Inconel 718 is provided as shown in Figure 4-2.

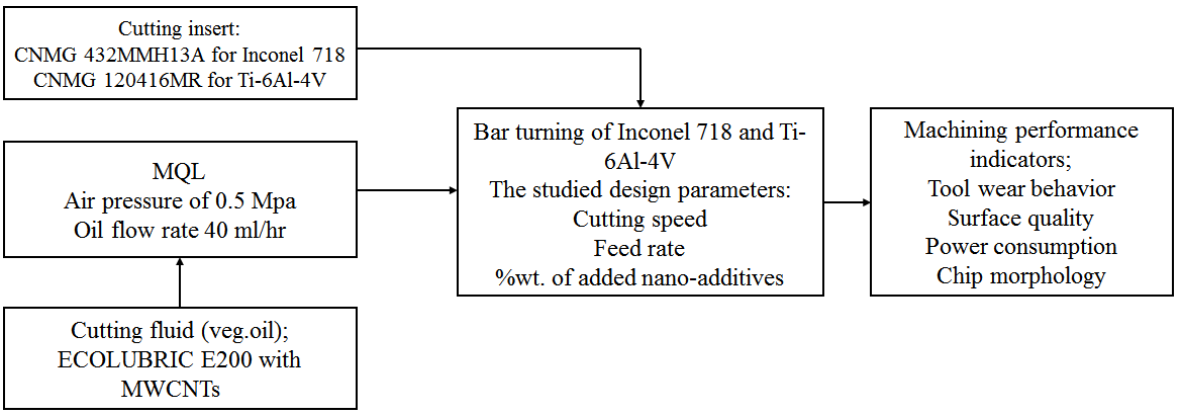

Figure 4-1 The experimental setup schematic

4.2. Nano-Cutting Fluid Preparation and Characterization

During the experimentation phase, multi-walled carbon nanotubes (MWCNTs) have 94% purity, 10-30 µm length, 12-20 nm average diameter, and 110 m2/g specific surface area have been employed for nano-cutting fluid preparations.

Also, it should be stated that nano-additives dispersion into the vegetable oil is a significant issue, which influences the thermal, rheological, and heat transfer characteristics of the proposed nano- fluid (e.g. thermal conductivity and viscosity).

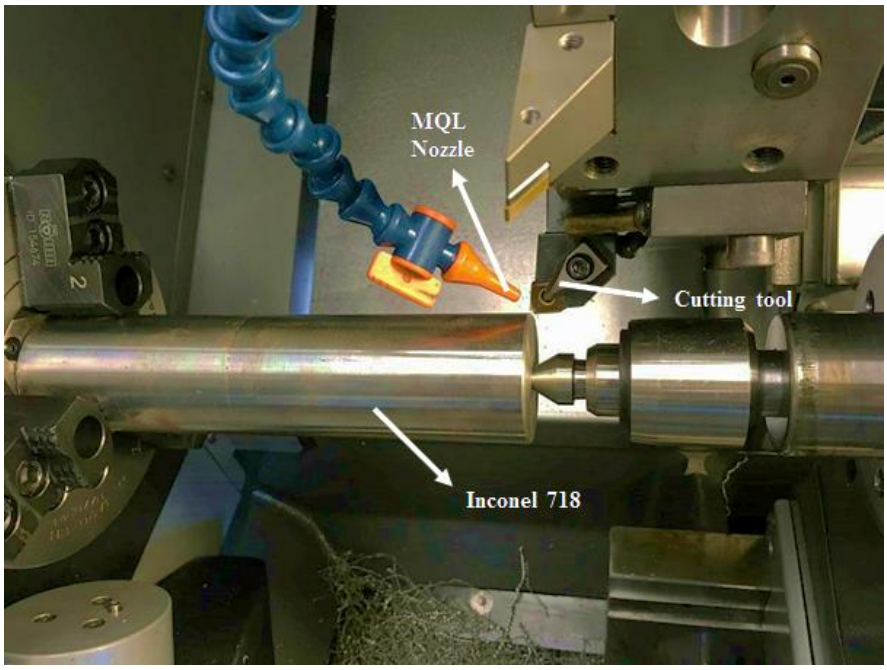

Figure 4-2 The experimental setup view when machining Inconel 718

In addition, Al_2O_3 nano-powder properties are; 20 nm size, 95% purity, and 138 m^2/g specific surface area. An ultrasonic device (AQUASONIC-50HT) has been used to disperse the nano-additives into the cutting oil over period of 3 hours at 60 ^oC, and then a magnetic stirrer (Hot Plate Stirrer-3073-21) has been used for the stirring step for 30 minutes to confirm fully dispersion of used nano-additives into the base cutting fluid. Zeta potential for stability analysis was conducted to measure the suspension stability of the resultant nano-fluid.

The Zetasizer-nano-device is used to measure the resultant nano-fluids zeta values with different weight percentages of added nano-additives (i.e., 2 wt. %, 4 wt. %). Two gold electrodes in a sample cell are used to measure the zeta potential index. A voltage source (i.e. 200 V) is implemented to the sample cell in order to capture the applied electric field effects during the nano-additives movements. Thus, the phase change in light scattered can be measured (electrophoresis). The phase change is proportional to the nano-additives electrophoresis mobility, from which the zeta potential can be calculated.

In addition, sodium dodecyl sulfate (surfactant) of 0.2 gm has been employed in preparing the nano-fluid. The surfactant's main function is to enhance the stability of the resultant nano-fluid to be more hydrophilic, and to increase the nano-additives surface charges; therefore, the repulsive forces between the nano-additives are increased as previously illustrated in literature [100, 101]. The zeta potential results for the nano-cutting fluids, which are used in this study, are provided in Table 4-4. It can be seen that all values are in the range of moderate stability according to the suspension stability evaluation criteria which has been mentioned and discussed in a previous work [109]. The nano-fluids usage when employing flood coolant can be an environmental concern; however, when using MQL technique, an optimal amount of oil is used and it results in a very fine mist where certain procedure is followed to eliminate any concern of using the nano-additives. Also, during the experimentation phase, certain safety procedures (i.e. standard nano-additives safety data sheets) have been applied to maintain a standard health and safety level in the workshop to avoid any harmful impacts for the machine operator. Regarding the disposal method, the nano-fluids have been carefully filtered before being released to the sewer according to a standard material safety data sheet [176]. A standard ventilator is employed in the workspace area to absorb the resultant nano-mist in the surrounded air.

Table 4-4 Zeta potential results

Nano-cutting fluid type (Nano-additives-wt. %)	Zeta potential absolute value
MWCNTs-2%	31
MWCNTs-4%	34
Al_2O_3-2%	29
Al_2O_3-4%	22

4.3. Plan of Experimentation

In this investigation, three design variables were employed with three levels each. Tables 4-5 and 4-6 indicate the studied independent process parameters and the assignment of the corresponding levels for Ti-6Al-4V and Inconel 718 cutting processes, respectively.

L9 orthogonal array (L9OA) based on the Taguchi method was implemented for cutting tests. L9OA has 9 rows corresponding to the number of tests with 4 columns at three levels. [177]. Tests were replicated 3 times and average values of measured responses were obtained. The full-factorial array in this study is L27OA (3^3); however, fractional factorial array L9OA based on the design of experiments approach was implemented to save time and cost. The conducted tests consist of nine experiments in which the first column was assigned to the cutting speed, the second column to the feed rate, and the third column to the weight percentage of added nano-additives as shown in Table 4-7.

Table 4-5 The levels assignment to design variables for Ti-6Al-4V cutting processes

Design Variables	Symbol	Level1	Level2	Level3
Cutting speed (m/min)	A	120	170	220
Feed rate (mm/rev)	B	0.1	0.15	0.2
Nano-additives (wt. %)	C	0%	2%	4%

Table 4-6 The levels assignment to design variables for Inconel 718 cutting processes

Design Variables	Symbol	Level1	Level2	Level3
Cutting speed (m/min)	A	30	40	50
Feed rate (mm/rev)	B	0.2	0.3	0.4
Nano-additives (wt. %)	C	0%	2%	4%

Table 4-7 L9OA used for experimentation plan

Run no.	Cutting speed (m/min)	Feed rate (mm/rev)	Nano-additive (wt. %)
1	1	1	1
2	1	2	2
3	1	3	3
4	2	1	2
5	2	2	3
6	2	3	1
7	3	1	3
8	3	2	1
9	3	3	2

Analysis of variance (ANOVA) is employed to analyze the influence of the studied design variables on the measured machining quality characteristics, which are average surface roughness, energy consumption, and flank tool wear. This technique includes determining the significant design parameters for each measured response, selecting an optimal level for each significant parameter, and verifying the improvement of quality characteristics using the optimal level of design parameters. As such, the studied cutting processes design, analysis, and optimization are achieved.

The modeling of the studied cutting processes is applied using response surface methodology (RSM) to analyze the influence of the independent process parameter s on the studied responses. The developed models are used to express; the average surface roughness, energy consumption, and flank tool wear for each studied cutting case. The purpose of mathematical models relates the process responses to facilitate the optimization of the process. The model's validation is demonstrated using the average percentage of deviation (Δ) which can be calculated as shown in equations (4.1) and (4.2) where R_m is the measured response value, R_p is the predicted response value, n is the number of tests, and Δ_i is the percentage of deviation per run (i).

$$\Delta_i = \left(\text{Abs}\frac{R_m - R_p}{R_m}\right) 100\ \% \tag{4.1}$$

$$\Delta = \frac{\sum_{i=1}^{n} \Delta_i}{n} \tag{4.2}$$

4.4. Summary

To summarize, the research methodology of the current work is concluded as shown in Figure 4-3.

As can be seen in the methodology schematic, there are four main stages throughout this study, namely; literature review, experimentation, experimental results analysis, and machining sustainability assessment. Literature review stage ends up with two main requirements; developing a general assessment model for machining processes, and performing cutting experiments in order to investigate the effects of the proposed nano-cutting fluid (i.e., based on MWCNT/Al_2O_3 nano-additives) on the machinability of Inconel 718 and Ti-6Al-4V. The experimentation stage shows the workpieces and their properties, selected cutting tool holder and inserts, MQL setup, studied design variables, nano-cutting fluids preparation, and characterization, and studied machining quality responses and their measurement methods. Finally, the experimental results analysis and investigations are presented and discussed through four phases illustrated as following:

- Modeling, optimization, and statistical analysis of the results related to average surface roughness, flank tool wear, and energy consumption using RSM, ANOVA, and implementation of the proposed sustainability assessment model.;

- Qualitative analysis for the resultant chips morphology and the cutting tool wear modes/mechanisms;

- A comparative study between the MWCNTs and Al_2O_3 nano-particles through discussing and analyzing the nano-cutting fluid tribological and heat transfer mechanisms;

- Developing an integrated finite element model in order to investigate various unique aspects of the studied cutting processes (e.g., the resultant nano-cutting fluid heat transfer characteristics and the interactions between the cutting tool and workpiece);

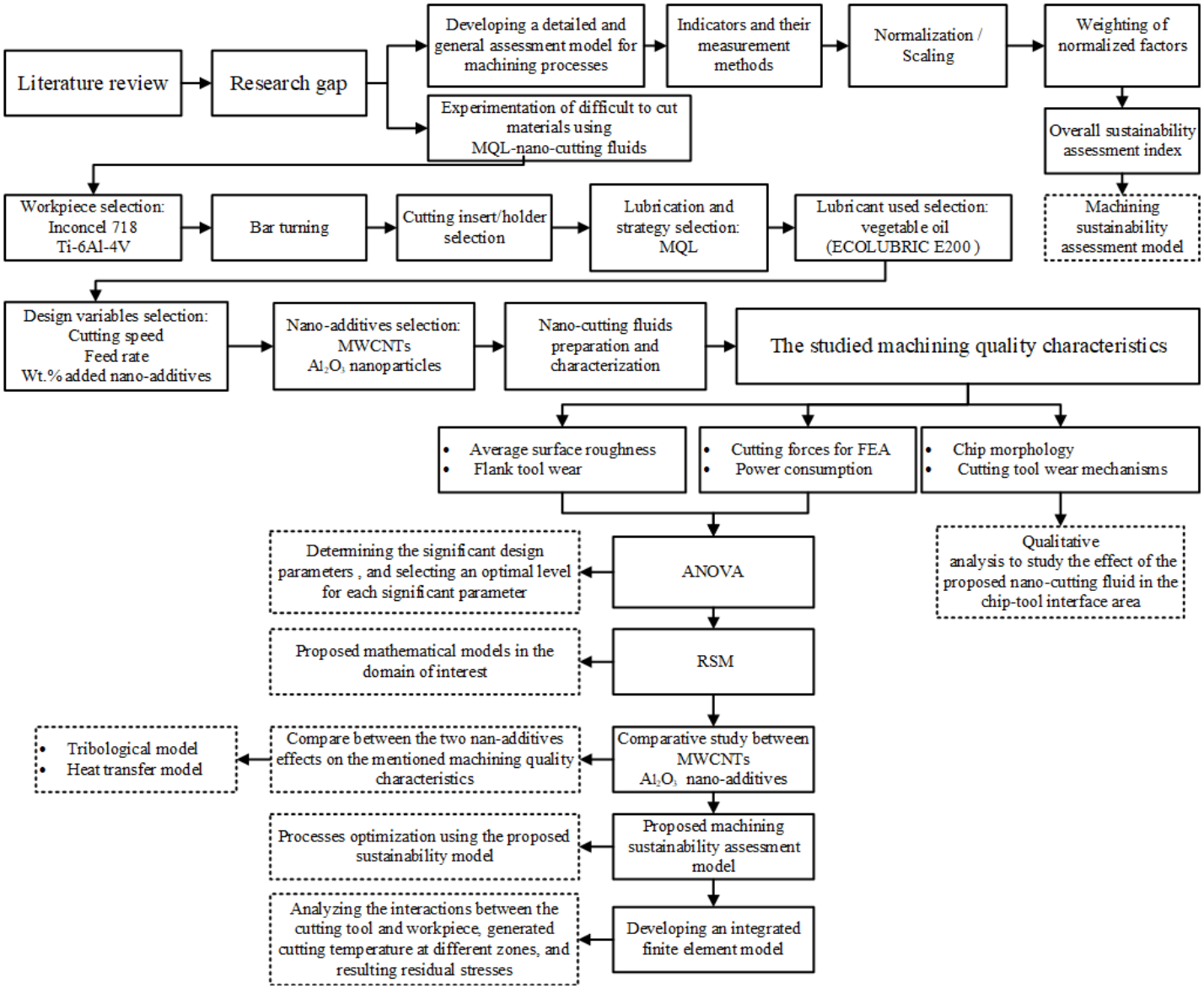

Figure 4-3 The current research methodology and roadmap

Chapter 5 Machining Inconel 718 with Nano-Fluids under Minimum Quantity Lubrication

5.1. Preamble

As have been mentioned earlier, the engineering application of nickel-based alloys could be increased through providing new proposed techniques in order to decrease the principal problems associated with the machining process. The focus of this chapter is mainly to investigate the effects of dispersed multi-wall carbon nano-tubes (MWCNTs) and Aluminum Oxide (Al_2O_3) gamma nano-particles into the conventional fluid (vegetable oil) under employing minimum quantity lubrication (MQL) technique during bar turning of Inconel 718. Investigations are carried out to study the tool wear behavior, energy consumption, surface quality and chip morphology.

The Inconel 718 is widely used in many industries including aerospace; however, the high temperature generated during machining is negatively affecting its machinability. Flood cooling is a commonly used remedy to improve machinability problems; however, the governmental regulation has called for further alternatives to reduce the environmental and health impacts of flood cooling.

This chapter aims to examine the effect of two types of nano-additives namely; multi-wall carbon nanotubes (MWCNTs) and aluminum oxide (Al_2O_3) gamma nanoparticles on enhancing the minimum quantity lubrication (MQL) technique cooling and lubrication capabilities during turning of Inconel 718. Machining tests were conducted and the generated surface and tools used were examined. In addition, the energy consumption data was recorded. The novelty focuses on improving the MQL heat capacity by employing different nano-fluids (i.e., nano-tubes and nano-particles) in order to improve Inconel 718 machinability.

5.2. Flank Wear Results

The collected flank wear data during machining with MWCNTs and Al_2O_3 nano-fluids are given in Figure 5-1. Regarding the tool life criteria, a maximum flank wear of 0.4 mm is used, otherwise, in case of not reaching the end of tool life criteria, the cutting stopped after nine cutting passes. The results revealed that both nano-fluids have shown effective results in comparison with the tests done without any nano-additives (i.e. tests 1, 6 and 8). The optimal flank wear value was obtained after test 2 when 2 wt. % MWCNTs nano-fluid is used. When 4 wt. % Al_2O_3 nano-fluid is used, test 4 showed the lowest tool wear. Additionally, test 8 showed the highest value of flank wear, this test has been done using pure MQL (without nan-additives) at cutting speed of 30 m/min and feed rate of 0.4 mm/rev. In general, the tool wear results revealed that the MWCNTs usage leads to a noticeable decrease in the measured flank wear compared to the cases when Al_2O_3 were employed except test 9 where Al_2O_3 nano-particles provided an improvement of 19.14 % more than MWCNTs. The progress of tool wear when using MWCNTs and Al_2O_3 nano-fluids is presented in Figure 5-2. The results presented in Figure 5-2 confirmed the obtained results in Figure 5-1. The main mechanism behind the tool wear improvements is the rolling effect as the induced mist penetrates the tool-workpiece interface area since the velocity of the resultant nano-mist is considerably higher than the velocity of the cutting tool, and hence it can pass through the tool pores and grain fractured groves. Thus, the nano-fluid droplets are formed on the cutting tool and workpiece surfaces and a tribo-film is also formed which considerably enhances the tribological and heat transfer characteristics.

The flank wear ANOVA results are listed in Table 5-1. Regarding MWCNTs fluids, the results showed that cutting speed and percentage of added nano-additives were the most significant process parameters affecting the flank wear at 90% and 95% confidence levels, respectively. Also, the plot of the studied parameters effects on the measured response (see Figure 5-3) is also used to visually present the most significant variables. A large difference in the flank wear results can be observed in all employed levels of cutting speed and nano-additive percentage. This finding support the claim that both cutting speed and nano-additive percentage are the most significant variables affecting the flank wear. Furthermore, the optimal levels were found to be 4 wt. % of added MWCNTs at cutting speed of 30 m/min and 0.2 mm/rev feed rate, as shown in Figure 5-3 (a).

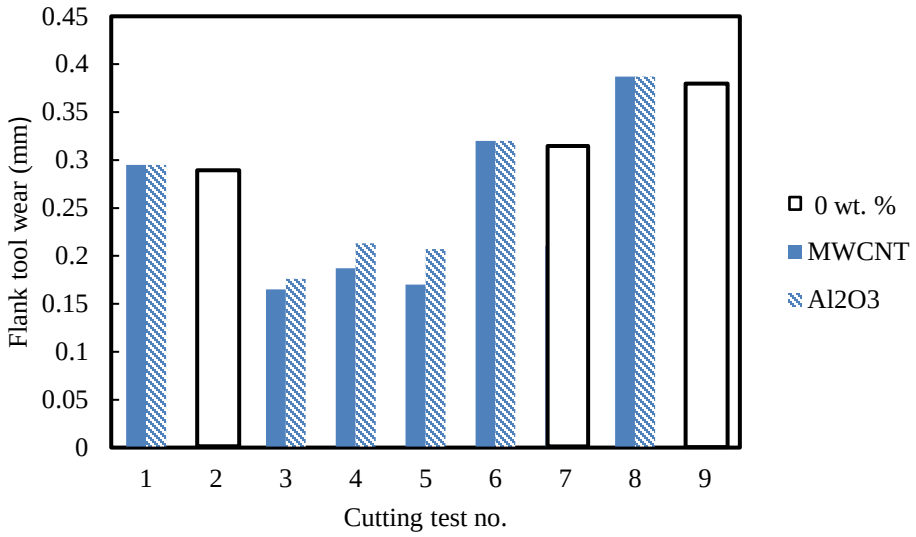

Figure 5-1 Flank wear results for Inconel 718

For the Al_2O_3 nano-fluid, the results confirmed that the wt.% of added nano-additives and cutting speed were the most significant design variables at 95% and 99% confidence levels, respectively (see Table 5-1). In addition, cutting speed of 30 m/min and 4 wt. % of added Al_2O_3 were the optimal levels (see Figure 5-3 (b)).

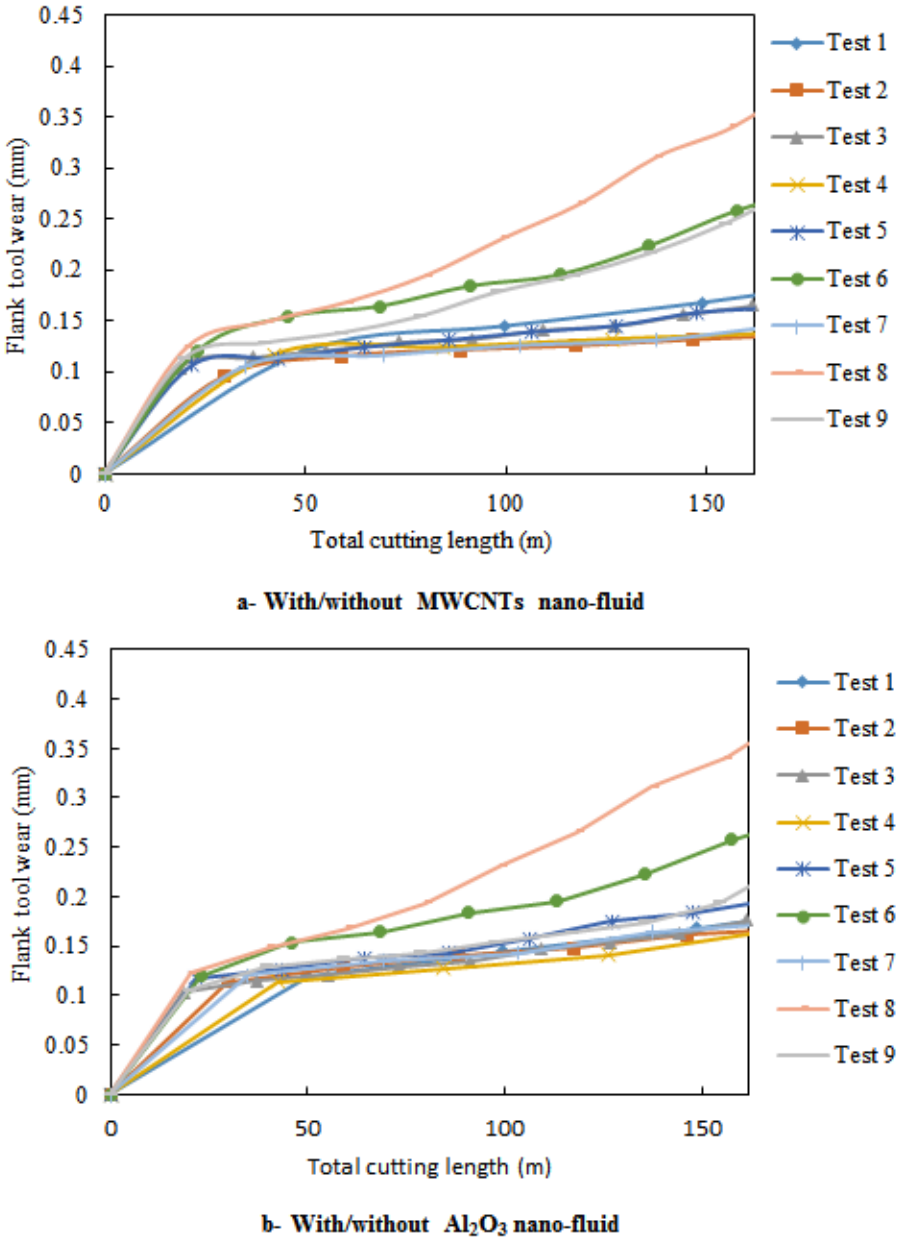

Figure 5-2 Progress of tool wear during cutting Inconel 718 using both nano-fluids

The feed rate hasn't shown any significant effect on both cases; however, it still has an acceptable statistical summation (see Table 5-1) which refers to its partial effect on the flank wear. It was found from Figure 5-3 (a) that 4 wt. % and 2 wt. % of added MWCNTs improve the flank wear results by 45.6% (C3 vs. C1) and 38.9% (C2 vs. C1) respectively compared to the tests conducted without any nano-additives (pure MQL).

Similarly, it was found from Figure 5-3 (b) that 4 wt. % and 2 wt. % of added Al_2O_3 nanoparticles enhance the tool wear results by 37.2% and 36%, respectively. Based on the results presented in Figures (5-1, 5-2, and 5-3), it is obvious that both employed nano-fluids offer significant improvements to flank wear. The improved in the measured tool wear when using the nano-fluid are attributed to the improvements in the wettability, convection, and conduction of the fluid as results of adding the nano-additives [26, 31, 178]. Also, the mentioned characteristics (wettability, convection, and conduction) extremely enhance the heat transfer and tribological functions of the proposed nano-fluids (either based on nano-tubes or nano-particles), and therefore the cutting tool hardness retains for a longer time which accordingly enhance the tool performance.

Table 5-1 ANOVA results for flank wear

Source	Statistical Sum	Variance	F (Calculated)	P-Value
		MWCTNs nano-fluid		
*A	0.0132	0.0066	13.19	0.07
B	0.0010	0.0005	1.04	0.49
**C	0.0406	0.0203	40.46	0.02
Error	0.0010	0.0052		
Total	0.0558			
		Al_2O_3 nano-fluid		
**A	0.0070	0.0035	27.61	0.035
B	0.0005	0.0002	2.09	0.333
***C	0.0302	0.0151	118.31	0.008
Error	0.0002	0.0001		
Total	0.0378			

*Significant at 90% confidence level
**Significant at 95% confidence level
***Significant at 99% confidence level

Also, some micrographs of worn flank faces were investigated under using different nano-additives weight percentage for MWCNTs and Al_2O_3 nano-fluids. The applied nano-fluids showed significant improvements in decreasing the flank tool wear compared to the test done without nano-additives as shown in Figure 5-4.

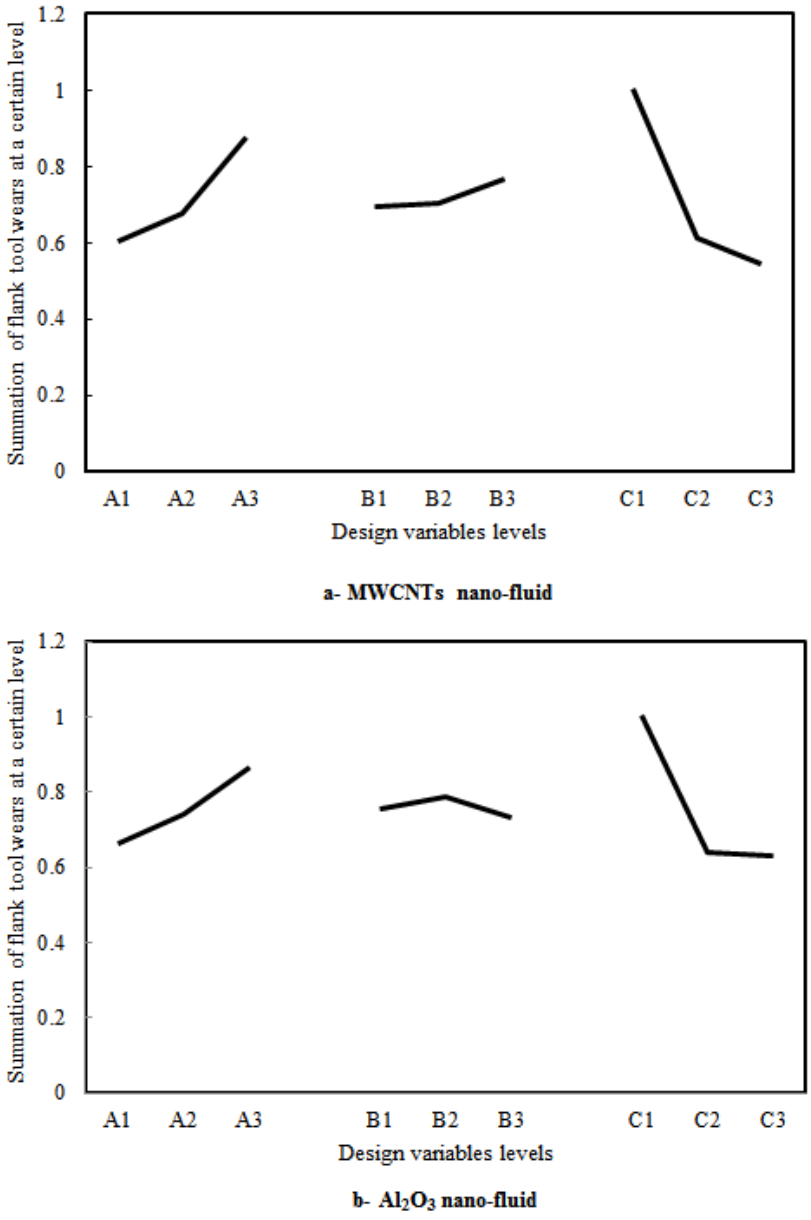

Figure 5-3 Plot of design variables effects on flank wear results when using both nano-cutting fluids

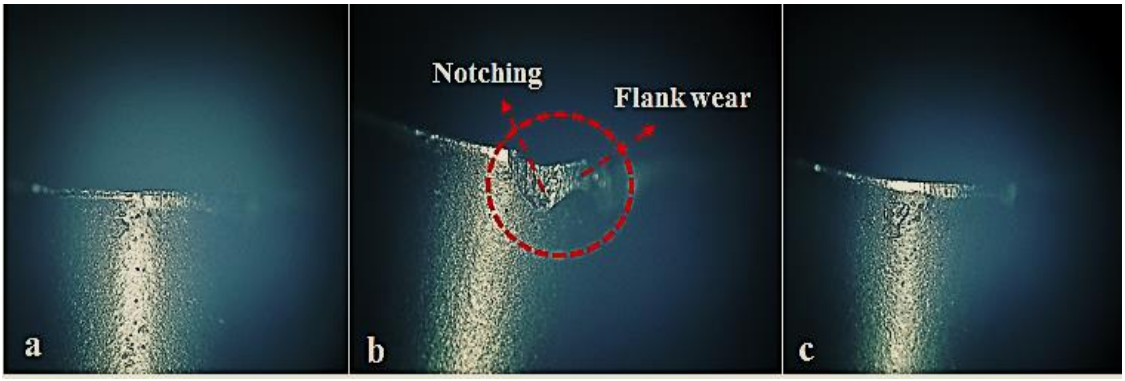

Figure 5-4 The observed flank wear at feed rate of 0.3 mm /rev and cutting speed of 50 m/min using; (a) 4 wt.% MWCNTs nano-fluid, (b) without nano-additives, (c) 2 wt.% Al_2O_3 nano-fluid

The adhesive mechanism of the workpiece on the tool surface followed by abrasive wear mechanism (due to hard elements in the workpiece material) is the main reason for the flank wear during machining Inconel 718. Thus, the observed flank wear without nano-additives (see Figure 5-4 (b)) is mainly attributed to a hybrid mechanism includes both abrasive and adhesive wear. However, the employed nano-fluids improved the base oil tribological and thermal functions which improve the interface bonding in the tool-chip area, and as a result, the adhesion wear severity was decreased and accordingly the flank wear has been reduced (see Figure 5-4 (a), and 5-4 (c)).

5.3. Average Surface Roughness Results

The average surface roughness results when using the two types of nano-additives are shown in Figure 5-5. Both types of nano-fluid showed improvement in machined surface quality; however, cutting tests 3 and 9 did not show significant improvements compared to other cutting tests performed using nano-additives which is attributed to the higher value of feed (0.4mm/rev) used in these two tests. Best surface quality is obtained after test 4 when using 2 wt. % MWCNTs nano-fluid. When 4 wt. % of added Al_2O_3 nano-particles is applied, it is found that cutting test 7 offered the better surface quality.

A comparison between the two types of nano-additives revealed that MQL-MWCNTs provided better performance in enhancing the surface quality; however, both cases (i.e. MWCNTs and Al_2O_3) provided almost the same performance at cutting test 7. The results revealed that the cooling and lubrication characteristics of nano-fluids improve the lubrication and wetting characteristics at the rake and flank regions and accordingly provide better heat dissipation as has been discussed in a previous study [179]. Thus, better average surface roughness values were noticed compared to the cutting tests done without any nano-additives, and these findings confirm the effectiveness of nano-fluids usage in improving the cutting processes performance as discussed in some previous studies [156, 164, 180]. Also, due to the increasing of nano-additive concentration, which increases the number of nano-additives at the tool-workpiece interface; these nano-additives perform a vital role as spacers, decreasing the contact between the tool and workpiece. Consequently, the coefficient of friction is decreased, and the surface roughness is improved. The ANOVA results for MWCNTs and Al_2O_3 cases are shown in Table 5-2. It can be seen that wt.% of added nano-additives and feed rate were the most significant design variables with 90% and 95% confidence levels, respectively.

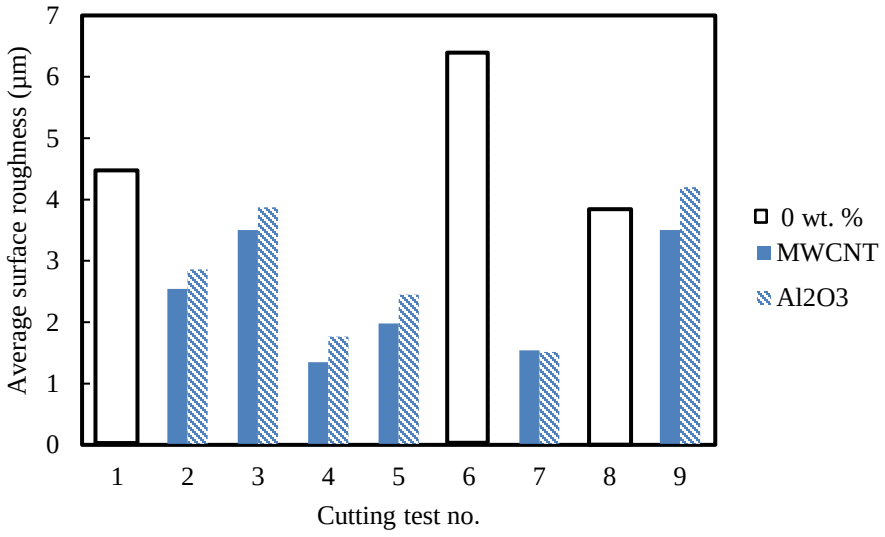

Figure 5-5 Average surface roughness results

In addition, the plots of the design variables are shown in Figure 5-6 and it was demonstrated that cutting feed rate of 0.2 mm/rev, cutting speed of 50 m/min and 4 wt. % added nano-additives were the optimal levels for both cases. From Figure 5-6 (a), it can be found that 4 wt. % of added MWCNTs decreased the machined surface roughness by 47.5% (C3 vs. C1) in comparison with the tests done without nano-additives, while 2 wt. % of added MWCNTs improved the surface quality by 44.8% (C2 vs. C1). Similarly, it was concluded from Figure 5-6 (b) that 4 wt. % and 2 wt. % of added Al_2O_3 nanoparticles enhanced the generated surface quality by 41.5% and 34%, respectively.

Table 5-2 ANOVA results for average surface roughness

Source	Statistical Sum	Variance	F (Calculated)	P-Value
MWCNTs nano-fluid				
A	0.0963	0.0481	0.1491	0.87
*B	9.087	4.5435	14.0662	0.06
*C	8.4962	4.2481	13.1517	0.07
Error	0.646	0.2321		
Total	18.3257			
Al_2O_3 nano-fluid				
A	0.2594	0.0797	0.623	0.617
**B	10.7751	5.3875	42.161	0.023
**C	5.8351	2.9175	22.831	0.042
Error	0.2556	0.1277		
Total	17.0251			

*Significant at 90% confidence level
**Significant at 95% confidence level

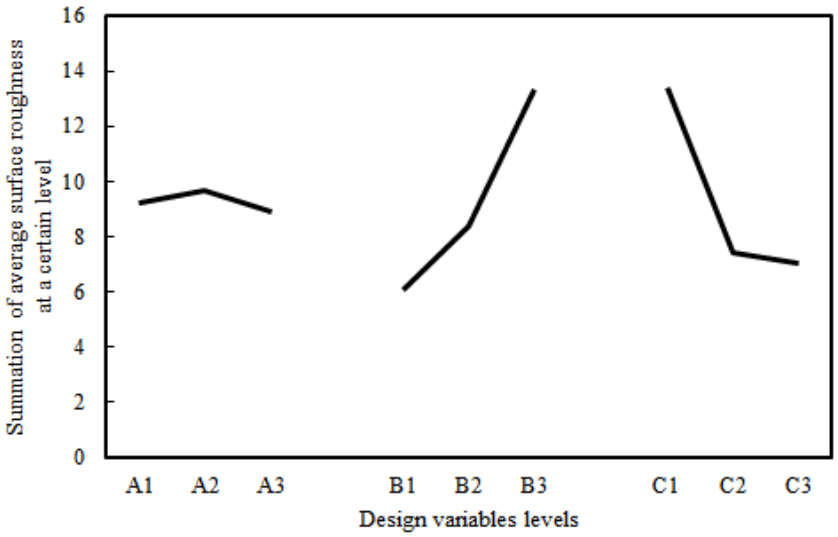

a- MWCNTs nano-fluid

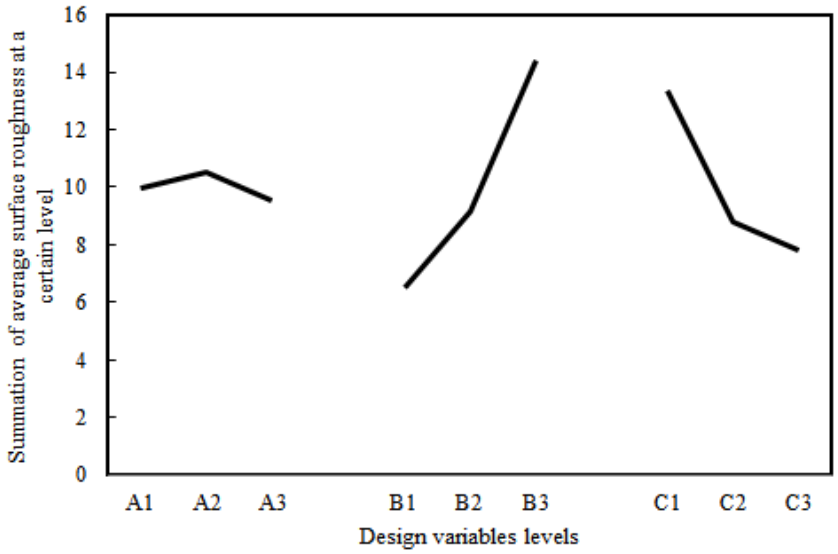

b- Al_2O_3 nano-fluid

Figure 5-6 Plot of design variable effects on average surface roughness results when using both MWCNTs and Al_2O_3 nano-fluids

5.4. Energy Consumption Results

Figure 5-7 shows the energy consumption results when using MWCNTs and Al_2O_3 nano-fluids. The lowest energy consumption was demonstrated at cutting test 2 when MWCNTs is used and test 3 for the case of Al_2O_3 nano-particles. In general, lower energy consumption is observed when MWCNTs is used except cutting test 3 which showed lower energy consumption of about 2% when Al_2O_3 nano-fluid is used. The change in the energy consumption when using nano-additives is mainly due to the improvements in the progression of tool wear due to the improvements in the cooling effectiveness, which led to decrease the tool material thermal softening [11, 86, 141, 142]. Also, the chips flow during machining Inconel 718 takes place within the workpiece (not at the tool–workpiece interface) because of the high induced friction, and hence high cutting force is required. Adequate applying of MQL-nano-fluid to the too-chip interface zone is an effective lubrication technique as the applied nano-additives play as rollers to improve the frictional behavior, and consequently the nano-additives rolling effect decreases the energy consumption.

The ANOVA results for both nano-fluids are listed as shown in Table 5-3. It can be found that cutting speed and wt. % of added nano-additives were the most significant design variables when using MWCNTs nano-fluid at 95% and 90% confidence levels, respectively. When using Al_2O_3 nano-fluid, the cutting speed and wt. % of added nano-additives were the most significant design variables at 99% and 95% confidence levels, respectively. Also, the cutting feed rate didn’t show any significant effect under using both cases; however, an acceptable statistical summation for feed rate can be only observed in the tests performed using Al_2O_3 nano-fluid. It can be concluded from Figure 5-8 that 2 wt. % of added nano-additives, feed rate of 0.2 mm/rev and cutting speed of 30 m/min showed the minimum energy consumption when employing MWCNTs nano-fluids.

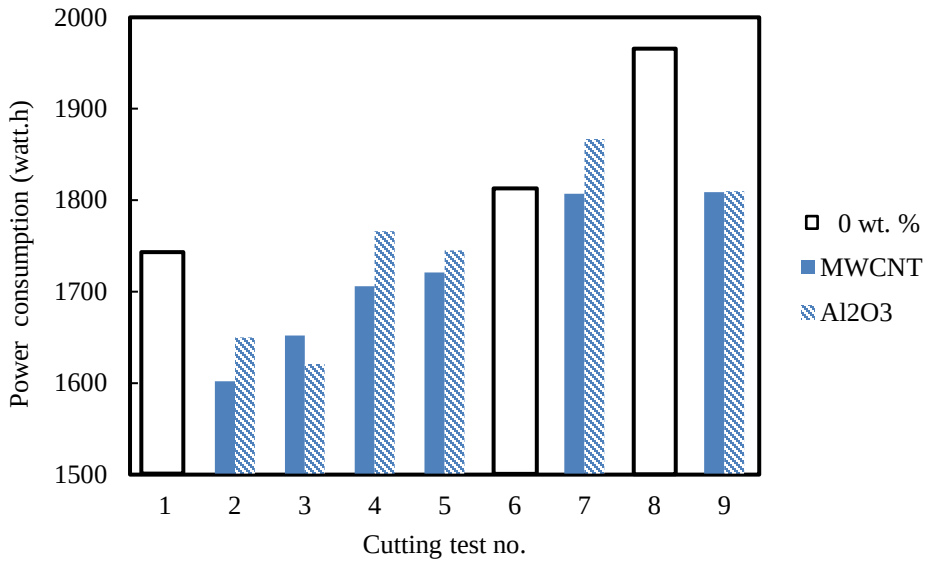

Figure 5-7 Energy consumption results

Table 5-3 ANOVA results for Energy consumption

Source	Statistical Sum	Variance	F (Calculated)	P-Value
		MWCNTs nano-fluid		
**A	58386.8	29193.4	31.75	0.03
B	228.2	114.1	0.12	0.89
*C	29062.9	14531.4	15.80	0.06
Error	1838.8	919.44		
Total	89516.9			
		Al_2O_3 nano-fluid		
***A	66788.22	33394.11	114.58	0.008
B	3520.22	1760.11	6.03	0.142
**C	16997.56	8498.77	29.16	0.033
Error	582.88	291.44		
Total	87888.88			

*Significant at 90% confidence level
**Significant at 95% confidence level
***Significant at 90% confidence level

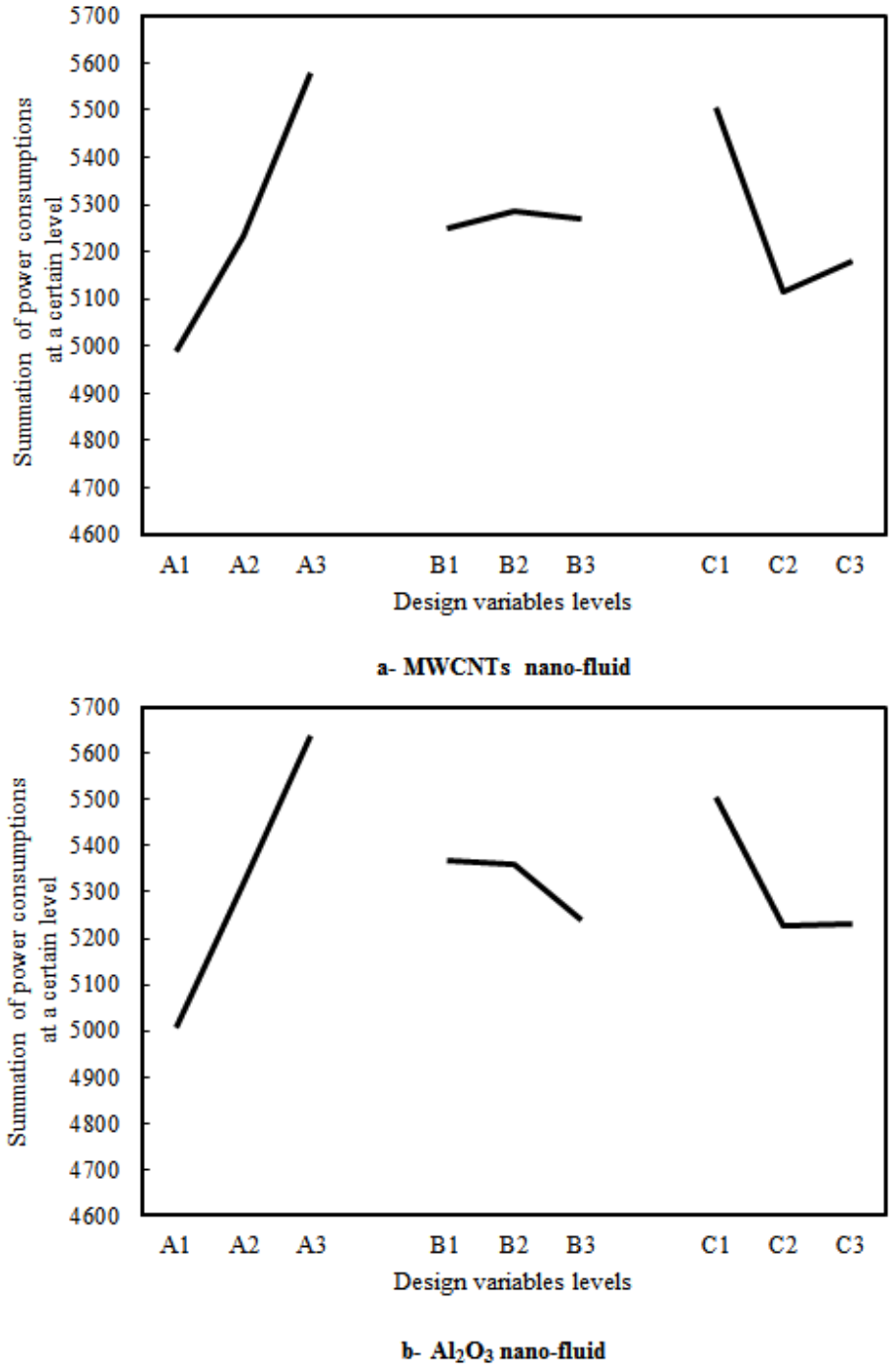

Figure 5-8 Independent process parameters effects on energy consumption results when using different nano-cutting fluids

Regarding Al_2O_3 nano-fluid, the lowest energy consumption has been revealed at 2 wt. % of added nano-additives, feed rate of 0.4 mm/rev, and cutting speed of 30 m/min. From Figure 5-8 (a), it can be found that 4 wt.% MQL-MWCNTs decreased the energy consumption by 5.9% (C3 vs. C1) compared to the cutting tests done without nano-additives, while 7% (C3 vs. C1) improvement percentage is determined for 2 wt.% MQL-MWCNTs. Similarly, as shown in Figure 5-8 (b), it is found that 4 wt. % and 2 wt. % of MQL-Al_2O_3 nano-fluid reduced the energy consumption results by 5% since no noticeable change between the two nano-particles concentrations has been observed.

5.5. ANOVA Verification

To verify the presented ANOVA results, equation (1) has been applied to estimate the optimal predicted levels as following:

$$Y_{predicted} = Y_{mean} + \sum_{i=1}^{n} (Y_i - Y_{mean}) \quad (5.1)$$

Where the optimal average response is Y_i and Y_{mean} is the overall mean. Table 5-4 shows the ANOVA verification results. Acceptable agreement is observed between the experimental and predicted optimal values. In addition, the verification accuracy results were calculated and acceptable results have been obtained.

Table 5-4 ANOVA verification results

Machining response	Nano-fluid type	Experimental value	Predicted value	Accuracy %
Flank wear (mm)	MWCNT	0.145	0.143	98.62%
Flank wear (mm)	Al_2O_3	0.176	0.178	98.86%
Surface roughness (µm)	MWCNT	1.35	1.28	94.81%
Surface roughness (µm)	Al_2O_3	1.51	1.44	95.36%
Energy consumption (watt. h)	MWCNT	1602	1613	99.31%
Energy consumption (watt. h)	Al_2O_3	1621	1637	99.01%

5.6. Machining Quality Characteristics Modeling

RSM is employed in the studied cutting processes to analyze the influence of the independent design variables on the measured machining responses. In addition, facilitating the optimization process is one of the mathematical model purposes. Three mathematical models have been developed for each nano-fluid type. The mathematical model commonly used for the process responses is represented as follows in equation (5.2).

$$Y = f(X_1 + X_2 + X_3 + \cdots) + \varepsilon \quad (5.2)$$

Where X_1, X_2, X_n are the process design variables and ε is the error which is usually normally distributed for the observed response Y. The developed models using MWCNTs nano-fluid for flank tool wear, average surface roughness, and energy consumption are provided as shown in equations (5.3-5.5), respectively. The design variables quadratic and interaction effects are used to accurately express the developed models since all studied design variables have three levels (2^{nd} degree of freedom). The average model accuracy for the flank tool wear under using MWCNTs nano-fluid is about 91.7%. The proposed model for the average surface roughness achieves an average model accuracy of 94.6%, while 93% average model accuracy is calculated for the energy consumption model. It can be concluded that acceptable average model accuracy has been noticed among all studied responses. The model's validation is demonstrated using the average percentage of deviation (Δ), as earlier mentioned in equations (4.1) and (4.2). The 3-D surface plots for flank wear, surface roughness, and energy consumption when using MWCNTs-nano-fluids are provided as shown in Figures 5-9, 5-10, and 5-11, respectively. In all 3-D surface plots, the third design variable is held constant at its second level.

$$VB_1 = 7.2\,E-05\,A^2 - 0.21\,B^2 + 106.71\,C^2 + 5.1\,E-03\,AB - 0.16\ - 5.08\,BC + 0.16 \quad (5.3)$$

$$Ra_1 = -7.3\,E-05\,A^2 + 34.85\,B^2 + 2015.75\,C^2 - 0.06\,AB - 0.75\,AC - 348.08\,BC + 1.95 \quad (5.4)$$

$$PC_1 = 0.14\,A^2 + 637.27\,B^2 + 178540.55\,C^2 + 7.72\,AB - 205.9\,AC - 4548.32\,BC + 1564.6 \quad (5.5)$$

As can be seen in Figures 5-9 (a) and 5-9 (b), increasing MWCNTs percentage results in decreasing the flank wear. Also, Figures 5-9 (a) and 5-9 (b) showed an agreement with the results obtained in Figure 5-3 as both of them confirmed that 4 wt. % MWCNTs provides the lowest flank wear. In addition, Figure 5-9 (c) confirmed the previous findings in Table 5-1 and Figure 5-3 since changing the cutting speed levels showed significant effects on the flank wear results. From Figure 5-10 (b) and 5-10 (c), it was found that 4wt. % provided the lowest surface roughness values. This finding is in agreement with the results obtained in Figure 5-6. Also, as can be seen in Figure 5-10 (a), the feed rate showed significant effect on the surface roughness values; however, the cutting speed did not show noticeable effects. This finding is consistent also with the surface roughness ANOVA results presented in Table 5-2.

In addition, from Figure 5-11 (a) and 5-11 (b), it was found that 2 wt. % provided the lowest energy consumption values. This finding is in agreement with the results obtained in Figure 5-8. Also, as can be seen in Figure 5-11 (c), the cutting speed showed significant effect on the energy consumption values; however, the feed rate did not show noticeable effects. This finding is consistent also with the energy consumption ANOVA results presented in Table 5-3.

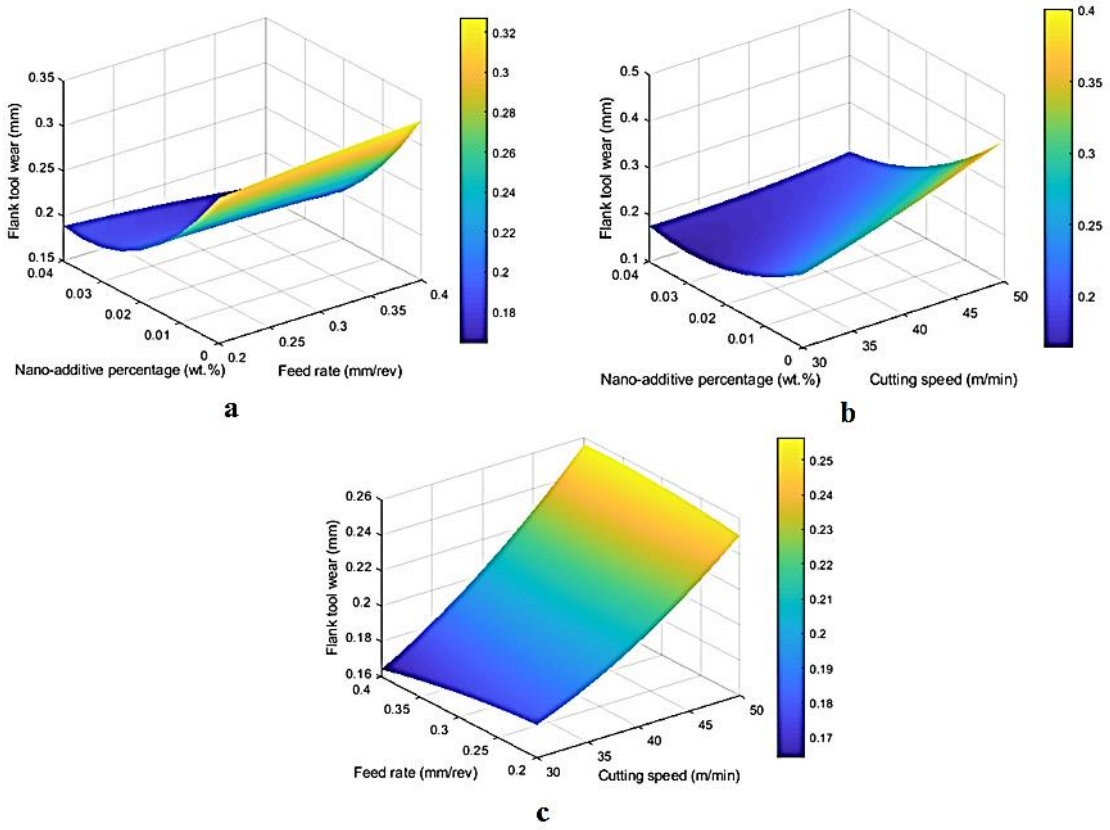

Figure 5-9 3-D surface plots for the flank wear model using MWCNTs-nano-fluids

Similarly, the proposed models for Al_2O_3 nano-fluid are provided in equations (5.6-5.8) for flank tool wear, average surface roughness, and energy consumption, respectively. The average model accuracy for the flank tool wear, average surface roughness and energy consumption models based on Al_2O_3 nano-fluid are 97.5%, 96.5%, and 99.3%, respectively.

The 3-D surface plots for flank wear, surface roughness, and energy consumption when using Al_2O_3-nano-fluids are provided as shown in Figures 5-12, 5-13, and 5-14, respectively. It should be stated that all developed models are valid for the studied design variables range.

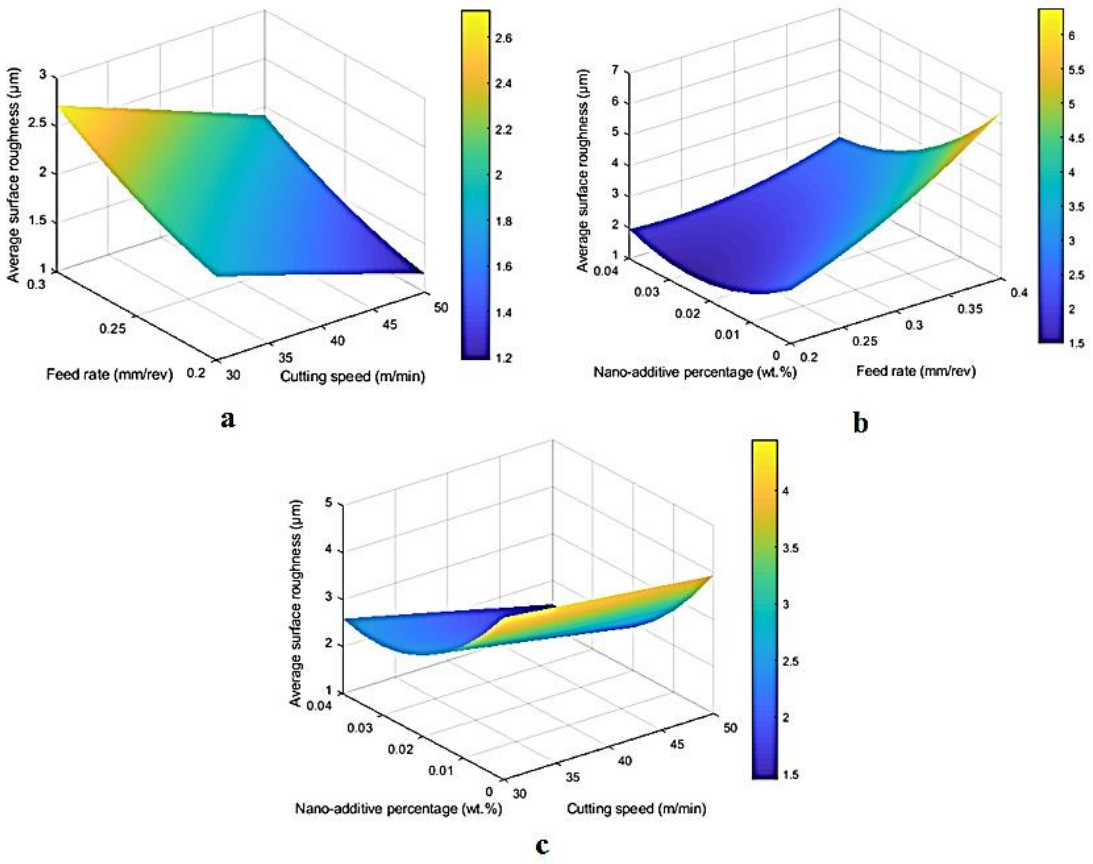

Figure 5-10 3-D surface plots for the surface roughness model using MWCNTs-nano-fluids

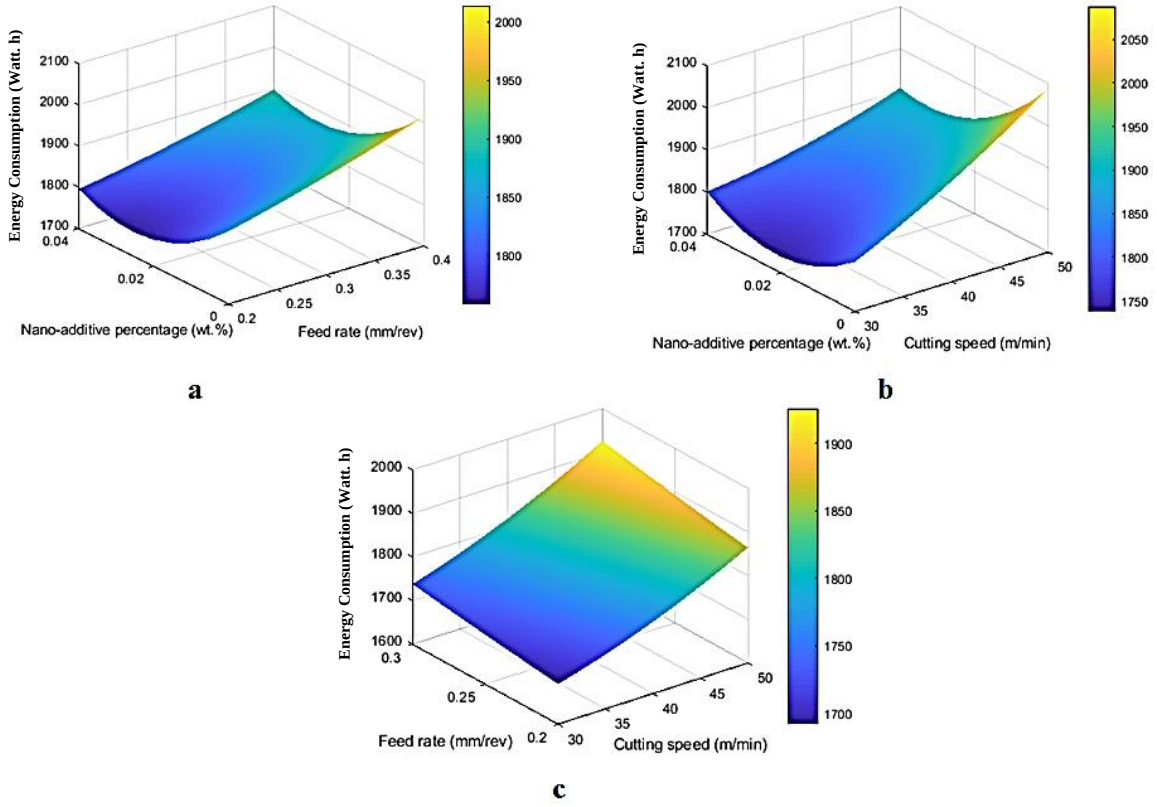

Figure 5-11 3-D surface plots for the energy consumption model using MWCNTs-nano-fluids

As can be seen in Figures 5-12 (b) and 5-12 (c), increasing Al_2O_3 percentage results in decreasing the flank wear. Also, Figures 5-12 (b) and 5-12 (c), showed an agreement with the results obtained in Figure 5-3 as both figures confirmed that no noticeable change is observed between 4 wt. % and 2 wt. % Al_2O_3. In addition, Figure 5-12 (a) confirmed the previous findings in Table 5-1 and Figure 5-3 since changing the cutting speed levels showed significant effects on the flank wear results. From Figure 5-13 (b) and 5-13 (c), it was found that 4wt. % provided the lowest surface roughness values. This finding is in agreement with the results obtained in Figure 5-6. Also, as can be seen in Figure 5-13 (a), the feed rate showed significant effect on the surface roughness values; however, the cutting speed did not show noticeable effects. This finding is consistent also with the surface roughness ANOVA results presented in Table 5-2. In addition, from Figure 5-14 (b) and 5-14 (c), it was found that 2 wt. % provided the lowest energy consumption values. This finding is in agreement with the results obtained in Figure 5-8.

Also, as can be seen in Figure 5-14 (a), the cutting speed showed significant effect on the energy consumption values; however, the feed rate did not show noticeable effects. This finding is consistent also with the energy consumption ANOVA results presented in Table 5-3.

$$VB_2 = 7.4\,E-05\,A^2 - 0.37\,B^2 + 141.11.71\,C^2 + 5.5\,E-03\,AB - 0.14\,AC - 8.97\,BC + 0.22 \quad (5.6)$$

$$Ra_2 = -5.1\,E-04\,A^2 + 26.56\,B^2 + 1350.22\,C^2 + 0.05\,AB - 0.43\,AC - 268.79\,BC + 2.01 \quad (5.7)$$

$$PC_2 = 0.12\,A^2 - 669.32\,B^2 + 128195.24\,C^2 + 5.81\,AB - 118.8\,AC - 8365.6\,BC + 1613.4 \quad (5.8)$$

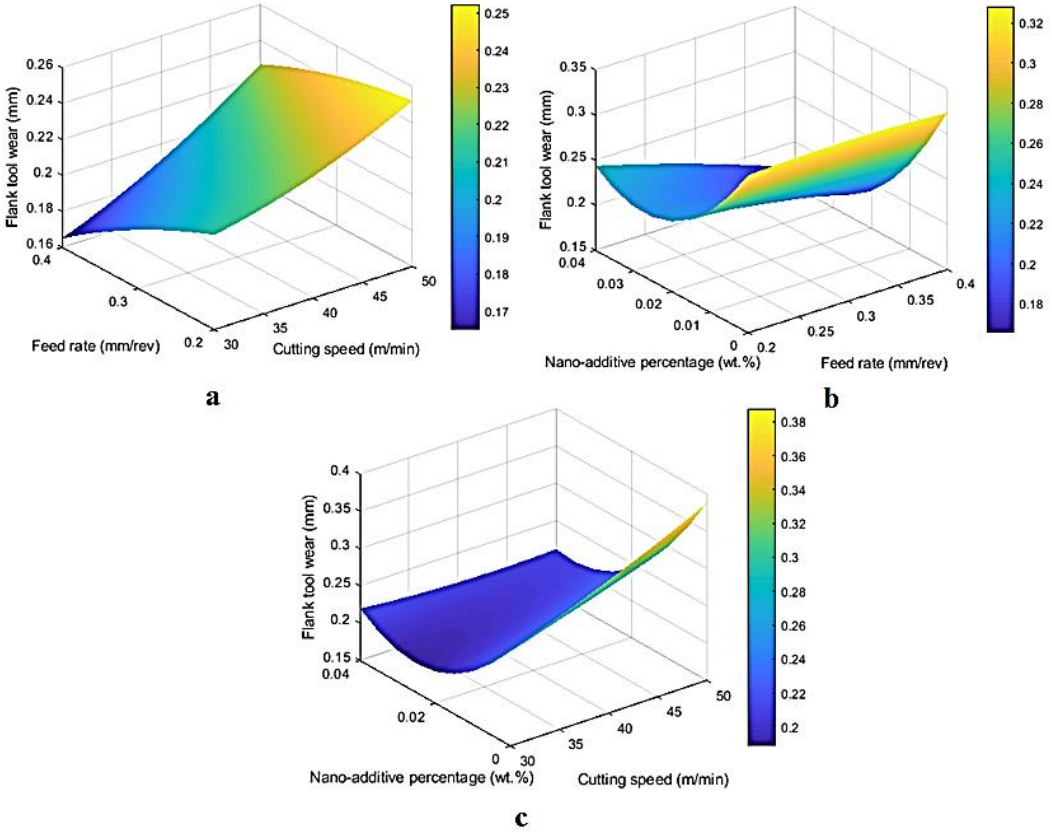

Figure 5-12 3-D surface plots for the flank wear model using Al_2O_3-nano-fluids

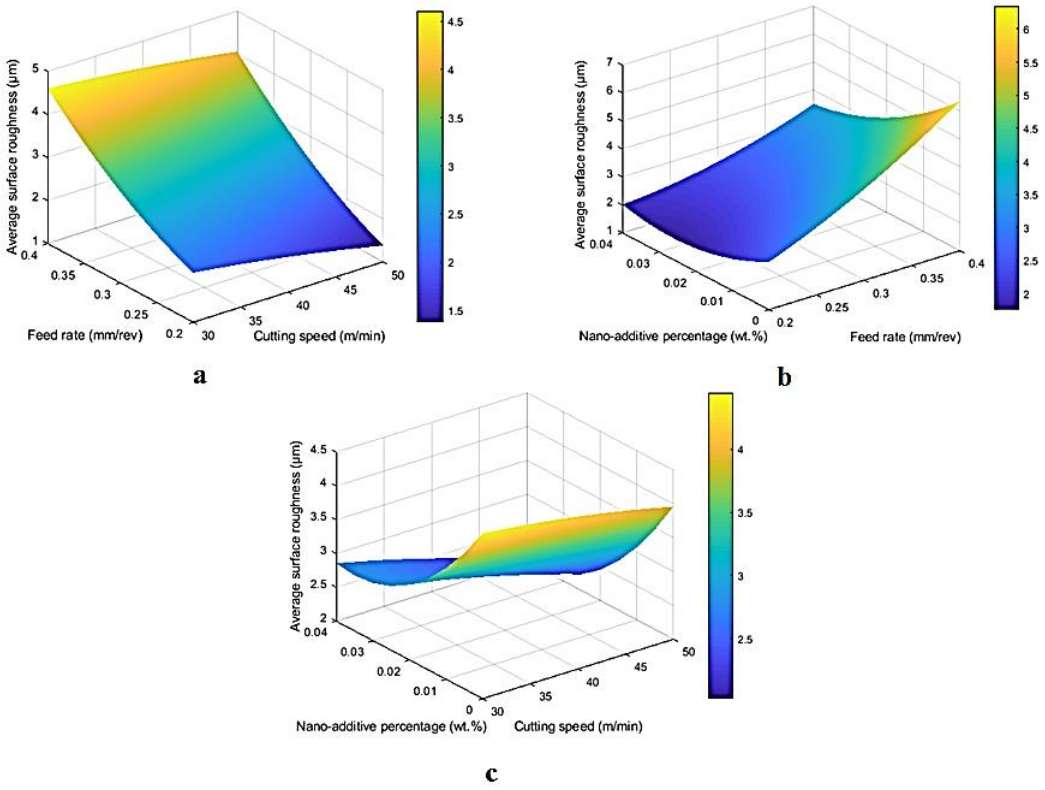

Figure 5-13 3-D surface plots for the surface roughness model using Al_2O_3-nano-fluids

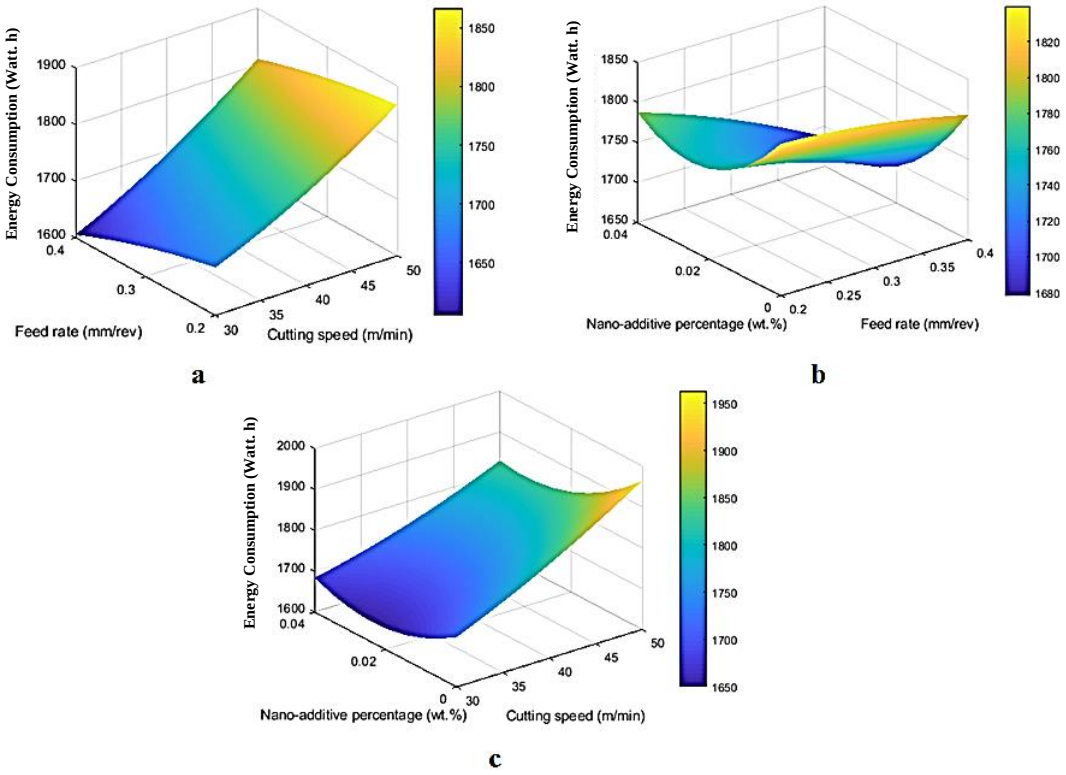

Figure 5-14 3-D surface plots for the energy consumption model using Al_2O_3-nano-fluids

5.7. Tool Wear Modes and Mechanisms

The modes of tool wear and their associated wear mechanisms are presented and discussed in this section. All micrographs of worn faces were captured at the end of cutting tests. The dominant wear modes when machining under mist coolant without nano-additives were; excessive flank wear, notching, built up edge (BUE), crater wear and oxidation. Regarding the tests performed using nano-additives either using MWCNTs or Al_2O_3 nano-fluids, it was demonstrated that the dominant wear modes were; flank tool wear, crater, and notching. The employed nano-fluids (i.e., MWCNTs and Al_2O_3) showed a significant improvement in reducing the flank tool wear compared to the tests performed without nano-additives as previously presented and discussed in Figure 5-4.

Regarding the notching mode, it occurs at the tool nose as seen in Figure 5-4 (b) which caused by adhesion. The adhesive mechanism during machining Inconel results due to the contact between the workpiece and cutting tool under sufficient pressure and temperature, which leads to plastic deformation in the actual contact area and it is called cold welding phenomenon as mentioned in a previous study [181].

However, the nano-fluids offer promising performance in terms of improving the flank wear. An observed notching wear has taken place when 4 wt. % Al_2O_3 nano-fluid was employed as these cutting test was performed at a higher value of cutting speed (see Figure 5-15). This result showed that MWCNTs nano-fluid provides a larger improvement than Al_2O_3 nano-fluid. It could be due to the superior thermal conductivity of MWCNTs (3000 W/m. K) compared to Al_2O_3 nano-particles (35 W/m. K). Also, MWCNTs nano-fluid offers higher zeta potential values than Al_2O_3 nano-fluid as previously presented in Table 6 which attributes to the better improvements obtained when using MWCNTs. There is no a clear physical evidence in the open literature proving that MWCNTs nano-fluid offers better tribological properties than Al_2O_3. However, based on the current research results, it is claimed that MWCNTs based nano-fluid could offer better performance than Al_2O_3 as a lubricant. Also, other aspects should be considered to emphasize this point correctly. The first aspect is the nano-additives dispersion level. Also, the induced nano-additives wear [182] (tribological aspect) is an important aspect which needs to be studied and analyzed in order to justify the current results. Thus, studying and understanding the nano-cutting fluids tribological and heat transfer mechanisms is highly required. Also, it was found that the crater wear (see Figure 5-16 (b)) was clearly noticed when pure MQL was employed (without nano-additives) at a higher value of cutting speed level (60 m/min). However, both nano-fluids showed a significant improvement in reducing the induced crater wear (see Figure 5-16 (a) & 5-16 (c)). It is mainly because of their superior cooling and lubrication properties which face the high generated temperature. During cutting without nano-additives, the high generated temperature is intensified by cutting speed preventing the hard constituents in the workpiece material to diffuse into softer material matrix. Consequently, that leads to a chemical reactivity between the tool and workpiece. Thus, the observed crater wear when pure MQL was employed is mainly attributed to a hybrid wear mechanism including both diffusion and chemical reactivity.

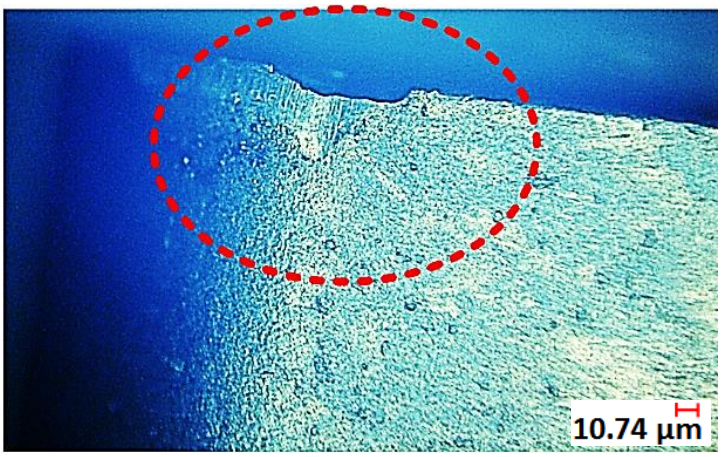

Figure 5-15 The observed notching wear when using 4 wt.% Al_2O_3 nano-fluid at cutting speed of 60 m/min and feed rate of 0.3 mm/rev

The oxidation and built-up-edge wear mechanisms (see Figure 5-17) have been only observed in the cutting tests performed without nano-additives. In terms of the oxidation wear mechanism which have been occurred at cutting speed of 50 m/min, it is mainly due to the chemical reactivity of Aluminum element in the carbide tools as has been confirmed in the literature review [183]. Also, it has been investigated that oxidation wear is also attributed to a combination of high generated temperature and oxygen from the surrounding air [184]. The built up edge phenomena has been observed at a feed rate of 0.4 mm/rev and a cutting speed of 50 m/min (without nano-additives) as shown in Figure 5-17. A previous work [181] claimed that it is mainly due to the adhesive form of carbide tools which leads to the chip pressure welding on the cutting insert. Also, the range of cutting speeds used in this investigation is considered as a low cutting speed which also increased the possibility of built-up-edge formation. It can be concluded that the employed nano-fluids offered significant improvements, it is mainly due to the promising cooling and lubrication properties which enhance the interface bonding between the tool and workpiece surfaces. In addition, the nano-fluids offer an effective heat dissipation performance which retains the cutting tool original hardness and accordingly the continuous sever rubbing of the workpiece with the flank face was decreased as discussed in some previous studies [26, 27, 31].

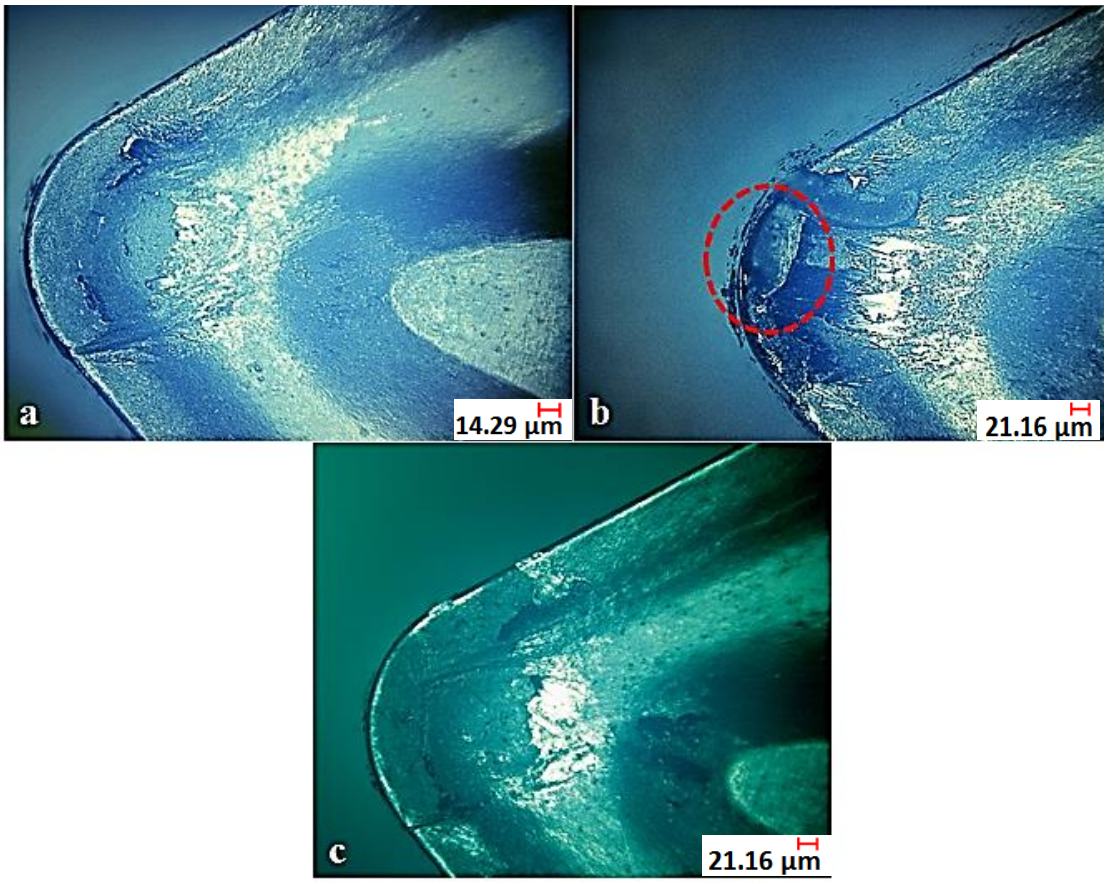

Figure 5-16 The observed crater wear at cutting speed of 60 m/min and feed rate of 0.2 mm/rev; (a) 4 wt.% Al_2O_3 nano-fluid, (b) without nano-additives, (c) 4 wt.% MWCNTs nano-fluid

Furthermore, the significant tribological properties of the resultant nano-cutting fluid reduced the coefficient of friction at the tool– chip interface as the employed nano-additives work as a spacers (see Figure 5-18) to limit the induced rubbing between the cutting tool and workpiece, as discussed previously [185]. As can be seen in Figure 5-18, the nano-cutting fluid is atomized into the MQL nozzle and it results in a very fine mist. Thus, the droplets of the nano-cutting-fluid are formed on the workpiece and cutting tool surfaces which significantly enhances the tribological characteristics and reduces the induced friction.

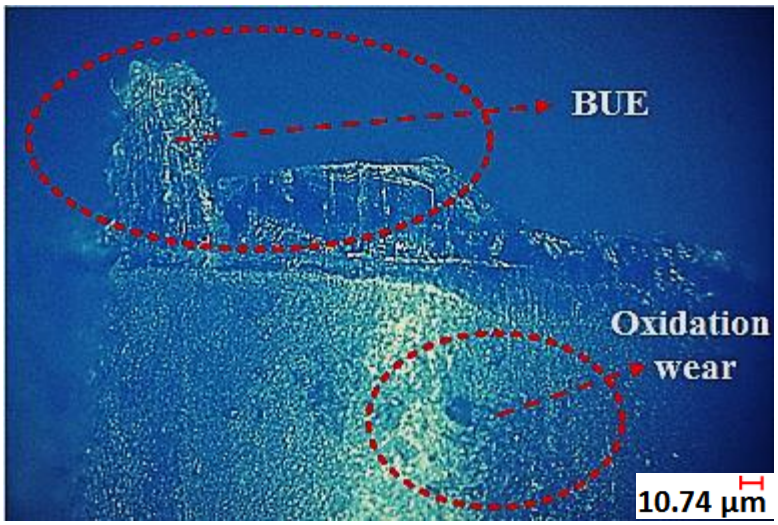

Figure 5-17 The observed oxidation wear and built-up-edge phenomena at cutting speed of 50 m/min without nano-additives

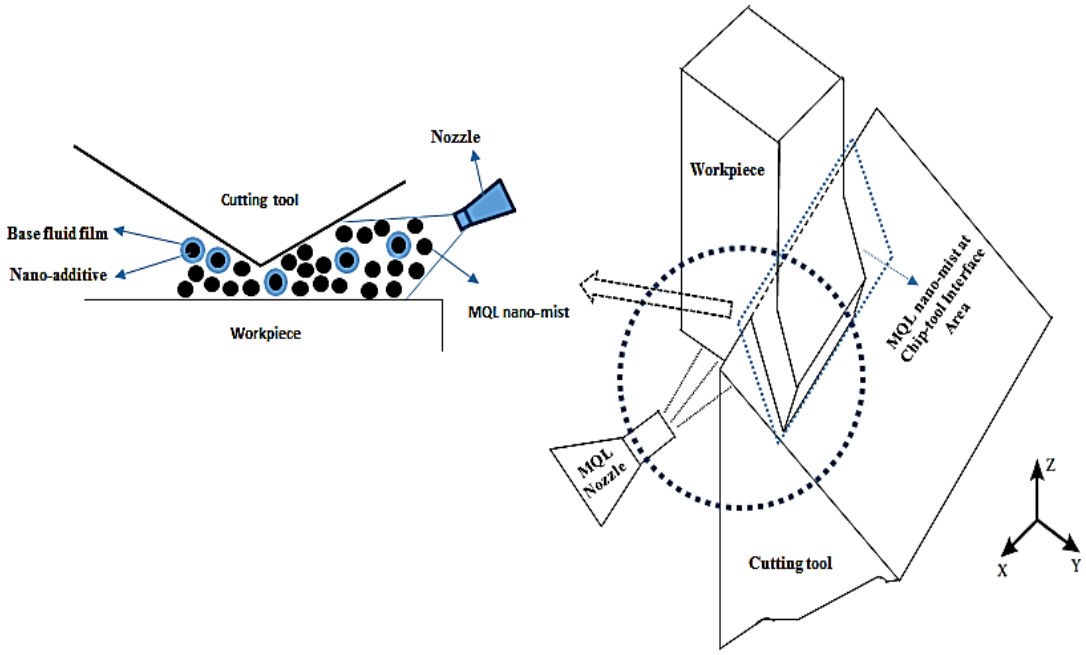

Figure 5-18 MQL-nano-fluid mechanism

5.8. Chip Morphology Examination

The chip morphology examination was carried out to provide details about the effects of dispersed MWCNTs/ Al_2O_3 nanoparticles on chip-tool interface temperature. For tests performed without nano-additives, the continuous helical chips (see Figure 5-19 (a)) were generated as the material becomes much softer compared to the cutting tool material due to the high generated temperature in the cutting shear zone. Al_2O_3 nano-fluid provides larger chip helix angles (θ) compared to the tests performed without nano-additives as shown in Figure 5-19 (b). It is attributed to forming a thin layer of nano-mist between the chip and tool rake face (see Figure 5-18) [26, 166]. This nano-mist layer increased the chip helix angle as can be seen in Figure (5-19 (b) & 5-20 (b)). The majority of tests performed using MWCNTs nano-fluid showed tiny segmented chips as shown in Figure 5-19 (c) because of the impingement of MWCNTs on the generated chips which increased the chip helix angle and forced the long chips for breaking. The schematic of the three cases is provided in Figure 5-20. The above results were confirmed with chip morphology examination revealed in a previous study [26] which applied Al_2O_3 nano-fluid during turning of AISI 4340. However, in the current study, the tiny segmented chips were observed only when MWCNTs have been employed. It is mainly due to the superior thermal properties of MWCNTs (thermal conductivity is about 3000 W/m K). Also, Inconel 718 has higher hardness and yield strength values (see Table 4-1) compared to AISI 4340 (i.e., yield strength of 470 MPa and hardness of 35 Rc) which accordingly prevented the occurrence of tiny segmented chips when using Al_2O_3 nano-fluid. Thus, this finding also confirms that MWCNTs have offered the best cooling and lubrication performance. In addition, BUE-chips have been observed at a higher cutting speed (60 m/min) and feed rate of 0.3 mm/rev without nano-additives. This phenomenon takes place due to the high generated temperature and pressure at the tool tip (see Figure 5-21 (a)). On the other hand, no built-up edge chips were observed when either using MWCNTs or Al_2O_3 nano-fluids (see Figure 5-21 (b)) as they offer promising cooling and lubrication properties.

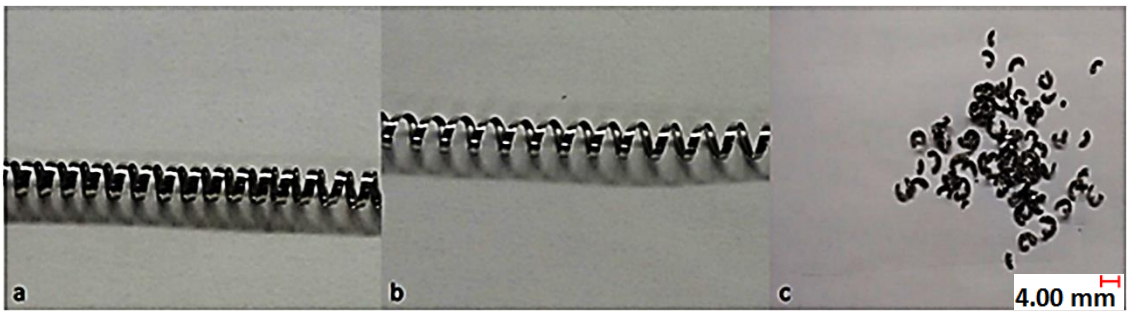

Figure 5-19 The generated chips during machining Inconel 718 at cutting speed of 60 m/min and feed rate of 0.3 mm/rev; (a) without nano-additives, (b) Al_2O_3 nano-fluid, (c) MWCNTs nano-fluid

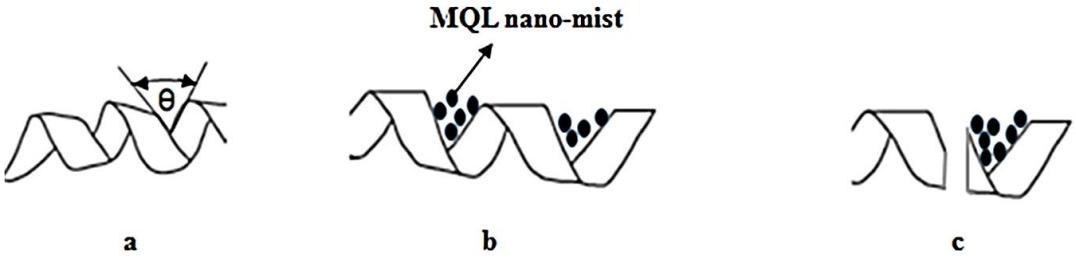

Figure 5-20 Schematic of the generated chips; (a) lower helix angle using pure MQL, (b) larger helix angle using Al_2O_3 nano-fluid, (c) segmented chips using MWCNTs nano-fluid

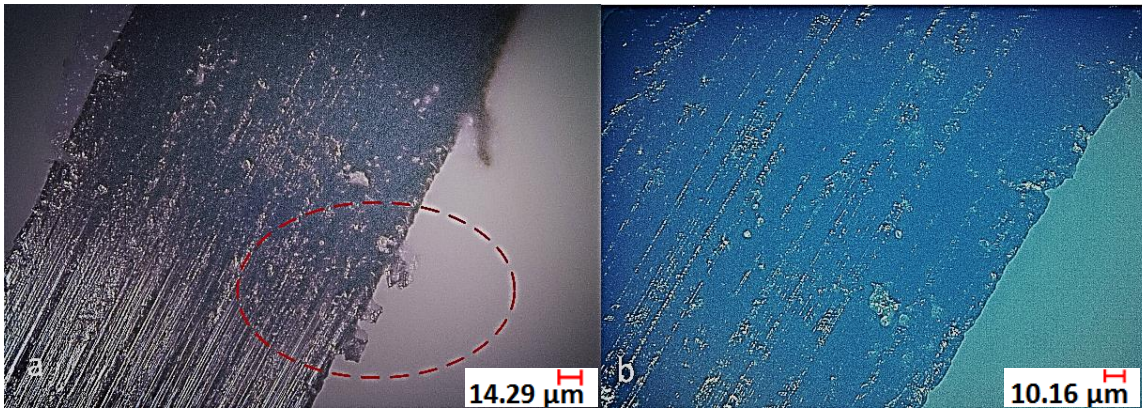

Figure 5-21 Micrographs of BUE effects on the generated chips at cutting speed of 60 m/min and feed rate of 0.3 mm/rev; (a) without nano-additives, (b) under MWCNTs nano-fluid

Also, the deformed chip thickness was measured for different cases and results were plotted at different feed rate levels as provided in Figure 5-22. It can be concluded that cutting tests performed without nano-additives showed the highest chip thickness due to the chip welding tendency to the top surface layers of the tool rake face. Based on the results provided in Figure 5-22, lower deformed chip thickness has been obtained using both nano-fluids. The chip thickness reduction would lead to shorter shear plane and larger shear angle [186]. Thus, lower cutting force [187] and induced friction coefficient [188] would occur as similarly discussed in previous studies. Furthermore, the chip breakability mechanism would be enhanced [189]. For MWCNTs tests, it was found that 4 wt. % provided lower deformed chip thickness than 2 wt. %. However, 2wt. % Al_2O_3 nano-fluid offered better performance than 4 wt. %. Thus, studying the MQL-nano-fluid heat transfer and tribological mechanisms is currently under investigation to obtain the nano-additives percentage and size effects on the cutting processes performance. In general, the chip morphology investigation showed the nano-fluids cooling and lubrication significantly improve the Inconel 718 machinability.

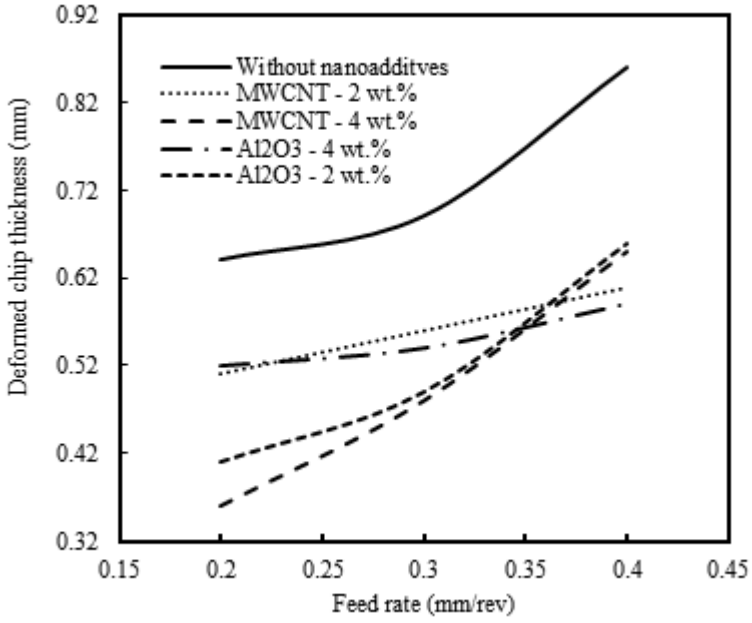

Figure 5-22 Effect of feed rate on chip thickness during machining Inconel 718 with/without nano-fluids

5.9. Discussions

It is an important aspect to understand the MQL nano-fluid mechanism. The technique schematic is shown at Figure 5-18. It can be concluded that the proposed nano-fluids are atomized using MQL device under employing certain amount of compressed air. Consequently, a fine mist walled with a vegetable oil layer is formed (see Figure 5-18). This mist is capable of penetrating into the tool-workpiece interfere area and creating a tribo-film which has a significant role in reducing the generated cutting heat as well as decreasing the coefficient of friction. Accordingly, these improvements significantly enhance the cooling and lubrication functions, and maintain the tool hardness for a longer period. Thus, the MQL-nano-fluid showed better performance in terms of tool wear behavior compared to other cutting tests done using pure MQL without any added nano-additives.

Also, the previous investigations revealed that both types of nano-fluids offer promising results in terms of flank wear, average surface roughness, and energy consumption; however, MWCNTs generally presents better performance than Al_2O_3 nano-fluid. The reasons for this finding were discussed as follows:

- The resultant nano-fluid based on MWCNTs offers higher thermal conductivity values even under employing lower concentration percentage (wt. %). This attributed to the fact that MWCNTs have superior thermal properties (thermal conductivity is about 3000 W/m K [33-35]). For example, the thermal conductivity value of MWCNTs nano-fluid using water as a base fluid showed an improvement percentage of 38% (using 0.6% volume fraction) [121], while Al_2O_3 nano-fluid using the same base fluid and 4.3% volume fraction showed 30% thermal conductivity improvement percentage [122].

- Zeta potential index expresses the repulsive force among the nano-additives and it is considered as a worthy dispersion stability indicator [92, 190]. Thus, higher values of zeta potential index mean the employed nano-fluid presents better performance which could prevent any possible obstacles such as nano-additives agglomeration, clogging, or sedimentation. In terms of the measured zeta potential results, MWCNTs nano-fluid offers higher values than Al_2O_3 nano-fluid as previously presented in Table 4-4 which attributes to the better improvements obtained when using MWCNTs.

- The range of cutting speeds used in the current investigation is considered as a low cutting speed. This emphasis the nano-fluid lubrication effect and its contribution to reduce the induced friction which improves the tribological aspects of the cutting process. Both employed nano-fluids have offered significant results in improving both the frictional behavior and tool wear performance. In a previous study [191] of a pin-on-flat tribo-tester showed that the worn weight and friction coefficient have been decreased by 43.4 % and 34.2% respectively under using Al_2O_3 nanoparticles in deionized water. Also, MoS2/CNTs hybrid nano-fluid showed reduction in the friction coefficient during grinding of Inconel 718, [192]. Regarding the CNTs tribological enhancements, a noticeable increment in the fire and flash points of SAE20W40 oil has been observed after adding MWCNTs so that it helps in improving both of tribological and heat absorption capabilities of the proposed nano-fluid [152].

- There is no a clear physical evidence in the open literature proves that MWCNTs nano-fluid offers better tribological properties than Al_2O_3; however, based on the current research results, it is claimed that MWCNTs based nano-fluid could offer better performance than Al_2O_3 as a lubricant. Thus, studying and understanding the nano-cutting fluids frictional and heat transfer functions is highly required and currently under investigation.

5.10. Summary

In this chapter, two nano-fluids (MWCNTs and Al_2O_3) were employed during machining Inconel 718 to study their influence on the machinability when MQL technology is used. The study revealed that:

- Both nano-fluids offer better results for tool wear, surface quality, and energy consumption; however, MWCNTs presents better performance than Al_2O_3 nano-fluid.

- The analysis of the measured flank wear, induced surface quality, and energy consumption results showed that the nano-additives weight percentage has a significant effect on all previous characteristics either using MWCNTs or Al_2O_3.

- 4 wt.% added MWCNTs or Al_2O_3 nanoparticles was the optimal level for flank wear and surface quality results; however, no noticeable change has been observed between 2 wt.% and 4 wt.% in case of energy consumption.

- The nano-fluids improvements are attributed its superior tribological and heat transfer characteristics, which improve the interface bonding between the cutting tool and workpiece surfaces. Also, the nano-fluids offer a better heat dissipation performance which retains the cutting tool original hardness and accordingly reduce the sever rubbing of the workpiece with the flank face.

- The dominant wear modes noticed when cutting without nano-additives were excessive flank wear, notching, built up edge, crater wear, and oxidation; however, both MWCNTs and Al_2O_3 nano-fluids have shown promising results in enhancing the cutting tool performance.

- It is revealed that both types of nano-fluids offer promising results in terms of flank wear, average surface roughness, and energy consumption; however, MWCNTs generally presents better performance than Al_2O_3 nano-fluid.

- There is no a clear physical evidence in the open literature proves that MWCNTs nano-fluid offers better tribological properties than Al_2O_3. Thus, studying and analyzing the nano-cutting fluid heat transfer and frictional mechanisms are required to physically investigate and emphasize this point.

It is concluded that MWCNTs and Al_2O_3 nanoparticles improve the thermal and tribological properties of the resultant nano-fluid compared with the base fluid. Thus, the obtained results showed improvements in the cutting performance of Inconel 718 (i.e. flank tool, surface quality, and energy consumption).

Chapter 6 Machining Ti-6Al-4V with Nano-Fluids under Minimum Quantity Lubrication

6.1. Preamble

Titanium alloys are the primary candidates in several applications due to its promising characteristics such as high strength to weight ratio, high yield strength, and high wear resistance. Despite its superior performance, some inherent properties such as low thermal conductivity and high chemical reactivity lead to poor machinability and result in premature tool failure. The engineering application of titanium alloys could be increased through providing proposed new techniques to decrease the principal problems associated with the machining process. In order to overcome the heat dissipation challenge during machining titanium alloys, nano-cutting fluids are utilized as they offer higher observed thermal conductivity values compared to the base oil. The focus of this chapter is mainly to investigate the effects of dispersed multi-wall carbon nanotubes (MWCNTs) into the conventional fluid (vegetable oil) under minimum quantity lubrication (MQL) technique during turning Ti-6Al-4V alloy. Similar to Chapter 5, the investigations are carried out to study the tool wear behavior, energy consumption, chip morphology and surface quality; however, only MWCNTs nano-fluid is employed as it offers better results than Al_2O_3 nano-fluid as has been clarified and discussed in the previous chapter.

6.2. Flank Wear Results

The flank wear results when cutting Ti-6Al-4V with MWCNTs nano-fluid are provided in Figure 6-1. A maximum flank wear of 0.4 mm [193] is used as the tool life criteria otherwise, in case of not reaching the end of tool life criteria, the cutting stopped after nine cutting passes. The results revealed that MWCNTs nano-fluid has shown promising results in comparison with the tests performed without any nano-additives (i.e. tests 1, 6 and 8). Test 3 shows the lowest flank wear value. The cutting conditions at test 3 are cutting speed of 120 m/min, feed rate of 0.15 mm/rev and 4 wt. % of added MWCNTs. The highest wear value was found after test 8 (i.e. after 6 cutting passes) and after test 6 (i.e. after 5 cutting passes). Both of cutting tests 8 and 6 have been performed without using nano-additives. Also, the tool wear progress is presented as shown in Figure 6-2.

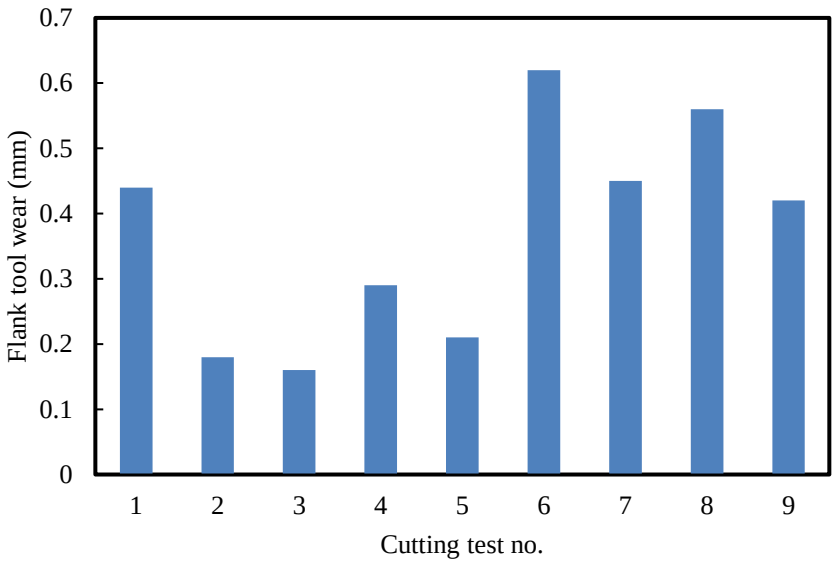

Figure 6-1 Flank tool wear results

The nano-fluid significant improvements are mainly attributed to the significant cooling and lubrication properties of nano-fluids which improve the rake and flank regions' lubrication and wetting properties so that better heat dissipation was accomplished.

Thus, partially smoothed cutting processes was achieved and lower flank wear values were observed in comparison with the processes performed without any nano-additives as has been discussed in previous studies [156, 180]. Also, the mentioned characteristics enormously improve the cooling and lubrication properties which retain the cutting tool hardness for a longer time as similarly confirmed in previous works [57, 60].

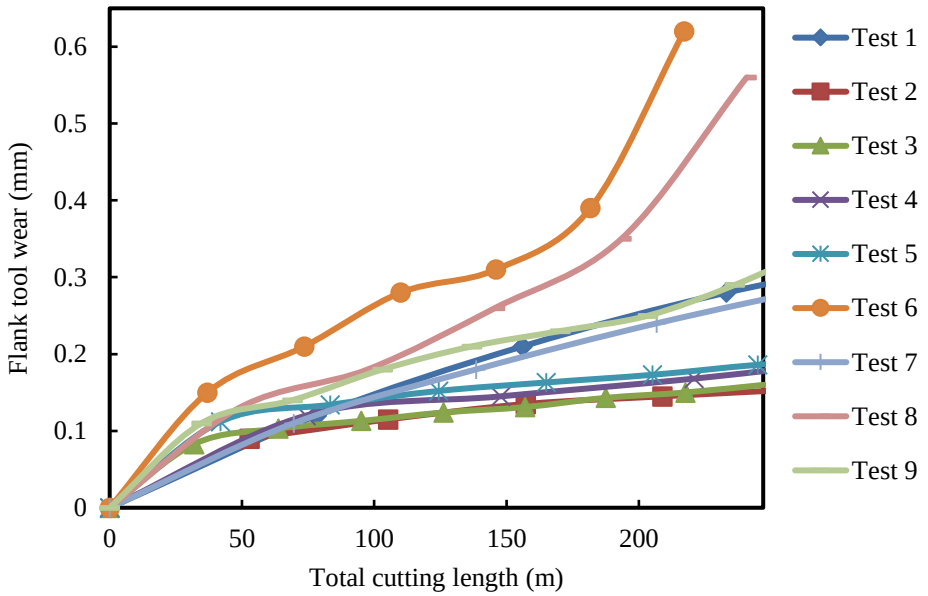

Figure 6-2 Tool wear progress during machining Ti-6Al-4V using MWNCTs nano-fluid

Analysis of variance (ANOVA) has been employed to study the machining design variables effects on the measured flank wear. It should be stated that ANOVA has been employed in previous studies [194, 195] , and it was an effective tool to clearly obtain the significant machining parameters affecting different machining characteristics. ANOVA results for the flank wear are listed in Table 6-1. It is revealed that weight percentage of added nano-additives is the main significant design variable affects the flank wear at 90% confidence level; however, cutting speed still has an acceptable statistical summation in comparison with the feed rate which can show the cutting speed effect on the induced tool wear (see Table 6-1).

Also, Figure 6-3 visually confirms the noticeable effect of cutting speed on the flank wear. Within the range of the investigated independent variables, the optimal levels were found to be cutting speed of 120 m/min, feed rate of 0.15 mm/rev and 4 wt. % of added MWCNTs (see Figure 6-3). It was also concluded that 4 wt. % and 2 wt. % of added MWCT reduced the flank wear by 49.4 % and 45%, respectively in comparison with the tests performed without any nano-additives (classical-MQL). Also, the modes of tool wear and their associated wear mechanisms are presented and discussed in this section. All micrographs of worn faces were captured at the end of cutting tests. The dominant wear modes when cutting under mist coolant without nano-additives were; excessive flank wear, crater wear, tool nose wear, and plastic deformation. Regarding the tests performed using nano-additives either using MWCNTs or Al_2O_3 nano-fluids, it was demonstrated that the dominant wear modes were; flank wear and crater.

The employed nano-fluids (i.e., MWCNTs) showed significant improvements in reducing both flank and crater wear compared to the tests performed without nano-additives as shown in Figure 6-4 and Figure 6-5, respectively. The crater wear is related to the diffusive wear mechanism as the rake face materials is dissolved into the generated chip due to the high-generated temperature during cutting processes (i.e., dissolution-diffusion) as discussed in a previous work [18]. On the other hand, the abrasion between the workpiece and the tool surface is main reason for the observed flank wear during cutting without MWCNTs. Regarding the employed nano-fluids significant effects, it is mainly due to the promising cooling and lubrication properties which enhance the interface bonding between tool and workpiece surfaces so that the abrasive wear severity is partially eliminated and the high-generated temperature is significantly decreased [26, 27].

Table 6-1 ANOVA results for flank wear (MWCNTs nano-fluid)

Source	Statistical Sum	Variance	F (Calculated)	P-Value
A	0.0701	0.0352	6.77	0.128
B	0.0128	0.0064	1.23	0.448
*C	0.1308	0.0654	12.58	0.073
Error	0.0104	0.0052		
Total	0.2246			
*Significant at 90% confidence level				

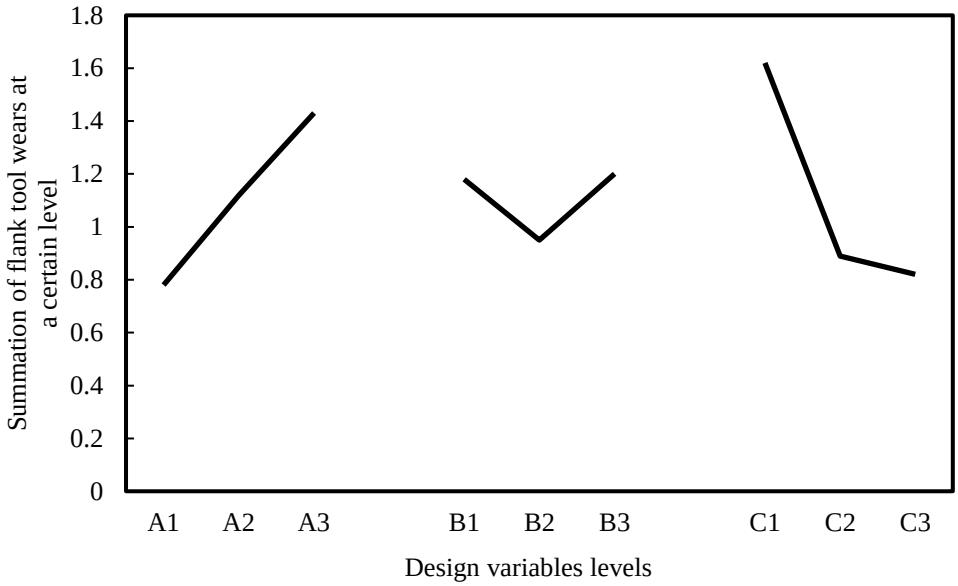

Figure 6-3 Plot of design variables effects for flank wear results

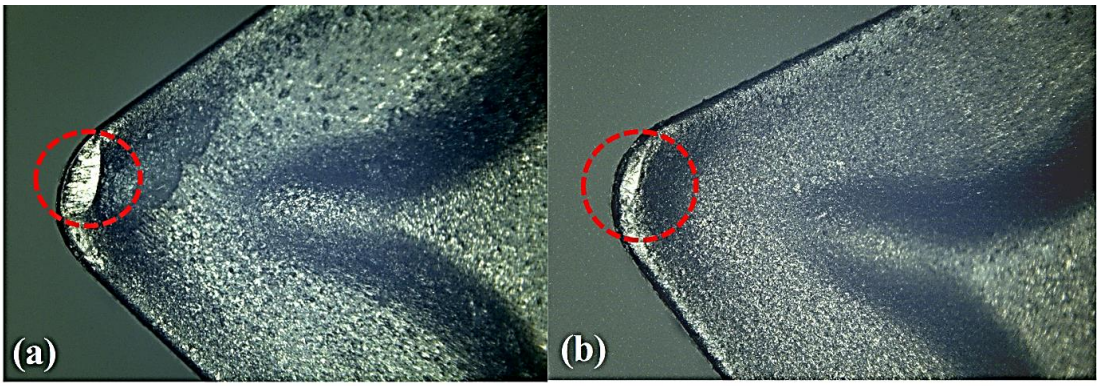

Figure 6-4 The observed crater wear at cutting speed of 170 m/min and feed rate of 0.15 mm/rev

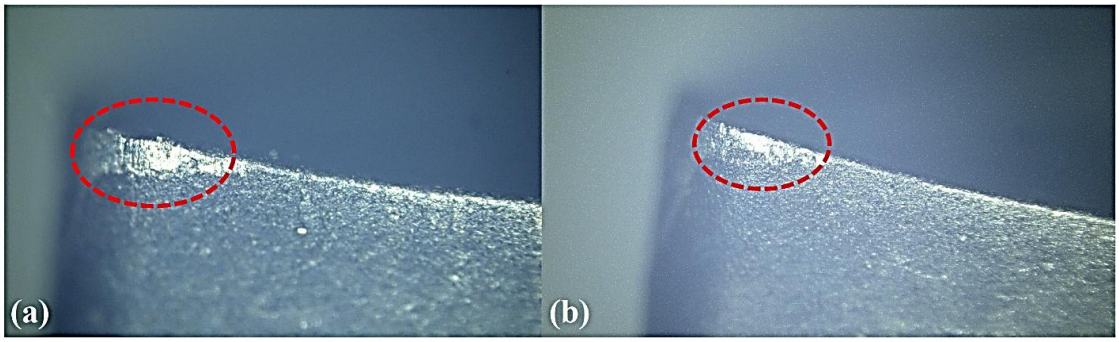

Figure 6-5 The observed flank tool wear at cutting speed of 170 m/min and feed rate of 0.1 mm /rev using; (a) without nano-additives, (b) 2 wt.% MWCNTs nano-fluid

Regarding the tool nose wear (see Figure 6-6 (a)), it is mainly attributed to an excessive localized damage on both the rake and flank faces appeared at the tool nose. It has been claimed in a previous study [196] that it is attributed to the abrasive wear mechanism because of the hard constituents in the workpiece material. Also, the plastic deformation was observed as can be seen in Figure 6-6 (b). It is mainly due to the high generated temperature as the thermal shock mechanism leads to softening the tool material and resulting in cracks developments and plastic deformation wear.

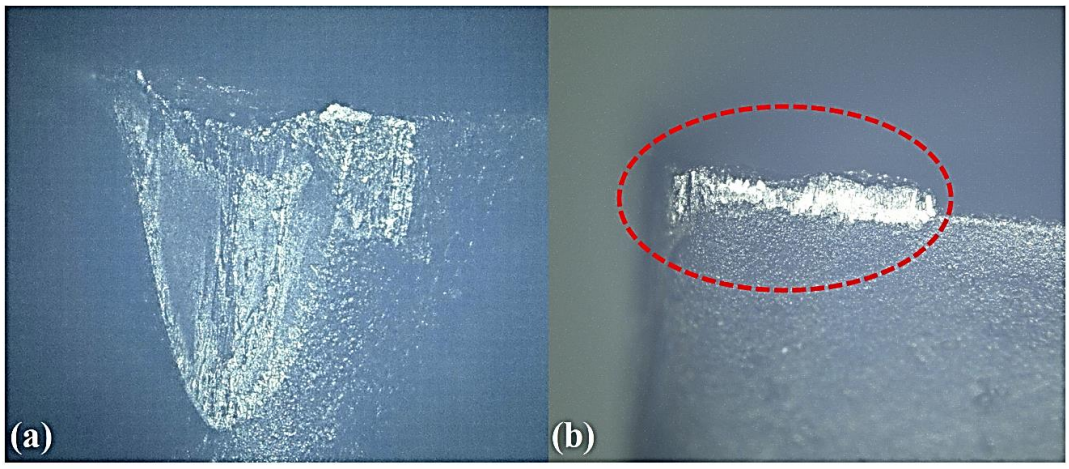

Figure 6-6 (a) the tool nose wear at cutting speed of 220 m/min, feed rate of 0.2 mm/rev and without nano-additives; (b) the plastic deformation at cutting speed of 120 m/min, feed rate of 0.15 mm/rev and 0 wt.% MWCNTs

6.3. Average Surface Roughness Results

The average surface roughness results are provided as shown in Figure 6-7. It is clear that MWCNTs nano-fluid shows promising results to improve the resultant surface quality; however, cutting tests 3 and 9 didn't show effective results compared to the other tests performed using nano-additives as these tests have been performed at the higher value of feed rate level (i.e., 0.4 mm/rev). Cutting test 4 showed the best surface quality. The cutting conditions of this test include cutting speed of 170 m/min, feed rate of 0.1 mm/rev and 2 wt. % of added MWCNTs.

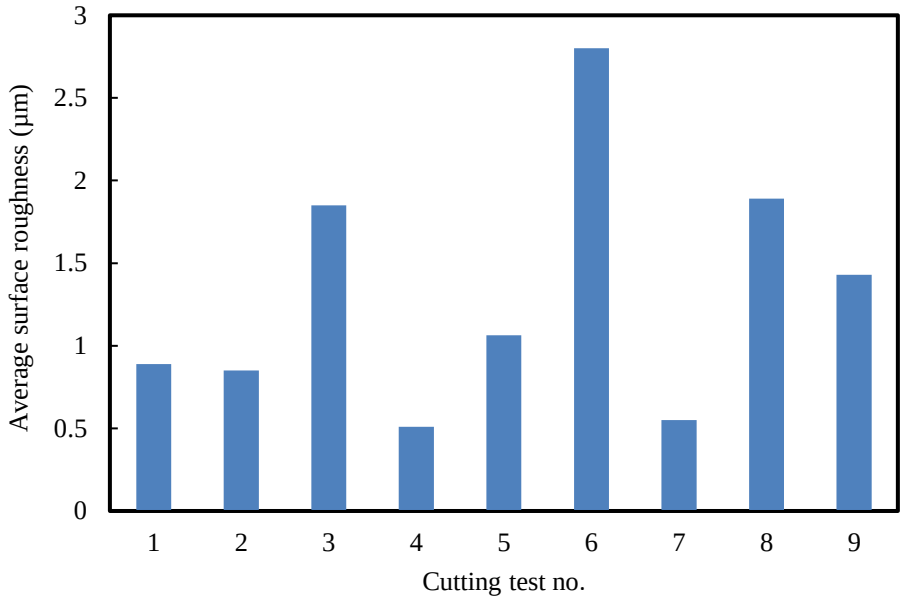

Figure 6-7 Average surface roughness results

ANOVA results are listed as shown in Table 6-2. Both cutting feed rate and wt. % of added nano-additives are the main significant design variables affecting the resultant surface quality at 90% confidence level. In addition, the plot of design variables effects is provided as shown in Figure 6-8. The cutting feed rate of 0.1 mm/rev, cutting speed of 120 m/min and 2 wt. % added nano-additives are the optimal design variables levels.

An improvement of 38 % is noticed for 4 wt. % of added MWCNTs in comparison with the tests performed without nano-additives, while 2 wt. % of added MWCNTs enhanced the surface quality by 50%. It can be noticed that increasing the added percentage of nano-additives usually results in higher thermal conductivity and better heat transfer performance; however, 2 wt. % MWCNTs offered better cutting performance than 4 wt. %. Thus, more investigations are needed in order to investigate the effect of nano-additives concentration on the tribological and heat transfer characteristics when machining with nano-fluids. Also, the nano-additives concentration and size effects on the thermal and frictional behavior should be emphasized. The cooling and lubrication properties of the nano-fluids improve the rake and flank regions' lubrication and wetting properties so that better heat dissipation could be achieved. Consequently, partially smoothed cutting processes is accomplished and better average surface roughness values are observed in comparison with the processes performed without any nano-additives as discussed previously [156, 180]. In addition, applying an appropriate lubrication and cooling system to the tool–workpiece interface area provides a viable role to reduce the coefficient of friction. Introducing the nano-cutting fluid system would decrease the induced friction and the machined surface roughness. This is mainly attributed to the significant tribological properties of the resultant nano-mist which decreases the friction at the tool– chip interface. Also, the nano-additives work as a spacers reducing the rubbing between the cutting tool and workpiece, as discussed previously [185]. The schematic of the lubrication/cooling system (MQL-nano-fluid) is provided in Figure 6-9. It can be seen that the nano-cutting fluid is atomized into the MQL nozzle and it results in a very fine mist. The resultant mist represents the nano-additives surrounded by a thin base fluid film. Thus, the droplets of the nano-cutting-fluid are formed on the workpiece and cutting tool surfaces and a tribo-film is also formed (see Figure 6-9) which significantly enhances the tribological characteristics and reduces the induced friction. In addition, increasing the added percentage of nano-additives results in higher thermal conductivity for the resultant nano-fluid and improves the heat transfer performance accordingly. However, in the current study, 2 wt. % MWCNTs nano-fluid offers better cutting performance than using 4 wt. %. This is mainly attributed to the ploughing mechanism (see Figure 6-9). When there is an abundance of nano-additives in the resultant nano-fluid, they collide with and are impeded by the

asperities on the work surface and hence generate higher cutting forces. As a result, the nano-additive induced wear is increased with increasing the nano-additives concretion as similarly discussed in a previous work [182]. Consequently, the resultant flank wear would increase and accordingly would affect the surface quality. On the other hand, as can be seen in Figure 6-9, increasing the nano-additives concentration means more nano-additives in the workpiece-interface area, and therefore the resultant friction would decrease since the employed mist serve as spacers in the cutting zone area. Based on above, it should be stated that the nano-additives concentration should be carefully selected and optimized in order to strike a balance between all previous considerations.

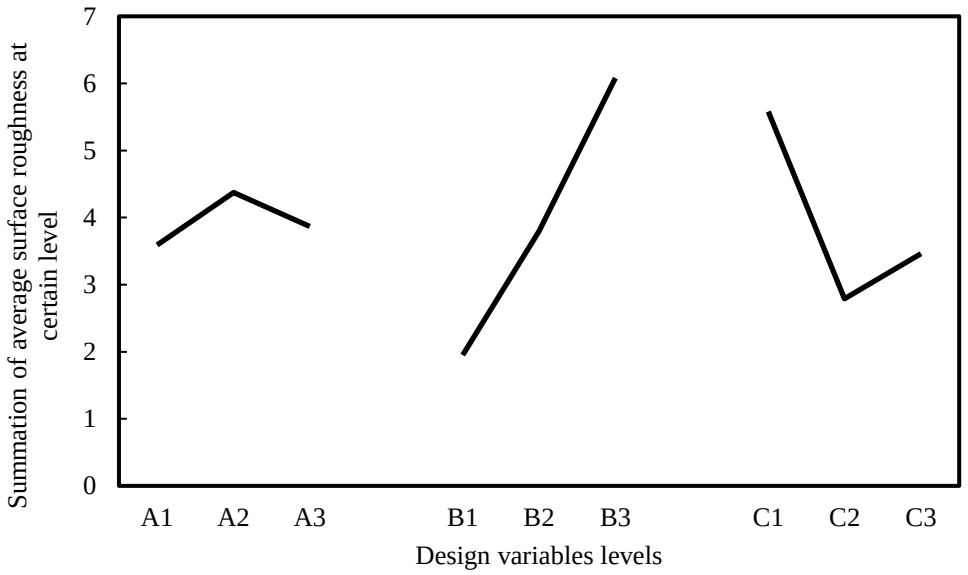

Figure 6-8 The plot of control variables effects on the measured surface quality

Table 6-2 ANOVA results for average surface roughness (MWCNTs nano-fluid)

Source	Statistical Sum	Variance	F (Calculated)	P-Value
A	0.1049	0.0524	0.664	0.608
*B	2.8528	1.4264	18.059	0.052
*C	1.4131	0.7065	8.94	0.1
Error	0.1579	0.0789		
Total	4.5289			

*Significant at 90% confidence level

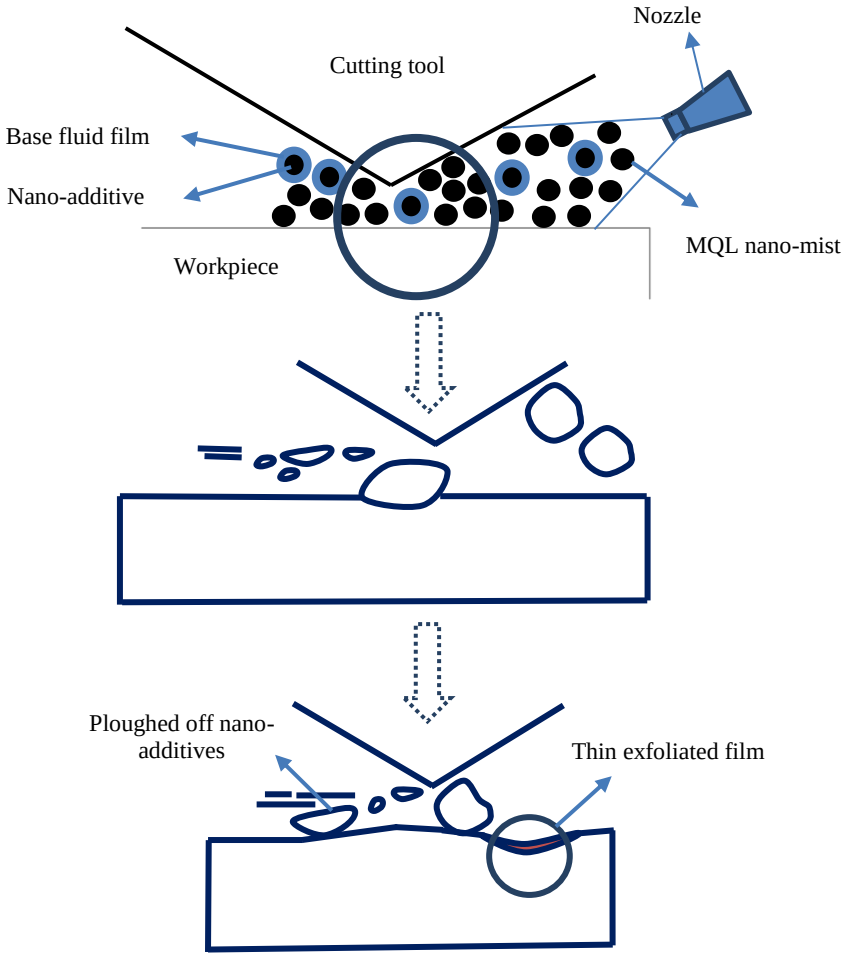

Figure 6-9 Schematic of the MQL-nano cutting fluid mechanism (rolling and ploughing)

6.4. Energy Consumption Results

The energy consumption results when using MWCNTs nano-fluid are provided in Figure 6-10. When 2 wt. % of added MWCNs is utilized, the results showed that cutting test 2 offered the lowest energy consumption. The cutting conditions at this test are cutting speed of 120 m/min and feed rate of 0.15 mm/rev. In general, MWCNTs nano-fluid has shown better performance in reducing the energy consumption compared to the tests performed without any nano-additives.

Due to the high induced friction occurred during machining difficult-to-cut materials, the higher frictional force component would lead to adhesive friction, and therefore the flow of chips will take place only within the workpiece (not at the tool–workpiece interface). Consequently, the deformed chip thickness would increase and accordingly the cutting ratio and shear angle would decrease. Therefore, the cutting force component required to remove the chip would significantly increase [197, 198]. Thus, applying an appropriate lubrication and cooling system to the tool–chip interface is required in order to reduce the induced coefficient of friction. The significant tribological properties of the resultant nano-cutting fluid could help in reducing the coefficient of friction at the tool–chip interface since the employed nano-additives work as spacers and decrease the induced rubbing between the cutting tool and workpiece (see Figure 6-9) [57, 185].

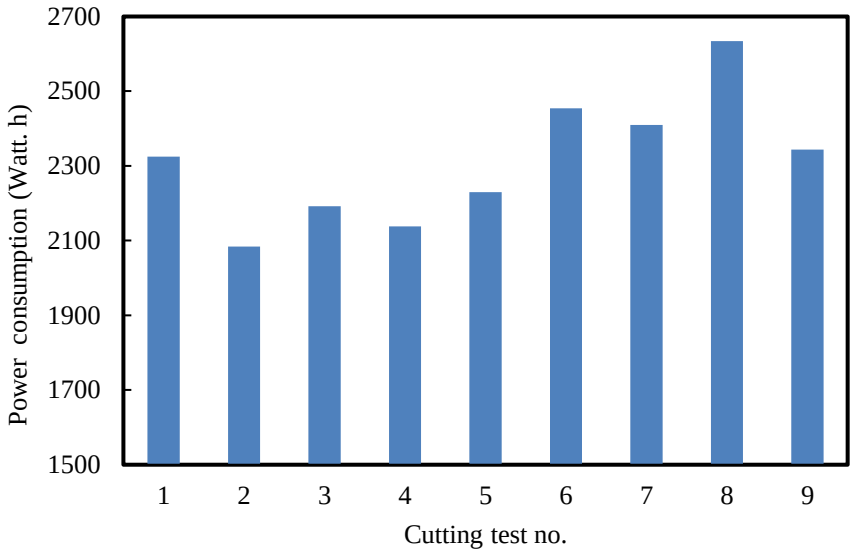

Figure 6-10 Energy consumption results

The ANOVA results (see Table 6-3) have shown that cutting speed and wt.% of added nano-additives were the main significant design variables affects the energy consumption at 99% confidence levels. In addition, the plot of the design variables effects is shown in Figure 6-11.

It is demonstrated that cutting speed of 120 m/min, feed rate of 0.1 mm/rev, and 2 wt.% of added nano-additives were the optimal levels which offer the lowest energy consumption when MWCNTs nano-fluid was employed. However, the cutting feed rate has not shown any significant effects (see Figure 6-11 and Table 6-3). From Figure 6-11, it can be concluded that of 4 wt.% of added MWCNTs reduced the energy consumption by 7.9% compared to the tests performed without nano-additives (i.e. C3 vs. C1), while 2 wt.% of added MWCNTs reduced the generated power by 11.5% (i.e. C2 vs. C1).

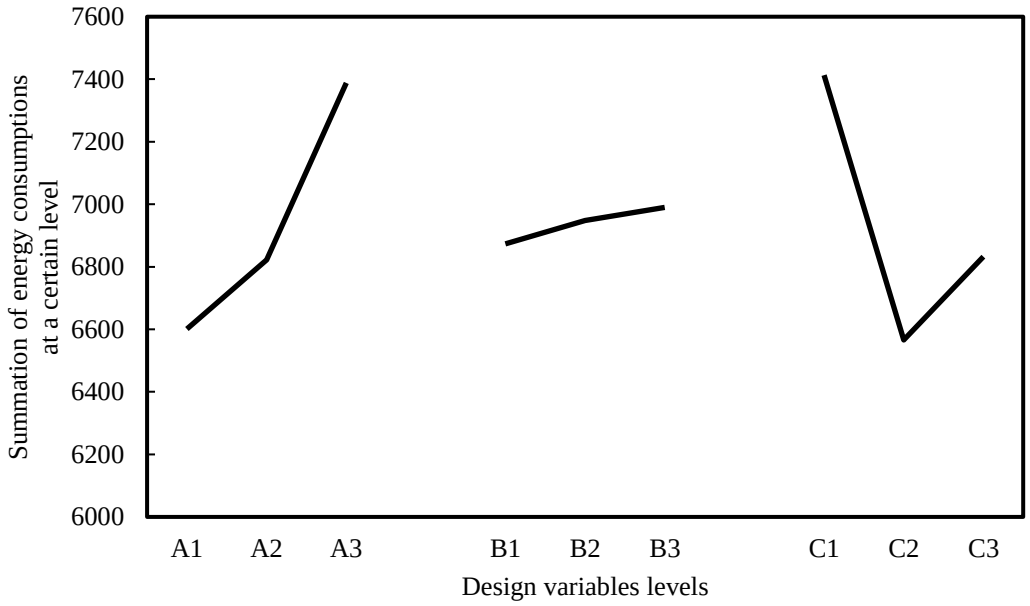

Figure 6-11 Plot of design variables effects on energy consumption results

Table 6-3 ANOVA results for energy consumption (MWCNTs nano-fluid)

Source	Statistical Sum	Variance	F (Calculated)	P-Value
*A	109840.6	54920.3	143.64	0.006
B	2342	1171	3.06	0.246
*C	125080.7	62540.35	163.57	0.005
Error	764.6	382.33		
Total	238028			

*Significant at 99% confidence level

However, increasing the added percentage of nano-additives increases the resultant nano-fluid thermal conductivity and accordingly improves the heat transfer performance, 2 wt. % offered less energy consumption than 4 wt. %. This finding could be attributed to the nano-additives dispersion into the base fluid (e.g. agglomeration, clogging, or sedimentation); however, zeta potential results offered an acceptable performance for both nano-additives percentages as has been mentioned earlier (see Table 4-4). On the other hand, 4 wt. % MWCNTs offered better results in reducing the flank wear compared to 2 wt. % of added MWCNTs. Thus, more investigations need to be focused on the effect of nano-additives concentration on the nano-cutting-fluid tribological and heat transfer mechanisms in order to physically justify why 2 wt. % nano-fluid occasionally offers better cutting performance than 4 wt. % nano-fluid.

6.5. ANOVA Verification

Similarly, to chapter 5, the ANOVA verification results have been determined using equation (5.1) as shown in Table 6-4. Good agreement can be noticed between the predicted and experimental optimal results.

Table 6-4 ANOVA verification results

Machining response	Experimental value	Predicted value	Accuracy %
Flank wear (mm)	0.16	0.163	98%
Surface roughness (μm)	0.51	0.45	89.3%
Energy consumption (watt)	2085	2077	99.6%

6.6. Machining Quality Characteristics Modeling

Similarly, to Chapter 5, RSM technique is employed to model the studied cutting processes. The developed models using MWCNTs nano-fluid for flank wear, average surface roughness, and energy consumption are provided as shown in equations (6.1-6.3), respectively. The design variables quadratic and interaction effects are used to express the developed model since all studied design variables have three levels (2^{nd} degree of freedom). The average model accuracy for the flank wear model under using MWCNTs nano-fluid is about 89.31%. The proposed model for the average surface roughness achieves an average model accuracy of 93.7%, while 98.6% average model accuracy is calculated for the energy consumption model. The 3-D surface plots for flank wear, surface roughness, and energy consumption when using MWCNTs-nano-fluids are provided as shown in Figures 6-12, 6-13 and 6-14, respectively.

$$VB_3 = 7.2\,E-06\,A^2 + 10.96\,B^2 + 188.6\,C^2 - 7\,E-03\,AB - 2.2\,E-03\;AC - 94\,BC + 0.22 \quad (6.1)$$

$$Ra_3 = 8.6\,E-06\,A^2 + 58.32\,B^2 + 1480.65\,C^2 - 2\,E-03\,AB - 0.21\,AC - 268.55\,BC + 0.27 \quad (6.2)$$

$$PC_3 = 0.01\,A^2 - 2579.76\,B^2 + 399783\,C^2 - 0.35\,AB - 75.26\,AC - 52343\,BC + 2071.63 \quad (6.3)$$

As can be seen in Figures 6-12 (b) and 6-12 (c), increasing MWCNTs percentage results in decreasing the flank wear. Also, Figures 7-12 (b) and 7-12 (c) showed an agreement with the results obtained in Figure 6-3 as both of them confirmed that 4 wt.% MWCNTs provides the lowest flank wear. In addition, 7-12 (b) confirmed the previous findings in Table 6-1 and Figure 6-3 since changing the cutting speed levels showed significant effects on the flank wear results.

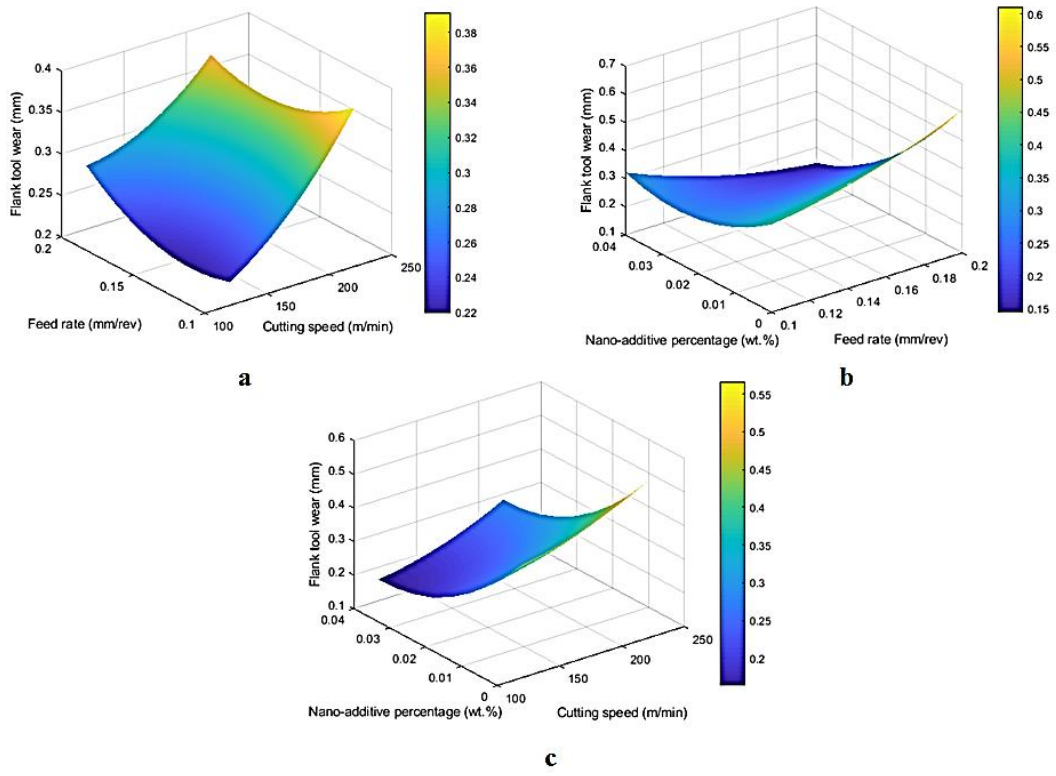

Figure 6-12 3-D surface plots for the flank wear model using MWCNTs-nano-fluids

From Figure 6-13 (b) and 6-13 (c), it was found that 2 wt. % provided the lowest surface roughness values. This finding is in agreement with the results obtained in Figure 6-8. Also, as can be seen in Figure 6-13 (a), the feed rate showed significant effect on the surface roughness values; however, the cutting speed did not show noticeable effects. This finding is consistent also with the surface roughness ANOVA results presented in Table 6-2.

From Figure 6-14 (a) and 6-14 (c), it was found that 2 wt. % provided the lowest energy consumption values. This finding is in agreement with the results obtained in Figure 6-11. Also, as can be seen in Figure 6-14 (b), the cutting speed showed significant effect on the energy consumption values; however, the feed rate did not show noticeable effects. This finding is consistent also with the energy consumption ANOVA results presented in Table 6-3.

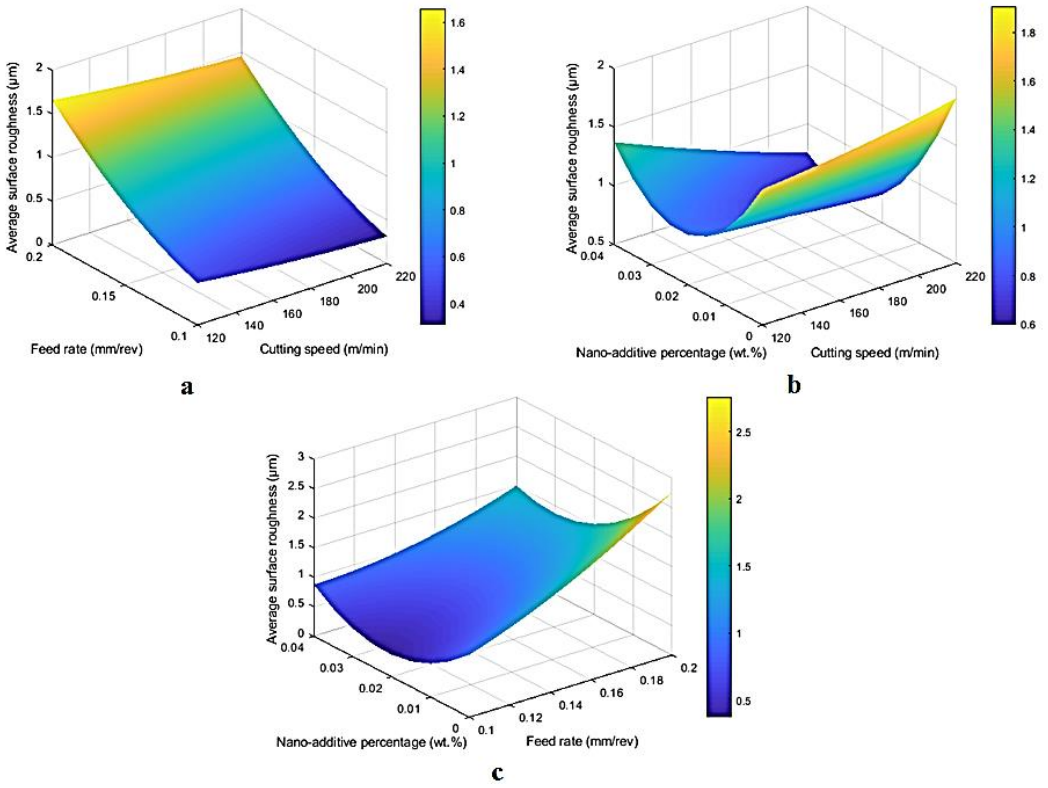

Figure 6-13 3-D surface plots for the surface roughness model using MWCNTs-nano-fluids

6.7. Chip Morphology Examination

Another investigation to evaluate the effects of the employed nano-fluids on the Ti-6Al-4V machining performance is the examination of chip morphology in order to provide details about the effects of dispersed MWCNT in the chip-tool interface area.

Regarding the tests performed without nano-additives, serrated chip or saw-tooth-like appearance (see Figure 6-15 (a)) are generated due to the non-uniform strain on the material during the cutting process (existence of low and high shear strain zones). In addition, it is usually observed when machining low-thermal-conductivity materials such as Ti-6Al-4V [199]. In the majority of cutting tests done using MWCNTs nano-fluid, wider saw-tooth spaces have been observed compared with the tests performed without nano-additives as shown in Figures 6-15 (b) and 6-15 (c). It is mainly due to forming a thin nano-mist layer between chip and tool rake face which enhances the heat dissipation performance. During cutting test 7, the non-homogenous serrated chips have not been observed as shown in Figure 6-15 (d), and it could be attributed to employing a higher percentage of added MWCNTs (i.e., 4 wt. %) which increases the induced heat convection coefficient and improves the heat dissipation performance.

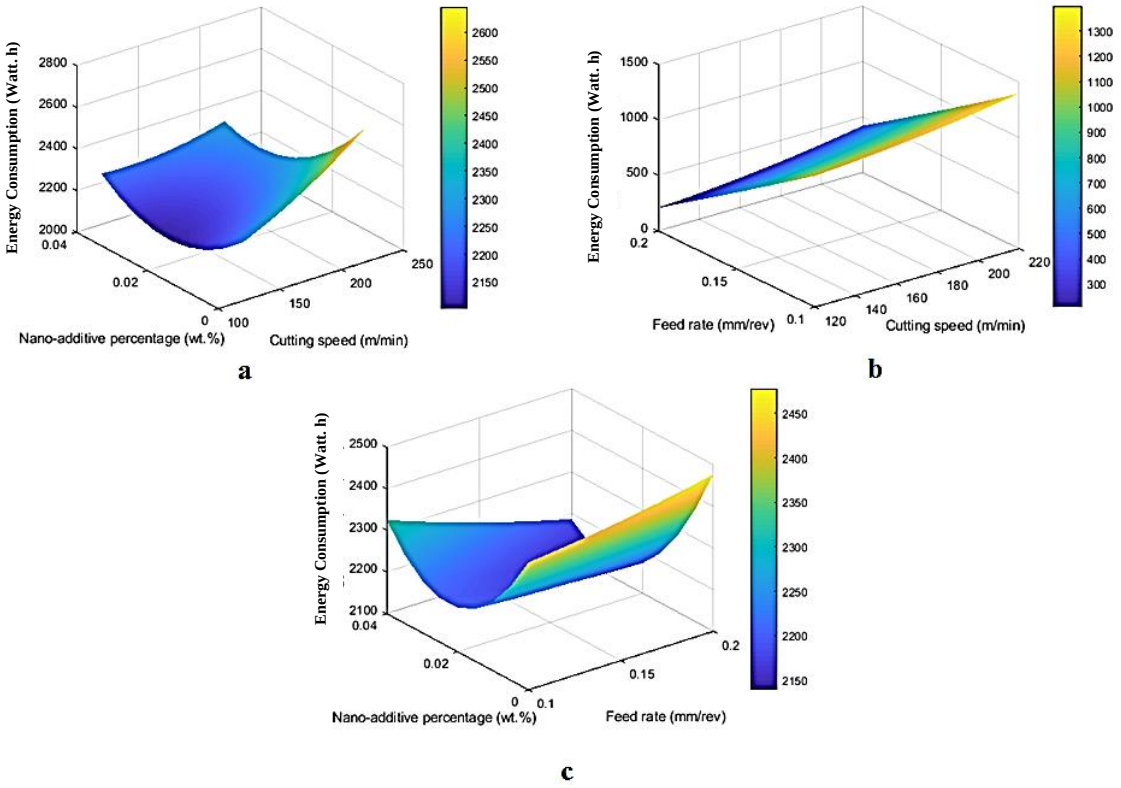

Figure 6-14 3-D surface plots for the energy consumption model using MWCNTs-nano-fluids

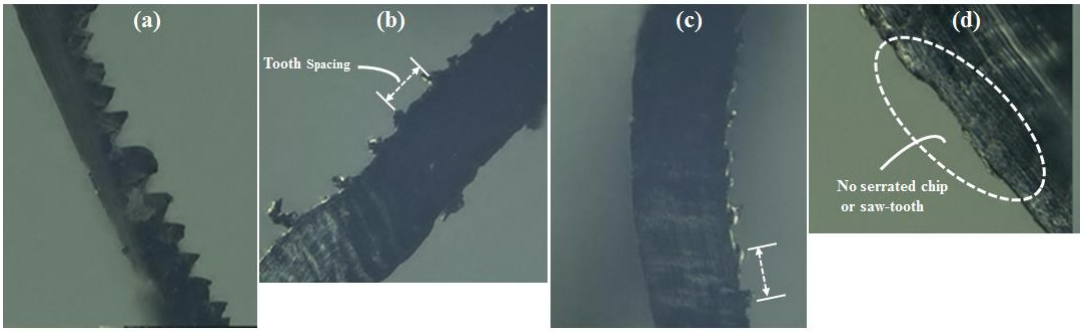

Figure 6-15 Micrographs of the generated chips; (a) without nano-additives, (b) at cutting test 2, (c) at cutting test 4 and (d) at cutting test 7

Also, the deformed chip thickness was measured for different cases during cutting Ti-6Al-4V alloy with/without MWCNTs nano-fluid, and the results were plotted at different feed rate levels as provided in Figure 6-16. The deformed chip thickness has been measured by analysis of micrographs captured using a digital optical microscope (KEYENCE VHX-1000) and ImageJ software under different feed rate levels. The cutting tests performed without nano-additives showed the highest chip thickness due to the chip welding tendency to the top surface layers of the tool rake face. Based on the results provided in Figure 6-16, lower deformed chip thickness has been obtained when using either 4 wt. % or 2 wt. % MWCNTs. It is mainly attributed to the effective cooling and lubrication properties upon using MQL-nano-fluid which help in reducing the severity of the chip welding tendency.

The chip thickness reduction would lead to shorter shear plane and larger shear angle. Thus, lower cutting force [187] and induced friction coefficient [188] would occur as similarly discussed in previous studies. Furthermore, the chip breakability mechanism would be enhanced [189]. On the other hand, the chip thickness results showed that 4 wt. % offered lower deformed thickness than 2 wt. %; however, 2 wt. % offered better surface quality. Thus, studying and analyzing the nano-cutting fluid tribological and heat transfer mechanisms are required in order to physically emphasize this concern, and understand the machining processes with MQL-nano-fluid.

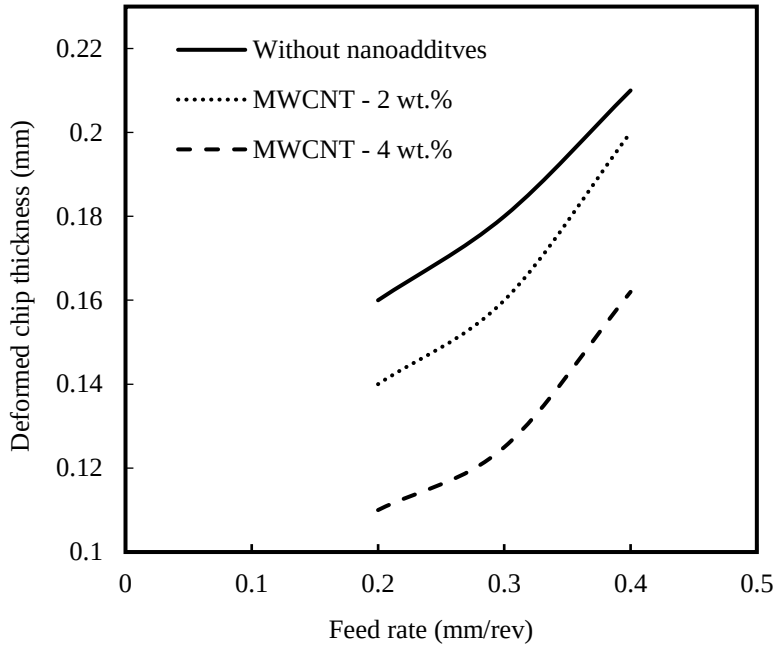

Figure 6-16 Effect of feed rate on the deformed chip thickness during machining Ti-6Al-4V with/without MWCNTs nano-fluids

6.8. Summary

In this chapter, MWCNTs nano-fluid has been employed during machining Ti-6Al-4V in order to study their influence on several cutting quality characteristics, namely; tool wear, surface roughness, energy consumption and chip morphology. The chapter findings are concluded as follows:

- Regarding the flank tool wear, average surface roughness and energy consumption results analysis, it is demonstrated that percentage of added nano-additives is a significant design variable through using ANOVA;

- It is observed that MWCNTs nano-fluid offers promising results in terms of tool wear, average surface roughness, and energy consumption;

- 4 wt.% added MWCNT is the optimal level for flank tool wear results; however, 2 wt.% nano-fluid offers better performance than 4 wt.% nano-fluid for both energy consumption and average surface roughness results;

- More investigations need to be focused on the effect of nano-additives concentration and size effects on the nano-fluid tribological and heat transfer mechanisms in order to physically justify why 2 wt. % nano-fluid offers occasionally better cutting performance than 4 wt. % nano-fluid;

- Three mathematical models have been developed for the studied cutting responses based on the studied design variables range and acceptable average model accuracy has been demonstrated for each proposed model;

- The dominant wear modes noticed for the cutting tests performed without nano-additives are; flank wear, crater wear, tool nose wear and plastic deformation. MWCNT nano-fluid has shown promising results in enhancing the cutting tool performance;

- In the majority of cutting tests done using MWCNTs nano-fluid, wider saw-tooth spaces have been observed compared with the tests performed without nano-additives due to forming a nano-mist layer between chip and tool rake face which enhances the heat dissipation performance. During cutting test 7, the non-homogenous serrated chips have not been observed, and it could be attributed to employing a higher percentage of added MWCNTs which increases the induced heat convection coefficient and enhances the heat dissipation performance;

- In addition, higher chip thickness values have been observed during the cutting tests conducted without nano-additives in comparison with the tests performed using MWCNTs nano-fluid. Thus, the chip morphology investigation also demonstrates the cooling and lubrication significant effects of the proposed nano-fluid on Ti-6Al-4V machining performance;

It is concluded that MWCNTs nano-fluid improves the thermal and tribological properties of the resultant nano-fluid compared with the base fluid, and hence promising cooling and lubrication properties are observed which accordingly affect the machining performance of Ti-6Al-4V (i.e., tool wear behavior, surface quality, and energy consumption);

Chapter 7 Nano-Cutting Fluids Tribological and Heat Transfer Mechanisms

7.1. Preamble

As yet, different nano-additives have been identified by advancements in modern technology of nano-lubricants which can afford lubricity along a varied range of temperatures [200, 201]. The nano-lubrication performance is mainly related to the quantity, structure, and morphology of the added nano-additives, and the way that resultant nano-fluids get presented to the tool–chip interface area [145]. The nano-cutting fluid usage showed effective results to decrease the induced friction between two contact surfaces. [202]. On the other hand, the physical analysis of nano-lubricants [141] demonstrates that dispersed nano-additives can easily penetrate into the rubbing surfaces and have a large elasto-hydro-dynamic lubrication effect. Also, nano-cutting fluids offered effective cooling capabilities which could withstand the high generated temperatures especially during cutting difficult-to-cut materials [203, 204]. In order to provide a solid physical understanding of the cutting processes using nano-fluids, this chapter is focused on studying and analyzing the nano-cutting fluid tribological mechanisms during machining processes.

Also, in this chapter, analyzing the nano-cutting fluid tribological and heat transfer mechanisms is presented and discussed through a comparative performance analysis between MWCNTs and Al_2O_3 nano-cutting fluids. Two proposed models are developed; the first model is discussing the induced wear by nano-additives, while the second model is investigating the nano-cutting fluids effects on the heat transfer characteristics. The proposed models findings provide a clear physical evidence which proves that MWCNTs nano-fluid offers better tribological and heat transfer characteristics than Al_2O_3 nano-fluids.

7.2. MQL Nano-Cutting Fluid Mechanisms

Nano-additives dispersed in lubricant are a novel engineering material consisting of nanometer-sized additives dispersed in a base fluid. It is an effective method of reducing the friction between two contact surfaces through the rolling effect of nano-additives. However, nano-additives are expected to be able to withstand high temperatures during machining, in addition to non-toxicity, ease of applicability and cost effectiveness. Nano-lubricant efficiency depends on morphology, crystal structure, size, quantity and the way nanoparticles are introduced to the tool-workpiece interface [145]. As mentioned before, using nano-additives with vegetable oil as a base cutting fluid under using MQL system could establish two desired objectives; enhancing the machining quality characteristics since nano-additives improve the friction and thermal behavior, and accomplishing a sustainable process as using MQL with vegetable oils provide effective environmental benefits. Thus, understanding the MQL nano-fluid mechanisms is so important. Two main mechanisms are concluded from different literature studies; rolling and ploughing mechanisms.

7.2.1. Rolling Mechanism

The rolling MQL nano-fluid mechanism is defined as following [205]:

- By applying a source of compressed air, the nano-cutting fluid is atomized into the MQL nozzle and it results in a very fine mist;

- The resultant mist represents the nano-additives surrounded by a thin base fluid film. This mist could penetrate the cutting zone as its velocity is significantly larger than cutting tool velocity since it can pass through the tool pores and grain fractured groves;

- Thus, the droplets of the nano-cutting-fluid are formed on the workpiece and cutting tool surfaces and a tribo-film is also formed which significantly enhances the tribological characteristics and reduces the induced friction;

- Due to the increasing of nano-additive concentration, which increases the number of nano-additives at the tool-workpiece interface; these nano-additives perform a vital role as spacers, eliminating the contact between the tool and workpiece. A schematic for the rolling mechanism is provided as shown in Figure 7.1;

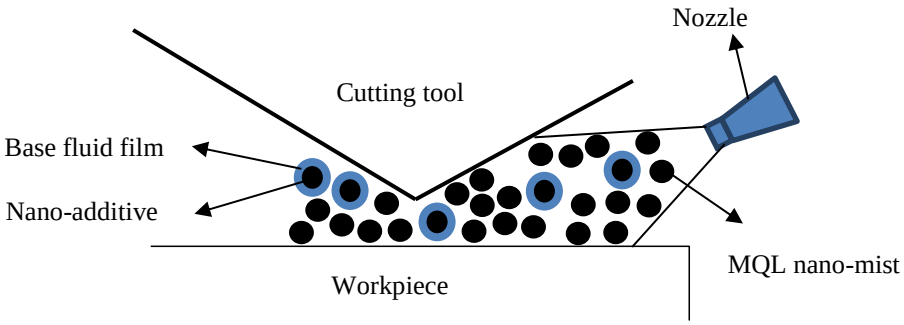

Figure 7-1 Schematic of the rolling MQL-nano cutting fluid mechanism

7.2.2. Ploughing Mechanism

The ploughing MQL nano-fluid mechanism is concluded as following:

- When the nano-fluid is dispersed in the cutting zone, a number of nano-additives are embedded into the machined surfaces. Some nano-additives have a rolling effect while others are sheared from the very high pressure in the cutting zone [139];

- Due to the high compression with increasing the nano-additives concertation, the nano-additive shape is changed and shearing would be more intense. Some of the nano-additives are partially ejected by other additives that left the nozzle into the cutting zone;

- The ploughed-off nano-additives left thin exfoliated film on the contact area due to the high loading damage as mentioned before in a previous study [206]. Meanwhile, at higher concentrations, the nano-additives that filled the surface cavity were sheared off by other nano-additives. Thus, when there is an abundance of nano-additives in the resultant cutting fluid, they collide with, and are impeded by the asperities on the work surface and hence generate higher cutting forces;

- Since the ploughed-off nano-additives left thin exfoliated film on the contact area due to the high contact resistance and the extreme pressure at the cutting zone, the formation of a protective nano-additive thin film (a chemical reaction layer) on the machined surface could be noticed and that prevents the induced cutting temperature from dissipating into the workpiece material. As a result, large amounts of heat generated in the cutting zone alter the elasto-hydrodynamic lubrication to boundary lubrication. A schematic for the ploughing mechanism is provided as shown in Figure 6-9;

- Therefore, due to the nano-additive extreme pressure in the resultant nano-cutting fluid and existence of a gap between tool–workpiece interfaces, nano-additives provide high contact resistance which helps in forming a chemical reaction film on the workpiece surface (see Figure 7-2). The increase of nano-additives concentration increases the growth of the thin protective film on the machined surface as has been discussed in a previous study [207];

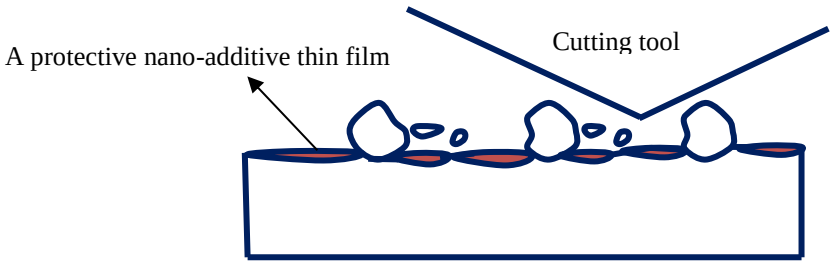

Figure 7-2 The formation of a protective nano-additives thin film

7.2.3. Nano-Cutting Fluid Wear Mechanism

Nano-additives ploughing on the surface can induce abrasive wear that is proportional to the cross section of nano-additives to surface interference as shown in equation (7.1) which has been developed in a previous study [182]. The wear schematic is also provided as shown in Figure 7-3 where V_{NA} is the wear volume induced by nano-additive, L is sliding distance, $n_p(y)$ is the number of nano-additives per nominal area of contact, ø is size distribution of nano-additives, A_{CS} is interference cross sectional area of nano-additive with surface, D is the nano-additive size, and ω is the nano-additive indentation.

During the cutting process using nano-cutting fluid, the induced nano-additive wear can be categorized into three cases:

- The nano-additive induced wear is greater than the cutting tool wear
- The nano-additive induced wear is less than the cutting tool wear
- The nano-additive induced wear is equaled to the cutting tool wear

$$\frac{V_{NA}}{L} = \int_{d}^{\infty} n_p(y)\, \phi(y)\, A_{CS}\, dy \qquad (7.1)$$

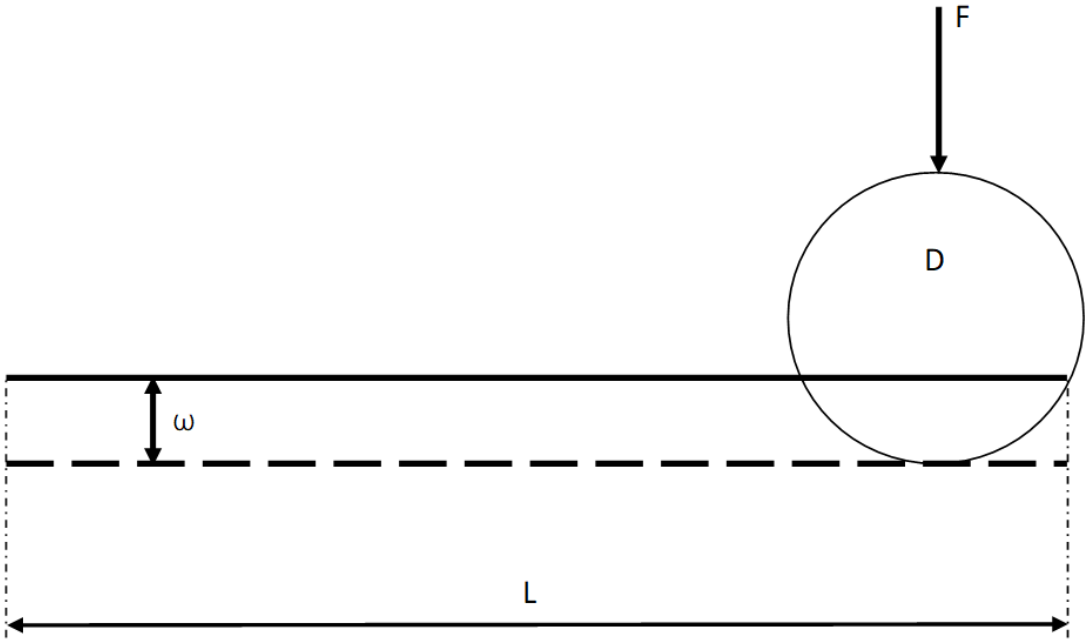

Figure 7-3 The nano-additive abrasive wear schematic

During the first case where the nano-additives induced wear is greater than the cutting tool wear, the nano-additives (wt. %) would increase the induced wear. Regarding the second case where the nano-additive induced wear is less than the cutting tool wear, the nano-additive (wt. %) would not change the wear practically. The mending effect could be observed in the third case as the nano-additives induced wear is almost equal to the cutting tool wear. The induced nano-additives wear categories offer a clear understanding of the ploughing and rolling mechanisms occurrence conditions. As long as the induced nano-additive wear is less than the cutting tool wear, it means that the dominant mechanism is rolling. On the other hand, if the induced nano-additive wear is greater than the cutting tool wear, it means that the dominant mechanism is ploughing. While the mending effect represents a critical condition between the ploughing and rolling effects.

7.2.4. Effects of Nano-Additives Concentration

Depending on the nano-additive rolling mechanism which has been discussed earlier, the increasing of nano-additives concentration would lead to increase the number of nano-additives at the tool-workpiece interface, and therefore these nano-additives would serve as spacers, eliminating the contact between tool and workpiece. As a result, the induced coefficient of friction would be decreased. This investigation confirms the same findings presented in a previous study (see Figure 7-4) [182]. On the other hand, when there is an abundance of nano-additives in the resultant nano-fluid, they collide with and are impeded by the asperities on the work surface (i.e., ploughing mechanism), and hence that generates higher cutting forces. As a result, the nano-additive induced wear is increased with increasing the nano-additives concretion as similarly discussed in the same mentioned study [182] (see Figure 7-4).

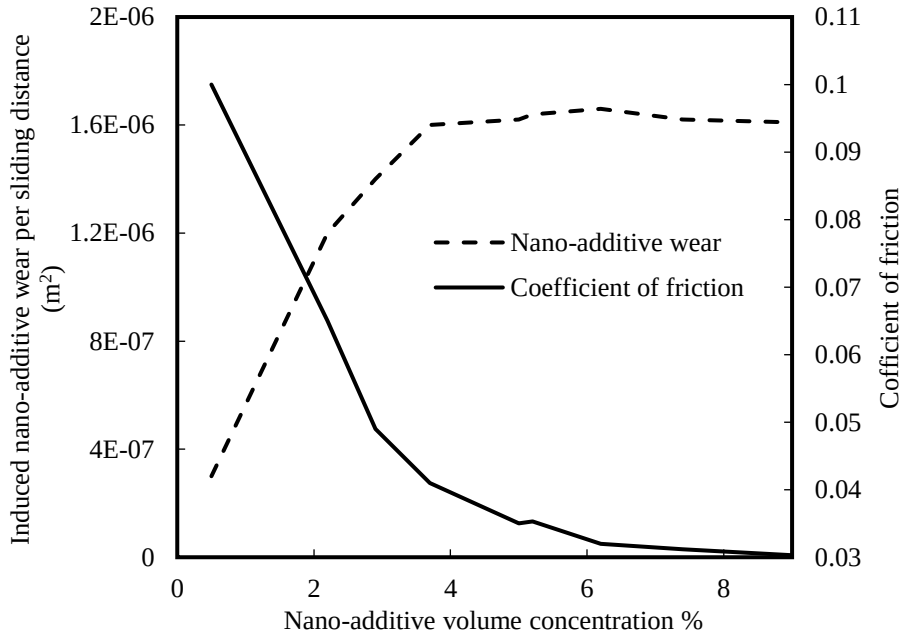

Figure 7-4 The induced nano-additive wear and coefficient of friction versus nano-additives concentration [182]

7.2.5. Effect of Nano-Additives Size

A previous study [208] found that the nano-additives ploughing effect rather than its rolling effect is predominant for larger size nano-additives, and it causes more craters, scratches, and grooves on both surface than that for small size nano-additives, and therefore the former would have higher surface roughness values. The previous investigation has discussed two main aspects; (a) the relationship between the nano-additive size and the ploughing and rolling occurrence conditions, and (b) the nano-additive size effects on the induced friction. The first aspect does not confirm the physical interpretation revealed through the proposed nano-additive wear model obtained in equation (7.1). According to equation (7.1), the nano-additive induced wear is directly proportional to the number of nano-additives per nominal area of contact ($n_p(y)$) which could be expressed as shown in equation (7.2). In this equation, d is the separation distance between the workpiece and cutting tool surfaces,N_{NA} is Number of nano-additives, $A_N$is the nominal area, ρ_e is the resultant nano-fluid density,ρ_{NA} is the nano-additive density, and $Vol_{NA}$is the nano-additive volume.

In addition, the nano-additive induced wear is directly proportional with interference cross-sectional area of nano-additives($V_{NA} \alpha A_{CS}$). From equations (7.1) and (7.2), it can be concluded that the induced nano-additive wear is inversely proportional to the nano-additive volume($V_{NA} \alpha N_{NA} \alpha \frac{1}{Vol_{NA}}$). Thus, in case of nanoparticles, the nano-additive induced wear is inversely proportional to the nano-additive diameter ($V_{NA} \alpha N_{NA} \alpha \frac{1}{D^3}$). Similarly, in case of nano-tubes, the nano-additive induced wear is inversely proportional to the nano-additive diameter at constant nanotube length ($V_{NA} \alpha N_{NA} \alpha \frac{1}{D^2 l}$).

$$n_p(d) = \frac{N_{NA}}{A_N} = \frac{\rho_e wt.\%\ d}{100\ \rho_{NA} \int_0^\infty Vol_{NA}\ \phi(D)\ dD} \tag{7.2}$$

On the other hand, in case of nanoparticles, the interference cross-sectional area of nano-additive would be approximately circular, so the nano-additive induced wear is directly proportional to the nano-additive diameter(V_{NA} α A_{CS} α D^2). Similarly, in case of nano-tubes, the nano-additive induced wear is directly proportional to the nano-additive diameter at constant nanotube length (V_{NA} α A_{CS} α Dl). The previous analysis schematic has been summarized as shown in Figure 7-5. Thus, it can be generally concluded that the nano-additive induced wear is inversely proportional to the nano-additive diameter for both cases; nano-particles or nano-tubes (V_{NA} α $\frac{1}{D}$).

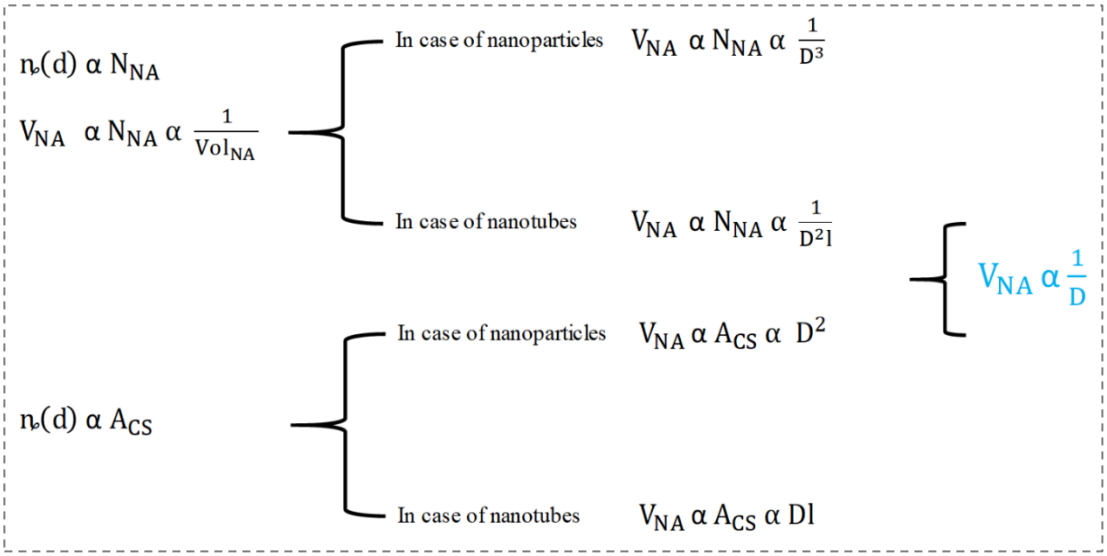

Figure 7-5 The nano-additive size effects analysis on the induced nano-additive wear for both cases; nano-particles and nano-tubes

As a result of the current analysis, using larger nano-additive would decrease the nano-additive wear and accordingly decrease the ploughing occurrence conditions. Some previous works [203, 204] studied experimentally the nano-additive size effects on the nano-additive induced wear and their results confirm that the nano-additive induced wear is inversely proportional to the nano-additive diameter as shown in Figure 7-6.

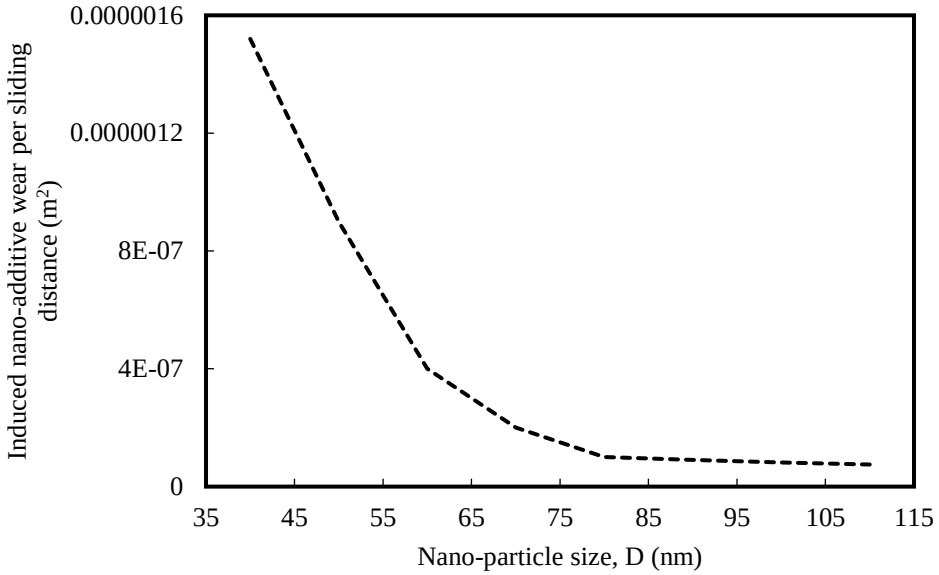

Figure 7-6 Nano-particles size effects on the induced nano-particles wear [182]

Although increasing the nano-additive size leads to decrease the nano-additive wear, it would decrease the number of nano-additives per nominal area which would accordingly lead to increase the induced friction. This investigation meets the same finding discussed by Choi, et al. [208] and Rahmati, et al. [139]. In addition, a previous work [182] studied the nano-additive size effects on the induced coefficient of friction and it confirms with the same previous findings (see Figure 7.7). Finally, it should be stated that the nano-additives concentration and size parameters should be controlled and optimized in order to avoid the drastic ploughing effects and high induced friction.

7.3. The Induced Nano-additive Wear Model

In this section, a comparative performance analysis between MWCNTs and Al_2O_3 in terms of the induced nano-additive wear is proposed and discussed.

The ratio between n_{NP} to n_{NT} at same nano-additive distribution, weight percentage, diameter and separation distance is provided as shown in equation (7.3).

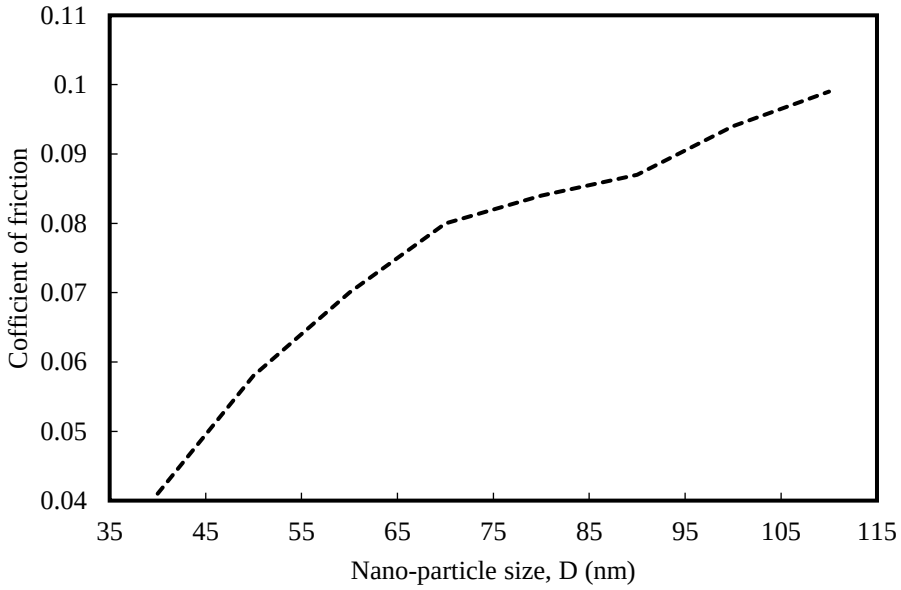

Figure 7-7 Nanoparticles size effects on the induced coefficient of friction [182]

$$\frac{n_{NP}}{n_{NT}} = \frac{\rho_{sol-NP}\,\rho_{NT}\,l\int_0^{\infty}\frac{\pi}{4}D^2\,\phi(D)\,dD}{\rho_{sol-NT}\,\rho_{NP}\int_0^{\infty}\frac{\pi}{6}D^3\,\phi(D)\,dD} \tag{7.3}$$

In addition, nano-additives are assumed to have a normal Gaussian size distribution which is characterized by nano-additive average size and standard deviation as shown in equation (7.4).

$$\phi(D) = \frac{1}{6_{avg}\sqrt{2\pi}}\exp[-0.5(\frac{D - D_{avg}}{6_{avg}})^2] \tag{7.4}$$

By approximation, the integration portion ratio in equation (7.2) can be numerically simplified as shown in equation (7.5):

$$\frac{\int_0^{\infty} \pi D^2 \, \phi(D) \, dD}{\int_0^{\infty} \pi D^3 \, \phi(D) \, dD} \approx \frac{1}{D} \tag{7.5}$$

Moreover, for nano-additives weight percentage up to 6 wt. % (which is commonly used limit in the previous studies), the nano-fluid density ratio $\left(\frac{\rho_{sol-NP}}{\rho_{sol-NT}}\right)$ given in equation (7.2) can be simplified as shown in equation (7.6)

$$\frac{\rho_{sol-NP}}{\rho_{sol-NT}} \approx 1 \tag{7.6}$$

From equations 7.5 and 7.6, $\frac{n_{NP}}{n_{NT}}$ can be simplified as shown in equation (7.7) where l and D should be in mm, and $\frac{\rho_{NT}}{\rho_{NP}}$ is the nano-tube to nanoparticle density ratio is:

$$\frac{n_{NP}}{n_{NT}} = \frac{3}{2}\left(\frac{\rho_{NT}}{\rho_{NP}}\right)\left(\frac{l}{D}\right)(10^3) \tag{7.7}$$

The interference cross-sectional area for both nanotubes and nanoparticles is provided in Figure 7.8 as has been discussed in the Hertz contact theory [209]. The contact area radii for cases I and II are provided as shown in equations 7.8 and 7.9 [209] where ν_2 is the workpiece Poisson ratio,E_2 is the work-piece Young's modulus, R is the nano-additive radius, and F is the resultant applied force (see Figure 7.8).

Nano-particle	Nano-tube
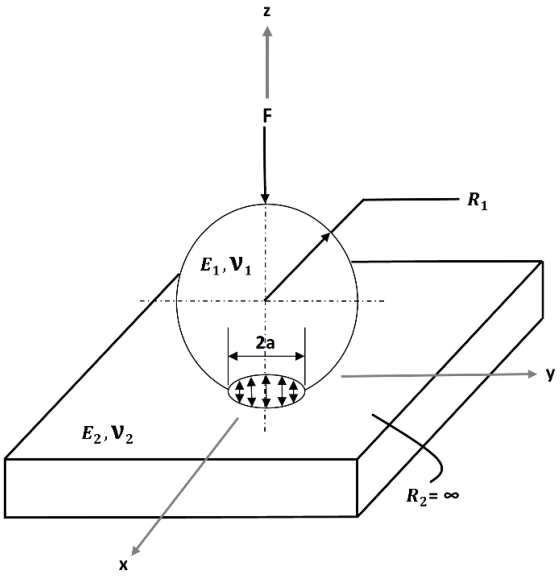	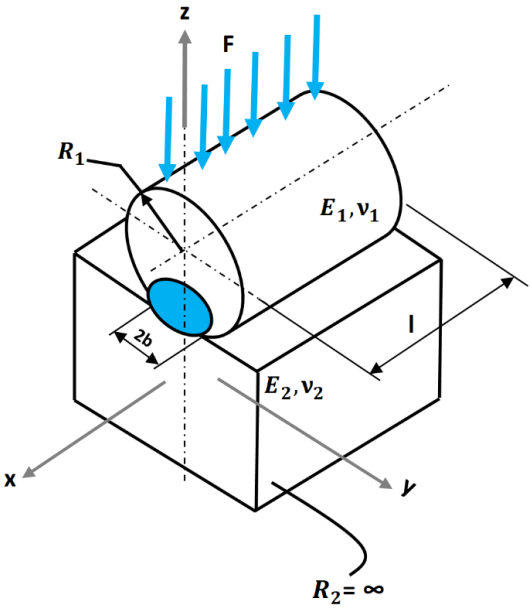
Circular contact area, resulting in a semi-elliptic pressure distribution	Rectangular contact area with semi-elliptical pressure distribution
$A_{CS-I} = \pi a^2$	$A_{CS-II} = \pi bl$
Case I: sphere on a flat plate	Case II: cylinder on a flat plate

Figure 7-8 The contact area schematic for two cases; case I: sphere on a flat plate, case II: cylinder on a flat plate

$$a = \sqrt[3]{\frac{3F\left(\frac{1-\nu_{NP}^2}{E_{NP}} + \frac{1-\nu_2^2}{E_2}\right)}{4\left(\frac{1}{R_{NP}}\right)}} = \sqrt[3]{\frac{3F\left(\frac{1-\nu_{NP}^2}{E_{NP}} + \frac{1-\nu_2^2}{E_2}\right)}{4\left(\frac{1}{R_{NP}}\right)}} \text{ (because } E_{NP} \text{ is a large value compared to } E_2) \quad (7.8)$$

$$b = \sqrt[2]{\frac{4F\left(\frac{1-\nu_{NT}^2}{E_{NT}} + \frac{1-\nu_2^2}{E_2}\right)}{\pi l\left(\frac{1}{R_{NT}}\right)}} = \sqrt[2]{\frac{4F\left(\frac{1-\nu_{NT}^2}{E_{NT}} + \frac{1-\nu_2^2}{E_2}\right)}{\pi l\left(\frac{1}{R_{NT}}\right)}} \text{ (because } E_{NT} \text{ is a large value compared to } E_2\text{)} \quad (7.9)$$

Using equations 7.8 and 7.9, the ratio between the contact area of case I to case II is calculated as shown in equation (7.10) assuming that $R_{NT} = R_{NP}$.

$$\frac{A_{CS-I}}{A_{CS-II}} = \frac{\pi a^2}{2bl} = 1.1481\, F^{\frac{1}{6}} \frac{D^{\frac{1}{6}}}{l^{\frac{1}{2}}} \left(\frac{1-\nu_2^2}{E_2}\right)^{\frac{1}{6}} \quad (7.10)$$

Using equations 7.7 and 7.10, $\left(\frac{n_{NP} A_{CS-NP}}{n_{NT} A_{CS-NT}}\right)$ could be calculated as shown in equation (7.11). Assuming that the sliding distance is constant during both cases, this ratio could express the induced wear volume ratio.

$$\frac{n_{NP} A_{CS-NP}}{n_{NT} A_{CS-NT}} = 1.7221\, F^{\frac{1}{6}} \frac{\sqrt{l}}{D^{\frac{5}{6}}} \frac{\rho_{NT}}{\rho_{NP}} \left(\frac{1-\nu_2^2}{E_2}\right)^{\frac{1}{6}}{}^{*} \quad (7.11)$$

The next step is implementing the proposed model into the studied experimental cases (i.e., using MWCNTs and Al_2O_3). The nano-additives density and size data is provided in Table 7-1. By substituting the nano-additives data listed in Table 7-1 into equation (7.11), the induced wear volume ratio $\left(\frac{V_{NP}}{V_{NT}}\right)$ could be expressed as shown in equation (7.12).

$$\frac{V_{NP}}{V_{NT}} = 1083.1\ F^{\frac{1}{6}}\left(\frac{1-\nu_2^2}{E_2}\right)^{\frac{1}{6}} \quad (7.12)$$

Table 7-1 MWCNTs and Al_2O_3 size and density data

	MWCNTs	Al_2O_3
ρ (gm/cm^3)	2.1	3.89
D (mm)	20	20
l (mm)	20	----

In order to validate the effectiveness of the proposed model with previous machining results, Inconel 718 has been used as workpiece material. The predicted model for Inconel 718 is provided as shown in equation (7.13). In addition, the resultant applied force effect on the induced wear volume ratio for Inconel 718 is plotted as shown in Figure 7-9. It can be clearly concluded from equation (7.13) and Figure 7-9 that MWCNTs offer better result than Al_2O_3 in terms of the induced nano-additive wear. This investigation would justify and provide a physical interpretation regarding the previously demonstrated machining results as MWCNTs-nano-fluid offers better cutting performance than Al_2O_3 nano-fluid in terms of flank wear, surface roughness and energy consumption. A schematic for the current conclusion is provided in Figure 7-10. It is claimed that both nano-fluids decrease the classical cutting tool wear; however, they cause another type of wear due to the nano-additives ploughing mechanism effects.

$$\frac{V_{NP}}{V_{NT}} = 139.6\ F^{\frac{1}{6}} \quad (7.13)$$

The proposed comparative performance analysis model discussed the induced nano-additive wear for both nanoparticles and nanotubes scenarios. The proposed model findings are consistent with the experimental results demonstrated in a previous study as both studies findings confirmed that MWCNTs nano-fluid offer better tribological performance than Al_2O_3 nano-fluid.

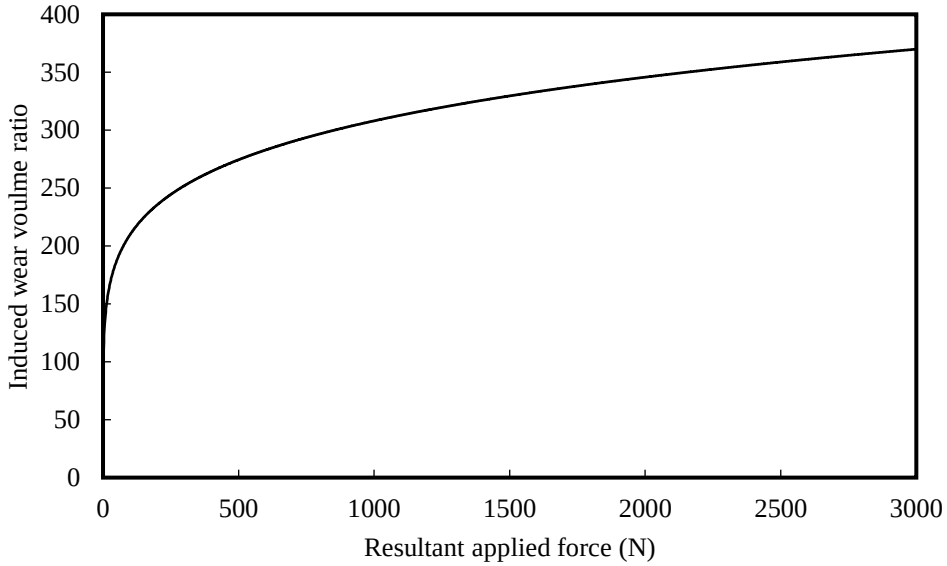

Figure 7-9 The resultant applied force effect on the induced nano-additive wear ratio in case of Inconel 718

To sum up the tribological effects of MQL-nano-fluid, two main mechanisms have been presented and discussed; rolling and ploughing mechanisms. In addition, the nano-additives size and concentration effects on the induced coefficient of friction and induced nano-additive wear have been discussed. Also, the induced nano-additive wear categorizations presented in this work offers a clear understanding of the occurrence conditions of the ploughing and rolling mechanisms. Finally, a proposed model has been developed throughout this work in order to evaluate the tribological effects of nanotubes and nanoparticles-based fluids on the cutting tool performance. The proposed model presents a solid physical evidence which proves that MWCNTs nano-fluid offers better tribological properties than Al_2O_3 nano-fluid and accordingly enhances the cutting tool performance.

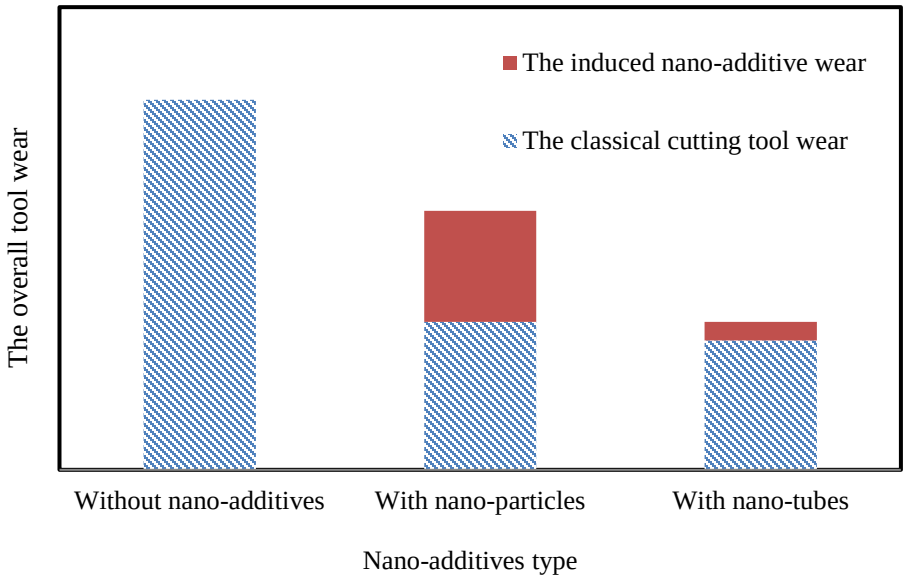

Figure 7-10 Schematic of the overall tool wear without/with nano-cutting fluids (i.e., nanoparticles or nanotubes)

7.4. The Nano-Cutting Fluid Heat Transfer Mechanisms: A Comparative Performance Analysis between MWCNTs and Al_2O_3

As mentioned earlier, the nano-cutting fluid heat transfer mechanisms could be categorized into two cases according to the induced nano-additives mechanisms (i.e., rolling or ploughing). In the case of rolling effect, the heat convection mechanism is only occurred as the nano-cutting fluids help in dissipating the generated cutting heat in the workpiece-tool interface area to the ambient environment. Regarding the ploughing effect, both heat convection and conduction mechanisms could occur as the ploughed-off nano-additives left thin exfoliated film which forms a protective nano-additive layer (a chemical reaction layer) on the machined surface.

This thin film/layer would decrease the cutting heat transfer into the workpiece. In this section, a general nano-cutting fluid heat transfer model is proposed. This model accommodates the general case (i.e. ploughing effect) which includes both the convection and conduction mechanisms. According to the first law of thermodynamics stated in equation (7.14), the change in the stored energy of a closed system($\frac{\Delta E_{stored}}{\Delta t}$) is equal to the input thermal energy rate ($\dot{E_{in}}$), minus the amount of work done by the system on its surroundings or it can be called the output thermal energy rate ($\dot{E_{out}}$).

$$\dot{E_{in}} - \dot{E_{out}} = \frac{\Delta E_{stored}}{\Delta t} \tag{7.14}$$

Regarding the input thermal energy rate during the nano-cutting fluid usage ($q'''d$), the making process of nano-additives transfers the potential energy from the cutting tool(q_1'''), and then it is converted into kinetic energy for the workpiece surface atoms and dissipated as heat. The nano-additives convert the kinetic energy to the workpiece surface in order to break the binding strength between the surface and sub-surface atoms of the workpiece. In addition, it is found that large interacting force between the nano-additives and workpiece would reduce the surface energy of workpiece as has been presented and discussed in a previous work [210]. The previous discussion (1st scenario) can be valid only in case of nano-additive rolling effects as shown in equation (7.15).

$$q''' = q_1''' \qquad \text{(in case of rolling effect only)} \tag{7.15}$$

Because of the incremental increase of nano-additive concentration (which increases the number of nano-additives at the tool-workpiece interface), an additional amount of heat generation (q_2''') should be considered since the nano-additives collide with each other, and are impeded by the asperities on the work surface, and they are sheared off by other new-ejected nano-additives. This extra amount is directly proportional to the wear volume induced by nano-additive(V_{NA}). The second scenario is valid in the case of nano-additive ploughing effect as shown in equation (7.16).

$$q''' = q_1''' + q_2''' \qquad \text{(in case of ploughing effect only)} \qquad (7.16)$$

As has been mentioned earlier, the proposed nano-cutting fluid heat transfer model considers the general case only (the second scenario) which includes both the convection and conduction mechanisms. By applying the 1st law of thermodynamics into the studied scenario, the preliminary model could be expressed as shown in equation (7.17). In this equation, h is the heat convection coefficient of the nano-cutting fluid mist, $T_{interface}$ is the workpiece-tool interface temperature, T_∞ is the ambient temperature, K is the heat conduction coefficient of the protective nano-additive layer, s is the protective nano-additive layer thickness, T_{film} is the protective nano-additive layer temperature, $T_{S1}$is the machined surface temperature, f_c is the cutting force, v is the cutting velocity, t_o is the undeformed chip thickness, w is the chip width, m_{film} is the protective nano-additive layer mass, A_s is the surface area of the protective nano-additive layer, and C is the protective film specific heat. The system schematic is provided as shown in Figure 7-11.

$$q'''d - h\,(T_{interface} - T_\infty) - \frac{k}{s}(T_{film} - T_{S1}) - \frac{f_c v}{t_o w} = \frac{C\, m_{film}}{A_s}\frac{dT_{film}}{dt} \qquad (7.17)$$

m_{film} can be expressed in terms of the protective nano-additive layer volume (V_{film}) and density(ρ_{film}). In addition, the protective film volume could be expressed in terms of $V_{film}$and s as shown in equation (7.18). The modified model could be expressed as shown in equation (7.19).

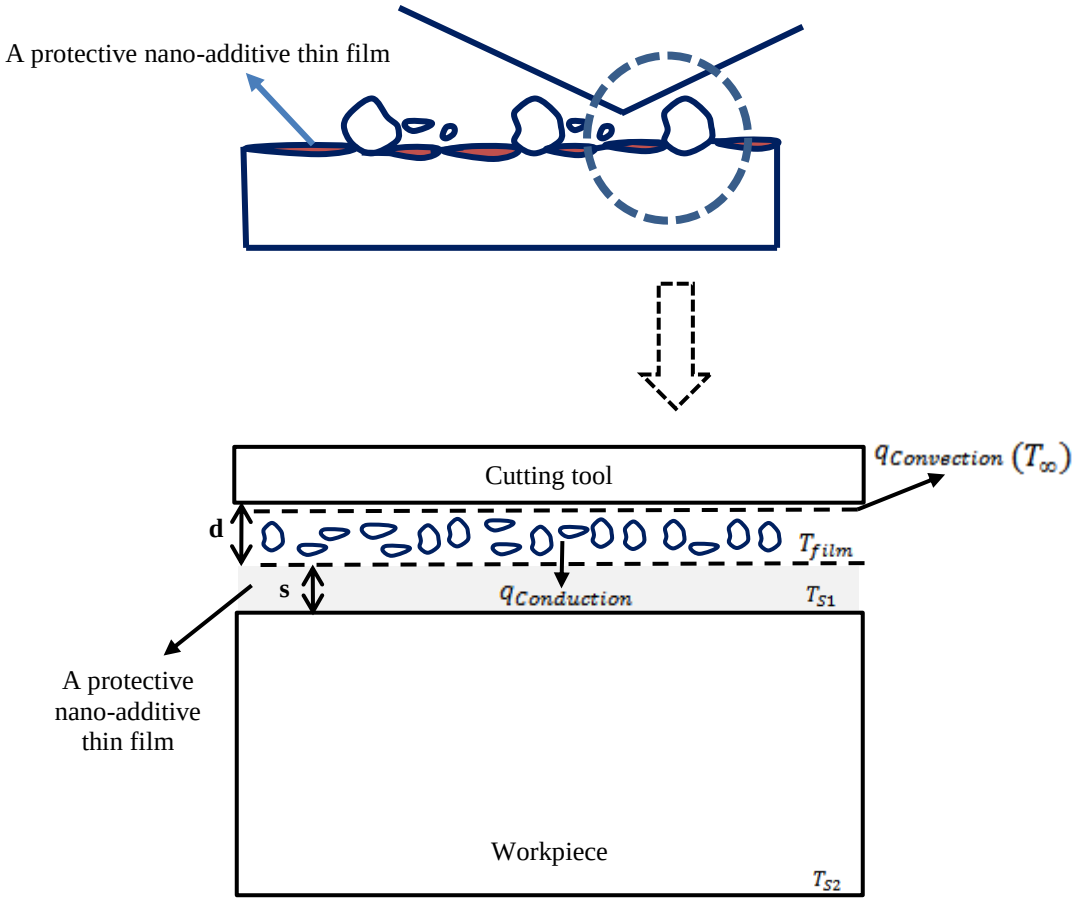

Figure 7-11 The schematic of the nano-cutting fluid heat transfer model

$$V_{film} = A_s\, s \tag{7.18}$$

$$q'''d - h(T_{interface} - T_\infty) - \frac{k}{s}(T_{film} - T_{S1}) - \frac{f_c v}{t_o w} = s\,\rho_{film}\, C \frac{dT_{film}}{dt} \tag{7.19}$$

By multiplying both sides by ($\frac{s}{k}$), the modified model could be expressed as shown in equation (7.20).

$$q''' \frac{ds}{k} - \frac{hs}{k}(T_{interface} - T_{\infty}) - (T_{film} - T_{S1}) - \frac{s\, f_c v}{k\, t_o w} = s^2 \frac{\rho_{film} C}{k} \frac{dT_{film}}{dt} \quad (7.20)$$

It can be found that $\frac{h\, s}{k}$ is expressing the Biot number (Bi) as shown in equation (7.21). It is an index used in heat transfer calculations, and it is used to express the ratio of the heat transfer resistances inside of and at the surface of a body. Since increasing the heat dissipation to the ambient environment is required during the cutting process, so the Biot number is considered as a higher-the-better index. It means also that increasing the heat convection coefficient of the nano-cutting fluid mist and the protective nano-additive layer thickness enhances the heat transfer resistances inside of and at the machined surface.

$$\frac{hs}{k} = Bi \quad (7.21)$$

Also, It can be found also from equation (7.20) that $\frac{\rho_{film} C_p}{k}$ is expressing the inverse of the thermal diffusivity ($\frac{1}{\alpha}$) as shown in equation (7.22). Thermal diffusivity measures the rate of heat transfer of a material from the hot side to the cold side. According to the modified model provided in equation (7.20), ($\frac{1}{\alpha}$) should be a higher value in order to enhance the heat transfer resistances inside of and at the machined surface. It means that α is considered as a lower-the-better index. From equations 7.20, 7.21, and 7.22, the final proposed could be expressed as shown in equation (7.23).

$$\frac{\rho_{film} C}{k} = \frac{1}{\alpha} \quad (7.22)$$

$$q''' \frac{ds}{k} - Bi(T_{interface} - T_{\infty}) - (T_{film} - T_{S1}) - \frac{s\, f_c v}{k\, t_o w} = \frac{s^2}{\alpha} \frac{dT_{film}}{dt} \quad (7.23)$$

The next step is to evaluate the MWCNTs and Al_2O_3 heat transfer performance depending on the previously proposed heat transfer model and its associated discussion. In order to perform a comparative performance analysis between MWCNTs and Al_2O_3 nano-fluids, the heat convection coefficient and thermal diffusivity of the resultant nano-mist should be calculated. The detailed steps for their calculations are presented and discussed throughout Chapter 8. The heat convection coefficient results for MWCNT and Al_2O_3 nano-fluids using different wt. % are provided as shown in Figure 7-12, while the thermal diffusivity results are provided in Figure 7-13.

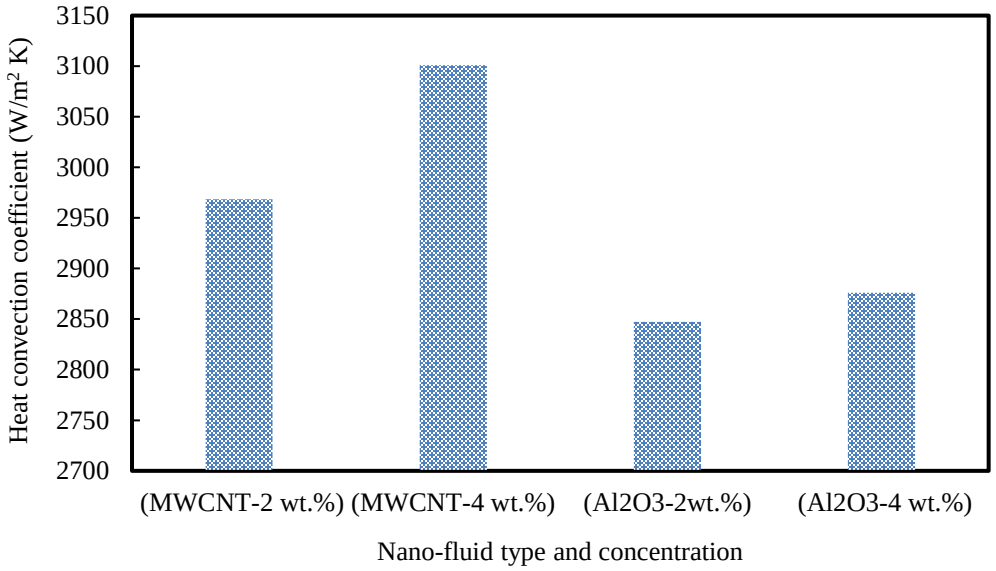

Figure 7-12 The heat convection coefficient results for MWCNTs and Al_2O_3 nano-fluids mist

Regarding the heat convection coefficient results (see Figure 7-12), an improvement percentage of 4.25% for 2 wt.% MWCNTs nano-fluid has been observed compared to Al_2O_3 nano-fluid with the same weight concertation, while 4 wt.% MWCNTs nano-fluid showed higher heat convection coefficient value by 7.82% in comparison with 4 wt.%. Al_2O_3 nano-fluid. In terms of the thermal diffusivity results (see Figure 7-13), an improvement percentage of 13% for 2 wt.% MWCNTs nano-fluid has been observed compared to 2 wt.% Al_2O_3 nano-fluid, while 4 wt.% MWCNTs nano-fluid showed lower thermal diffusivity value by 22.8% in comparison with Al_2O_3 nano-fluid with 4 wt.%.

It can be concluded from Figures 7-12 and 7-13 that MWCNTs nano-fluid provides better heat transfer performance than Al_2O_3 nano-fluid for both thermal diffusivity and heat convection coefficient results.

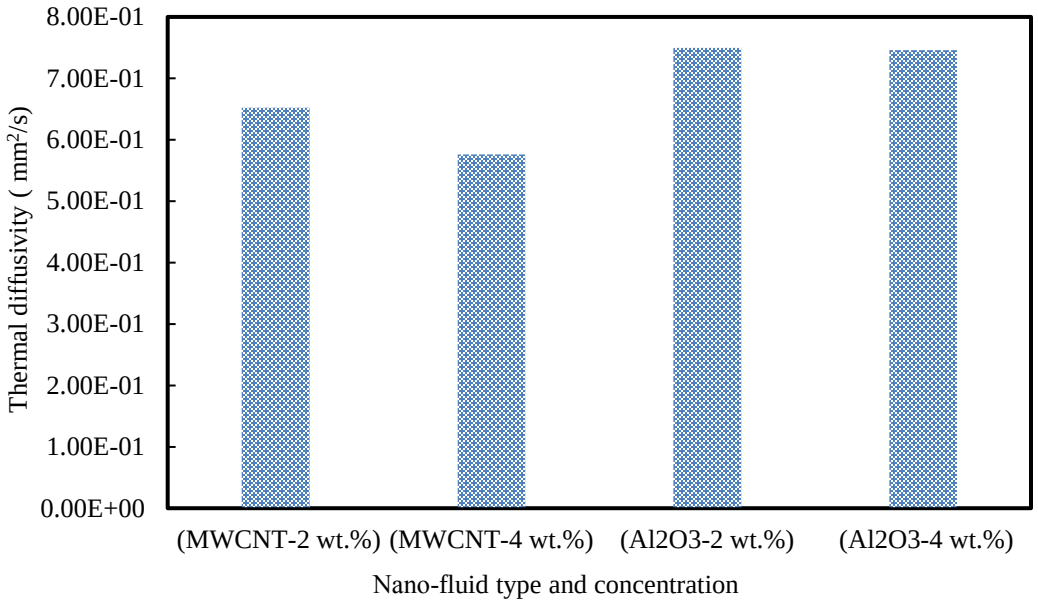

Figure 7-13 The thermal diffusivity results for MWCNTs and Al_2O_3 nano-fluids mist

7.5. Summary

This chapter provides a clear understanding of the MQL-nano-cutting fluids mechanism. Two main mechanisms have been presented and discussed; rolling and ploughing mechanisms. In addition, the nano-additives size and concentration effects on the induced coefficient of friction and induced nano-additive wear have been discussed. Two proposed models have been developed throughout this chapter in order to evaluate MWCNTs and Al_2O_3 nano-cutting fluids performance. The first model is related to the induced nano-additive wear, while the second model is discussing the heat transfer performance analysis when machining with MQL-nano-fluids. MWCNTs-based nano-fluid provides better results within both proposed models. The proposed models present a solid physical evidence which proves that MWCNT nano-fluid offers better tribological and heat transfer properties than Al_2O_3, and that accordingly enhances the machining quality characteristics.

Chapter 8 Finite Element Modeling of Machining with Nano-Cutting Fluids under MQL

8.1. Preamble

The generated heat during cutting processes doesn't only accelerate the tool wear rate, but also affects the physical properties of the machined surface. Measuring the generated cutting temperature and resulting residual stress directly during machining processes is a challenge task because of the dynamic nature of cutting process and the small contact areas at the tool-workpiece and tool-chip interfaces. Thus, the finite element (FE) modeling is a useful tool to provide an adequate and quick estimation of the induced heat and residual stresses under different machining conditions. Previous studies have focused on developing FE models to investigate different characteristics during machining difficult-to-cut materials such as cutting forces [211], lubrication and cooling effects [212], and chip shape characteristics [213]. Also, different studies have focused on the aspects of the numerical modeling and simulation of machining Inconel 718 [214-217] and Ti-6Al-4V [218, 219]. In addition, some researchers focused on finite element analysis of minimum quantity lubrication machining Ti-6Al-4V using a developed friction model [220]. Additional research works have developed computational fluid dynamics models to investigate the MQL effects on machining processes [221-223].

In spite of many published studies on FE modeling and simulation of machining with MQL, there is a research gap in finite element modeling of machining with MQL-nano-cutting fluids. In this chapter, an integrated finite element model is developed in order to analyze various unique aspects of machining with nano-fluids under minimum quantity lubrication during cutting Inconel 718 and Ti-6Al-4V alloys. These aspects include the characteristics of heat transfer of the resultant nano-cutting fluid, the interactions between the cutting tool and workpiece, the temperature at different zones, and the machining induced resulting residual stresses. The novelty of this work lies on developing an integrated finite element model to analyze various unique aspects of machining with nano-fluids under minimum quantity lubrication during cutting Inconel 718 and Ti-6Al-4V alloys.

Two main phases have been employed to develop the integrated finite element model. The first phase simulated the thermal effect of the resultant nano-fluid mist through developing a 2-D Axisymmetric Computational Fluid Dynamics (CFD) domain representing the volume occupied by the mixture from inside the MQL nozzle to the interface area between the machined surface and the tool. In the second phase, the effectiveness of the use of MQL-nano-cutting fluid in terms of cutting temperature and resulting residual stresses have been presented using Lagrangian modeling approach using ABAQUS/Explicit.

8.2. Modeling Phases Descriptions

In order to develop a finite element model which provides an accurate prediction of the cutting processes using MQL-nano-cutting fluids, an integrated finite element model has been established. The integrated model includes two main phases:

Phase I: (MQL-nano-cutting fluid simulation): developing a computational fluid dynamics model to analyze the heat transfer characteristics of MQL-nano-cutting fluid at different cutting temperatures. In order to simulate the thermal effect of the resultant nano-fluid mist, a boundary film on the machined and cutting tool surfaces is applied. This boundary film expresses the nano-fluid mist using different heat convection coefficients values at different cutting temperatures. ANSYS-FLUENT module (two-phase flow) has been used in order to determine the heat convection coefficients of the boundary film under different cutting temperatures. The previous studies have focused on simulating the applied coolant (boundary film) with constant heat convection coefficient; however, the coolant's convection coefficient varies with the induced cutting temperature. Thus, the current model accommodates this situation to accurately simulate the effect of MQL-nano-fluid.

Phase II: (cutting process simulation): the effectiveness of the use of MQL-nano-cutting fluid in terms of cutting forces, temperature and resulting residual stresses has been analyzed using finite element modeling based on the Lagrangian approach.

The schematic of the proposed integrated model is provided in Figure 8-1.

8.3. MQL-Nano-Cutting-Fluids Thermo-Physical and Heat Characteristics (Theoretical Approach)

The characteristics of the nano-cutting fluids used in this study are as follows:

- The resultant thermal conductivity is (K_e)
- The resultant viscosity (μ_e)
- The resultant density (ρ_e)
- The resultant specific heat (C)

The used nano-additives and vegetable oil properties are provided in Table 8-1.

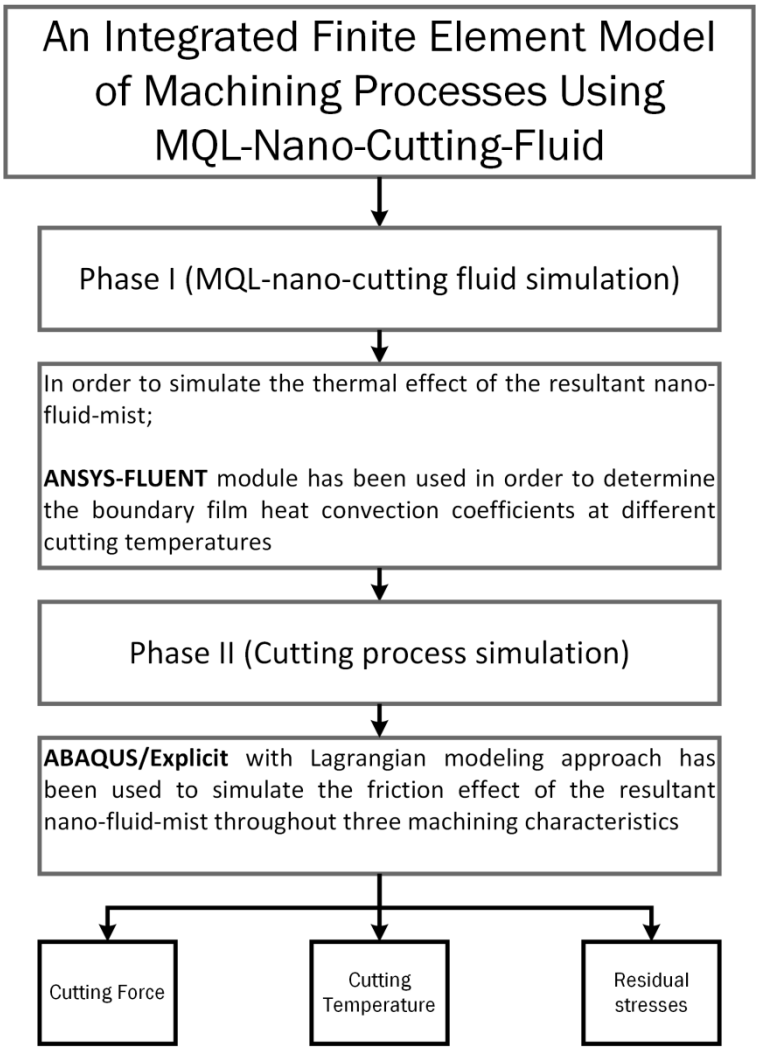

Figure 8-1 The integrated FE model phases

Table 8-1 The used nano-additives and base oil thermo-physical properties

	MWCNTs	Base oil
ρ (gm/cm^3)	2.1	0.92
K (W/m K)	3000	0.58
C (KJ/Kg K)	35	1.67

In order to determine the resultant thermal conductivity (K_e), equation (8.1) [224] could be used knowing that n value should be 3 in the case of nano-particles and 6 in the case of carbon-nano tubes, U_p is the nano-additive volume fraction, "m" refers to the base oil and "p" refers to the nano- additives.

$$K_e = K_m\left(1 + \frac{\frac{K_p}{K_m} + (n-1) - (n-1)\left(1 - \frac{K_p}{K_m}\right) U_p}{\frac{K_p}{K_m} + (n-1) + \left(1 - \frac{K_p}{K_m}\right) U_p}\right) \quad (8.1)$$

The resultant nano-fluid viscosity (μ_e) is determined as shown in equation (8.2) [225], while the resultant nano-fluid density (ρ_e) is provided as shown in equation (8.3).

$$\mu_e = \mu_m\,(1 + 2.5\ U_p) \quad (8.2)$$

$$\rho_e = \rho_m\left(1 - U_p\right) + U_p\rho_p \quad (8.3)$$

The resultant nano-fluid specific heat (C) can be determined as mentioned in equation (8.4). The studied nano-cutting fluids characteristics for both MWCNTs are calculated according to the previous equations and their results are given in Table 8-2.

$$C = C_{bf}\left(1 - U_p\right) + U_p C_p \quad (8.4)$$

As mentioned in previous studies, with utilizing compressed air, the nano-fluid is atomized into the MQL nozzle and it results in a very fine mist. Thus, in order to investigate the MQL-nano-fluid effects, the induced mist (mixture) characteristic should be calculated depending on the air and resultant nano-fluid volumetric concentrations; for example, the mist density is calculated as shown in equation (8.5). The resultant mist characteristics results are determined and provided as shown in Table 8-3.

Table 8-2 The studied nano-cutting fluids characteristics results

	MWCNTs- 2 wt. %	MWCNTs- 4 wt. %
ρ_e (Kg/m^3)	930.384	940.65
μ_e (N s/m^2)	0.07154	0.0730625
K_e (W/m K)	1.191	1.222
C (J/Kg K)	1963.304	2253.275

$$\rho_{mist} = \rho_{nano-fluid}(1 - \upsilon_{air}) + \upsilon_{air}\,\rho_{air} \tag{8.5}$$

Table 8-3 The resultant mist characteristics

	MWCNTs- 2 wt. %	MWCNTs- 4 wt. %
ρ_{mist} (Kg/m^3)	414.14	418.70
μ_{mist} (N s/m^2)	0.0318	0.0325
K_{mist} (W/m K)	0.5645	0.5774
C_{mist}(J/Kg K)	1441.32	1570.18

In order to simulate the MQL-nano-cutting fluids effects, the heat convection coefficients should be determined using equation (8.6):

$$h = \frac{K_e Nu_x}{L_c} \tag{8.6}$$

Where h is the heat convection coefficient, Nu_x is the MQL-nano-cutting fluid Nusselt number, and Lc is the characteristics length. The characteristic length in the current case should be the distance between nozzle and target plane. In addition, MQL-nano-cutting fluid mechanism is categorized as a liquid jet impingement cooling mechanism. In order to predict the resultant mist flow regime, Reynolds number should be calculated as shown in equation (8.7), where V_{mist} is the average mist velocity which can be determined from the principle of conservation of mass as shown in equation (8.8) assuming constant nozzle cross-sectional area. Reynolds number results at an average value of L_c (2.5 mm) are provided as shown in Table 8-4.

$$\mathrm{Re}_{L_c,\mathrm{mist}} = \frac{\rho_e L_c V_{\mathrm{mist}}}{\mu_e} \tag{8.7}$$

$$V_{\mathrm{mist}} = \frac{\rho_{\mathrm{nano-fluid}} V_{\mathrm{nano-fluid}} + \rho_{\mathrm{air}} V_{\mathrm{air}}}{\rho_{\mathrm{mist}}} \tag{8.8}$$

Table 8-4 The average Reynolds number results

	MWCNTs- 2 wt. %	MWCNTs- 4 wt. %
$\mathrm{Re}_{L_c,\mathrm{mist}}$	12	11.88

Since the MQL-nano-cutting fluid mechanism is categorized as a liquid jet impingement cooling mechanism and the flow regime is laminar depending on the Reynolds number results, the "laminar stagnation-zone boundary layer" case has been selected [226] in order to determine the Nusselt number values as provided in equation (8.9). As can be seen in equation (8.9), the Nusselt number depends on the Prandtl number function (G(Pr)) and the dimensionless velocity gradient (B'). The Prandtl number should be determined as shown in equation (8.10) in order to select the appropriate Prandtl function as can be observed in equation (8.11). The Prandtl number results are calculated as shown in Table 8-5. According to these results, the third Prandtl number function in equation (11) is selected to calculate the Nusselt number. In addition, the dimensionless velocity gradient (B=1.486) value has been selected as mentioned in some previous studies [226, 227] as it mainly depends on the nozzle size, distance between nozzle and target plane, and jet Weber number.

Once the appropriate Prandtl function has been selected and determined, the average Nusselt number and heat convection coefficients values are calculated using equations (8.9) and (8.6), respectively. The Nusselt number and heat convection coefficients results are given in Table 8-6.

$$\overline{Nu_{L_c}} = G(Pr)Re_{L_c,mist}^{0.5}\sqrt{B'} \tag{8.9}$$

$$Pr = \frac{C_{mist}\,\mu_{mist}}{K_{mist}} \tag{8.10}$$

$$G(Pr) \approx \begin{cases} \dfrac{\sqrt{\frac{2\,Pr}{\pi}}}{1 + 0.80455\sqrt{\frac{2\,Pr}{\pi}}} & Pr \le 0.15 \\ 0.5389\,Pr^{0.4} & 0.15 < Pr < 3.0 \\ 0.60105\,Pr^{0.333} - 0.05084 & Pr \ge 3.0 \end{cases} \tag{8.11}$$

Table 8-5 Prandtl number results

	MWCNTs- 2 wt.%	MWCNTs- 4 wt.%
Pr	81.24	88.37

Table 8-6 The theoretical Nusselt number and heat convection coefficients results

	MWCNTs- 2 wt. %	MWCNTs- 4 wt. %
$\overline{Nu_{L_c}}$	10.78	11.04
$\bar{h}$ (W/m2 K)	2968.41	3108.52

8.4. Phase I (MQL-Nano-Cutting Fluid Simulation)

A 2-D Axisymmetric Computational Fluid Dynamics (CFD) domain has been constructed to represent the volume occupied by the mixture from inside the MQL nozzle to the interface area between the cutting tool and machined surface as shown in Figure 8-2. The length of the mist channel inside the nozzle is integrated into the domain to obtain a fully developed velocity profile of the mist before it leaves the nozzle tip. The Length of

the considered interface area has been chosen long enough to ensure insignificant end condition effects on the simulated domain. Quadrilateral elements have been used in the meshing construction. The CFD model simulates the MQL function of a stand-alone booster system (MQL-Unist) which was installed on the machine tool, and it has a nozzle diameter of 2.5 mm. Then, the CFD model results were ensured to be independent of mesh size through conducting several comparisons with other models have smaller mesh size. The CFD model uses the governing equations which are the conservation of mass, momentum, and the energy equations to simulate the global behavior of the air-mist mixtures. While for the detailed air-mist interaction, the mist's void fraction transport equation augmented with the algebraic mixture model is used. The numerical results convergence is claimed when the scaled imbalance in each of the conservation equations summed over all computational cells (residuals) becomes less than 10^{-3} (continuity equation) in any two successive iterations, while for all other governing equations, the convergence is satisfied when residual becomes less than 10^{-4}.

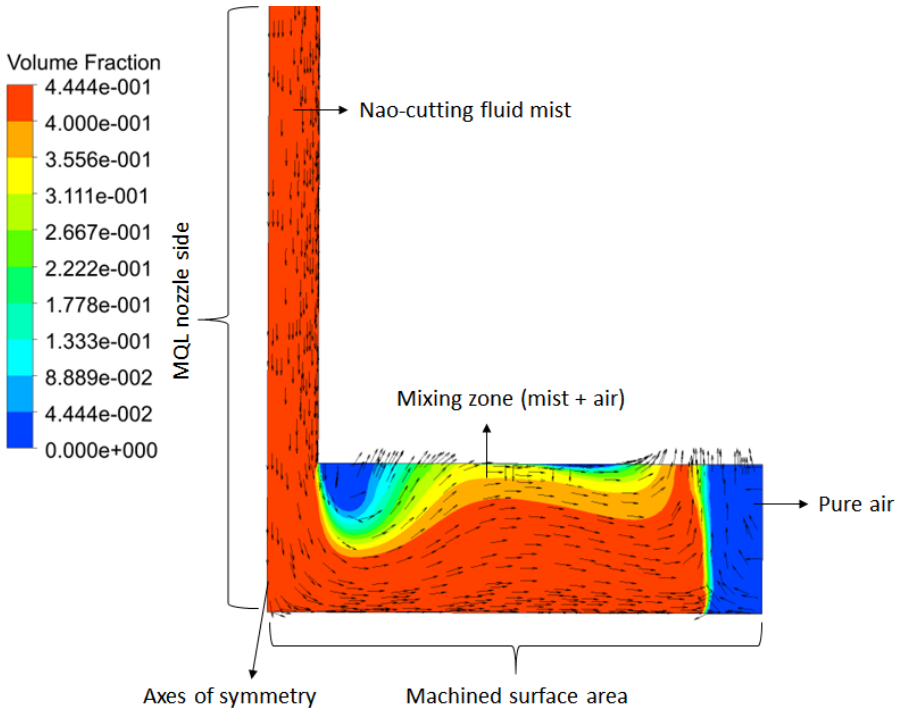

Figure 8-2 (2-D) Axisymmetric domain used in the CFD simulation

The results of average heat convection coefficients obtained from the proposed CFD model at standard room temperature demonstrated a good agreement with the theoretical values calculated in the previous section. Figure 8-3 shows the CFD simulation and theoretical results for the average heat convection coefficients results. The highest accuracy has been observed under using MWCNT with 4 wt. % (about 99.7%), while using 2 wt. % offered 97.7% accuracy. Once the CFD model has been validated, it can be used to determine the heat convection coefficients at different temperatures.

The results of average heat convection results for the studied cases with different applied temperatures are provided as shown in Figure 8-4.

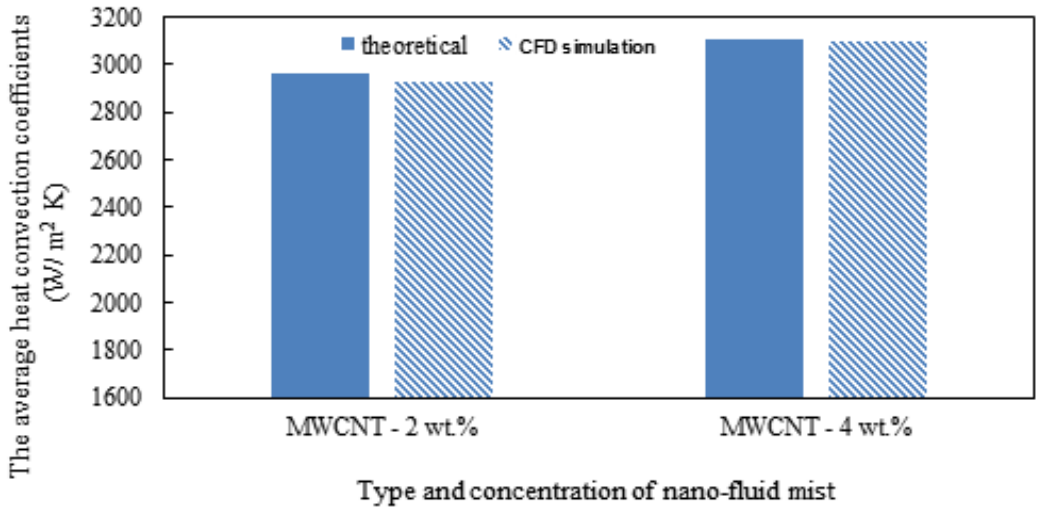

Figure 8-3 The CFD simulation and theoretical results for the average heat convection coefficients results

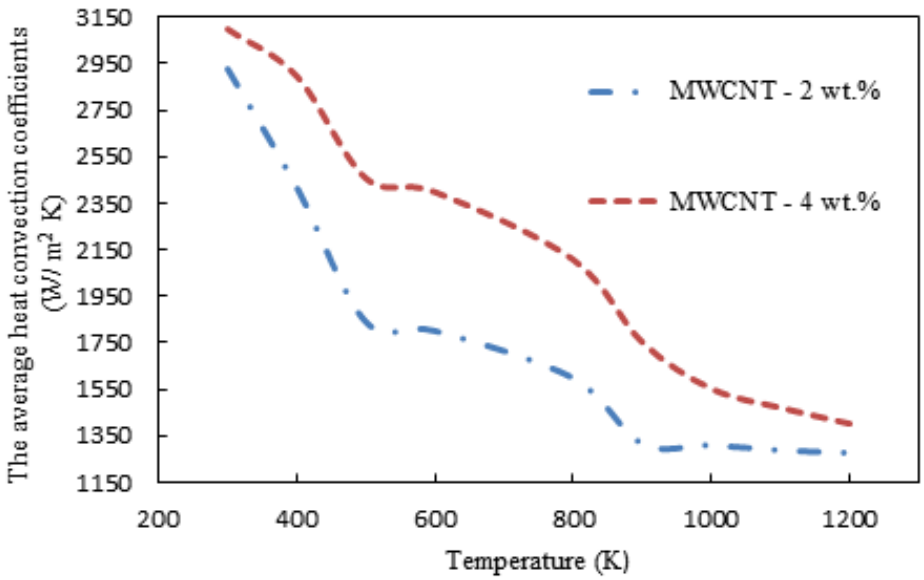

Figure 8-4 The average heat convection results versus temperature

8.5. Phase II (Cutting Process Simulation)

In this phase, Lagrangian based FE model is developed and used to analyze the studied cutting processes after specifying the nano-fluid mist heat convection coefficient results throughout phase I. As mentioned earlier, a boundary film on the machined and cutting tool (rake and flank) surfaces is applied to model and simulate the resultant nano-mist effect. The quadratic-thermal-displacement plane strain elements have been used to mesh the current FE model. Meshing sensitivity has been performed to ensure the independency of mesh size of the obtained results. Several comparisons were made using models with different mesh size. The cutting force was used to validate the proposed FE model with the experimental results. The meshed parts (i.e., tool and workpiece) are provided as shown in Figure 8-5. In order to investigate the effects of MQL- MWCNTs performance, different orthogonal cutting trials for Ti-6Al-4V and Inconel 718 were performed with/without MWCNTs. The tests were conducted on a CNC lathe machine (Hass ST-10 CNC). The used depth of cut was 0.2 mm and the information of the used cutting tool is provided in Table 4-3. The thermo-viscous-plastic behavior of the workpiece material has been expressed using the Johnson–Cook (J-C) material model, while the element deletion (i.e., using Johnson–Cook's model for progressive damage and fracture)

has been used to model and simulate the chip separation using an approximate layer of elements. The material flow stress has been expressed by using the J-C hardening model provided in equation (8.12). This model can fit problems with higher strain rate ranges and temperatures variations because of the plastic deformation caused by thermal softening [228]. Also, the thermal conductance-option in ABAQUS has been used to simulate the thermal interaction effect between the workpiece and cutting tool.

$$\bar{\sigma} = [A + B\,\bar{\varepsilon}^{\,n}][1+c \ln(\frac{\dot{\bar{\varepsilon}}}{\dot{\bar{\varepsilon}}_o})][1-(\frac{T-T_{room}}{T_{melt}-T_{room}})^{m}] \quad (8.12)$$

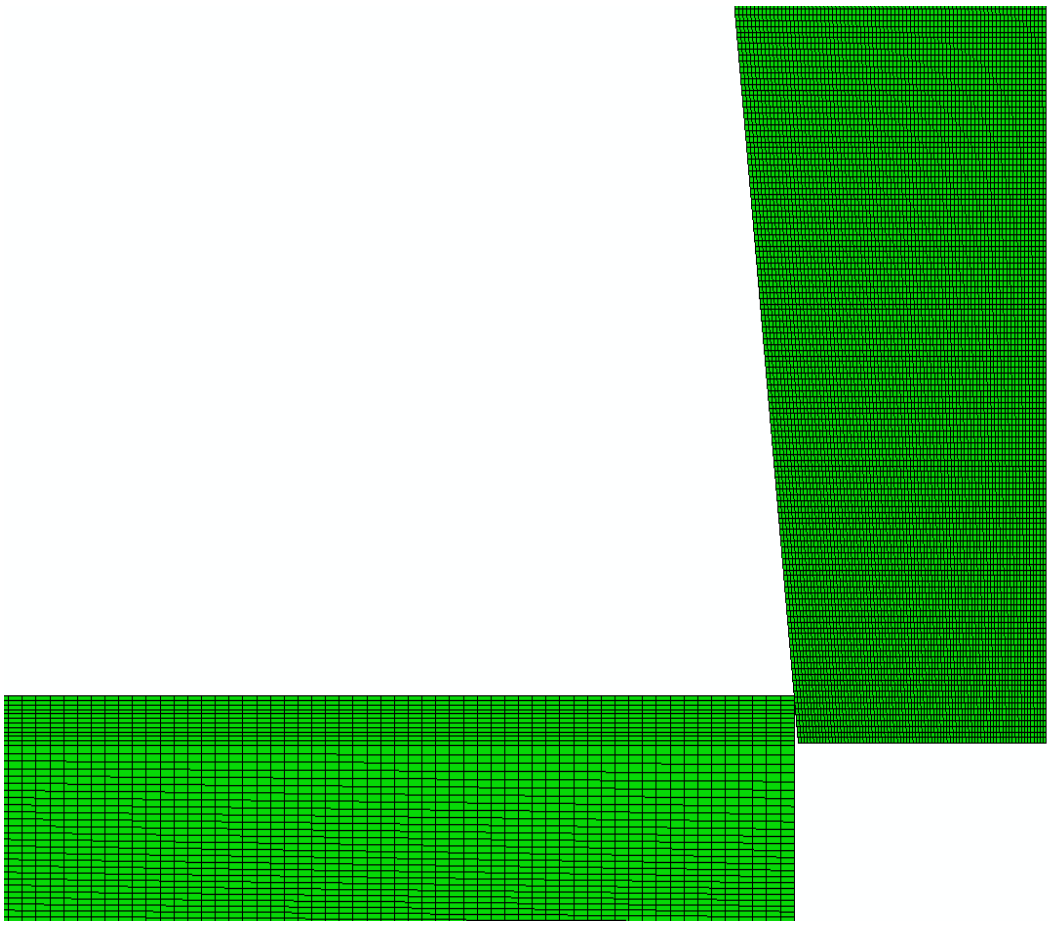

Figure 8-5 Finite element modeling of machining Inconel 718 (meshing view)

Where equivalent stress is $\bar{\sigma}$, the hardening modulus is B, the yield strength of the workpiece material at room temperature is A, the work-hardening exponent is n, the coefficient dependent on the strain rate is c, m is the thermal softening coefficient and $\bar{\varepsilon}$ denotes the equivalent plastic strain. The strain rate $\dot{\bar{\varepsilon}}$ is normalized with a reference strain rate $\dot{\bar{\varepsilon}}_o$ of 1 s^{-1}. T_{melt} and T_{room} represent the melting temperature and room temperature, respectively. Moreover, the Johnson-Cook damage model is used with J-C yield model. The fracture/damage of an element is defined by equation (8.13).

$$D = \sum \frac{\Delta\bar{\varepsilon}}{\bar{\varepsilon}^f} \tag{8.13}$$

Where the increment of equivalent plastic strain is $\Delta\bar{\varepsilon}$, and $\bar{\varepsilon}^f$ the equivalent strain to fracture. The element fracture is occurred when D =1.0, and then these elements are eliminated from the FE computation. The general expression for the fracture strain based on J-C damage is given in equation (8.14).

$$\bar{\varepsilon}^f = (D_1 + D_2 \exp D_3 \frac{\sigma_m}{\bar{\sigma}}) (1 + D_4 \ln \frac{\dot{\bar{\varepsilon}}}{\dot{\bar{\varepsilon}}_o}) [1 - D_5 (\frac{T - T_{room}}{T_{melt} - T_{room}})^m] \tag{8.14}$$

Where σ_m is the average of the three normal stresses and $\bar{\sigma}$ is the equivalent stress. The J-C damage model accounts for high strain rate deformation, and so, it is appropriate to investigate the dynamic simulations. Jonson-Cook parameters and progressive damage model parameters for Inconel 718 [229] and Ti-6Al-4V [230] used in FE simulations are presented in Tables 8-7 and 8-8, respectively. The other properties for Inconel 718 and Ti-6Al-4V are provided in Tables 4-1 and 4-2, respectively.

Table 8-7 Jonson-Cook parameters and progressive damage model parameters for Inconel 718 [229]

	Johnson-Cook model parameters		Johnson–Cook progressive damage model parameters
A (MPa)	450	D_1	0
B (MPa)	1700	D_2	0.66
c	0.017	D_3	-0.4
n	0.65	D_4	-0.017
m	1.3	D_5	0
T_{melt} (^oC)	1350		

Table 8-8 Jonson-Cook parameters and progressive damage model parameters for Ti-6Al-4V [230]

	Johnson-Cook model parameters		Johnson–Cook progressive damage model parameters
A (MPa)	1098	D_1	-0.099
B (MPa)	1092	D_2	0.27
c	0.014	D_3	0.48
n	0.93	D_4	0.014
m	1.1	D_5	3.87
T_{melt} (^oC)	1649		

Regarding the FE model boundary conditions, a constant cutting velocity has been used, and the workpiece bottom surface was restricted to move in all directions. In order to model the tool-workpiece and tool-chip contact areas, the Coulomb's friction law has been employed. The mentioned assumption has been used based on previous available results for finite element modeling of cutting processes [231]. According to the Coulomb's law, when the chip shear stress τ is equal to or greater than the critical friction stress τ_c, the relative motion (slip) occur at the contact point. When τ is smaller than τ_c there is no relative motion and the contact point is in a state of sticking [232]. The critical friction stress can be calculated as shown in equation (8.15), where p is the normal pressure at the contact point, and τ_{th} is the threshold value associated with the material failure. In addition, it should be stated here that τ_{th} is infinity when applying the law of conventional Coulomb frictional. In the current FE simulations, penalty method is used as a friction formulation. In addition, the equivalent strain to fracture and the induced coefficient of friction have been used in the current simulation in order to accurately represent the experimental cutting processes by comparing the FE and experimental cutting forces results. Using the measured

cutting and feed forces (i.e., for all cutting tests), and the cutting tool rake angle, the coefficients of friction were determined. The coefficient of friction during cutting Inconel 718 with 4 wt. % MQL-MWCNTs-fluid was about 0.41, while using 2 wt. % MWCNTs provides coefficient of friction of 0.49, and the coefficient of friction when machining with classical MQL was about 0.63. Regarding cutting Ti-6Al-4V, the coefficient of friction when using classical MQL was 0.51, while the coefficients of friction when using 2 wt. % and 4 wt. % MWCNTs, were found to be 0.37, and 31, respectively.

$$\tau_c = \min\ (\mu p, \tau_{th}) \tag{8.15}$$

The generated cutting forces, residual stresses, and temperatures have been selected to evaluate the performance of the applied MQL-nano-cutting fluid, as will be discussed in the next sections.

8.5.1. Effect of MQL-Nano-Cutting Fluid on Cutting Forces

Cutting force is an important characteristic which can offer an adequate prediction of the tool performance. The cutting parameters settings during orthogonal turning of Inconel 718 are speed of 40 m/min, feed rate of 0.2 mm/rev, and depth of cut of 0.2 mm. In the orthogonal cutting of Ti-6Al-4V, the cutting conditions are as following: cutting speed 170 m/min, feed rate 0.1 mm/rev, and depth cut of 0.2 mm. During the cutting tests, the force sensors (KISTLER) have been mounted on specially designed fixture in order to measure the induced cutting forces. In the current work, the experimental cutting forces have been used to validate the developed finite element model. Three cases have been used to obtain the effectiveness of using MQL (see Table 8-9). The variation of cutting force generated in experiments and FE simulations during machining Inconel 718 using 2 wt. % MWCNTs (cutting test 2), 4 wt. % MWCNTs (cutting test 3), and without MWCNTs (cutting test 1) can be found as shown in Figure 8-6. The improvement in the machining performance when using MWCNTs-nano-fluid is obvious, as shown in Figure 8-6. It is noticed that the cutting force magnitude during cutting with MWCNTs is lower compared to the cutting processes done without-MWCNTs. It is mainly due to the boundary film effect that

enhances the heat capacity performance as well as the simulated friction behavior (coefficient of friction) presented and discussed in the previous section.

Table 8-9 The studied lubrication scenarios (cutting tests)

Lubrication technique	Cutting test #
Pure MQL	1
MQL + 2 wt. % MWCNTs	2
MQL + 4 wt. % MWCNTs	3

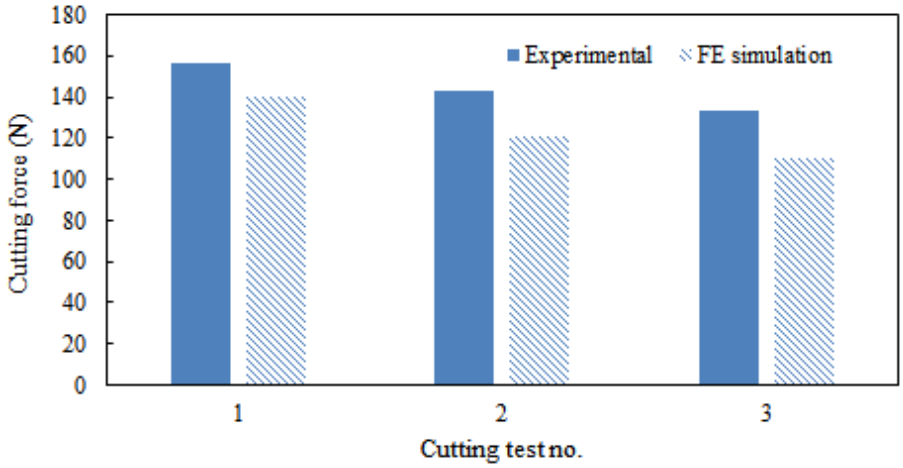

Figure 8-6 Cutting forces results with/without MWCNTs during machining Inconel 718

As shown from Figure 8-6, the simulated and experimentally measured cutting forces showed better agreement in cutting test 1 (accuracy % ≈ 90%) than cutting test 2 (accuracy % ≈ 82.3%) or cutting tests 3 (accuracy % ≈ 79.6 %). It is mainly due to neglecting the ploughing effect during the simulation. When the nano-fluid mist is dispersed in the cutting zone, a number of nano-additives are embedded into the machined surfaces. Some nano-additives have a rolling effect while others are sheared due to very high pressure in the cutting zone (i.e., ploughing effect) as shown previously in Figure 6-9 [139]. Thus, the current integrated FE model can be enhanced by constructing a hybrid model that can simulate both the chip formation mechanism as well as the nano-additives collisions occurred when they are sheared off by other new-ejected nano-additives. Similarly, for cutting tests performed on Ti-6Al-4V (see Figure 8-7), the experimental and simulated cutting forces showed better agreement in cutting test 1 (accuracy ≈93.7%) than cutting test 2 (accuracy ≈ 79.6%), or cutting tests 3 (accuracy % ≈ 82.2 %). As shown in Figure

8-6 and Figure 8-7, the cutting forces accuracy during tests performed with 2 wt. % and 4 wt.% MWCNTs-nano fluid is lower than cutting test 1 (without MWCNTs). During cutting Inconel 718, cutting test 2 (2 wt. % MWCNTs) showed better agreement than cutting test 3 (4 wt. % MWCNTs). However, during cutting Ti-6Al-4V, cutting test 3 (4 wt. % MWCNTs) showed better agreement than cutting test 2 (2 wt. % MWCNTs). It is mainly attributed to the dual-effect of the nano-additives concentration which has been previously discussed in Chapter 7. In other words, increasing the nano-additives percentage reduces the coefficient of friction; however, it could increase the induced nano-additives wear as mentioned in some previous studies [261-263].

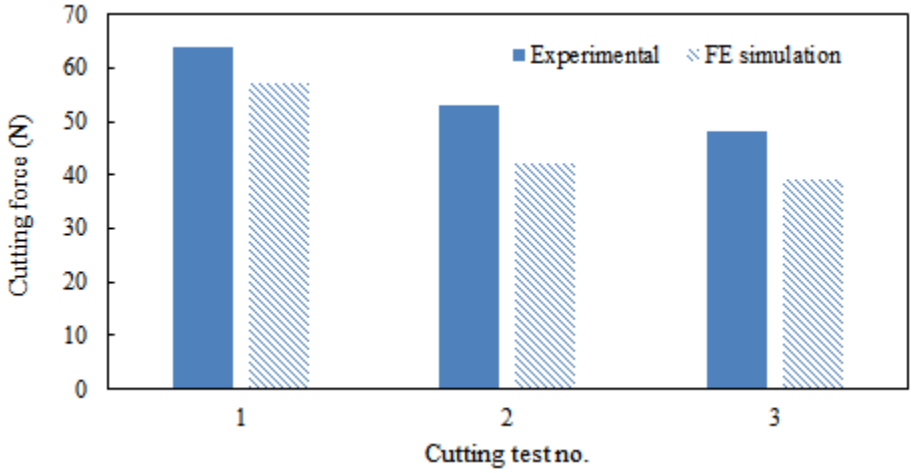

Figure 8-7 Cutting forces results with/without MWCNTs during machining Ti-6Al-4V

8.5.2. Effect of MQL-Nano-Cutting Fluid on Cutting Temperature

The developed finite element model showed also another evidence to verify the improvement in the machining performance with MWCNTs-nano-fluid. The FE simulated temperatures generated along the cutting edge with/without MWCNTs-nano-fluid during machining Inconel 718 are obtained. In comparison with the test performed without MWCNTs, the average cutting temperature during machining with 2 wt. % or 4 wt. % MWCNTs-nano-fluid tools is rather low. It is mainly due to the boundary film effect which enhances the heat dissipation performance and accordingly lower values of cutting temperature have been observed beneath the cutting tool. According to the FE results, a

reduction percentage of 47.1% in the average generated cutting temperature at the tool-chip interface area has been observed between cutting tests 1 and 2, while a reduction percentage about 60% has been observed between cutting test 1 and 3 as shown in Figure 8-8. The difference in the generated temperature results between cutting test 2 and cutting test 3 is mainly due to the heat transfer convection effect which previously presented and discussed (see Table 8-6 and Figure 8-4). Also, Figure 8-9 shows the temperature distribution along the tool-chip interface zone for all cases, which demonstrates the significance of using MQL-nano-fluid.

Similarly, during machining Ti-6Al-4V, a reduction percentage about 51% in the average generated cutting temperature has been noticed between cutting tests 1 and 2, while a reduction percentage of 60% has been observed between cutting test 1 and 3 as shown in Figures 8-10. Also, similarity to the results of Inconel 718, the temperature distribution along the tool-chip interface zone when machining Ti-6Al-4V with/without MWCNTs-nano-fluid is provided as shown Figure 8-11. The results obtained the significance of using MWCNTs-nano-fluids.

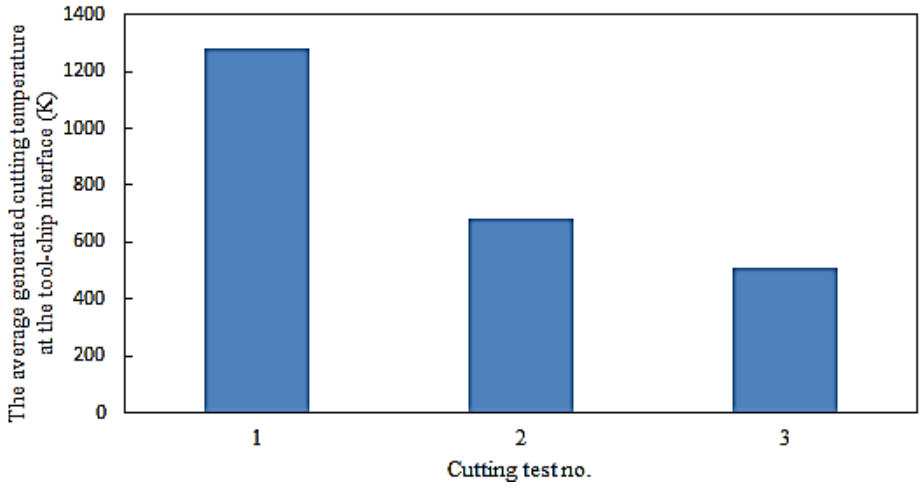

Figure 8-8 Simulated results of average cutting temperatures with/without MWCNTs-nano-fluid during machining Inconel 718

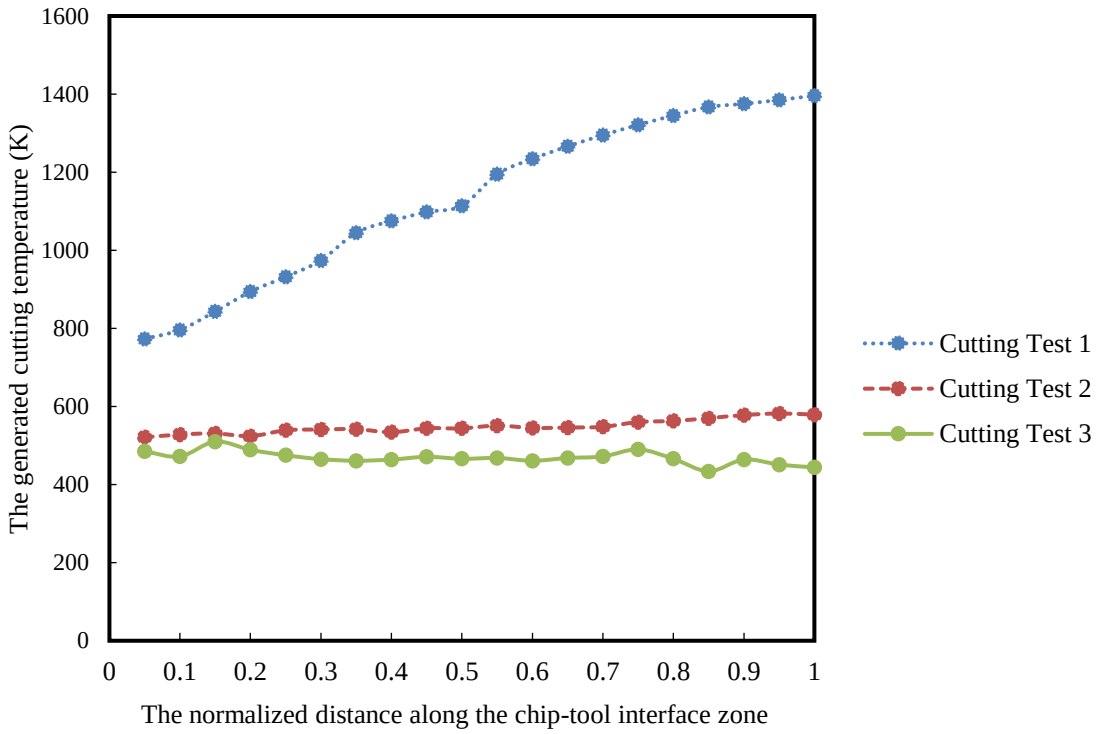

Figure 8-9 The temperature distribution along the chip-tool interface with/without MWCNTs-nano-fluid during machining Ti-6Al-4V

The previous investigations demonstrate the advantage of using MQL-nano-fluid technique in terms of enhancing the cutting process performance by forming a tribo-film along the workpiece and tool surface which decreases the induced friction as well as the shear stresses in the secondary and tertiary shear zones. Thus, that decrease the generated heat which is an important step towards enhancing the machinability in general.

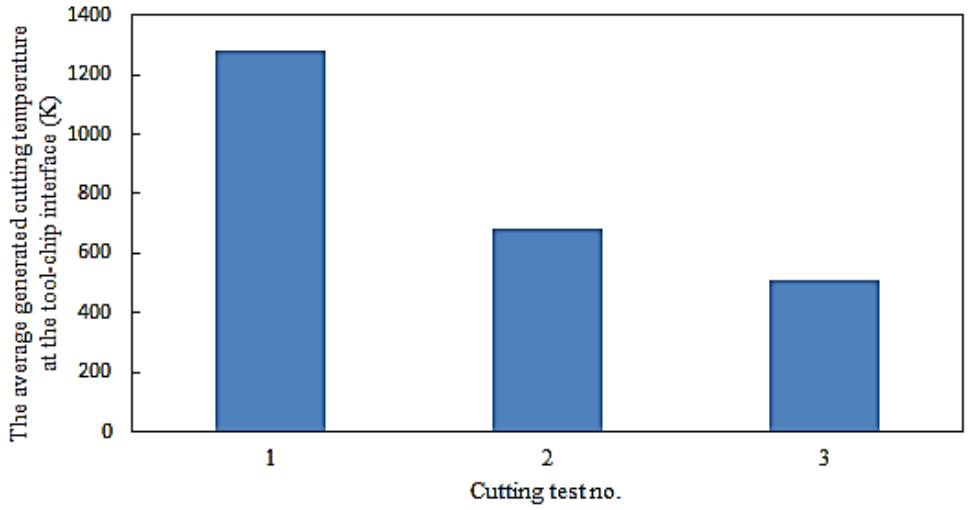

Figure 8-10 Simulated results of average cutting temperatures with/without MWCNTs-nano-fluid during machining of Ti-6Al-4V

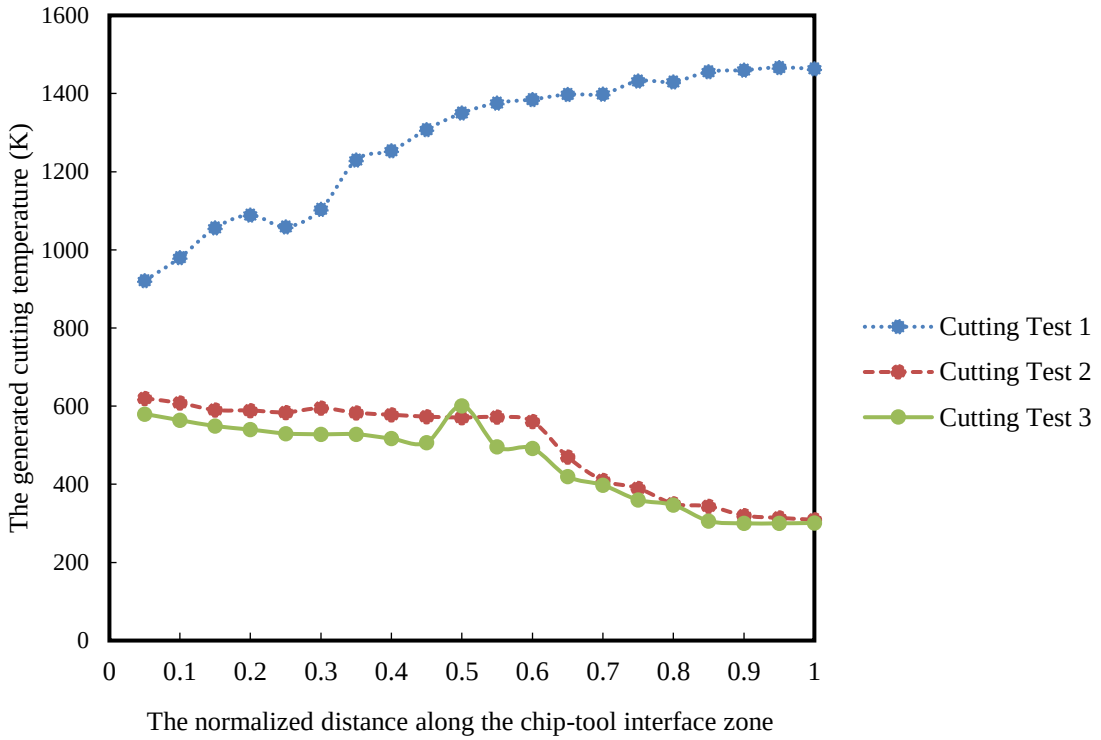

Figure 8-11 The temperature distribution along the chip-tool interface with/without MWCNTs-nano-fluid during machining Ti-6Al-4V

8.5.3. Effect of MQL-Nano-Cutting Fluid on Residual Stresses

The machining induced residual stress is an important characteristic that affect the surface integrity. Machining induced residual stresses depend on different design parameters such as rake angle, cutting speed, and friction as discussed in some previous studies [233, 234]. Also, the resultant residual stresses during machining processes have major effect on the surface quality, especially, its corrosion resistance and fatigue life [235, 236]. In this chapter, the residual stresses which generated beneath the machined surface (i.e., at 100 µm below the machined surface) with/without MWCNTs-nano-fluid during machining Inconel 718 have been calculated. As shown in Figure 8-12, the test performed with employing MQL-MWCNTs-fluid (2 wt. %) showed lower average residual stresses value (max principle stress) than the test employed without MWCNTs. Also, in Figure 8-13, a reduction percentage of about 12.5 % has been noticed between cutting tests 1 and 2, while a reduction percentage about 1of 5.9 % has been observed between after cutting test 1 and 3.

Similarly, for the cutting tests performed on Ti-6Al-4V (see Figure 8-15), the test done using 2 wt. % MWCNTs showed average residual stresses less than the test done using classial MQL. Also, as shown in Figure 8-14, a reduction percentage about 19 % has been noticed between cutting tests 1 and 2, while a reduction percentage about 25 % has been observed between cutting test 1 and 3. Also, it should be stated that the difference between the results of the induced residual stresses during machining Inconel 718 and Ti-6Al-4 is attributed to the difference in the material mechanical properties as well as the used cutting speed.

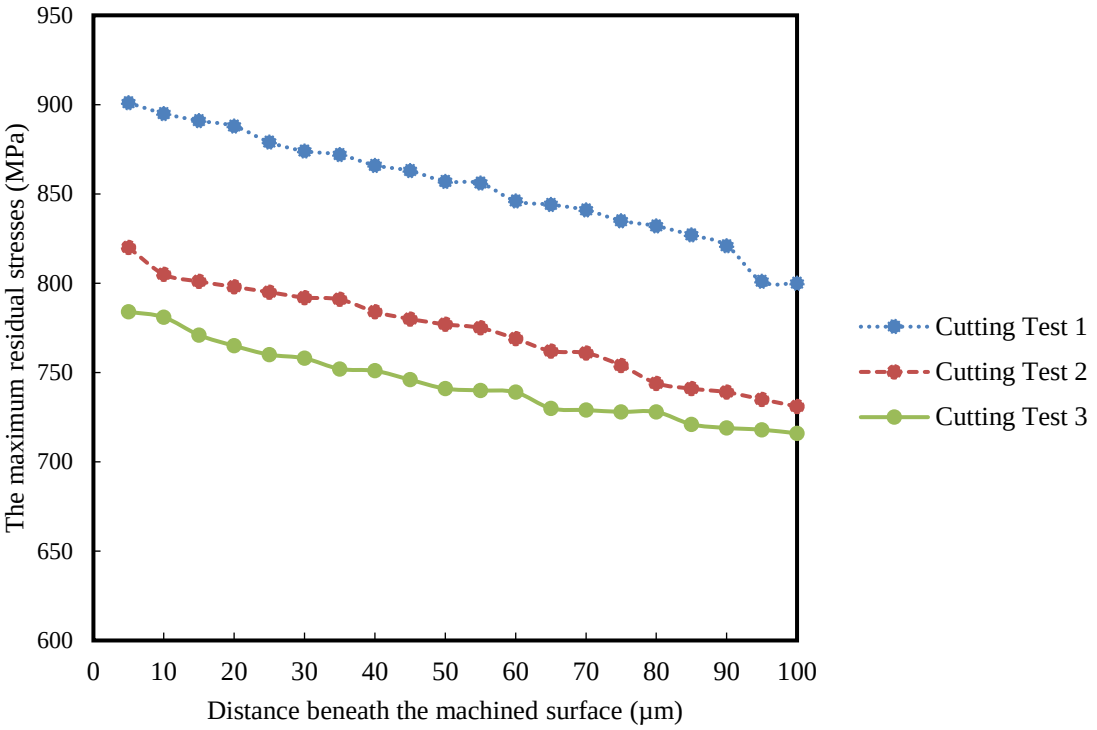

Figure 8-12 FE simulation of maximum residual stresses generated beneath the machined surface during machining Inconel 718 with/without MWCNTs-nano-fluid

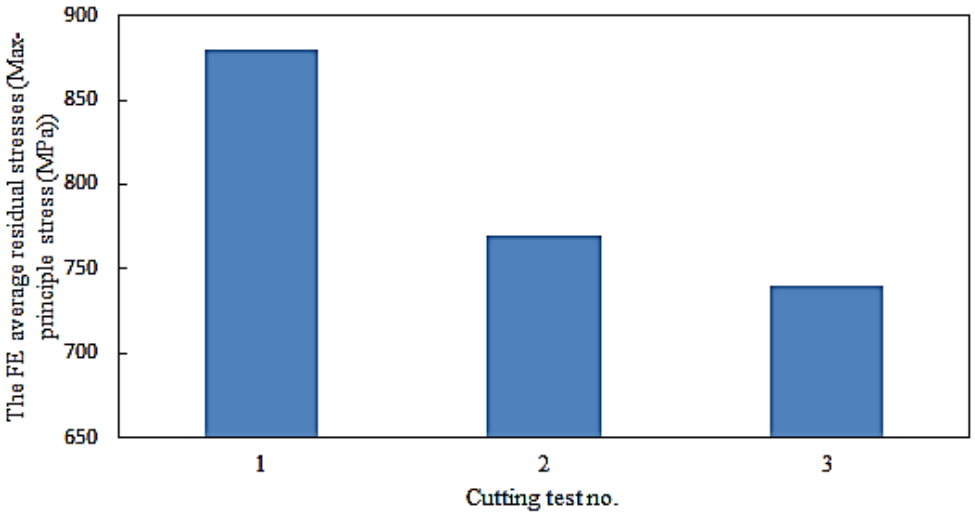

Figure 8-13 Simulated results of average residual stresses with/without MWCNT-nano-fluid during machining Inconel 718

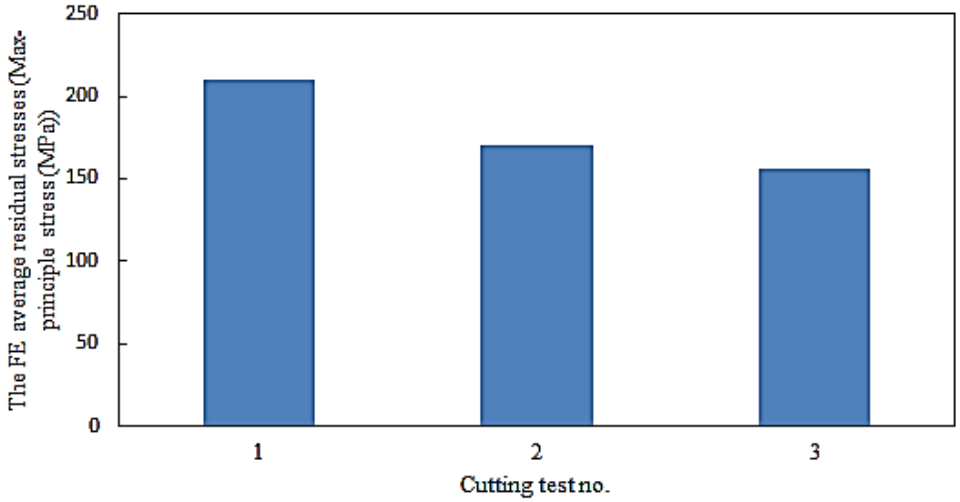

Figure 8-14 Simulated results of average residual stresses with/without MWCNTs-nano-fluid during machining Ti-6Al-4V

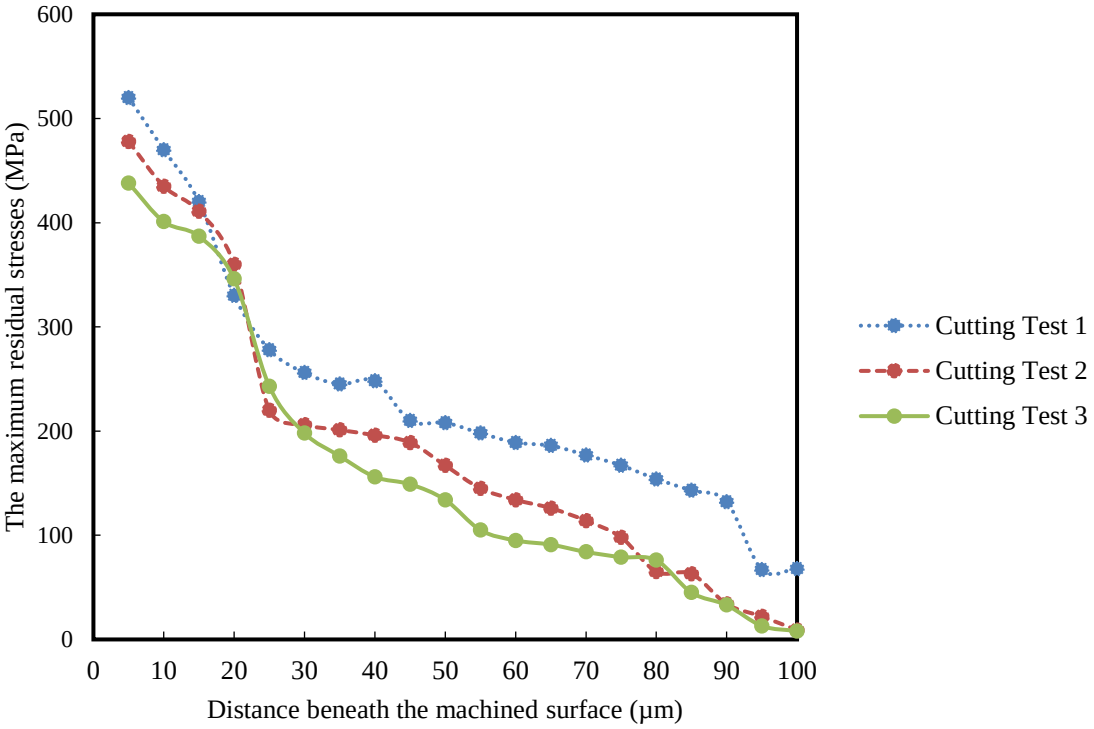

Figure 8-15 FE results for the maximum residual stresses generated beneath the machined surface during machining Ti-6Al-4V with/without MWCNTs-nano-fluid

The nano-cutting fluid technology helps in decreasing the thermal softening and coefficient of friction as mentioned earlier, and it also forms a protective nano-additive thin film during the cutting process which has a vital role in reducing the induced residual stresses in the machined surface. As a result, it is claimed that using nano-cutting fluid could achieve lower induced friction and thermal softening rate without deteriorating the resultant machined surface in terms of generated residual stresses.

8.6. Summary

Details of finite element simulation of machining Inconel 718 and Ti-6Al-4V using MQL-nano-cutting fluids have been presented in this chapter. Two main phases have been employed in order to develop the integrated finite element model. The first phase simulated the thermal effect of the resultant nano-fluid mist through developing a 2-D Axisymmetric Computational Fluid Dynamics (CFD) domain representing the volume occupied by the mixture from inside the MQL nozzle to the interface area between the machined surface and the tool. The average heat convection coefficients results, obtained from the proposed CFD model at standard room temperature demonstrated a good agreement with the theoretical values calculated throughout this chapter. In the second phase, the effectiveness of the use of MQL-nano-cutting fluid in terms of cutting forces, temperature and resulting residual stresses has been analyzed using Lagrangian modeling approach with ABAQUS/Explicit. A boundary film on the machined and cutting tool surfaces is applied to represent the MQL-nano-cutting fluid. The boundary film expresses the nano-fluid mist using different heat convection coefficients values at different cutting temperatures as presented and discussed in the first phase. The experimental and simulated cutting forces showed better agreement in the cutting test performed without nano-additives (accuracy % $\approx$ 90%) than the cutting test performed with nano-additives (accuracy % $\approx$ 82.3%), and that is mainly attributed to neglecting the ploughing effect simulation. Both generated cutting temperature and residual stresses results revealed better performance in the tests performed using MQL-nano-cutting fluid. It is mainly attributed to the promising thermal effect of the added boundary film as well as the lower coefficient of friction values employed in the simulation tests performed using MQL-nano-cutting fluid.

This chapter presents a first attempt to simulate the machining processes using MQL-nano-fluid; however, more improvements are still required in the future work to enhance this integrated model accuracy, particularly providing an accurate simulation of the nano-additives ploughing effects.

Chapter 9 Sustainability Assessment of Machining Processes

9.1. Preamble

Developing a detailed and general assessment model for machining processes is an essential requirement as it can be used in providing optimal cutting conditions and analyzing the flows of energy and materials. In this chapter, a general sustainability assessment algorithm for machining processes is developed and discussed. The four life-cycle stages (pre-manufacturing, manufacturing, use and post-use) are included in the proposed algorithm. Energy consumption, machining costs, waste management, environmental impact, and personal health and safety are used to express the overall sustainability assessment index. A list of indicators is employed under each sustainable metric and a measurement method for each indicator is defined. In addition, the proposed assessment algorithm has the flexibility to assign different weighting importance factors for each metric, indicator, and measured machining characteristic. The current proposed assessment algorithm of machining processes is developed and discussed in order to find the optimal and sustainable process parameter levels by considering both machining quality characteristics as well as the sustainable metrics presented in a previous work [8]. Furthermore, a solid sustainable machining guideline is developed by providing a list of indicators under each sustainable metric and defining the measurement method for each given indicator.

Thus, general assessment algorithm and guideline for sustainable machining processes are proposed in this study. In order to validate the proposed algorithm, three literature case studies have been implemented and results discussed. In addition, the proposed algorithm has been applied to the studied nano-cutting fluid cases and a good agreement with the experimentally measured results has been observed.

9.2. Sustainable Machining Background

Nowadays, a solid comprehensive sustainability assessment methodology is essential in the manufacturing processes. Life cycle assessment (LCA) methodology can be used to assess the manufacturing processes; however, more concern needs to be focused on the product manufacturing and machine tool use phases through obtaining and classifying their corresponding metrics as obtained by Badurdeen et al. [4]. Jayal et al. [3] mentioned that it is necessary to study the concept of sustainable manufacturing through three different levels which include product, process, and system levels as their connection can provide the required sustainable target. In addition, Joshi et al. [5] showed the new sustainable manufacturing 6R approach (reduce, reuse, recover, redesign, remanufacture, recycle) which replaced the 3R approach (reduce, reuse, recycle) of green manufacturing since it theoretically achieves a closed loop and multiple life-cycle paradigms. Although the 6R approach covers a wider range of sustainability aspects it lacks an independent tool to optimize the process. Therefore, a solid assessment tool which could offer an optimal and sustainable solution is highly required. In this chapter, developing a general sustainability assessment algorithm for machining processes is presented and discussed. This algorithm focuses on the main aspects of sustainability (i.e. environmental, economic, and societal). It mainly based on the four life-cycle stages (pre-manufacturing, manufacturing, use and post-use). Five major sustainable metrics which presented by Lu [8] are employed to express the overall sustainability assessment index throughout the proposed algorithm; namely; energy consumption, machining costs, waste management, personal health and operational safety, and environmental impact.

The current proposed assessment algorithm of machining processes is developed and discussed in order to find the optimal and sustainable process parameter levels by considering both machining quality characteristics as well as the sustainable metrics presented in a previous research work [8]. Furthermore, a solid sustainable machining guideline is developed by providing a list of indicators under each sustainable metric and defining the measurement method for each given indicator. Thus, general assessment algorithm and guideline for sustainable machining processes are proposed in this study.

9.3. Sustainability Modeling: Review

Several studies in sustainability modeling have been performed in many manufacturing sectors; however, the machining sector still requires further improvements in terms of providing advanced sustainable techniques to enhance the process and product quality characteristics [237]. In this section, various studies related to sustainability assessment of machining are presented. Identification of the main pillars for achieving sustainable machining processes has been established in a previous work [238]. These pillars are; environmental impact, energy consumption, machining costs, waste management, and personnel health and operational safety. They have mainly focused on presenting a comparative study of two machining processes with and without applying cryogenic systems at different cutting conditions to evaluate the overall cost in terms of energy consumption. Also, another work [239] presents an effective guideline for measuring and assessment of sustainability at GM company (General Motors). It has been based on the identification of stakeholder needs, standardization of business operations and units through national and international levels, and implementation of the continuous improvement concept. Additional work [240] studied the effect of energy consumption since it is an important pillar for manufacturing processes assessment. This work has focused on measuring the energy consumption in both manufacturing and use phases including several energy consumption elements such as cutting fluid, transportation, manufacturing environment, and automation. The results showed the energy consumption and CO_2 emissions for two milling machine tools, and it is recommended to extend this approach with including more sustainable metrics and manufacturing processes.

In addition, a previous study [241] developed a sustainable manufacturing measurement model which includes several sustainable metrics, indicators, guidelines, methods of measurements and techniques of performance evaluation. Several available systems for evaluating the sustainability concept have been listed with their corresponding number of indicators as shown in Table 9-1. Furthermore, a previous research work [242] discussed the product safety index and the different sustainable indicators in the Ford Motor Company. These indicators have been based on LCA methodology and guidelines of ISO 14040 namely; Life Cycle Global Warming Potential, Life Cycle Air Quality Potential, Sustainable Materials, Restricted Substances, Drive-by-Exterior-Noise, Mobility Capability, Safety, and Life Cycle Cost of Ownership.

Table 9-1 Different rating systems of sustainability concept

Sustainability rating systems	No. indicators
Global Report Initiative (GRI)	70
Dow Jones Sustainability Index (DJSI)	12 criteria based single indicators
2006 Environment Performance Indicators	19
United Nations Committee on Sustainable Development Indicators	50
Ford Product Sustainability Index	8
GM Metrics for Sustainable Manufacturing	46
ISO 14031 environmental performance evaluation	155 example indicators
Environmental Indicators for European Union	60
Eco-Indicators 1999	3 main factors based single indicator

Regarding the environmental impact metric, a previous study [243] have discussed the machining processes environmental burden calculations by obtaining emission intensity of CO_2 per consumption resource as it is an important indicator for sustainability evaluation, and it can be used for expressing the coolant usage and energy consumption. Additional work [244] presented the carbon emission signature (CESTM) and carbon emission label concepts in order to evaluate the manufacturing processes environmental effects by calculating the carbon emission intensity associated with each component energy consumption and its corresponding rating factor.

Another study [245] focused on developing and optimizing the energy footprint for machining specific material under dry cutting conditions. The model is developed to express an optimized tool life based on minimum cost and minimum energy consumption through determining the optimal cutting conditions. Also, a previous research work [246] revealed the cryogenic machining promising results in terms of tool wear, cutting temperature, and cutting forces as this study proves that the cryogenic techniques have significant effects of reducing the environmental and social impact. Furthermore, higher production rates and lower wastes have been obtained under using this sustainable cooling technique. Another work presented [50] several machining technologies effects on providing better processes outcomes from a sustainable perspective. High pressure jet-assisted, cryogenic and conventional machining have been used during cutting of Inconel 718 to express their impact on environmental emissions, waste management, machining costs, energy consumption, and personal health. The sustainable machining technologies have obtained better economic, societal and environmental performance in comparison with conventional techniques; however, higher initial setup cost for these technologies is still the main challenge. Additionally, a previous attempt [247] has been presented to develop a thermodynamic framework for sustainable manufacturing processes to determine the processes components efficiencies. The exergy analysis approach has been implemented for the proposed model's development.

Another work [248] showed the exergy analysis implementation to investigate the dry cutting process through studying several cutting parameters effects on exergy loss and efficiency. The proposed model is mainly based on developing a tool life equation which can provide minimum exergy loss. On the other hand, a previous study [249] proposed a new approach for sustainable process measurement (SPM). This approach has been built using four basic pillars; resources and value indicators organization, environmental/economical/societal representation, product life cycle consideration, and concerning with leading system outcomes over business indicators. In terms of measuring sustainable development, several sustainable metrics, and their classifications have been obtained by in a previous work [250]; however, all these metrics are related to certain manufacturing organizations (e.g., OECD toolkit, General Motors metrics for sustainable manufacturing, Ford's PSI).

Thus, there is a need to develop a general guideline for measuring sustainability aspects in the manufacturing sector. Also, another study [251] presented a solid literature review which focused on the energy-efficient machine tools through modelling and analysis of energy loss and evaluating the machine tools energy efficiency. Additional work [252] developed an assessment model in order to evaluate and compare the machining performance of three technological cooling systems which are flood, cryogenic and near dry for a specific machining cases. The used assessment index included only machining cost, quality, and environmental impact. Also, a previous study [253] presented a big data analytics platform evaluate the sustainability performance of machining processes. The proposed platform included big data infrastructure and data analytics to create models which could be used to identify the required function for specific machine tools. An additional work [254] proposed a sustainability assessment framework for turning process. The proposed framework is considering the environmental and economical perspectives along with the cutting tool wear performance.

Another work [255] proposed a frame work for sustainability of machining processes which includes design, modelling, optimization, and assessment through building an integrated framework. In addition, a previous study [256] proposed a model to provide better understanding of machining sustainability under dry, and flood coolant and water vapor environments condition when cutting Inconel 718. It was expected to see a very bad performance during dry cutting of Inconel 718 and thus the authors have concluded their work on a comparison between the flood and water vapor environment and concluded their study by recommending the use of water vapor as an eco-friendly machining technique.

Based on the above mentioned work, it can be concluded that various efforts have been performed in area of sustainable machining; however, there is no generalized and detailed model or tool that can assess the sustainable machining system. Thus, this work is focused on developing a solid and detailed assessment algorithm which could be used as effective tool to quantify the sustainability of machining processes.

9.4. Sustainable Machining Guideline

A previous work [4] presented a proposed guideline for the sustainable manufacturing systems through showing the major manufacturing metrics, their associated indicators and how these indicators can be measured. Similarly, using the same concept under focusing on certain machining considerations, developing a general guideline for the sustainable machining processes is accomplished throughout the current work. This guideline will be used as a preliminary step for developing the sustainable machining algorithm. The proposed sustainable machining guideline depends on five major metrics which are; energy consumption, machining costs, waste management, environmental impact, and personal health and safety.

Figure 9-1 shows a schematic diagram for the sustainable machining guideline which will be briefly discussed during this section. Regarding the indicators measurements, it can be determined using the analytical and numerical models especially for energy consumption, machining costs, process/product quality as will be discussed in the current section. On the other hand, the non-quantifiable indicators can be evaluated depending on the designer's experience and judgment especially for the personal health and operational safety effects as will be clarified in the current section too. In this section, all associated indicators for each metric and their measurements methods are discussed.

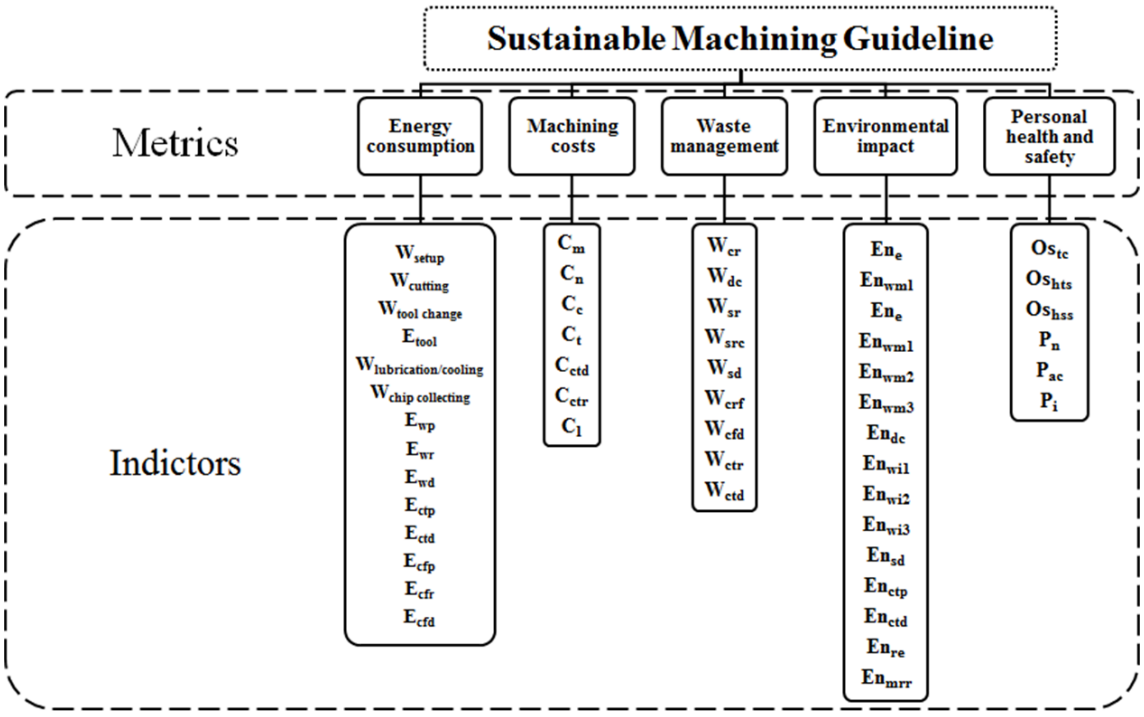

Figure 9-1 The sustainable machining guideline

9.4.1. Energy Consumption

Several assessment indicators are presented for energy consumption as following:

- W_{setup} is the energy consumed by the machine during setup and can be evaluated from the machine's power consumption with the spindle turned off ($\dot{W}_o$) and the total time required for tool and workpiece setup as shown in equation (9.1), where t_{setup} is the required setup time [245];

$$W_{setup} = \dot{W}_o t_{setup} \tag{9.1}$$

- $W_{cutting}$ is the energy required during the machining process and is evaluated from the energy spent on powering the machine modules ($\dot{W}_o$) and the energy for

material removal as shown in equation (9.2), where k is the specific cutting energy (J/mm^3), $\dot{V}$ is material removal rate (mm^3/min), and $t_{cutting}$ is the required cutting time (min) [245];

$$W_{cutting} = (\dot{W}_o + k\dot{v})\, t_{cutting} \tag{9.2}$$

- $W_{tool\ change}$ is defined as the energy consumption during tool change. Since the tool is usually changed with the spindle turned off, the power during tool change is equal to the machine's idle condition power consumption as shown in equation (9.3), where $t_{toolchange}$ is the required time to change the cutting tool, and T is the cutting tool life [245];

$$W_{tool\ change} = \dot{W}_o t_{tool\ change}\left(\frac{t_{cutting}}{T}\right) \tag{9.3}$$

- E_{tool} is the energy footprint of the cutting tool and can be calculated from the product of the energy per cutting edge, $E_{cutting\ edge}$, and the number of the cutting edges required to complete the machining pass as shown in equation (9.4);

$$E_{tool} = E_{cutting\ edge}\left(\frac{t_{cutting}}{T}\right) \tag{9.4}$$

- $W_{lubrication/cooling}$ is the lubrication/cooling system required energy which can be determined as a function of the volume flow rate ($\dot{V}$) and applied pressure of the used cutting fluid ($\dot{P}$) as shown in equation (9.5), where t_{cus} is the cutting usage time;

$$W_{lubrication/cooling} = \dot{P}\,\dot{V}\,t_{cus} \tag{9.5}$$

- $W_{chip\ collecting}$ is the required energy to lift up process's chips;
- E_{wp} is the required energy for production of the used workpiece;
- E_{wr} is the required energy to recycle/recover scrap parts (workpiece);
- E_{wd} is the required energy to dispose of the scrap parts (workpiece);
- E_{ctp} is the required energy for production the used cutting tool;
- E_{ctr} is the required energy to recycle/recover scrap parts (cutting tool);
- E_{ctd} is the required energy to dispose of scrap parts (cutting tool);
- E_{cfp} is the required energy for production of the used cutting fluid;
- E_{cfr} is the required energy to recycle/recover the used cutting fluid;
- E_{cfd} is the required energy to dispose of the used cutting fluid;

9.4.2. Machining Costs

In this section, several machining costs components are presented [257]:

- C_m is the cutting cost which can be expressed using the following terms as shown in equation (9.6), where t_m is the machining time per piece (including the time the feed is engaged whether or not the tool is cutting), l_m is the labor cost of a production operator per unit time, o_m is the overhead charge for the machine, including depreciation, indirect labor, and maintenance cost;

$$C_m = t_m (l_m + o_m) \tag{9.6}$$

- C_n is the cost associated with non-machining time, i.e., setup cost, preparation, time for loading & unloading, idle machine time (unit cost/piece);
- C_c is the cost of tool changing which can be expressed using the following terms as shown in equation (9.7) where t_g is the time required to grind and change a cutting edge, t_{ac} is the actual cutting time per piece, T is the tool life for a cutting edge, l_g is the labor rate for a tool room operator, o_g is the overhead rate for the tool room operation;

$$C_c = t_g \frac{t_{ac}}{T}(l_g + o_g) \tag{9.7}$$

- C_t is the tool cost per piece which can be expressed as shown in equation (9.8), where C_e is the cost of a cutting edge, and $\frac{t_{ac}}{T}$ is the number of tool changes required per piece;

$$C_t = C_e \frac{t_{ac}}{T} \tag{9.8}$$

- C_{ctd} is the cost of cutting tool disposal (unit cost/Kg);
- C_{ctr} is the recycling cost of cutting tool (unit cost/Kg);
- C_l is the cutting fluid preparation costs and it can be expressed using the following terms as shown in equation (9.9), where C_{co} is the production cost of cutting oil (unit cost/liter), C_{ad} is the cost of additives (unit cost/liter), C_{di} is the required cost to disperse the additives into the main cutting oil (unit cost/liter), C_{setup} is the required cost for lubrication/cooling system setup (unit cost/liter), C_{dis} is the cost of cutting fluid disposal (unit cost/liter), and C_{lr} is the recycling cost of cutting fluid (unit cost/liter);

$$C_l = C_{co} + C_{ad} + C_{di} + C_{setup} + C_{dis} + C_{lr} \tag{9.9}$$

9.4.3. Waste Management

Several indicators are used to predict the waste management and it is based on the same way of assessment which presented in a previous work [4]; however, more focus has been given to the machining processes considerations within this guideline as following:

- W_{rc} is the ratio of recycled chips which can be expressed using the following terms as shown in equation (9.10), where m_{cr} is the total mass of recycled chips and m_c is the total mass of chips;

$$W_{rc} = \frac{m_{rc}}{m_c} \tag{9.10}$$

- W_{dc} is the ratio of disposed of chips and it can be expressed using the following terms in equation (9.11), where m_{dc} is the total mass of disposed of chips;

$$W_{dc} = \frac{m_{dc}}{m_c} \tag{9.11}$$

- W_{sr} is the ratio of remanufactured scrap parts and it can be expressed using the following terms in equation (9.12), where m_{sr} is the total mass of remanufactured scrap parts and m_s is the total mass of scrap parts;

$$W_{sr} = \frac{m_{sr}}{m_s} \tag{9.12}$$

- W_{src} is the ratio of recycled scrap parts and it can be expressed using the following terms as shown in equation (9.13), where m_{src} is the total mass of recycled scrap parts;

$$W_{src} = \frac{m_{src}}{m_s} \tag{9.13}$$

- W_{sd} is the ratio of disposed scrap parts and it can be expressed using the following terms as shown in equation (9.14), where m_{sd} is the total mass of disposed of scrap parts;

$$W_{sd} = \frac{m_{sd}}{m_s} \tag{9.14}$$

- W_{cfr} is the mass of recycled/recovered cutting fluid;
- W_{cfd} is the mass of disposed of cutting fluid;
- W_{ctr} is the mass of recycled/recovered cutting tool;
- W_{ctd} is the mass of disposed of cutting tool;

9.4.4. Environmental Impact

The environmental impact of different elements of the machining process can be expressed by multiplication of the used resource quantity with its respective emission intensity. The set of emission intensity values (i.e., based on a Japanese energy mix) and quantification of the resources used are listed in Table 9-2 [243].

9.4.5. Personal Health and Operational Safety

Indicators for personal health and operational safety are developed and discussed as following:

- OS_{tc} is an operational safety index used to express the exposure of the toxic chemical during cutting fluid preparation or cutting process itself (mist/dust level). This value can be 1, 2, or 3 depending on its harmful effects (type and concentration %), where 1 is the lowest level and 3 is the highest level. It should be selected manually;
- OS_{hts} is an operational safety index used to express the high-temperature surface exposure during the cutting processes. This value can be 1 or 2 depending on the measured cutting temperature level, where it will be given by 1 at cutting temperature less than 600^{o}C, and 2 during cutting temperature above this level. In addition, it can be selected manually without considering the previous criteria;

Table 9-2 Environmental impact ratings based on CO_2 emission intensities

Symbol	Resources	Rate	Measurement method
En_e	Electricity (kg-CO_2/kWh)	0.38	$W_{setup} + W_{machining} + W_{tool} + E_{tool} + W_{lubrication/cooling} + W_{chip\ collecting}$
En_{wm1}	Cutting fluid disposal, water-miscible cutting fluid; type A1 (kg-CO_2/L)	3.78	The volume of water-miscible cutting fluid which disposed of by normal techniques
En_{wm2}	Cutting fluid disposal, water-miscible cutting fluid; type A2 (kg-CO_2/L)	5.14	The volume of water-miscible cutting fluid which disposed of by thermal recycle
En_{wm3}	Cutting fluid disposal, water-miscible cutting fluid; type A3 (kg-CO_2/L)	8.10	The volume of water-miscible cutting fluid which disposed of by material recycle
En_{dc}	Cutting fluid disposal, distilling and condensing process (kg-CO_2/L)	3.42	The volume of cutting fluid which disposed of using distilling and condensing process (L)
En_{wi1}	Cutting fluid disposal, water-insoluble cutting fluid; normal (kg-CO_2/L)	2.55	The volume of water-insoluble cutting fluid which disposed of by normal techniques
En_{wi2}	Cutting fluid disposal, water-insoluble cutting fluid; thermal recycle (kg-CO_2/L)	1.77	The volume of water-insoluble cutting fluid which disposed of by thermal recycle
En_{sd}	Spindle lubricant oil production and disposal (kg-CO_2/L)	0.46	The volume of spindle lubricant oil (L)
En_{ctp}	Cutting tool production (kg-CO_2/kg)	33.7	The mass of the used cutting tool (Kg)

- OS_{hss} is an operational safety index used to express the high-speed surface exposure during the cutting processes. This value can be 1 or 2 depending on the used cutting speed level, where it will be given by 1 at cutting speed less than 900 rpm, and 2 during cutting speed above this level. In addition, it can be selected manually without considering the previous criteria;

- P_n is a personal health index used to express the noise level of working environment during the cutting processes. This value can be 1 or 2 depending on the measured noise level, where it will be given by 1 at noise level less than 90 dB, and 2 during noise level above this value. In addition, it can be selected manually without considering the previous criteria;

- P_{ac} is a personal health index used to express the working environment atmospheric conditions during the cutting processes. This value can be 1 or 2 depending on the measured wet-bulb globe temperature (WBGT). WBGT is a measure for atmospheric conditions which considers humidity, temperature, wind speed, and solar radiation. This index will be given by 1 at WBGT level less than 82^oF, and 2 during WBGT level above this value. In addition, it can be selected manually without considering the previous criteria;

- P_i is a personal health index used to express the illumination level of working environment during the cutting processes. This value can be 1 or 2 depending on the measure illumination level, where it will be given by 2 at illumination level less than 75 fc, and 1 during illumination level above this value. In addition, it can be selected manually without considering the previous criteria;

At the end of this section, it can be obtained that all sustainable metrics are associated with a list of indicators to express and evaluate the sustainability major aspects through the four life-cycle stages by obtaining what/how must be measured. In the next section, the proposed assessment algorithm will be presented and discussed.

9.5. The Proposed Sustainable Machining Algorithm

The main objective of the proposed algorithm [264] is to find the optimal and sustainable process parameters levels by considering both machining quality characteristics as well as the sustainable indicators presented in the previous section. The proposed algorithm provides an overall assessment index which expresses the whole sustainable machining system in terms of the studied machining metrics, indicators and machining responses. Furthermore, the current algorithm accommodates several machining responses and sustainable indicators regardless of their criteria (higher-the-better, lower-the-better, or nominal-the-better). In general, the developed algorithm is a heuristic approach (multi-objectives solver) and specific for the sustainable machining optimization. The proposed algorithm notations are defined as following:

N_{dp}	number of selected design parameters
N_{li}	number of levels per each design parameter (i)
M	number of selected machining quality characteristics (responses)
N	number of experimental cutting tests
NM	number of studied sustainable metrics
N_k	number of selected indicators for each sustainable metric (k)
I_{kp}	value for each sustainable indicator (p)
Mr_j	value for each machining response (j)
MQW_j	weighting importance factor for each machining response (j)
SMW_k	weighting importance factor for each sustainable metric (k)
IW_{kp}	weighting importance factor for each sustainable indicator (p)
SF_{kpjn}	sustainable factor for each cutting test (n)
SI_{kpjn}	sustainable index for each cutting test (n)
WSI_{kpjn}	weighted sustainable index for each cutting test (n)
$TWSI_n$	total weighted sustainable index for each cutting test (n)
$AWSI_{jn}$	average weighted sustainable index for each machining characteristic (j)
$AWSI_{kn}$	average weighted sustainable index for each sustainable assessment metric (k)
$OAWSI_n$	overall average weighted sustainable index for each cutting test (n)

n	cutting tests counter
i	design parameter levels counter
k	sustainable metrics counter
p	sustainable indicators counter
j	machining responses counter

The proposed sustainable algorithm is presented and discussed in this section. Figure 9-2 shows the main steps for the proposed sustainable assessment process. The experimental cutting tests results are used beside its corresponding sustainable indicators in order to predict the sustainable factor for each cutting test. The sustainable factor per each cutting test is calculated as shown in equation (9.15).

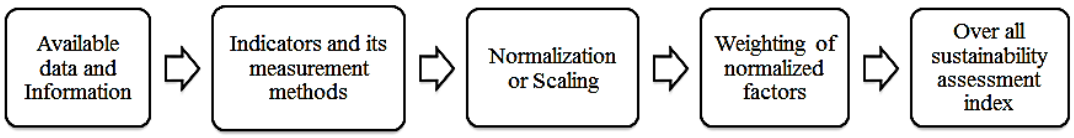

Figure 9-2 Sustainability assessment of machining processes

$$SF_{kpjn} = \begin{cases} I_{kp} Mr_j & \text{if } I_{kp} \text{ and } Mr_j \text{ are both LB or HB} \\ \dfrac{Min(I_{kp}, Mr_j)}{Max(I_{kp}, Mr_j)} & \text{otherwise,} \end{cases} \tag{9.15}$$

The optimal sustainable factor is then selected depending on the studied indicators and responses criteria (higher-the-better (HB) or lower-the-better (LB)). The optimal sustainable factor is then compared with the other sustainable factors to predict the sustainable index for each cutting test (i.e., Normalization/Scaling). The sustainable index per each cutting test can be determined as shown in equation (9.16).

$$SI_{kpjn} = \begin{cases} \dfrac{Min(SF_{kpj})}{SF_{kpjn}} & \text{if } SF_{kpj} \text{is based on LB} \\ \dfrac{SF_{kpjn}}{Min(SF_{kpj})} & \text{if } SF_{kpj} \text{is based on HB} \end{cases} \quad (9.16)$$

Thus, the maximum sustainable index value should be 1. Furthermore, different weighting importance factors for the studied metrics, indicators, and machining characteristics are provided in order to calculate the weighted sustainable index for each cutting test as can be obtained in equation (9.17).

$$WSI_{kpjn} = SMW_k MQW_j IW_{kp} SI_{kpjn} \quad (9.17)$$

The last step is calculating the total weighted sustainable index for each cutting test. As shown in equation (9.18).

$$TWSI_n = \sum_{k=1}^{NM} \sum_{p=1}^{N_k} \sum_{j=1}^{M} WSI_{kpj} \quad (9.18)$$

In addition, the average weighted sustainable index for each cutting test can be determined as shown in equation (9.19).

$$OWSI_n = \frac{\sum_{k=1}^{NM} \sum_{p=1}^{N_k} \sum_{j=1}^{M} WSI_{kpj}}{(M)\sum_{k=1}^{NM} N_k} \quad (9.19)$$

Furthermore, other assessment indices are also presented using this algorithm to analyze the machining process sustainability with more focusing on the studied machining characteristics or sustainable metrics such as; $AWSI_{jn}$ and $AWSI_{kn}$, respectively. These indices can be determined as shown in equations (9.20) and (9.21).

$$AWSI_{jn} = \sum_{k=1}^{NM} \sum_{P=1}^{N_k} WSI_{kp} \tag{9.20}$$

$$AWSI_{jn} = \frac{\sum_{p=1}^{N_k} \sum_{j=1}^{M} WSI_{pj}}{(M)(N_k)} \tag{9.21}$$

The proposed algorithm flow chart which obtains the previously mentioned steps is established as shown in Figure 9-3. To sum up, $TWSI_n$ can be used as an overall assessment index which expresses the whole sustainable machining system in terms of the studied machining metrics, indicators, and machining responses.

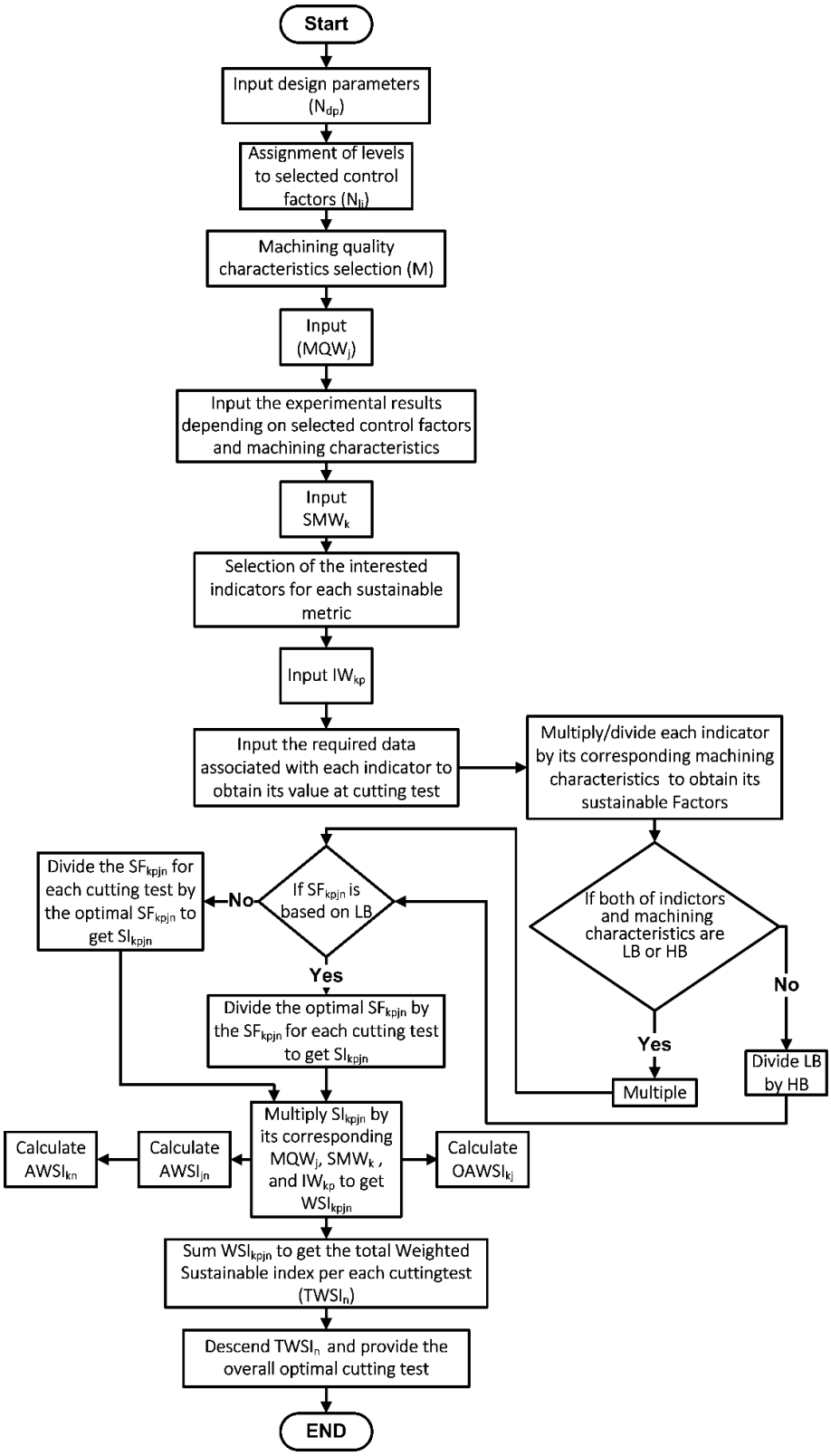

Figure 9-3 Proposed algorithm of sustainability assessment of machining processes

9.6. Assessment Model Validation (Case Studies)

The proposed algorithm is validated using several experimental data to ensure that the optimal conditions predicted by the proposed algorithm are consistent with the physical findings in different experimental studies. Attention was made to ensure that cases studies have a wide range of process parameters and process outputs. The process parameters include feed rate, cutting speed, depth of cut, tool geometry, and lubrication strategy, while the process outputs include energy consumption, flank tool wear, average surface roughness and tool life. Furthermore, in order not to overweight the sustainable indicators over other indicators and to handle the redundancy issue, lower weighting factors can be used. The proposed approach provides the decision makers the flexibility to select and assign different weighting factors for the measured machining process outputs, metrics and indicators (see Figure 9-3 & Equation (9.17)), so that the current algorithm can handle the redundancy problem.

9.6.1. Case Study I

The proposed assessment algorithm is utilized in a literature case study to validate the developed assessment model. A previous study [258] has performed thirty cutting tests during turning of AA7075-15 wt. % SiC Particles (20-40 µm) composite using CNMG 12040EM cutting inserts. The process parameters include; cutting speed, feed rate, depth of cut and nose radius while each design parameter includes three different levels. Investigations have been carried out to study the tool life and energy consumption. The proposed algorithm is implemented to predict the optimum tool life and energy consumption in these tests based on the following assumptions:

- Energy consumed, and environmental impact (CO_2 emissions) are the two sustainable metrics used;
- The sustainable indicator for environmental impact is E_{ne} which is evaluated based on Table 9-2;
- Equally weighting factors for sustainable metrics are assumed;

Based on these assumptions, the sustainable weighted index for each experimental cutting test is calculated and plotted in Figure 9-4. As can be seen in the Figure 9-4, cutting test 1 has the highest weighted sustainable index. The process parameters employed in this test were: cutting speed of 90 m/min, feed rate of 0.15 mm/min, depth of cut of 0.2 mm and nose radius of 0.4 mm. The highest weighted sustainable index predicted the same measured optimal energy consumption and tool life results which were 1.012 kWh and 6.5 min respectively. In addition, the lowest index is obtained at cutting test 16 which has the highest energy consumption and the lowest tool life results of 2.16 kWh and 0.6 min respectively. Based on this case study the proposed algorithm has predicted identical values (see Table 9-3) for best and worst cases scenarios for energy consumption and tool life.

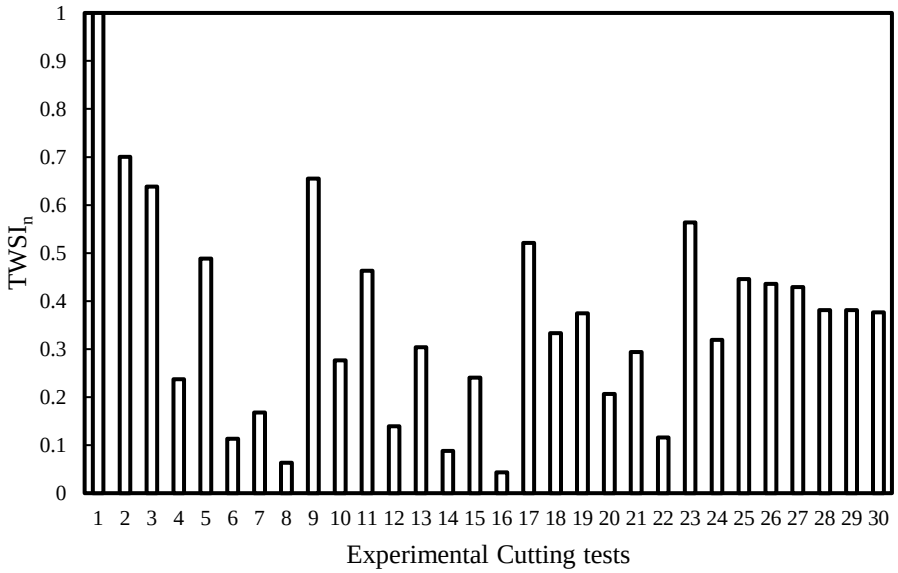

Figure 9-4 Total weighted sustainable indices results (Case I)

Table 9-3 The proposed assessment algorithm results versus optimal results (Case I)

The measured machining responses	The proposed assessment algorithm results	The optimal machining responses results
Energy consumption (kWh)	1.012	1.012
Tool life (min)	6.5	6.5

9.6.2. Case Study II

A previous research work [259] performed 27 cutting tests to evaluate the machined average surface roughness and energy consumption during turning of AISI 1045 steel. Uncoated tungsten carbide tool (TNMG 16 04 12) has been used in the tests. The process parameters include cutting speed, feed rate and depth of cut. The presented assessment algorithm is employed to evaluate the optimum surface roughness and power consumption in these tests based on the following assumptions and the weighted sustainable index is calculated. The employed assumptions are:

- The energy consumed during the cutting process is the only studied sustainable metric;
- The average surface roughness is the only studied machining quality characteristic

Figure 9-5 shows the proposed algorithm results based on the above assumptions. The predicted data based on the assessment algorithm revealed that the highest assessment index is obtained at cutting test 10 in (see Figure 9-5), which was performed at cutting speed of 134.3 m/min, feed rate of 0.12 mm/min and depth of cut of 0.5mm. At this predicted optimal condition, the measured surface roughness and energy consumption values were 1.284 µm and 0.574 kW respectively. The measured average surface roughness and energy consumption revealed optimum values of 1.257 µm and 0.543 kW, respectively at cutting test 11 in (see Figure 9-5). This confirms a good agreement between the measured optimal process response and the one predicted by the proposed assessment algorithm (see Table 9-4). On the other hand, cutting test 27 shows the lowest assessment index which is also represented the highest surface roughness and energy consumption results of 3.574 µm and 2.43 kW respectively. In that case, the predicted and measured values are identical.

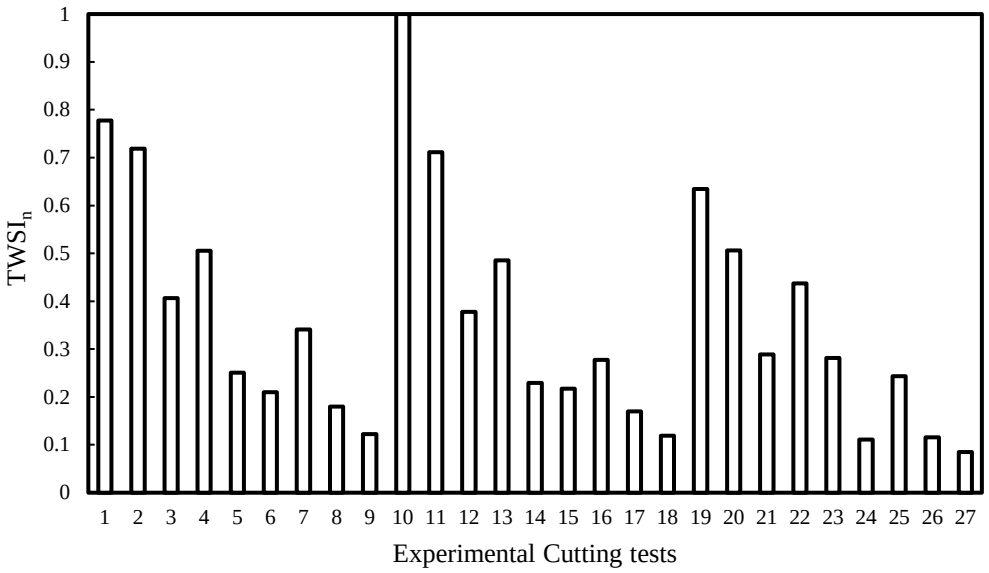

Figure 9-5 Total weighted sustainable indices results (Case II)

Table 9-4 The proposed assessment algorithm results versus optimal results (Case II)

The measured machining responses	The proposed assessment algorithm results	The optimal machining responses results
Energy consumption (kW)	0.574	0.543
surface roughness (μm)	1.284	1.257

9.6.3. Case Study III

A previous work [260] presented 27 experimental trials on PEEK-CF30 composite (i.e. reinforced PEEK with 30% of carbon fibers (PEEK-CF30)). Dry turning trials have been carried out on a GORATU GCRONO 4S CNC using TiN coated cutting tools (WNMG080408-TF). The processes parameters include; cutting speed, feed rate and depth of cut. Investigations have been carried out to study the average surface roughness and energy consumption through using L27OA based on the Taguchi experimental design. The following points have been assumed to accommodate the developed algorithm implementation:

- The studied metrics are the energy consumption, and environmental impact (CO_2 emissions);
- The studied sustainable indicator for environmental impact is En_e (kg-CO_2/kWh);
- The average surface roughness is the only studied machining quality characteristic;
- Equally weighting factors for sustainable metrics are assumed;

The total weighted indices are calculated depends on the previous assumptions and the results are provided as shown in Figure 9-6. It is obtained that cutting test 27 has the highest weighted sustainable index as shown in Figure 9-6. Cutting test 27 is performed at cutting speed of 100m/min, feed rate of 0.05 mm/min and depth of cut of 0.25mm. At this predicted optimal condition, the average surface roughness and power consumption values were 1.14 µm and 7.3 kW respectively. This cutting test offers the optimal power consumption value (see Table 9-5); however, the average surface roughness isn't the same as the measured optimal value as the proposed assessment algorithm is designed to achieve a multi-objective optimization depends mainly on the provided assumptions (e.g. studied indicators, weighting factors). On the other hand, cutting test 1 shows the lowest assessment index as it has the highest surface roughness and energy consumption of 1.855 µm and 49.7 kW respectively. In that case, the predicted and measured values are identical.

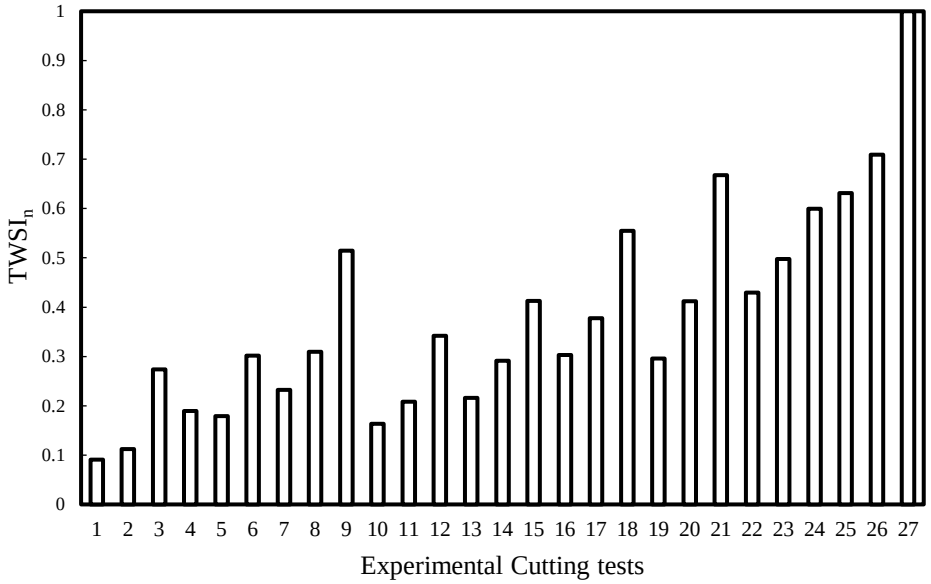

Figure 9-6 Total weighted sustainable indices results (Case III)

Table 9-5 The proposed assessment algorithm results versus optimal results (Case III)

The measured machining responses	The proposed assessment algorithm results	The optimal machining responses results
Energy consumption (kW)	7.3	7.3
surface roughness (μm)	1.14	0.98

These studies have focused only on using equally weighting factors for machining characteristics, metrics, and indicators to find the optimal process parameter levels; however, different weighting factors can be implemented through this proposed algorithm. Therefore, this assessment algorithm has the flexibility to be utilized in any further case studies.

9.7. Nano-Cutting Fluids Case Studies

The proposed assessment algorithm has been implemented in the studied nano-cutting fluid cases in order to ensure that the optimal conditions predicted by the proposed algorithm are consistent with the physical findings in the studied experimental cases. The following points have been assumed to accommodate the developed algorithm implementation;

- The studied metrics are the energy consumption, environmental impact (CO_2 emissions), and personal health and operational safety

- The sustainable indicator for environmental impact is E_{ne} which is evaluated based on Table 9-2.

- The sustainable indicators for the personal health and operation safety metric are OS_{tc}, OS_{hts}, and OS_{tc}

- Equally weighting factors for sustainable metrics and machining quality characteristics are implemented.

The assessment results for the three studied cases are provided as shown in Tables 9-6, 9-7 and 9-8. In the all studied cases; Ti-6Al-4V with MWCNT (see Figure 9-7), Inconel 718 with MWCNT (see Figure 9-8), and Inconel 718 with Al_2O_3 (see Figure 9-9), the highest index is demonstrated at cutting test 4 which includes the medium level of cutting speed, the lowest level of feed rate, and 2 wt.% of added nano-additives. While the lowest index in all case studies (see Tables 9-4, 9-5, and 9-6) is revealed at cutting test 6 that has been performed at the medium level of cutting speed, the highest level of feed rate, and without any added nano-additives.

The current findings are confirmed by the previous experimental investigations provided in chapters 5 and 6 as the employed nano-cutting fluids offers promising results in comparison with the tests performed without nano-additives; however, the optimal added nano-additive percentage was 2 wt.%. This finding provides more physical sense as the highest percentage of nano-additive (4 wt. %) could cause more deteriorations to the cutting processes because of the highest occurrence possibility of the drastic ploughing effects and high induced friction.

Table 9-6 Total weighted sustainable indices results of machining Ti-6Al-4V with MWCNTs

Cutting test #	Machining quality characteristics		Energy consumption metric	Environmental impact metric (kg-CO_2/kWh)	Personal health and operational safety metrics			$TWSI_n$
	Flank wear	Surface roughness	Energy consumption	En_e	OS_{tc}	OS_{hts}	OS_{hss}	
1	0.44	0.89	2325	885.825	1	2	1	0.354553
2	0.18	0.85	2084	794.004	2	2	1	0.598868
3	0.16	1.85	2192	835.152	2	2	1	0.493268
4	0.29	0.51	2138	814.578	2	2	1	0.607399
5	0.21	1.063	2230	849.63	2	2	1	0.471409
6	0.62	2.8	2454	934.974	1	2	1	0.160113
7	0.45	0.55	2410	918.21	2	2	1	0.452747
8	0.56	1.89	2634	1003.554	1	2	1	0.190617
9	0.42	1.43	2344	893.064	2	2	1	0.267851

With more focus on the studied cases associated with cutting Inconel 718, it was found that cutting test 4 has the highest weighted sustainablity index as shown in both Figure 9-8 and Figure 9-9. Cutting test 4 has been performed at cutting speed of 40 m/min, feed rate of 0.2 mm/rev and nano-additives weight percentage of 2 wt.%. At this predicted optimal condition, the average surface roughness values were 1.35 µm and 1.76 µm, while the flank wear values were 0.187 mm and 0.213 mm for MWCNTs, and Al_2O_3 nano-fluids, respectively. This cutting test offers the same optimal average surface roughness value when machining Inconel 718 with MWCNTs nano-fluid (see Figure 5-5 and Table 9-9); however, the predicted average surface roughness in the case of Al_2O_3 nano-fluid is not the same as the measured optimal value. This is due to the fact that the proposed assessment algorithm is designed to achieve a multi-objective optimization and it depends mainly on the provided assumptions (e.g. studied indicators, weighting factors). However, the predicted and optimal average surface roughness values in case of Al_2O_3 nano-fluid were in close agreement as shown in Table 9-9. Regarding the flank wear results, the model offers the same optimal flank wear values when machining Inconel 718 with Al_2O_3 nano-fluid (see Figure 5-1 and Table 9-9). The predicted flank wear in case of MWCNTs nano-fluid is not the same as the measured optimal value; however, the predicted and optimal flank wear values were in close agreement as shown in Table 9-9.

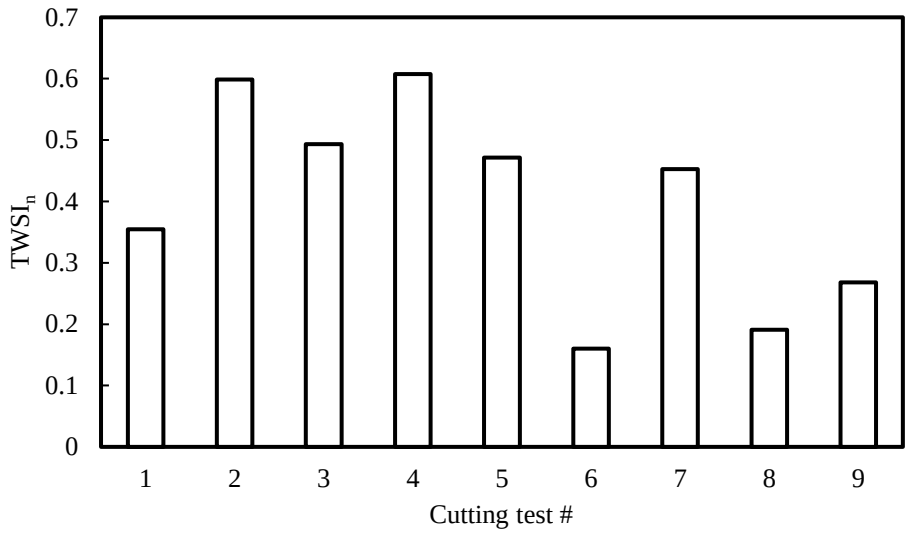

Figure 9-7 Total weighted sustainable indices results of machining Ti-6Al-4V with MWCNTs

Table 9-7 Total weighted sustainable indices results of machining Inconel 718 with MWCNTs

Cutting test #	Machining quality characteristics		Energy consumption metric	Environmental impact metric (kg-CO_2/kWh)	Personal health and operational safety metrics			$TWSI_n$
	Flank wear	Surface roughness	Energy consumption	E_{ne}	OS_{tc}	OS_{hts}	OS_{hss}	
1	0.295	3.21	1736	661.416	1	2	1	0.351883
2	0.145	2.54	1602	610.362	2	2	1	0.606391
3	0.165	3.5	1652	629.412	2	2	1	0.48653
4	0.187	1.35	1706	649.986	2	2	1	0.673904
5	0.17	1.98	1721	655.701	2	2	1	0.57455
6	0.32	6.32	1807	688.467	1	2	1	0.247136
7	0.21	1.54	1807	688.467	2	2	1	0.56633
8	0.387	3.85	1963	747.903	1	2	1	0.253571
9	0.28	3.5	1809	689.229	2	2	1	0.323941

On the other hand, cutting test 6 showed the lowest assessment index in both employed cases (see Figure 9-8 and Figure 9-9). This cutting test has been performed at cutting speed of 40 m/min, feed rare 0.4 mm/rev, and without nano-additives. The flank wear and average surface roughness results at cutting test 6 were; 0.32 mm and 6.23 µm, respectively. Regarding the average surface roughness results, the model and measured values are identical since both of them confirmed that the worst surface quality occurred after cutting test 6 (see Figure 5-5, Figure 9-8 and Figure 9-9). In terms of the flank wear results, the model and measured values weren't in agreement since cutting test 8 showed the highest flank wear (see Figure 5-1); however, both of them confirmed that the highest flank wear occurred during machining Inconel 718 without nano-additives. Thus, it can be concluded that the model outputs are consistent with the physical findings in the current experiments since the optimal experimental values and model indices have been obtained under using the MQL-nano-fluids.

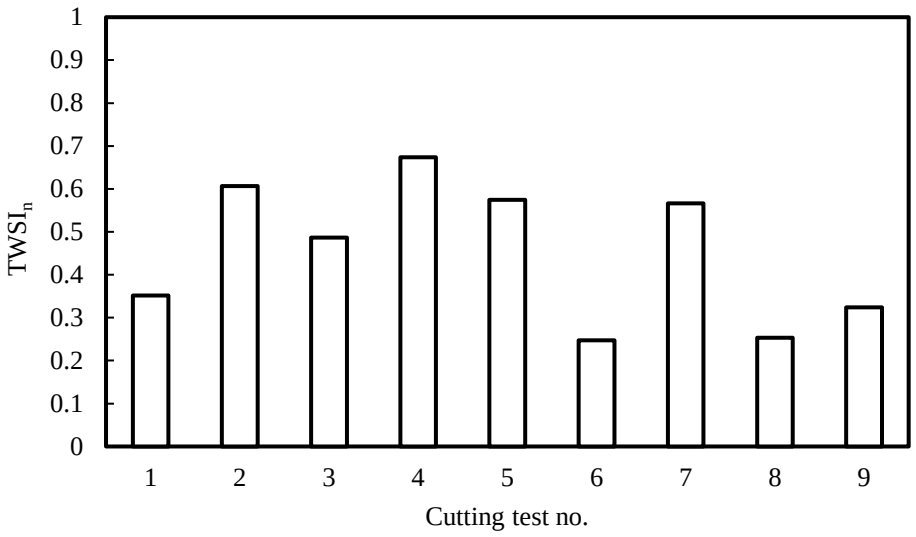

Figure 9-8 Total weighted sustainable indices results of machining Inconel 718 with MWCNTs

Table 9-8 Total weighted sustainable indices results of machining Inconel 718 with Al_2O_3

Cutting test #	Machining quality characteristics		Energy consumption metric	Environmental impact metric (kg-CO2/kWh)	Personal health and operational safety metrics			TWSIn
	Flank wear	Surface roughness	Energy consumption	E_{ne}	OS_{tc}	OS_{hts}	OS_{hss}	
1	0.295	3.21	1736	661.416	1	2	1	0.381151
2	0.145	2.86	1602	610.362	2	2	1	0.622218
3	0.165	3.87	1652	629.412	2	2	1	0.501623
4	0.187	1.763	1706	649.986	2	2	1	0.640188
5	0.17	2.45	1721	655.701	2	2	1	0.566734
6	0.32	6.32	1807	688.467	1	2	1	0.264737
7	0.21	1.513	1807	688.467	2	2	1	0.634532
8	0.387	3.85	1963	747.903	1	2	1	0.278177
9	0.28	4.2	1809	689.229	2	2	1	0.324196

Regarding the optimal levels of the nano-additives concentration, it has been found that 4 wt. % for both Al_2O_3 and MWCNTs nano-fluids showed the best experimentally surface quality and tool wear; however, no noticeable change has been observed between 2 wt. % and 4 wt. % in the energy consumption results. The assessment model showed that cutting test 4 is the optimal test which has the highest total weighted index. The nano-additives concentration at this test is 2 wt. %. At this point, the experimental investigations were not the same as the assessment model findings; however, the model finding provides more physical sense as the highest percentage of nano-additive (4 wt. %) could cause more deteriorations to the cutting processes. This can be attributed to the highest occurrence possibility of the drastic ploughing effects which could increase the induced nano-additives wear and accordingly increase the overall tool wear. When there is an abundance of nano-additives in the resultant nano-fluid, they collide with and are impeded by the asperities on the work surface and hence generate higher cutting forces. As a result, the nano-additive induced wear is increased with increasing the nano-additives concretion as similarly discussed in a previous work [182] (see Figure 7-4). On the other hand, increasing the nano-additives concentration would increase the resultant nano-fluid thermal conductivity and would improve the heat dissipation performance. Moreover, increasing the nano-additives concentration means more nano-additives in the workpiece-interface area, and therefore the induced friction would decrease as can be seen in Figure 7-4. Thus, the nano-

additives concentration should be carefully selected and optimized in order to strike a balance between all previous considerations.

Table 9-9 The assessment model results versus optimal experimental results

Machining outputs	MWCNTs		Al_2O_3	
	Model	Exp.	Model	Exp.
Average surface roughness (μm)	1.35	1.35	1.76	1.513
Flank wear (mm)	0.187	0.145	0.213	0.213

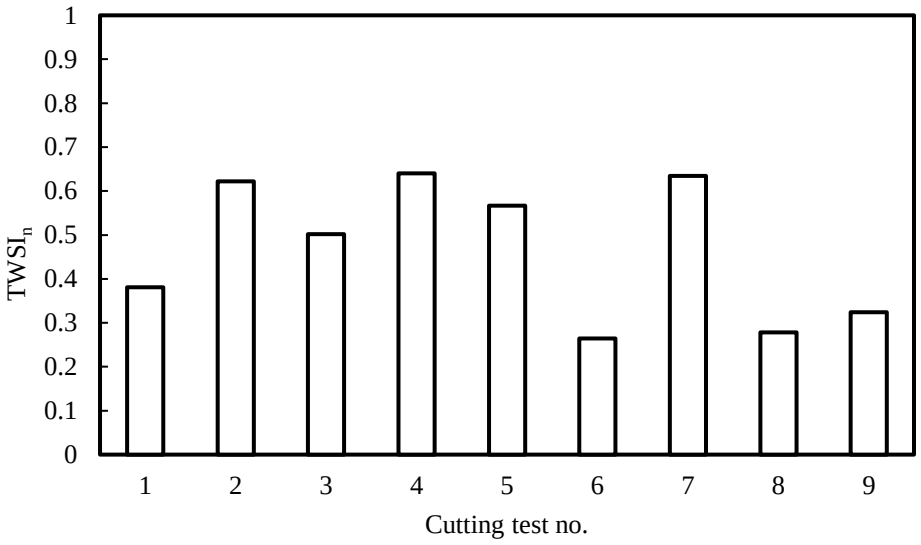

Figure 9-9 Total weighted sustainable indices results of machining Inconel 718 with Al_2O_3

Finally, it is recommend to study/include other sustainable indicators such as the consumption of nano-additives and the energy required for the dispersion in the cutting fluid in order to provide a more comprehensive understanding of the sustainability assessment of machining with nano-cutting fluids.

9.8. Summary

In this chapter, a proposed sustainability assessment algorithm of machining processes is developed and discussed. The proposed algorithm is mainly based on considering both machining quality characteristics and sustainable machining metrics results to find the optimal process parameter levels. Using weighting factors for the measured machining process outputs, metrics and indicators provide this assessment algorithm the flexibility to be applied to any experimental case. Five major sustainable metrics are utilized through this algorithm; energy consumption, machining costs, waste management, environmental impact, and personal health and safety. All sustainable metrics are associated with a list of indicators to express and evaluate the major aspects of sustainability through the four life-cycle stages by obtaining what must be measured.

Three literature case studies have been implemented to validate using the proposed algorithm. In each of the cases studies, the predicted optimal parameters were in close agreement with the experimentally measured results. In addition, the proposed algorithm has been implemented in the studied nano-cutting fluids cases in order to ensure that the optimal conditions predicted by the proposed algorithm are consistent with the physical findings in different experimental studies. It should be stated that the proposed algorithm is considered as a valuable tool for the sustainable machining processes optimization. Finally, it is recommended to study/include other sustainable indicators such as the consumption of nano-additives and the energy required for the dispersion in the cutting fluid in order to provide a more comprehensive understanding of the sustainability assessment of machining with nano-cutting fluids.

Chapter 10 Conclusions and Future Works

10.1. Preamble

Flood cooling is a typical cooling strategy used in industry to dissipate the high temperature generated during machining difficult-to-cut materials; however, the use of flood coolant has raised environmental and health concerns which call for different alternatives. Minimum Quaintly Lubricant (MQL) has been successfully introduced as an acceptable coolant strategy; however, its potential to dissipate heat is much lower than the one achieved using flood coolant. The main objective of this thesis is focused on achieving sustainable machining processes for difficult-to-cut materials using nano-cutting fluids under MQL. In order to achieve this objective, several research phases have been achieved. The first phase has mainly focused on performing experimental cutting trials to investigate the effects of MWCNTs and Al_2O_3 nano-fluids on several machining quality characteristics such as flank tool wear and energy consumption. The first phase has ended up with several required investigations such as the importance of understanding the MQL-nano-fluids heat transfer and wear mechanisms which have been presented and discussed briefly in the second phase. Two analytical models have been developed in order to fully understand the induced nano-additive wear and heat transfer mechanisms during the cutting processes using MQL-nano-fluids. These models have been also presented through a comparative performance analysis between using nano-particles (Al_2O_3) and nano-tubes (MWCNTs).

The third phase has focused on developing an integrated finite element model which can be used to simulate the thermal and frictional effects of the MQL-nano-fluid in order to study various unique cutting aspects such as generated cutting temperature and residual stresses. In order to provide a tool to obtain the sustainable and optimal cutting conditions, the fourth phase of analysis has focused on developing a detailed assessment model for machining processes over a wide range of sustainability aspects. Using weighting factors for the measured machining process outputs, metrics and indicators provide this assessment algorithm the flexibility to be applied to any experimental case. The proposed assessment model is considered as a valuable tool for the sustainable machining processes optimization. The most important findings revealed from these four phases are presented in the next section.

10.2. Conclusions

The most important findings of the current work are concluded as following:

- During machining Inconel 718 and Ti-6Al-4V, it is observed that both nano-fluids offer promising results in terms of tool wear, average surface roughness, and energy consumption; however, MWCNTs nano-fluid presents better performance than Al_2O_3 nano-fluid;

- During machining Inconel 718 and Ti-6Al-4V under using MQL-nano-cutting fluids, the percentage of added nano-additives is a significant design variable for all studied machining characteristics;

- When machining Inconel 718, 4 wt.% added MWCNT or Al_2O_3 nano-particles was the optimal level for flank tool wear and average surface roughness results; however, no noticeable change has been observed between 2 wt.% and 4 wt.% for the energy consumption results;

- When machining Ti-6Al-4V, 4 wt.% added MWCNT is the optimal level for flank tool wear results; however, 2 wt.% nano-fluid offers better performance than 4 wt.% nano-fluid for both energy consumption and average surface roughness results;

- During machining Inconel 718 and Ti-6Al-4V, it is observed that both nano-fluids offer promising results in terms of tool wear, average surface roughness, and energy consumption; however, MWCNTs nano-fluid presents better performance than Al_2O_3 nano-fluid;

- The dominant wear modes noticed for the cutting tests performed without nano-additives during machining Inconel 718 are; excessive flank wear, notching, built up edge (BUE), crater wear and oxidation. In addition, both MWCNTs and Al_2O_3 nano-fluids have shown promising results in enhancing the tool performance due to the improved cooling and lubrication properties, which enhance the interface bonding between tool and workpiece surfaces;

- The dominant wear modes observed when machining Ti-6Al-4V without nano-additives are; flank wear, crater wear, tool nose wear and plastic deformation. The use of MWCNTs nano-fluid resulted in a better tool performance as it offers an effective heat dissipation characteristic which retains the cutting tool original hardness;

- The chip morphology investigations for Inconel 718 and Ti-6Al-4V cutting tests confirmed the significant cooling and lubrication effects of the proposed nano-fluid on both alloys machinability;

- Different mathematical models for each alloy have been developed to express the studied cutting responses based on the range of studied design variables. An acceptable average model accuracy has been obtained for each proposed model;

- Two main mechanisms (i.e., rolling and ploughing mechanisms) are used to explain the cooling and lubrication functions when using MQL-nano-fluids.

- In terms of the rolling mechanism effects, the incremental increase of nano-additives concentration decreases the induced coefficient of friction as these nano-additives serve as spacers, eliminating the contact between tool and workpiece;

- In terms of the ploughing mechanism, when there is an abundance of nano-additives in cutting oil, they collide with, and are impeded by, the asperities on the work surface, and thus generates higher cutting forces. As a result, the nano-additive induced wear is increased with increasing the concentration of nano-additives;

- The induced nano-additive wear classification offers a clear understanding about the ploughing and rolling mechanisms occurrence conditions. As long as the induced nano-additive wear is less than the lubricated surface wear, it means that the dominant mechanism is rolling. On the other hand, if the induced nano-additive wear is greater than the lubricated surface wear, it means that the dominant mechanism is ploughing. While the mending effect represent a critical condition between the ploughing and rolling mechanisms effects;

- It has been proved that the nano-additive induced wear is inversely proportional to the nano-additive diameter for both cases; nano-particles or nano-tubes. Because of this investigation, using large nano-additives would decrease the nano-additive wear and accordingly decreases the ploughing occurrence percentage. Although increasing the nano-additive size leads to decrease the nano-additive wear, it would decrease the number of nano-additives per nominal area of contact which would lead to increase the induced friction. Thus, the nano-additives concentration and sizes parameter should be controlled and optimized in order to avoid the drastic ploughing effects and high induced friction;

- Depending on the proposed nano-additive wear models using nano-particles and nano-tubes, it can be clearly concluded that MWCNTs offer promising result than Al_2O_3. This investigation would justify and provide a physical interpretation regarding the experimental results demonstrated throughout chapter 5 since MWCNTs-nano-fluid offers better results than Al_2O_3 nano-fluid for all studied machining responses.

- Two main scenarios have been presented in order to express the energy transfer mechanisms during the cutting process using MQL-nano-cutting fluids;

- Depending on the proposed general heat transfer model using nano-particles and nano-tubes, it has been demonstrated that increasing the heat convection coefficient of the nano-cutting fluid mist and the protective nano-additive layer thickness enhances the heat transfer resistances inside of and at the machined surface. In addition, it has been concluded that decreasing the thermal diffusivity of the nano-cutting fluid mist would enhance the heat transfer resistance performance inside the workpiece;

- It has been concluded that MWCNTs nano-fluid provides better performance than Al_2O_3 nano-fluid for both thermal diffusivity and heat convection coefficient results. Regarding the heat convection coefficient results, an improvement percentage of 4.25% for MWCNTs nano-fluid with 2 wt. % has been observed compared to Al_2O_3 nano-fluid with 2 wt. %, while 7.82% improvement percentage has been noticed for MWCNTs nano-fluid with 4 wt. % in comparison with 4 wt. % of Al_2O_3 nano-fluid. In terms of the thermal diffusivity results, an improvement percentage of 13% for 2 wt.% MWCNTs nano-fluid with has been observed compared to 2 wt. % Al_2O_3 nano-fluid, while 22.8 % improvement percentage has been noticed for 4 wt. % MWCNTs nano-fluid in comparison with 4 wt. % Al_2O_3 nano-fluid;

- The nano-additive wear and heat transfer models present a solid physical evidence which proves that MWCNT nano-fluid offers better tribological and heat transfer properties than Al_2O_3, and accordingly enhances the machining quality characteristics;

- An integrated finite element modeling of machining Inconel 718 and Ti-6Al-4V using MQL-nano-cutting fluids has been presented through two main phases. The first phase simulated the thermal effect of the resultant nano-fluid mist through developing a 2-D Axisymmetric Computational Fluid Dynamics (CFD) domain, while the second phase studied the effectiveness of the use of MQL-nano-cutting fluid in terms of machining temperature and resulting residual stresses using ABAQUS/Explicit with Lagrangian modeling approach;

- The average heat convection coefficients results obtained from the proposed CFD model at standard room temperature demonstrated a good agreement with the theoretical heat transfer characteristics. The highest accuracy has been observed under using MWCNTs with 4 wt. % (about 99.7%). Thus, the proposed CDF has been used to determine the heat convection coefficients at different temperatures for the studied MQL-nano-fluids with MWCNTs;

- The experimental and simulated cutting forces during machining Inconel 718 shows better agreement in the cutting test performed without nano-additives (i.e., accuracy % ≈ 90%) than the cutting test performed with 2 wt. % MWCNTs (i.e., accuracy % ≈ 82.3%). Similarly for cutting tests performed on Ti-6Al-4V, the experimental and simulated cutting forces shows better agreement in cutting test 1 (i.e., accuracy ≈93.7%) than cutting test 4 (i.e., accuracy ≈ 79.6%). It is mainly attributed to neglecting the ploughing effect simulation (q_2'');

- Both generated cutting temperature and residual stresses results reveal better performance in the tests performed using MQL-nano-cutting fluid during machining Inconel 718 and Ti-6Al-4V. It is mainly attributed to the promising thermal effect of the added boundary film as well as the lower coefficient of friction values employed in the tests performed using MQL-nano-cutting fluid;

- A general proposed sustainability assessment model of machining processes has been developed and discussed. Three literature case studies have been implemented to validate using the proposed algorithm. In each of the cases studies, the predicted optimal parameters were in close agreement with the experimentally measured results. In addition, the proposed algorithm has been implemented in the studied nano-cutting fluids cases in order to ensure that the optimal conditions predicted by the proposed algorithm are consistent with the physical findings in different experimental studies;

- In the all studied cases, Ti-6Al-4V with MWCNTs, Inconel 718 with MWCNTs and Inconel 718 with Al_2O_3, the highest index has been demonstrated at cutting test 4, which includes the medium level of cutting speed, the lowest level of feed rate, and 2 wt. % of added nano-additives. While the lowest index in all case studies is revealed at cutting, test 6 that has been performed at the medium level of cutting speed, the highest level of feed rate, and without any added nano-additives;

- The proposed sustainability model findings are confirmed by the previous experimental investigations provided in chapters 5 and 6 as the employed nano-cutting fluids offers promising results in comparison with the tests performed without nano-additives; however, the optimal added nano-additive percentage was 2 wt. %. This finding provides more physical sense as the highest percentage of nano-additive (4 wt. %) could cause more deteriorations to the cutting processes because of the highest occurrence possibility of the drastic ploughing effects and high induced friction;

10.3. Current Research Contributions

- The current research addresses the research gap in the literature which relates to investigation of nano-fluids technology when machining titanium and nickel-based alloys using both nano-particles and nano-tubes;

- The current research provides a clear understanding of the role of MQL-nano-cutting fluids, its cooling and lubrication mechanisms, and clarification of the possible induced nano-additive wear, and the occurrence conditions of the ploughing and rolling mechanisms. In addition, two main scenarios have been presented in order to express the energy transfer mechanisms during the cutting process using MQL-nano-cutting fluids;

- A comparative performance analysis model for the induced nano-additive wear has been developed and utilized for both nano-particles and nano-tubes scenarios;

- A general nano-cutting-fluid heat transfer model has been developed to understand the role of nano-additives in enhancing the cooling and characteristics of the cutting fluid;

- An integrated finite element model of machining process using MQL-nano-cutting fluid has been developed and discussed in order to simulate the thermal and frictional effects of the applied nano-fluid mist (i.e., the cooling and lubrication aspects of nano-fluid based MQL);

- A detailed and general assessment model for sustainable machining processes has been developed and discussed. This model offers a tool to obtain not only the optimal cutting conditions, but also the optimal sustainable aspects. Moreover, it is considered as a valuable tool for the sustainable machining processes optimization;

10.4. Future Research

Finally, the current research could be extended in the future work by considering the following points:

- Including more design variables effects (e.g. applied MQL air pressure, MQL nozzle orientation, MQL volume flow rate, and cutting tool geometry).

- Proposing a dual nano-cutting-fluid; for example, mixture between MWCNTs and Al_2O_3 nano-particles, and then investigating the tribological and heat transfer characteristics of the proposed dual fluid on the machining processes performance;

- Developing an analytical model to explain the relationship between the induced nano-additive wear and the nano-additive size and concentrations;

- Enhancing the current integrated finite element model by simulating the nano-additive ploughing effects in order to accurately predict the effectiveness of using MQL-nano-fluid;

- Enhancing the current sustainability assessment model by studying/including other sustainable indicators such as the consumption of nano-additives and the energy required for the dispersion in the cutting fluid in order to provide a more comprehensive understanding of the sustainability assessment of machining with nano-cutting fluids;

References

1. Jawahir, I. S. (2008, August). Beyond the 3R's: 6R concepts for next generation manufacturing: recent trends and case studies. In Symposium on Sustainability and Product Development.

2. Jawahir, I. S., Wanigarathne, P. C., & Wang, X. (2006). Product design and manufacturing processes for sustainability. Mechanical Engineers' Handbook: Manufacturing and Management, Volume 3, Third Edition, 414-443.

3. Jayal, A. D., Badurdeen, F., Dillon Jr, O. W., & Jawahir, I. S. (2010). Sustainable manufacturing: Modeling and optimization challenges at the product, process and system levels. CIRP Journal of Manufacturing Science and Technology, 2(3), 144-152.

4. Badurdeen, F., Shuaib, M. A., Lu, T., & Jawahir, I. S. (2015). Sustainable Value Creation in Manufacturing at Product and Process Levels: Metrics-Based Evaluation. In Handbook of Manufacturing Engineering and Technology (pp. 3343-3375). Springer London.

5. Joshi, K., Venkatachalam, A., & Jawahir, I. S. (2006, October). A new methodology for transforming 3R concept into 6R concept for improved product sustainability. In IV global conference on sustainable product development and life cycle engineering (pp. 3-6).

6. Jawahir, I. S., & Dillon, O. W. (2007, October). Sustainable manufacturing processes: new challenges for developing predictive models and optimization techniques. In Proceedings of the first international conference on sustainable manufacturing, Montreal, Canada (pp. 1-19).

7. Badurdeen, F., Iyengar, D., Goldsby, T. J., Metta, H., Gupta, S., & Jawahir, I. S. (2009). Extending total life-cycle thinking to sustainable supply chain design. International Journal of Product Lifecycle Management, 4(1-3), 49-67.

8. Lu, T. (2014). A metrics-based sustainability assessment of cryogenic machining using modeling and optimization of process performance. University of Kentucky.

9. Sharma, V. S., Dogra, M., & Suri, N. M. (2009). Cooling techniques for improved productivity in turning. International Journal of Machine Tools and Manufacture, 49(6), 435-453.

10. Krishna, P. V., Srikant, R. R., Padmini, R., & Viswaditya, J. L. P. P. (2013, July). Application of nanomaterials as coolants/lubricants in machining. In Advanced Nanomaterials and Emerging Engineering Technologies (ICANMEET), 2013 International Conference on (pp. 674-682). IEEE.

11. Krajnik, P., Pusavec, F., & Rashid, A. (2011). Nanofluids: Properties, applications and sustainability aspects in materials processing technologies. In Advances in Sustainable Manufacturing (pp. 107-113). Springer, Berlin, Heidelberg.

12. Shokrani, A., Dhokia, V., & Newman, S. T. (2012). Environmentally conscious machining of difficult-to-machine materials with regard to cutting fluids. International Journal of Machine Tools and Manufacture, 57, 83-101.

13. Abukhshim, N. A., Mativenga, P. T., & Sheikh, M. A. (2006). Heat generation and temperature prediction in metal cutting: A review and implications for high speed machining. International Journal of Machine Tools and Manufacture, 46(7-8), 782-800.

14. Aggarwal, A., Singh, H., Kumar, P., & Singh, M. (2008). Optimization of multiple quality characteristics for CNC turning under cryogenic cutting environment using desirability function. Journal of materials processing technology, 205(1-3), 42-50.

15. Sun, S., M. Brandt, and M. Dargusch, Machining Ti–6Al–4V alloy with cryogenic compressed air cooling. International Journal of Machine Tools and Manufacture, 2010. 50(11): p. 933-942.

16. Choragudi, A., Kuttolamadom, M. A., Jones, J. J., Mears, M. L., & Kurfess, T. (2010). Investigation of the machining of titanium components in lightweight vehicles. In SAE International Congress.

17. Schauerte, O. (2003). Titanium in automotive production. Advanced Engineering Materials, 5(6), 411-418.

18. Ezugwu, E. and Z. Wang, Titanium alloys and their machinability—a review. Journal of materials processing technology, 1997. 68(3): p. 262-274.

19. Abrão, A.M., J.L.S. Ribeiro, and J.P. Davim, Surface integrity, in Machining of Hard Materials. 2011, Springer. p. 115-141.

20. Miller, S., Advanced materials mean advanced engines. Interdisciplinary Science Reviews, 1995. 20(4): p. 117-129.

21. Davim, J.P., Machining of hard materials. 2011: Springer Science & Business Media.

22. Kuttolamadom, M. (2012). Prediction of the Wear & Evolution of Cutting Tools in a Carbide/Ti-6Al-4V Machining Tribosystem by Volumetric Tool Wear Characterization & Modeling.

23. Alauddin, M. M. B. M. H. M., Mazid, M. A., El Baradi, M. A., & Hashmi, M. S. J. (1998). Cutting forces in the end milling of Inconel 718. Journal of Materials Processing Technology, 77(1-3), 153-159.

24. Dudzinski, D., Devillez, A., Moufki, A., Larrouquere, D., Zerrouki, V., & Vigneau, J. (2004). A review of developments towards dry and high speed machining of Inconel 718 alloy. International Journal of Machine Tools and Manufacture, 44(4), 439-456.

25. Amrita, M., R. Srikant, and A. Sitaramaraju, Performance evaluation of nanographite-based cutting fluid in machining process. Materials and Manufacturing Processes, 2014. 29(5): p. 600-605.

26. Khandekar, S., Sankar, M. R., Agnihotri, V., & Ramkumar, J. (2012). Nano-cutting fluid for enhancement of metal cutting performance. Materials and Manufacturing Processes, 27(9), 963-967.

27. Sharma, A.K., A.K. Tiwari, and A.R. Dixit, Progress of nanofluid application in machining: a review. Materials and Manufacturing Processes, 2015. 30(7): p. 813-828.

28. Rajmohan, T., S. Sathishkumar, and K. Palanikumar, Effect of a nanoparticle-filled lubricant in turning of AISI 316L stainless steel (SS). Particulate Science and Technology, 2017. 35(2): p. 201-208.

29. Singh, R. K., Sharma, A. K., Dixit, A. R., Tiwari, A. K., Pramanik, A., & Mandal, A. (2017). Performance evaluation of alumina-graphene hybrid nano-cutting fluid in hard turning. Journal of cleaner production, 162, 830-845.

30. Bakalova, T., Svobodová, L., Rosická, P., Borůvková, K., Voleský, L., & Louda, P. (2017). The application potential of SiO_2, TiO_2 or Ag nanoparticles as fillers in machining process fluids. Journal of cleaner production, 142, 2237-2243.

31. Paul, S., A.K. Singh, and A. Ghosh, Grinding of Ti-6Al-4V Under Small Quantity Cooling Lubrication Environment Using Alumina and MWCNT Nanofluids. Materials and Manufacturing Processes, 2017. 32(6): p. 608-615.

32. Liu, G., Li, C., Zhang, Y., Yang, M., Jia, D., Zhang, X., ... & Zhai, H. (2017). Process parameter optimization and experimental evaluation for nanofluid MQL in grinding Ti-6Al-4V based on grey relational analysis. Materials and Manufacturing Processes, 1-14.

33. Reich, S., C. Thomsen, and J. Maultzsch, Carbon nanotubes: basic concepts and physical properties. 2008: John Wiley & Sons.

34. Popov, V.N., Carbon nanotubes: properties and application. Materials Science and Engineering: R: Reports, 2004. 43(3): p. 61-102.

35. Kim, P., Shi, L., Majumdar, A., & McEuen, P. L. (2001). Thermal transport measurements of individual multi-walled nanotubes. Physical review letters, 87(21), 215502.

36. Ulutan, D. and T. Ozel, Machining induced surface integrity in titanium and nickel alloys: A review. International Journal of Machine Tools and Manufacture, 2011. 51(3): p. 250-280.

37. Hong, S.Y., Y. Ding, and R.G. Ekkens, Improving low carbon steel chip breakability by cryogenic chip cooling. International Journal of Machine Tools and Manufacture, 1999. 39(7): p. 1065-1085.

38. Jaffery, S. and P. Mativenga, Assessment of the machinability of Ti-6Al-4V alloy using the wear map approach. The International Journal of Advanced Manufacturing Technology, 2009. 40(7-8): p. 687-696.

39. Ezugwu, E., Z. Wang, and A. Machado, The machinability of nickel-based alloys: a review. Journal of Materials Processing Technology, 1999. 86(1): p. 1-16.

40. Richards, N. and D. Aspinwall, Use of ceramic tools for machining nickel based alloys. International Journal of Machine Tools and Manufacture, 1989. 29(4): p. 575-588.

41. Ezugwu, E., Key improvements in the machining of difficult-to-cut aerospace superalloys. International Journal of Machine Tools and Manufacture, 2005. 45(12): p. 1353-1367.

42. Tools, S., Turning Difficult-To-Machine Alloys. Technical Guide, 2002: p. 21.

43. Rosen, M.A. and H.A. Kishawy, Sustainable manufacturing and design: Concepts, practices and needs. Sustainability, 2012. 4(2): p. 154-174.

44. Harland, J., T. Reichelt, and M. Yao. Environmental sustainability in the semiconductor industry. in Electronics and the Environment, 2008. ISEE 2008. IEEE International Symposium on. 2008. IEEE.

45. Dahmus, J.B. and T.G. Gutowski. An environmental analysis of machining. in ASME 2004 international mechanical engineering congress and exposition. 2004. American Society of Mechanical Engineers.

46. Munoz, A. and P. Sheng, An analytical approach for determining the environmental impact of machining processes. Journal of Materials Processing Technology, 1995. 53(3): p. 736-758.

47. Narita, H., N. Desmira, and H. Fujimoto, Environmental burden analysis for machining operation using LCA method, in Manufacturing Systems and Technologies for the New Frontier. 2008, Springer. p. 65-68.

48. Byrne, G. and E. Scholta, Environmentally clean machining processes—a strategic approach. CIRP Annals-Manufacturing Technology, 1993. 42(1): p. 471-474.

49. Klocke, F. and G. Eisenblätter, Dry cutting. CIRP Annals-Manufacturing Technology, 1997. 46(2): p. 519-526.

50. Pusavec, F., Kramar, D., Krajnik, P., & Kopac, J. (2010). Transitioning to sustainable production–part II: evaluation of sustainable machining technologies. Journal of Cleaner Production, 18(12), 1211-1221.

51. Thompson, D., Kriebel, D., Quinn, M. M., Wegman, D. H., & Eisen, E. A. (2005). Occupational exposure to metalworking fluids and risk of breast cancer among female autoworkers. American journal of industrial medicine, 47(2), 153-160.

52. Kamata, Y. and T. Obikawa, High speed MQL finish-turning of Inconel 718 with different coated tools. Journal of Materials Processing Technology, 2007. 192: p. 281-286.

53. Cabanettes, F., Faverjon, P., Sova, A., Dumont, F., & Rech, J. (2017). MQL machining: from mist generation to tribological behavior of different oils. The International Journal of Advanced Manufacturing Technology, 90(1-4), 1119-1130.

54. Kishawy, H., An experimental evaluation of cutting temperatures during high speed machining of hardened D2 tool steel. 2002.

55. Kishawy, H., L. Li, and A. El-Wahab, Prediction of chip flow direction during machining with self-propelled rotary tools. International Journal of Machine Tools and Manufacture, 2006. 46(12): p. 1680-1688.

56. Srikant, R. R., Rao, D. N., Subrahmanyam, M. S., & Krishna, V. P. (2009). Applicability of cutting fluids with nanoparticle inclusion as coolants in machining. Proceedings of the Institution of Mechanical Engineers, Part J: Journal of Engineering Tribology, 223(2), 221-225.

57. Li, B., Li, C., Zhang, Y., Wang, Y., Jia, D., Yang, M., ... & Sun, K. (2017). Heat transfer performance of MQL grinding with different nanofluids for Ni-based alloys using vegetable oil. Journal of Cleaner Production, 154, 1-11.

58. Ghadimi, A., R. Saidur, and H. Metselaar, A review of nanofluid stability properties and characterization in stationary conditions. International Journal of Heat and Mass Transfer, 2011. 54(17): p. 4051-4068.

59. Sharma, A.K., A.K. Tiwari, and A.R. Dixit, Effects of Minimum Quantity Lubrication (MQL) in machining processes using conventional and nanofluid based cutting fluids: A comprehensive review. Journal of Cleaner Production, 2016. 127: p. 1-18.

60. Su, Y., Gong, L., Li, B., Liu, Z., & Chen, D. (2016). Performance evaluation of nanofluid MQL with vegetable-based oil and ester oil as base fluids in turning. The International Journal of Advanced Manufacturing Technology, 83(9-12), 2083-2089.

61. Nanomaterials, U.R., US Research Nanomaterials, Inc, The Advanced Nanomaterials Provider. US Research Nanomaterials.

62. Sales, W., Becker, M., Barcellos, C. S., Landre Jr, J., Bonney, J., & Ezugwu, E. O. (2009). Tribological behavior when face milling AISI 4140 steel with minimum quantity fluid application. Industrial Lubrication and Tribology, 61(2), 84-90.

63. Ghandehariun, A., Y. Nazzal, and H. Kishawy, Sustainable manufacturing and its application in machining processes: a review. International Journal of Global Warming, 2016. 9(2): p. 198-228.

64. Kishawy, H. A., Dumitrescu, M., Ng, E. G., & Elbestawi, M. A. (2005). Effect of coolant strategy on tool performance, chip morphology and surface quality during high-speed machining of A356 aluminum alloy. International Journal of Machine Tools and Manufacture, 45(2), 219-227.

65. Su, Y., He, N., Li, L., Iqbal, A., Xiao, M. H., Xu, S., & Qiu, B. G. (2007). Refrigerated cooling air cutting of difficult-to-cut materials. International Journal of Machine Tools and Manufacture, 47(6), 927-933.

66. Hong, S.Y., Economical and ecological cryogenic machining. Journal of manufacturing science and engineering, 2001. 123(2): p. 331-338.

67. Hong, S.Y. and Y. Ding, Cooling approaches and cutting temperatures in cryogenic machining of Ti-6Al-4V. International Journal of Machine Tools and Manufacture, 2001. 41(10): p. 1417-1437.

68. Bermingham, M. J., Kirsch, J., Sun, S., Palanisamy, S., & Dargusch, M. S. (2011). New observations on tool life, cutting forces and chip morphology in cryogenic machining Ti-6Al-4V. International Journal of Machine Tools and Manufacture, 51(6), 500-511.

69. Bermingham, M. J., Palanisamy, S., Kent, D., & Dargusch, M. S. (2012). A comparison of cryogenic and high pressure emulsion cooling technologies on tool life and chip morphology in Ti–6Al–4V cutting. Journal of Materials Processing Technology, 212(4), 752-765.

70. Venugopal, K., S. Paul, and A. Chattopadhyay, Tool wear in cryogenic turning of Ti-6Al-4V alloy. Cryogenics, 2007. 47(1): p. 12-18.

71. Rivero, A., Aramendi, G., Herranz, S., & de Lacalle, L. L. (2006). An experimental investigation of the effect of coatings and cutting parameters on the dry drilling performance of aluminum alloys. The International Journal of Advanced Manufacturing Technology, 28(1-2), 1-11.

72. Weinert, K., Inasaki, I., Sutherland, J. W., & Wakabayashi, T. (2004). Dry machining and minimum quantity lubrication. CIRP Annals-Manufacturing Technology, 53(2), 511-537.

73. Krain, H., A. Sharman, and K. Ridgway, Optimisation of tool life and productivity when end milling Inconel 718TM. Journal of materials processing technology, 2007. 189(1): p. 153-161.

74. Jen, T. C., Gutierrez, G., Eapen, S., Barber, G., Zhao, H., Szuba, P. S., ... & Manjunathaiah, J. (2002). Investigation of heat pipe cooling in drilling applications.: part I: preliminary numerical analysis and verification. International Journal of Machine Tools and Manufacture, 42(5), 643-652.

75. Daungthongsuk, W. and S. Wongwises, A critical review of convective heat transfer of nanofluids. Renewable and Sustainable Energy Reviews, 2007. 11(5): p. 797-817.

76. Chol, S., Enhancing thermal conductivity of fluids with nanoparticles. ASME-Publications-Fed, 1995. 231: p. 99-106.

77. Elcock, D., Potential impacts of nanotechnology on energy transmission applications and needs. 2007, Argonne National Laboratory (ANL).

78. Saidur, R., K. Leong, and H. Mohammad, A review on applications and challenges of nanofluids. Renewable and sustainable energy reviews, 2011. 15(3): p. 1646-1668.

79. Bhogare, R.A. and B. Kothawale, A review on applications and challenges of nanofluids as coolant in automobile radiator. International journal of scientific and research publications, 2013. 3(8).

80. Wu, D., Zhu, H., Wang, L., & Liu, L. (2009). Critical issues in nanofluids preparation, characterization and thermal conductivity. Current Nanoscience, 5(1), 103-112.

81. Hiemenz, P.C., Principles of colloid and surface chemistry. Vol. 188. 1986: M. Dekker New York.

82. Das, S. K., Choi, S. U., Yu, W., & Pradeep, T. (2007). Nanofluids: science and technology. John Wiley & Sons.

83. Swanson, E.J., J. Tavares, and S. Coulombe, Improved dual-plasma process for the synthesis of coated or functionalized metal nanoparticles. IEEE transactions on plasma science, 2008. 36(4): p. 886-887.

84. Li, Y., Tung, S., Schneider, E., & Xi, S. (2009). A review on development of nanofluid preparation and characterization. Powder Technology, 196(2), 89-101.

85. Wang, X.-Q. and A.S. Mujumdar, Heat transfer characteristics of nanofluids: a review. International journal of thermal sciences, 2007. 46(1): p. 1-19.

86. Sharma, P., B.S. Sidhu, and J. Sharma, Investigation of effects of nanofluids on turning of AISI D2 steel using minimum quantity lubrication. Journal of cleaner production, 2015. 108: p. 72-79.

87. Rajmohan, T., S. Sathishkumar, and K. Palanikumar. Experimental Investigation of Machining Parameters during Turning of AISI 316L Stainless Steel Using Nano Cutting Environment. in Applied Mechanics and Materials. 2015. Trans Tech Publ.

88. Doshi, S.J., P. Jain, and N. Mehta, Prospective applications of nano fluid during machining process. International Journal of Machining and Machinability of Materials, 2013. 14(3): p. 257-274.

89. Hwang, Y., Park, H. S., Lee, J. K., & Jung, W. H. (2006). Thermal conductivity and lubrication characteristics of nanofluids. Current Applied Physics, 6, e67-e71.

90. Li, X. F., Zhu, D. S., Wang, X. J., Wang, N., Gao, J. W., & Li, H. (2008). Thermal conductivity enhancement dependent pH and chemical surfactant for Cu-H2O nanofluids. Thermochimica Acta, 469(1-2), 98-103.

91. Zhu, H., Zhang, C., Tang, Y., Wang, J., Ren, B., & Yin, Y. (2007). Preparation and thermal conductivity of suspensions of graphite nanoparticles. Carbon, 45(1), 226-228.

92. Chang, H., Wu, Y. C., Chen, X. Q., & Kao, M. J. (2000). Fabrication of Cu based nanofluid with superior dispersion. National Taipei University of Technology Journal, 5, 201-208.

93. Zhu, D., Li, X., Wang, N., Wang, X., Gao, J., & Li, H. (2009). Dispersion behavior and thermal conductivity characteristics of Al_2O_3–H_2O nano-fluids. Current Applied Physics, 9(1), 131-139.

94. Wang, X.-j. and D.-s. Zhu, Investigation of pH and SDBS on enhancement of thermal conductivity in nanofluids. Chemical Physics Letters, 2009. 470(1): p. 107-111.

95. Pantzali, M. N., Kanaris, A. G., Antoniadis, K. D., Mouza, A. A., & Paras, S. V. (2009). Effect of nanofluids on the performance of a miniature plate heat exchanger with modulated surface. International Journal of Heat and Fluid Flow, 30(4), 691-699.

96. Chandrasekar, M., S. Suresh, and A.C. Bose, Experimental investigations and theoretical determination of thermal conductivity and viscosity of Al_2O_3/water nanofluid. Experimental Thermal and Fluid Science, 2010. 34(2): p. 210-216.

97. Assael, M. J., Metaxa, I. N., Arvanitidis, J., Christofilos, D., & Lioutas, C. (2005). Thermal conductivity enhancement in aqueous suspensions of carbon multi-walled and double-walled nanotubes in the presence of two different dispersants. International Journal of Thermophysics, 26(3), 647-664.

98. Wei, X., Kong, T., Zhu, H., & Wang, L. (2010). CuS/Cu_2S nanofluids: synthesis and thermal conductivity. International Journal of Heat and Mass Transfer, 53(9-10), 1841-1843

99. Meibodi, M. E., Vafaie-Sefti, M., Rashidi, A. M., Amrollahi, A., Tabasi, M., & Kalal, H. S. (2010). The role of different parameters on the stability and thermal conductivity of carbon nanotube/water nanofluids. International Communications in Heat and Mass Transfer, 37(3), 319-323.

100. Hwang, Y. J., Lee, J. K., Lee, C. H., Jung, Y. M., Cheong, S. I., Lee, C. G., ... & Jang, S. P. (2007). Stability and thermal conductivity characteristics of nanofluids. Thermochimica Acta, 455(1-2), 70-74.

101. Huang, J., Wang, X., Long, Q., Wen, X., Zhou, Y., & Li, L. (2009, August). Influence of pH on the stability characteristics of nanofluids. In Photonics and Optoelectronics, 2009. SOPO 2009. Symposium on (pp. 1-4). IEEE.

102. Chang, H., Jwo, C. S., Fan, P. S., & Pai, S. H. (2007). Process optimization and material properties for nanofluid manufacturing. The International Journal of Advanced Manufacturing Technology, 34(3-4), 300-306.

103. Lee, D., J.-W. Kim, and B.G. Kim, A new parameter to control heat transport in nanofluids: surface charge state of the particle in suspension. The Journal of Physical Chemistry B, 2006. 110(9): p. 4323-4328.

104. Lee, K., Hwang, Y., Cheong, S., Kwon, L., Kim, S., & Lee, J. (2009). Performance evaluation of nano-lubricants of fullerene nanoparticles in refrigeration mineral oil. Current Applied Physics, 9(2), e128-e131.

105. Hwang, Y., Lee, J. K., Lee, J. K., Jeong, Y. M., Cheong, S. I., Ahn, Y. C., & Kim, S. H. (2008). Production and dispersion stability of nanoparticles in nanofluids. Powder Technology, 186(2), 145-153.

106. Munson, B.R., D.F. Young, and T.H. Okiishi, Fundamentals of fluid mechanics. New York, 1990. 3: p. 4.

107. Xian-Ju, W. and L. Xin-Fang, Influence of pH on nanofluids' viscosity and thermal conductivity. Chinese Physics Letters, 2009. 26(5): p. 056601.

108. Hong, K., T.-K. Hong, and H.-S. Yang, Thermal conductivity of Fe nanofluids depending on the cluster size of nanoparticles. Applied Physics Letters, 2006. 88(3): p. 031901.

109. Vandsburger, L., Synthesis and covalent surface modification of carbon nanotubes for preparation of stabilized nanofluid suspensions. 2010: Library and Archives Canada= Bibliothèque et Archives Canada.

110. Maxwell, J., Electricity and Magnetism Clarendon Press. 1873, Oxford, UK.

111. Xuan, Y., Q. Li, and W. Hu, Aggregation structure and thermal conductivity of nanofluids. AIChE Journal, 2003. 49(4): p. 1038-1043.

112. Vadász, P., Nanofluid suspensions and bi-composite media as derivatives of interface heat transfer modeling in porous media, in Emerging Topics in Heat and Mass Transfer in Porous Media. 2008, Springer. p. 283-326.

113. Tavman, S. and I. Tavman, Measurement of effective thermal conductivity of wheat as a function of moisture content. International communications in heat and mass transfer, 1998. 25(5): p. 733-741.

114. Yu, W., France, D. M., Routbort, J. L., & Choi, S. U. (2008). Review and comparison of nanofluid thermal conductivity and heat transfer enhancements. Heat transfer engineering, 29(5), 432-460.

115. Pak, B.C. and Y.I. Cho, Hydrodynamic and heat transfer study of dispersed fluids with submicron metallic oxide particles. Experimental Heat Transfer an International Journal, 1998. 11(2): p. 151-170.

116. Xuan, Y. and W. Roetzel, Conceptions for heat transfer correlation of nanofluids. International Journal of heat and Mass transfer, 2000. 43(19): p. 3701-3707.

117. Duangthongsuk, W. and S. Wongwises, Measurement of temperature-dependent thermal conductivity and viscosity of TiO_2-water nanofluids. Experimental thermal and fluid science, 2009. 33(4): p. 706-714.

118. Chen, H., Y. Ding, and C. Tan, Rheological behaviour of nanofluids. New journal of physics, 2007. 9(10): p. 367.

119. Murshed, S., K. Leong, and C. Yang, Enhanced thermal conductivity of TiO 2—water based nanofluids. International Journal of Thermal Sciences, 2005. 44(4): p. 367-373.

120. Eastman, J. A., Choi, S. U. S., Li, S., Yu, W., & Thompson, L. J. (2001). Anomalously increased effective thermal conductivities of ethylene glycol-based nanofluids containing copper nanoparticles. Applied physics letters, 78(6), 718-720.

121. Assael, M., Chen, C. F., Metaxa, I., & Wakeham, W. A. (2004). Thermal conductivity of suspensions of carbon nanotubes in water. International Journal of Thermophysics, 25(4), 971-985.

122. Masuda, H., A. Ebata, and K. Teramae, Alteration of thermal conductivity and viscosity of liquid by dispersing ultra-fine particles. Dispersion of Al_2O_3, SiO_2 and TiO_2 ultra-fine particles. 1993.

123. Liu, M. S., Lin, M. C. C., Tsai, C. Y., & Wang, C. C. (2006). Enhancement of thermal conductivity with Cu for nanofluids using chemical reduction method. International Journal of Heat and Mass Transfer, 49(17-18), 3028-3033.

124. Xuan, Y. and Q. Li, Investigation on convective heat transfer and flow features of nanofluids. Journal of Heat transfer, 2003. 125(1): p. 151-155.

125. Li, C.H. and G. Peterson, Experimental investigation of temperature and volume fraction variations on the effective thermal conductivity of nanoparticle suspensions (nanofluids). Journal of Applied Physics, 2006. 99(8): p. 084314.

126. Patel, H. E., Das, S. K., Sundararajan, T., Sreekumaran Nair, A., George, B., & Pradeep, T. (2003). Thermal conductivities of naked and monolayer protected metal nanoparticle based nanofluids: Manifestation of anomalous enhancement and chemical effects. Applied Physics Letters, 83(14), 2931-2933.

127. Xie, H., Wang, J., Xi, T., Liu, Y., Ai, F., & Wu, Q. (2002). Thermal conductivity enhancement of suspensions containing nanosized alumina particles. Journal of applied physics, 91(7), 4568-4572.

128. Das, S. K., Putra, N., Thiesen, P., & Roetzel, W. (2003). Temperature dependence of thermal conductivity enhancement for nanofluids. Journal of heat transfer, 125(4), 567-574.

129. Kang, H.U., S.H. Kim, and J.M. Oh, Estimation of thermal conductivity of nanofluid using experimental effective particle volume. Experimental Heat Transfer, 2006. 19(3): p. 181-191.

130. Wen, D. and Y. Ding, Formulation of nanofluids for natural convective heat transfer applications. International Journal of Heat and Fluid Flow, 2005. 26(6): p. 855-864.

131. Wen, D. and Y. Ding, Natural convective heat transfer of suspensions of titanium dioxide nanoparticles (nanofluids). IEEE Transactions on Nanotechnology, 2006. 5(3): p. 220-227.

132. Chon, C. H., Kihm, K. D., Lee, S. P., & Choi, S. U. (2005). Empirical correlation finding the role of temperature and particle size for nanofluid (Al_2O_3) thermal conductivity enhancement. Applied Physics Letters, 87(15), 153107.

133. Choi, S. U. S., Zhang, Z. G., Yu, W., Lockwood, F. E., & Grulke, E. A. (2001). Anomalous thermal conductivity enhancement in nanotube suspensions. Applied physics letters, 79(14), 2252-2254.

134. Lee, C. G., Hwang, Y. J., Choi, Y. M., Lee, J. K., Choi, C., & Oh, J. M. (2009). A study on the tribological characteristics of graphite nano lubricants. International Journal of Precision Engineering and Manufacturing, 10(1), 85-90.

135. He, Y., Jin, Y., Chen, H., Ding, Y., Cang, D., & Lu, H. (2007). Heat transfer and flow behavior of aqueous suspensions of TiO_2 nanoparticles (nanofluids) flowing upward through a vertical pipe. International journal of heat and mass transfer, 50(11-12), 2272-2281.

136. Park, K.-H., B. Ewald, and P.Y. Kwon, Effect of nano-enhanced lubricant in minimum quantity lubrication balling milling. Journal of Tribology, 2011. 133(3): p. 031803.

137. Sarhan, A.A., M. Sayuti, and M. Hamdi, Reduction of power and lubricant oil consumption in milling process using a new SiO_2 nanolubrication system. The International Journal of Advanced Manufacturing Technology, 2012. 63(5-8): p. 505-512.

138. Sayuti, M., Sarhan, A. A., Tanaka, T., Hamdi, M., & Saito, Y. (2013). Cutting force reduction and surface quality improvement in machining of aerospace duralumin AL-2017-T4 using carbon onion nanolubrication system. The International Journal of Advanced Manufacturing Technology, 65(9-12), 1493-1500.

139. Rahmati, B., A.A. Sarhan, and M. Sayuti, Morphology of surface generated by end milling AL6061-T6 using molybdenum disulfide (MoS_2) nanolubrication in end milling machining. Journal of Cleaner Production, 2014. 66: p. 685-691.

140. Sayuti, M., Erh, O. M., Sarhan, A. A., & Hamdi, M. (2014). Investigation on the morphology of the machined surface in end milling of aerospace AL6061-T6 for novel uses of SiO2 nanolubrication system. Journal of cleaner production, 66, 655-663.

141. Sayuti, M., A.A. Sarhan, and M. Hamdi, An investigation of optimum SiO_2 nanolubrication parameters in end milling of aerospace Al6061-T6 alloy. The International Journal of Advanced Manufacturing Technology, 2013. 67(1-4): p. 833-849.

142. Rahmati, B., A.A. Sarhan, and M. Sayuti, Investigating the optimum molybdenum disulfide (MoS_2) nanolubrication parameters in CNC milling of AL6061-T6 alloy. The International Journal of Advanced Manufacturing Technology, 2014. 70(5-8): p. 1143-1155.

143. Shen, B., Malshe, A. P., Kalita, P., & Shih, A. J. (2008). Performance of novel MoS_2 nanoparticles based grinding fluids in minimum quantity lubrication grinding. Trans. NAMRI/SME, 36(357), e364.

144. Shen, B., A.J. Shih, and S.C. Tung, Application of nanofluids in minimum quantity lubrication grinding. Tribology Transactions, 2008. 51(6): p. 730-737.

145. Alberts, M., K. Kalaitzidou, and S. Melkote, An investigation of graphite nanoplatelets as lubricant in grinding. International Journal of Machine Tools and Manufacture, 2009. 49(12): p. 966-970.

146. Lee, P. H., Nam, T. S., Li, C., & Lee, S. W. (2010, December). Environmentally-friendly nano-fluid minimum quantity lubrication (MQL) meso-scale grinding process using nano-diamond particles. In Manufacturing Automation (ICMA), 2010 International Conference on (pp. 44-49). IEEE.

147. Prabhu, S. and B. Vinayagam, Nano surface generation of grinding process using carbon nano tubes. Sadhana, 2010. 35(6): p. 747-760.

148. Lee, P. H., Nam, J. S., Li, C., & Lee, S. W. (2012). An experimental study on micro-grinding process with nanofluid minimum quantity lubrication (MQL). International Journal of Precision Engineering and Manufacturing, 13(3), 331-338.

149. Setti, D., S. Ghosh, and P.V. Rao. Application of nano cutting fluid under minimum quantity lubrication (MQL) technique to improve grinding of Ti–6Al–4V alloy. in Proceedings of World Academy of Science, Engineering and Technology. 2012. World Academy of Science, Engineering and Technology.

150. Kalita, P., Malshe, A. P., Kumar, S. A., Yoganath, V. G., & Gurumurthy, T. (2012). Study of specific energy and friction coefficient in minimum quantity lubrication grinding using oil-based nanolubricants. Journal of Manufacturing Processes, 14(2), 160-166.

151. Kalita, P., A.P. Malshe, and K.P. Rajurkar, Study of tribo-chemical lubricant film formation during application of nanolubricants in minimum quantity lubrication (MQL) grinding. CIRP Annals-Manufacturing Technology, 2012. 61(1): p. 327-330.

152. Prabhu, S. and B.K. Vinayagam, AFM investigation in grinding process with nanofluids using Taguchi analysis. The International Journal of Advanced Manufacturing Technology, 2012. 60(1-4): p. 149-160.

153. Mao, C., Tang, X., Zou, H., Huang, X., & Zhou, Z. (2012). Investigation of grinding characteristic using nanofluid minimum quantity lubrication. International Journal of Precision Engineering and Manufacturing, 13(10), 1745-1752.

154. Mao, C., Zou, H., Huang, X., Zhang, J., & Zhou, Z. (2013). The influence of spraying parameters on grinding performance for nanofluid minimum quantity lubrication. The International Journal of Advanced Manufacturing Technology, 64(9-12), 1791-1799.

155. Nam, J.S., P.-H. Lee, and S.W. Lee, Experimental characterization of micro-drilling process using nanofluid minimum quantity lubrication. International Journal of Machine Tools and Manufacture, 2011. 51(7): p. 649-652.

156. Krishna, P.V., R. Srikant, and D.N. Rao, Experimental investigation on the performance of nanoboric acid suspensions in SAE-40 and coconut oil during turning of AISI 1040 steel. International Journal of machine Tools and manufacture, 2010. 50(10): p. 911-916.

157. Rao, S.N., B. Satyanarayana, and K. Venkatasubbaiah, Experimental estimation of tool wear and cutting temperatures in MQL using cutting fluids with CNT inclusion. International Journal of Engineering Science and Technology, 2011. 3(4).

158. Huang, W. T., Lin, S. P., & Chen, J. T. (2014). Robust design of using MWCNTs in minimum quantity lubrication. Applied Mechanics and Materials, 670, 11.

159. Hegab, H., Umer, U., Deiab, I., & Kishawy, H. (2018). Performance evaluation of Ti–6Al–4V machining using nano-cutting fluids under minimum quantity lubrication. The International Journal of Advanced Manufacturing Technology, 1-13.

160. Setti, D., Sinha, M. K., Ghosh, S., & Rao, P. V. (2015). Performance evaluation of Ti–6Al–4V grinding using chip formation and coefficient of friction under the influence of nanofluids. International Journal of Machine Tools and Manufacture, 88, 237-248.

161. Zhang, Y., Li, C., Jia, D., Zhang, D., & Zhang, X. (2015). Experimental evaluation of MoS_2 nanoparticles in jet MQL grinding with different types of vegetable oil as base oil. Journal of Cleaner Production, 87, 930-940.

162. Rao, P. and R. Srikant. Sustainable machining utilizing vegetable oil based nanofluids. in Smart Technologies and Management for Computing, Communication, Controls, Energy and Materials (ICSTM), 2015 International Conference on. 2015. IEEE.

163. Najiha, M. and M. Rahman, Experimental investigation of flank wear in end milling of aluminum alloy with water-based TiO_2 nanofluid lubricant in minimum quantity lubrication technique. The International Journal of Advanced Manufacturing Technology, 2016: p. 1-11.

164. Prabhu, S., M. Uma, and B. Vinayagam, Surface roughness prediction using Taguchi-fuzzy logic-neural network analysis for CNT nanofluids based grinding process. Neural Computing and Applications, 2015. 26(1): p. 41-55.

165. Vasu, V. and G. Pradeep Kumar Reddy, Effect of minimum quantity lubrication with Al_2O_3 nanoparticles on surface roughness, tool wear and temperature dissipation in machining Inconel 600 alloy. Proceedings of the Institution of Mechanical Engineers, Part N: Journal of Nanoengineering and Nanosystems, 2011. 225(1): p. 3-16.

166. Sinha, M. K., Madarkar, R., Ghosh, S., & Rao, P. V. (2017). Application of eco-friendly nanofluids during grinding of Inconel 718 through small quantity lubrication. Journal of cleaner production, 141, 1359-1375.

167. Zhang, Y., Li, C., Jia, D., Li, B., Wang, Y., Yang, M., ... & Zhang, X. (2016). Experimental study on the effect of nanoparticle concentration on the lubricating property of nanofluids for MQL grinding of Ni-based alloy. Journal of Materials Processing Technology, 232, 100-115.

168. Pavan, R. B., Venu Gopal, A., Amrita, M., & Goriparthi, B. K. (2017). Experimental investigation of graphene nanoplatelets–based minimum quantity lubrication in grinding Inconel 718. Proceedings of the Institution of Mechanical Engineers, Part B: Journal of Engineering Manufacture, 0954405417728311.

169. Das, S.K., Nanofluids—the cooling medium of the future. 2006.

170. Lee, J. and I. Mudawar, Assessment of the effectiveness of nanofluids for single-phase and two-phase heat transfer in micro-channels. International Journal of Heat and Mass Transfer, 2007. 50(3): p. 452-463.

171. Pantzali, M., A. Mouza, and S. Paras, Investigating the efficacy of nanofluids as coolants in plate heat exchangers (PHE). Chemical Engineering Science, 2009. 64(14): p. 3290-3300.

172. Ding, G., Peng, H., Jiang, W., & Gao, Y. (2009). The migration characteristics of nanoparticles in the pool boiling process of nano-refrigerant and nano-refrigerant–oil mixture. International Journal of Refrigeration, 32(1), 114-123.

173. Deiab, I., S.W. Raza, and S. Pervaiz, Analysis of lubrication strategies for sustainable machining during turning of titanium Ti-6Al-4V alloy. Procedia CIRP, 2014. 17: p. 766-771.

174. Maity, T.K., Development and Study of the Mechanical Properties of Silica Glass Based Composite. 2014.

175. Davim, J.P., Surface integrity in machining. Vol. 1848828742. 2010: Springer.

176. Loos, M., Carbon Nanotube Reinforced Composites: CNT Polymer Science and Technology. 2014: Elsevier.

177. Phadke, M., Quality engineering using design of experiments, quality control, robust design, and the Taguchi method. Wadsworth, Los Angeles, CA, 1998.

178. Najiha, M. and M. Rahman, Experimental investigation of flank wear in end milling of aluminum alloy with water-based TiO_2 nanofluid lubricant in minimum quantity lubrication technique. The International Journal of Advanced Manufacturing Technology, 2016. 86(9-12): p. 2527-2537.

179. Rabiei, F., A. Rahimi, and M. Hadad, Performance improvement of eco-friendly MQL technique by using hybrid nanofluid and ultrasonic-assisted grinding. The International Journal of Advanced Manufacturing Technology, 2017: p. 1-15.

180. Prasad, M. and R. Srikant, Performance evaluation of nano graphite inclusions in cutting fluids with MQL technique in turning of AISI 1040 steel. International Journal of Research in Engineering and Technology, 2013. 2(11): p. 381-393.

181. Zhu, D., X. Zhang, and H. Ding, Tool wear characteristics in machining of nickel-based superalloys. International Journal of Machine Tools and Manufacture, 2013. 64: p. 60-77.

182. Ghaednia, H. and R.L. Jackson, The effect of nanoparticles on the real area of contact, friction, and wear. Journal of Tribology, 2013. 135(4): p. 041603.

183. Winer, W.O. and M.B. Peterson, Wear Control Handbook. 1980: American society of mechanical engineers.

184. Sayit, E., K. Aslantas, and A. Çiçek, Tool wear mechanism in interrupted cutting conditions. Materials and Manufacturing Processes, 2009. 24(4): p. 476-483.

185. Sayuti, M., Sarhan, A. A., Tanaka, T., Hamdi, M., & Saito, Y. (2013). Cutting force reduction and surface quality improvement in machining of aerospace duralumin AL-2017-T4 using carbon onion nanolubrication system. The International Journal of Advanced Manufacturing Technology, 65(9-12), 1493-1500.

186. Stanford, M., Lister, P. M., Morgan, C., & Kibble, K. A. (2009). Investigation into the use of gaseous and liquid nitrogen as a cutting fluid when turning BS 970-80A15 (En32b) plain carbon steel using WC–Co uncoated tooling. Journal of Materials Processing Technology, 209(2), 961-972.

187. Suresh, R., Basavarajappa, S., Gaitonde, V. N., & Samuel, G. L. (2012). Machinability investigations on hardened AISI 4340 steel using coated carbide insert. International Journal of Refractory Metals and Hard Materials, 33, 75-86.

188. Hong, S.Y., Y. Ding, and W.-c. Jeong, Friction and cutting forces in cryogenic machining of Ti–6Al–4V. International Journal of Machine Tools and Manufacture, 2001. 41(15): p. 2271-2285.

189. Jerold, B.D. and M.P. Kumar, Experimental investigation of turning AISI 1045 steel using cryogenic carbon dioxide as the cutting fluid. Journal of Manufacturing Processes, 2011. 13(2): p. 113-119.

190. Vandsburger, L., Synthesis and covalent surface modification of carbon nanotubes for preparation of stabilized nanofluid suspensions. 2009.

191. Mao, C., Huang, Y., Zhou, X., Gan, H., Zhang, J., & Zhou, Z. (2014). The tribological properties of nanofluid used in minimum quantity lubrication grinding. The International Journal of Advanced Manufacturing Technology, 71(5-8), 1221-1228.

192. Zhang, Y., Li, C., Jia, D., Zhang, D., & Zhang, X. (2015). Experimental evaluation of the lubrication performance of MoS_2/CNT nanofluid for minimal quantity lubrication in Ni-based alloy grinding. International Journal of Machine Tools and Manufacture, 99, 19-33.

193. Ezugwu, E. O., Da Silva, R. B., Bonney, J., & Machado, A. R. (2005). Evaluation of the performance of CBN tools when turning Ti–6Al–4V alloy with high pressure coolant supplies. International Journal of Machine Tools and Manufacture, 45(9), 1009-1014.

194. Selvaraj, D.P., P. Chandramohan, and M. Mohanraj, Optimization of surface roughness, cutting force and tool wear of nitrogen alloyed duplex stainless steel in a dry turning process using Taguchi method. Measurement, 2014. 49: p. 205-215.

195. Patole, P. and V. Kulkarni, Experimental investigation and optimization of cutting parameters with multi response characteristics in MQL turning of AISI 4340 using nano fluid. Cogent Engineering, 2017. 4(1): p. 1303956.

196. Jawaid, A., C. Che-Haron, and A. Abdullah, Tool wear characteristics in turning of titanium alloy Ti-6246. Journal of Materials Processing Technology, 1999. 92: p. 329-334.

197. Sarhan, A.A. and A. Matsubara, Compensation method of the machine tool spindle thermal displacement for accurate monitoring of cutting forces. Materials and Manufacturing Processes, 2011. 26(12): p. 1511-1521.

198. Alabi, A., T. Ajiboye, and H. Olusegun, Investigating the cutting forces in heat treated medium carbon steel when turning on a lathe machine. Journal of Engineering, Design and Technology, 2010. 8(1): p. 80-93.

199. Kahles, J. F., Field, M., Eylon, D., & Froes, F. H. (1985). Machining of titanium alloys. JOM, 37(4), 27-35.

200. Miaosun, S., Solid lubrication materials. China Chemistry, Beijing, 2000.

201. Nakamura, T., Tanaka, S., Hayakawa, K., & Fukai, Y. (2000). A study of the lubrication behavior of solid lubricants in the upsetting process. Journal of tribology, 122(4), 803-808.

202. Deshmukh, S. and S. Basu, Significance of solid lubricants in metal cutting. 22nd AIMTDR, 2006.

203. Keblinski, P., Phillpot, S. R., Choi, S. U. S., & Eastman, J. A. (2002). Mechanisms of heat flow in suspensions of nano-sized particles (nanofluids). International journal of heat and mass transfer, 45(4), 855-863.

204. Murshed, S., K. Leong, and C. Yang, A combined model for the effective thermal conductivity of nanofluids. Applied Thermal Engineering, 2009. 29(11): p. 2477-2483.

205. Mao, C., Zhang, J., Huang, Y., Zou, H., Huang, X., & Zhou, Z. (2013). Investigation on the effect of nanofluid parameters on MQL grinding. Materials and Manufacturing Processes, 28(4), 436-442.

206. Rapoport, L., Nepomnyashchy, O., Lapsker, I., Verdyan, A., Moshkovich, A., Feldman, Y., & Tenne, R. (2005). Behavior of fullerene-like WS_2 nanoparticles under severe contact conditions. Wear, 259(1-6), 703-707.

207. Lin, Y. and H. So, Limitations on use of ZDDP as an antiwear additive in boundary lubrication. Tribology International, 2004. 37(1): p. 25-33.

208. Choi, C., Jung, M., Choi, Y., Lee, J., & Oh, J. (2011). Tribological properties of lubricating oil-based nanofluids with metal/carbon nanoparticles. Journal of nanoscience and nanotechnology, 11(1), 368-371.

209. Shigley, J.E., Shigley's mechanical engineering design. 2011: Tata McGraw-Hill Education.

210. Tu-Chieh, H. and S. Yaw-Terng, A method for reducing tool wear in a polishing process. International Journal of Machine Tools and Manufacture, 2006. 46(3): p. 413-423.

211. Pan, Z., Shih, D. S., Tabei, A., Garmestani, H., & Liang, S. Y. (2017). Modeling of Ti-6Al-4V machining force considering material microstructure evolution. The International Journal of Advanced Manufacturing Technology, 91(5-8), 2673-2680.

212. Tahri, C., Lequien, P., Outeiro, J. C., & Poulachon, G. (2017). CFD simulation and optimize of LN2 flow inside channels used for cryogenic machining: application to milling of titanium alloy Ti-6Al-4V. Procedia CIRP, 58, 584-589.

213. Li, A., Pang, J., Zhao, J., Zang, J., & Wang, F. (2017). FEM-simulation of machining induced surface plastic deformation and microstructural texture evolution of Ti-6Al-4V alloy. International Journal of Mechanical Sciences, 123, 214-223.

214. Jafarian, F., Ciaran, M. I., Umbrello, D., Arrazola, P. J., Filice, L., & Amirabadi, H. (2014). Finite element simulation of machining Inconel 718 alloy including microstructure changes. International Journal of Mechanical Sciences, 88, 110-121.

215. Vijayaraghavan, V., Garg, A., Gao, L., Vijayaraghavan, R., & Lu, G. (2016). A finite element based data analytics approach for modeling turning process of Inconel 718 alloys. Journal of cleaner production, 137, 1619-1627.

216. Chien, S. E. M., Reddy, M. M., Lee, V. C. C., & Sujan, D. (2017). The Study of Coated Carbide Ball End Milling Tools on Inconel 718 Using Numerical Simulation Analysis to Attain Cutting Force and Temperature Predictive Models at the Cutting Zone. In Materials Science Forum (Vol. 882, pp. 28-35). Trans Tech Publications.

217. Soo, S., D. Aspinwall, and R. Dewes, 3D FE modelling of the cutting of Inconel 718. Journal of Materials Processing Technology, 2004. 150(1-2): p. 116-123.

218. Rao, B., C.R. Dandekar, and Y.C. Shin, An experimental and numerical study on the face milling of Ti–6Al–4V alloy: tool performance and surface integrity. Journal of Materials Processing Technology, 2011. 211(2): p. 294-304.

219. Thepsonthi, T. and T. Özel, Experimental and finite element simulation based investigations on micro-milling Ti-6Al-4V titanium alloy: Effects of cBN coating on tool wear. Journal of Materials Processing Technology, 2013. 213(4): p. 532-542.

220. Banerjee, N. and A. Sharma, Development of a friction model and its application in finite element analysis of minimum quantity lubrication machining of Ti-6Al-4 V. Journal of Materials Processing Technology, 2016. 238: p. 181-194.

221. Balan, A. S. S., Kullarwar, T., Vijayaraghavan, L., & Krishnamurthy, R. (2017). Computational fluid dynamics analysis of MQL spray parameters and its influence on superalloy grinding. Machining Science and Technology, 21(4), 603-616.

222. Rohit, J. N., Kumar, S., Sura Reddy, N., Kuppan, P., & Balan, A. S. S. (2016). Computational Fluid Dynamics Analysis of MQL Spray Parameters and its Influence on MQL Milling of SS304.

223. Abd Rahim, E., H Dorairaju, D., Asmuin, N., Mantari, A. R., & Hanafi, M. (2014). Determination of mist flow characteristic for MQL technique using particle image velocimetry (PIV) and computer fluid dynamics (CFD).

224. Kleinstreuer, C., & Feng, Y. (2011). Experimental and theoretical studies of nanofluid thermal conductivity enhancement: a review. Nanoscale research letters, 6(1), 229.

225. Saarinen, S., Heat Transfer in Nanoscale Colloids. 2014.

226. Lienhard, J. Heat transfer by impingement of circular free-surface liquid jets. in Proceedings of 18th National and 7th ISHMT-ASME Heat and Mass Transfer Conference, Guwahati, India. 2006.

227. Shen, Y., Theoretical analysis of jet-ground plane interaction. 1962: Institute of the Aerospace Sciences.

228. Duan, C. Z., Dou, T., Cai, Y. J., & Li, Y. Y. (2009). Finite element simulation and experiment of chip formation process during high speed machining of AISI 1045 hardened steel. International Journal of Recent Trends in Engineering, 1(5), 46-50.

229. Oh, J.W., Experimental Investigation and Analysis of Chip Rebonding Phenomenon in Turning Superalloys. 2013, The University of Michigan.

230. Kay, G., Failure modeling of Ti-6A1-4V and aluminum 2024-T3 with the Johnson-Cook material model. 2003.

231. Özel, T., The influence of friction models on finite element simulations of machining. International Journal of Machine Tools and Manufacture, 2006. 46(5): p. 518-530.

232. Shet, C. and X. Deng, Finite element analysis of the orthogonal metal cutting process. Journal of Materials Processing Technology, 2000. 105(1): p. 95-109.

233. Miguélez, M. H., Zaera, R., Molinari, A., Cheriguene, R., & Rusinek, A. (2009). Residual stresses in orthogonal cutting of metals: the effect of thermomechanical coupling parameters and of friction. Journal of Thermal Stresses, 32(3), 269-289.

234. Miguélez, M. H., Zaera, R., Molinari, A., & Muñoz-Sánchez, A. (2009, May). The influence of cutting speed in the residual stresses induced by HSM in AISI 316L steel. In 12th CIRP Conference on Modelling of Machining Operations, San Sebastián, España (pp. 7-8).

235. Brinksmeier, E., Cammett, J. T., König, W., Leskovar, P., Peters, J., & Tönshoff, H. K. (1982). Residual stresses—measurement and causes in machining processes. CIRP Annals-Manufacturing Technology, 31(2), 491-510.

236. König, W., A. Berktold, and K.-F. Koch, Turning versus grinding–a comparison of surface integrity aspects and attainable accuracies. CIRP Annals-Manufacturing Technology, 1993. 42(1): p. 39-43.

237. Jovane, F., Y. Koren, and C. Boer, Present and future of flexible automation: towards new paradigms. CIRP Annals-Manufacturing Technology, 2003. 52(2): p. 543-560.

238. Pusavec, F. and J. Kopac, Achieving and implementation of sustainability principles in machining processes. Journal of Advances in Production Engineering and Management, 2009. 3: p. 58-69.

239. Dreher, J., Lawler, M., Stewart, J., Strasorier, G., & Thorne, M. (2009). General motors metrics for sustainable manufacturing. Laboratory for Sustainable Business, Massachusetts Institute of Technology.

240. Diaz, N., Helu, M., Jayanathan, S., Chen, Y., Horvath, A., & Dornfeld, D. (2010, May). Environmental analysis of milling machine tool use in various manufacturing environments. In Sustainable systems and technology (ISSST), 2010 IEEE international symposium on (pp. 1-6). IEEE.

241. Feng, S.C. and C.B. Joung. An overview of a proposed measurement infrastructure for sustainable manufacturing. in Proceedings of the 7th Global Conference on Sustainable Manufacturing, Chennai, India. 2009.

242. Schmidt, W.-P. and A. Taylor. Ford of Europe's product sustainability index. in Proceedings of 13th CIRP International Conference on Life Cycle Engineering. Leuven May 31st–June 2nd. 2006. Citeseer.

243. Narita, H., N. Desmira, and H. Fujimoto, Environmental burden analysis for machining operation using LCA method. Manufacturing Systems and Technologies for the New Frontier, 2008: p. 65-68.

244. Jeswiet, J. and S. Kara, Carbon emissions and CES™ in manufacturing. CIRP Annals-Manufacturing Technology, 2008. 57(1): p. 17-20.

245. Rajemi, M., P. Mativenga, and A. Aramcharoen, Sustainable machining: selection of optimum turning conditions based on minimum energy considerations. Journal of Cleaner Production, 2010. 18(10): p. 1059-1065.

246. Pusavec, F., P. Krajnik, and J. Kopac, Transitioning to sustainable production–Part I: application on machining technologies. Journal of Cleaner Production, 2010. 18(2): p. 174-184.

247. Gutowski, T. G., Branham, M. S., Dahmus, J. B., Jones, A. J., Thiriez, A., & Sekulic, D. P. (2009). Thermodynamic analysis of resources used in manufacturing processes. Environmental science & technology, 43(5), 1584-1590.

248. Ghandehariun, A., Nazzal, Y., Kishawy, H., & Al-Arifi, N. S. (2015). Investigation of sustainability in machining processes: exergy analysis of turning operations. International Journal of Exergy, 17(1), 1-16.

249. Fiksel, J., J. McDaniel, and C. Mendenhall. Measuring progress towards sustainability principles, process, and best practices. in Greening of Industry Network Conference Best Practice Proceedings, http://www. economics. com/images/Sustainability Measurement GIN. pdf, Accessed June. 1999.

250. Feng, S.C., C.-B. Joung, and G. Li. Development overview of sustainable manufacturing metrics. in Proceedings of the 17th CIRP International Conference on Life Cycle Engineering, Hefei, PRC. 2010.

251. Zhang, Y., Review of recent advances on energy efficiency of machine tools for sustainability. Proceedings of the Institution of Mechanical Engineers, Part B: Journal of Engineering Manufacture, 2015. 229(12): p. 2095-2108.

252. Singh, K. and J. Madan. Sustainability Performance Assessment of Alternate Machining Technologies. in ASME 2015 International Manufacturing Science and Engineering Conference. 2015. American Society of Mechanical Engineers.

253. Woo, J., S.-J. Shin, and W. Seo. Developing a big data analytics platform for increasing sustainability performance in machining operations. in Proceedings of 26th International Conference on Flexible Automation and Intelligent Manufacturing, Seoul, Republic of Korea. 2016.

254. Bhanot, N., P.V. Rao, and S. Deshmukh, An Assessment of Sustainability for Turning Process in an Automobile Firm. Procedia CIRP, 2016. 48: p. 538-543.

255. Álvarez, M.E.P., M.M. Bárcena, and F.A. González, On the sustainability of machining processes. Proposal for a unified framework through the triple bottom-line from an understanding review. Journal of Cleaner Production, 2017. 142: p. 3890-3904.

256. Kadam, G.S. and R.S. Pawade, Surface integrity and sustainability assessment in high-speed machining of Inconel 718–An eco-friendly green approach. Journal of Cleaner Production, 2017. 147: p. 273-283.

257. Edwards, L. and M. Endean, Manufacturing with materials. 1990: Butterworth-Heinemann.

258. Bhushan, R.K., Optimization of cutting parameters for minimizing power consumption and maximizing tool life during machining of Al alloy SiC particle composites. Journal of Cleaner Production, 2013. 39: p. 242-254.

259. Kant, G. and K.S. Sangwan, Prediction and optimization of machining parameters for minimizing power consumption and surface roughness in machining. Journal of cleaner production, 2014. 83: p. 151-164.

260. Hanafi, I., Khamlichi, A., Cabrera, F. M., Almansa, E., & Jabbouri, A. (2012). Optimization of cutting conditions for sustainable machining of PEEK-CF30 using TiN tools. Journal of Cleaner Production, 33, 1-9.

261. Hegab, H., Umer, U., Deiab, I., & Kishawy, H. (2018). Performance evaluation of Ti–6Al–4V machining using nano-cutting fluids under minimum quantity lubrication. The International Journal of Advanced Manufacturing Technology, 1-13.

262. Hegab, H., Umer, U., Soliman, M., & Kishawy, H. A. (2018). Effects of nano-cutting fluids on tool performance and chip morphology during machining Inconel 718. The International Journal of Advanced Manufacturing Technology, 1-10.

263. Hegab, H., Kishawy, H. A., Gadallah, M. H., Umer, U., & Deiab, I. (2018). On machining of Ti-6Al-4V using multi-walled carbon nanotubes-based nano-fluid under minimum quantity lubrication. The International Journal of Advanced Manufacturing Technology, 1-11.

264. Hegab, H. A., Darras, B., & Kishawy, H. A. (2018). Towards sustainability assessment of machining processes. Journal of Cleaner Production, 170, 694-703.